Alternative methods for the crosslinking of poly(vinyl alcohol) by the use of functionalised inorganic particles

A water-based approach towards environmentally benign coating materials

Thesis by Jörg Guido Schauberger

In Partial Fulfilment of the Requirements

For the Degree of

Doctor of Mining Sciences

Chair of Chemistry of Polymeric Materials

University of Leoben

Supervision: Ass.Prof. Dipl.-Chem. Dr.rer.nat. Gisbert Rieß

Univ.-Prof. Mag.rer.nat. Dr.techn. Wolfgang Kern

Leoben, August 2013

"Indifference is the revenge the world takes on mediocrities."

Vera, or the Nihilists; Oscar Wilde

Acknowledgement

Abstract

The use of environmentally benign coatings and resist materials has come to attention in the past decades. Besides established polymeric materials poly(vinyl alcohol) is of major interest, as this polymer is water soluble and regarded as safe for packaging technologies as well as for biomedical applications.

New methods for the crosslinking of PVA by radiation were investigated in this work, with emphasis on non-toxicity and biocompatibility of the employed crosslinking agents and cleavage products. Additionally a number of functionalised particles such as cation exchanged montmorillonites were prepared and characterised. The aim was to immobilise functional groups at the surface of inorganic particles that capable of initiating crosslinking reactions. Furthermore these additives were employed to prepare organic-inorganic composite materials with poly(vinyl alcohol) as matrix polymer.

The distribution of the modified particles was investigated by microscopic methods, while optical spectroscopy was employed to observe covalent crosslink formation, due to heat treatment of UV light exposure. Additionally covalent crosslink formation and polymer-filler interactions were investigated by determination of the swelling behaviour in deionised water.

Kurzfassung

Die Verwendung umweltfreundlicher Beschichtungen und Resistmaterialien ist für zahlreiche technische Anwendungen relevant. Neben bewährten Polymersystemen ist Poly(vinylalkohol) aufgrund seiner Wasserlöslichkeit von größtem Interesse. Ein weiterer Vorteil ist die Biokompatibilität und physiologische Unbedenklichkeit dieses Polymers, das für Anwendungen im Bereich der Verpackungstechnologien und für medizinische Produkte zugelassen ist.

In der vorliegenden Arbeit wurden alternative Methoden für die Vernetzung von Poly(vinylalkohol) durch Strahlung (e-Beam, UV) untersucht. Der Schwerpunkt wurde auf die Unbedenklichkeit der eingesetzen Vernetzungchemikalien und deren Spaltprodukte gelegt. Zusätzlich wurde eine Vielzahl an funktionalisierten anorganischen Partikeln, wie kationen-getauschte Schichtsilikate, hergestellt und charakterisiert. Das Ziel war die Immobilisierung funktioneller Gruppen an der Oberfläche von anorganischen Partikeln, um Vernetzungsreaktionen der Polymermatrix zu initiieren. Zusätzlich wurden die modifizierten anorganischen Komponenten zur Herstellung von Kompositmaterialien mit Poly(vinylalkohol) als Matrixpolymer eingesetzt.

Die Verteilung der modifizierten Partikel wurde mittels mikroskopischer Methoden untersucht, während spektroskopische Methoden zur Untersuchung der Ausbildung von Vernetzungsstellen (z.B. durch UV Bestrahlung oder thermische Reaktionen) eingesetzt wurden. Quellversuche in deionisiertem Wasser wurden durchgeführt, um zusätzliche Informationen über die Wechselwirkungen zwischen Matrix und Polymer, und die Ausbildung von Vernetzungsstellen zu erhalten.

Affidavit

I hereby confirm that my thesis entitled "Alternative methods for the crosslinking of poly(vinyl alcohol) by the use of functionalised inorganic particles - A water-based approach towards environmentally benign coating materials" is the result of my own work. I did not receive any help or support from commercial consultants. All sources and / or materials applied are listed and specified in the thesis.

Furthermore, I confirm that this thesis has not yet been submitted as part of another examination process neither in identical nor in a similar form.

Leoben, August 2013   Jörg Guido Schauberger

Table of Contents

Abbreviations

Abbreviation	Description
DSC	Differential scanning calorimetry
EDX	Energy dispersive X-ray spectroscopy
EVOH	Poly(ethylene-co-vinyl alcohol)
FTIR spectroscopy	Fourier transform infrared spectroscopy
GC-MS	Gas chromatography – mass spectrometer
GPC	Gel permeation chromatography
LOD	Limit of detection
LS	Light scattering detector
MAXS	Medium angle X-ray scattering
MMD	Molar mass distribution
MMT	Montmorillonite
M_n	Number average molecular weight
M_w	Weight average molecular weight
NMR spectroscopy	Nuclear magnetic resonance spectroscopy
PDI	Polydispersity index
phr	Per hundred parts of rubber
PVA	Poly(vinyl alcohol)
RI	Refractive index detector (GPC)

Abbreviation	Description
RT	Room temperature
SEC	Size exclusion chromatography
SEM	Scanning electron microscope
TGA	Thermogravimetric analysis
UV/Vis spectroscopy	Ultraviolet/visible light spectroscopy
XNBR	Carboxylated nitrile butadiene rubber

Formula symbols

Symbol	Unit(s)	Meaning
D	kGy	Radiation dose (e-Beam)
M_n	$gmol^{-1}$	Number average molecular weight
M_w	$gmol^{-1}$	Weight average molecular weight
n^D	-	Refractive index at sodium D-line
PDI	-	Polydispersity index
RT	°C	Room temperature (23 ± 2°C)
T	°C	Temperature
w_d	g, mg	Dry sample weight
w_i	g, mg	Initial sample weight
w_s	g, mg	Swollen sample weight
η	mPas	Viscosity
λ	nm, (Å)	Wavelength of visible / UV-light or (X-rays)
ν	cm^{-1}	Wavenumber

I. INTRODUCTION

In the recent decades environmental compliance became of growing importance in the packaging industry and for the application of chemical technologies. Hence the critical values for organic solvents in sewage water and in exhaust air got tighter, production processes have to be adapted to recirculate solvents and process chemicals. This brought forth reduced emissions and water contamination.[1]

As an example, the food packaging industry would benefit from the employment of water based coating systems. As the guidelines and regulations in the field of packaging regarding the migration of organic substances (e.g. di-isobutyl phthalate) into packaged goods such as food get more and more tight, the need arises to develop water-based coating materials and barrier films to prevent migration of such substances.[2–7]Great effort is devoted to the research in such materials, which have to be environmentally benign and recyclable as well.[8]

Moreover, water-based coatings and resist materials may find application in the field of printed circuit boards. Furthermore the preparation of photoresist materials that are water soluble and therefore can be developed by water could provide an alternative to common resist technologies for the preparation of flexible polymer waveguides and holographic recording materials.[9–11]

The immobilisation of functional groups onto inorganic surfaces (e.g. silicon dioxide) bearing hydroxyl groups, provides a way to prevent leaching out of the active substances of organic-inorganic composite materials. This also provides the possibility to employ new classes of materials in the field of biomedical technologies and water purification (e.g. removal of heavy metal cations and dyes).[4,12,13]

The substitution of established processes and chemicals by water-based systems would pose alternatives that are environmentally benign as well as lead to cost reduction after implementation. Hence no additional safety measures and closed loop process conduction have to be employed.

The major goals of this work are the investigation of alternative ways for the crosslinking of poly(vinyl alcohol) by the employment of radiation and thermally induced methods. On the

other hand, new classes of functionalised filler materials have been envisaged, by either cation exchange reactions to obtain modified layered clays as well as surface modification of inorganic particles such as silica. These particles have been assessed as functional additives for both covalent and physical crosslinking of organic-inorganic composite materials with PVA as matrix polymer.

II. STATE OF THE ART: A LITERATURE REVIEW

1. POLY(VINYL ALCOHOL) (PVA)

1.1 SYNTHESIS AND PROPERTIES

Poly(vinyl alcohol) (PVA) is usually prepared by polymer analogous saponification of poly(vinyl acetate), which has been polymerised by free radical polymerisation.[14] The chemical and physical properties of the water soluble polymer are strongly influenced by the degree of polymerisation as well as by the degree of saponification.[15,16]

PVA is employed as adhesive for packaging applications[17], as sizing agent for paper processing[3,16], for water soluble glues and modelling materials [18] as well as encapsulation agent and dispersing aid.[19] Due to its biocompatibility this polymer is regarded as safe for coatings in contact with foodstuff and suitable for the preparation of hydrogels for biomedical applications.[20–22]

Furthermore PVA is able to form an intricate network of hydrogen bonds between the polymer chains, which leads to outstanding barrier properties of the dry polymer against oxygen and non-polar substances as the polymer itself is highly polar.[23,24] As PVA exhibits strong hygroscopy, the absorption of aerial humidity leads to deterioration of the hydrogen bonding network, resulting in swelling of the polymer and diminishing of the barrier properties.[25,26]

In order to prevent this adverse effect, crosslinking has to be achieved. Numerous crosslinking reactions are well described in the literature and are in many cases acid catalysed.

1.2 CROSSLINKING

1.2.1 *Acid catalysed methods*

Acid catalysed crosslinking of PVA can be performed with a number of multifunctional crosslinking agents, but the majority of these reactions are performed in accordance to three concepts that are depicted in Fig. 1. As aldehydes are highly reactive, crosslinking reactions with PVA lead to the formation of stable acetal and unstable hemiacetal structures, of which the latter are further hydrolysed because of lacking stability.[27,28] Crosslinking by the

employment of difunctional acids, such as adipic acid or oxalic acid leads to the formation of ester bonds, which prevent swelling and thus further deterioration of the barrier properties due to water uptake.[22,29,30]

By the addition of multifunctional silanes, such as tetraethyl orthosilicate (TEOS), the formation of an organic-inorganic hybrid network is described by a series of authors. Also the formation of silica nanoparticles due to acid induced hydrolysis of the ethoxy groups is reported and demonstrated by Bandyopadhyay, Sarkar and Bhowmick by in-situ sol-gel processes.[31–35]
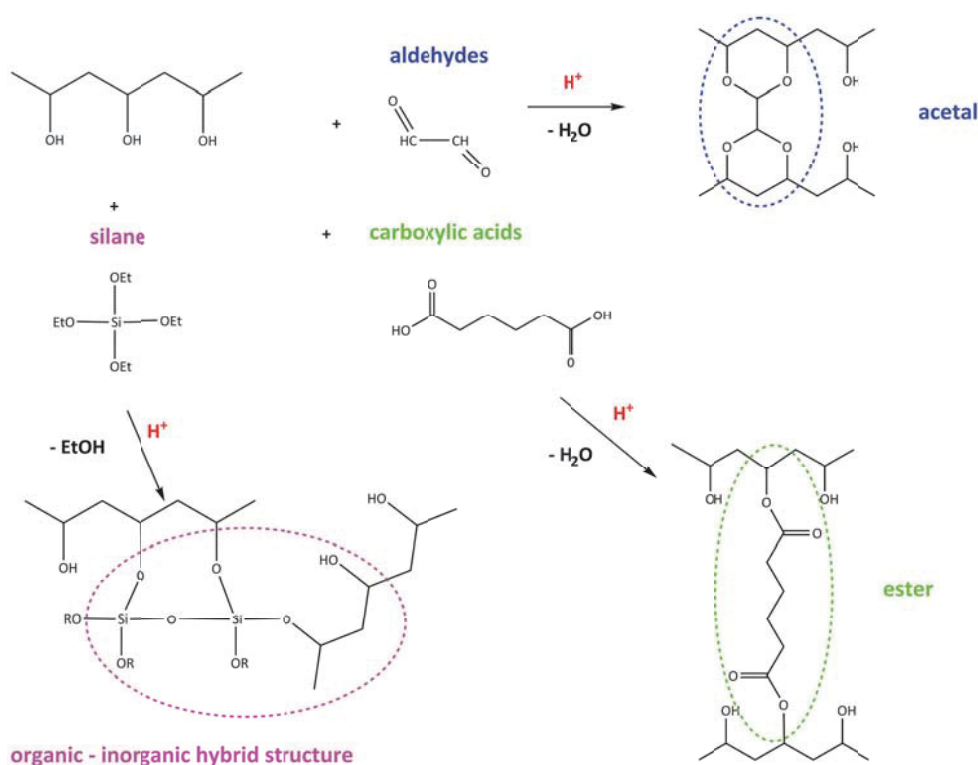
Fig. 1: Overview of acid catalysed crosslinking mechanisms for poly(vinyl alcohol).

An alternative to the employment of low molecular crosslinking agents would be the utilisation of polymers with carboxylic moieties such as poly(acrylic acid). Pal describes the preparation of crosslinked hydrogel membranes by use of acid catalysed esterification between PVA and the free carboxylic acid groups of gelatin.[30,36]

1.2.2 Radiation induced crosslinking

Poly(vinyl alcohol) can be crosslinked by exposure to ionising radiation such as β/γ-rays or X-rays, resulting in statistic formation of free radicals and their subsequent recombination.[29,37]

A number of authors report that ionising radiation can be employed for co-crosslinking PVA blends with chitosan or gelatine in order to prepare hydrogels without the addition of any crosslinking agents.[38–40]

A more convenient method to crosslink PVA is the doping with transition metal chlorides such as iron chloride or chromates such as potassium dichromate, which leads to photosensitising of the polymer. The mechanism of crosslinking can be compared to the well-known gelatine/dichromate systems in the field of photographic and holographic recording materials. But it has to be stated that chromates are highly toxic compounds, which are hazardous to the environment and carcinogenic as well. [41–43]

Manivannan, Kuncser and Filoti have investigated the mechanism of crosslinking for Fe^{3+} doped PVA and found that photoreduction of the Fe^{3+} ions to Fe^{2+} takes place, which leads to radical formation and recombination, thus leading to crosslink formation.[44–48] The aim of these UV crosslinking experiments was the preparation of holographic recording materials and nonlinear optics. As $FeCl_3$ is employed as flocculation agent for waste water treatment, it is considered environmentally benign and poses an alternative way to chromate doping of PVA.[48–51]

Another approach to attain UV curable PVA is the grafting of copolymers with acrylic moieties attached to the polymer backbone. By the addition of a radical photoinitiator such as 2-hydroxy-2-methylpropiophenone (Irgacure® 1173; BASF GmbH; Ludwigshafen; Germany), UV induced crosslinking via free radical reaction can be performed, which leads to samples that are insoluble in deionised water.[52–55]

2.   AZOSULPHONATES

2.1.1   *State of the art*

Labile azo functionalities bearing aliphatic or mixed aliphatic aromatic moieties have a long tradition in the field of polymer chemistry. Thermally cleavable azo compounds are widely used as initiators for free radical polymerisation, with 2,2'-azoisobutyronitrile and its derivatives the most well-known examples of this class.[56,57] Also polymers with azo functions in the main chain or side groups that can be thermally decomposed are employed as macroinitiators for the synthesis of block and graft polymers.[58–60]

The preparation of photolabile and thermally stable low molecular aromatic azo compounds such as azosulphonates and azophosphonates came to interest, for the employment in the field of photoresist materials, laser ablation and recording materials.[61–63] Also the preparation and characterisation of polymers and copolymers that can be decomposed by UV irradiation has been reported by Matusche, Nuyken and Trogisch.[60,64,65]

2.1.2   *Decomposition mechanism of aromatic azosulphonates*

The photolysis behaviour of aromatic azosulphonate compounds was investigated by Nuyken and Voit in the early 1990s. It was found, that the mechanism of decomposition is depending on the chemical environment. As a result of UV irradiation, the stable trans-form of the azosulphonate is rearranged to the unstable cis-form, which leads to decomposition upon further exposure (see Fig. 2). In the presence of water an ionic scission mechanism is prevalent, leading to the formation of hydroxyphenyl residue groups. On the other hand, in the presence of alcohols, a radical cleavage mechanism is dominant, which leads to the formation of phenyl groups. Due to UV induced decomposition, the described mechanisms lead to formation of nitrogen gas, showing no dependence on the chemical environment.[57,61,66]
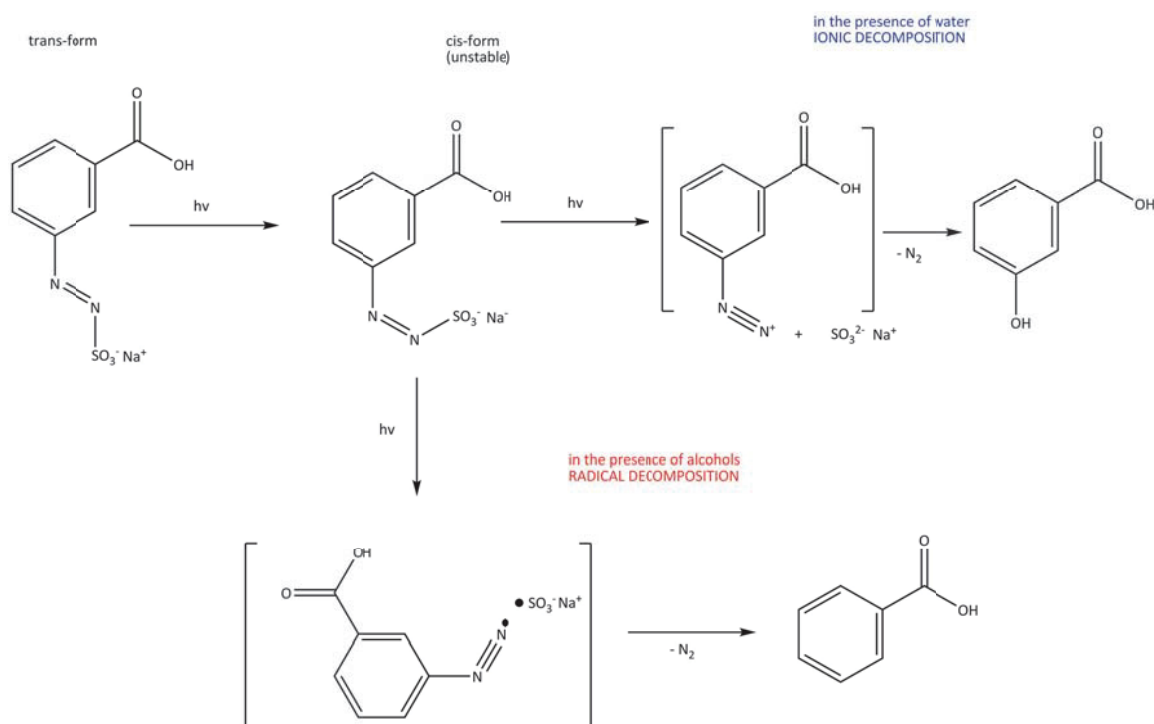
Fig. 2:   Decomposition mechanism of aryl azosulphonate compounds in dependence of the chemical environment as published by Nuyken, Voit and Riess.[57,61]

3. FUNCTIONALISATION OF INORGANIC PARTICLES

3.1 MONTMORILLONITE

The smectite-group mineral montmorillonite (MMT) is a layered alumosilicate with the general composition $[Si_8]^{IV}[Al_{4-x}Mg_x]^{VI}O_{20}(OH)_4(M_{x/n})^{n+}\cdot yH_2O$.[67,68] Due to its special layer structure consisting of two tetrahedral sheets sandwiching one octahedral sheet, negative surface charges between the clay platelets exist, that are balanced by Ca^{2+}, Mg^{2+} or Na^+ cations (see Fig. 3). The absorption of water leads to swelling of the layered silicate, thus increasing the layer-to-layer distance. Therefore the interlayer cations can be more easily exchanged with other metal cations or with organic cations to further increase the layer-to-layer distance and thus improve the exfoliation behaviour and dispersibility. Neat montmorillonite is one of the main components of drilling muds and can also be employed as thickening agent for aqueous suspensions or for geotextiles.[69–71]
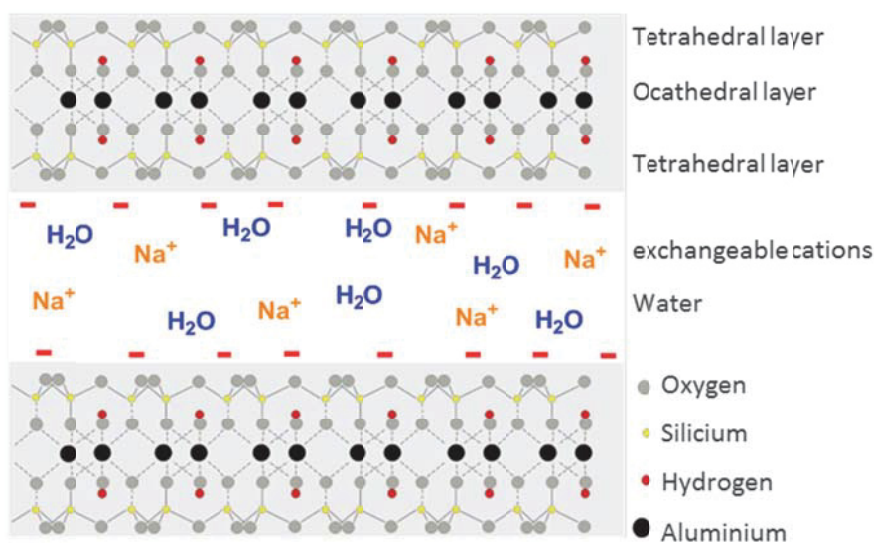
Fig. 3: Triple layered structure of a sodium montmorillonite aggregate consisting of two platelets, water and interlayer cations.([©]Andreas Trepte).

A variety of cation exchange reactions can be performed on montmorillonites, the most of them are employed to incorporate non-polar ammonium salts, bearing tallow groups to attain organophilic behaviour. Such modified materials may find application as flame retardants; active filler materials that enhance the mechanical strength of polymer composites as well increase the gas barrier properties of a number of polymeric composite

materials. The main aim is often to facilitate the compatibility of the layered silicate with polyolefins such as PE and PP and to enable melt processing of the obtained composites.[70,72]

3.1.1   *Activation*

The treatment of montmorillonite clays with mineral acids such as hydrochloric, sulphuric or nitric acid leads to a volume increase of the MMT as well as to decomposition of accessory minerals and biological contaminants.[73,74] The first step of the acid treatment process leads to a rise of the surface acidity as well as to partial delamination. [75] This results in an increase of the surface area of the montmorillonite and introduces permanent mesoporosity.[76] Due to the activation step additional silanol groups are formed, which act as hydrogen bonding sites.[77]

A series of authors report the activation of montmorillonite clays using phosphoric acid, which does not only lead to delamination of the platelets, but also to a decomposition of the triple layer structure of the particles. It is found that the formation of aluminium phosphate takes place, which is a lead that aluminium ions, which are located at the broken edges of the MMT platelets are conversed by the acid treatment.[78–80]

Acid activated montmorillonite clays may find application as solid catalysts for alkylation and acylation reactions [76], and their suitability as adsorbents for heavy metals, radioactive waste materials and dyes from aqueous solution has been investigated as well. [81–83] Furthermore Tyagi and Chudasama report the employment of the modified clays in the field of paper technology and in beverage and foodstuff applications (e.g. fining agent for wine).[75]

3.1.2   *Metal-cation exchange*

As the interlayer cations of montmorillonite can be leached out easily, cation exchange reactions to immobilise transition metal ions can be performed by the addition of an excess of the particular metal salt. It is reported that these modified MMTs are outstanding solid state heterogenic catalysts, for a series of reaction types including esterification, alkylation, acetalisation and oxidation reactions.[80,84–86]

The immobilisation of zinc cations in the interlayer galleries leads to antimicrobially active clays, which may also find application as crosslinking agents for XNBR lattices as substitute

for common crosslinking chemicals such as ZnO.[87–89] Abollino reports that Mn^{2+} cations exhibit strong affinity to montmorillonite, while Hothi states that manganese cation exchanged MMTs can be employed as environmentally compliant solid state catalyst for the production of hydrogen peroxide as well as hydroxylamine.[90,91]

Gerstl et al. report that the intercalation of Fe^{3+} ions leads to enhanced catalytic activity of such prepared montmorillonite, which may be employed as environmentally benign solid state catalysts.[92–96] As the Fe^{3+} cation can be reduced by UV light exposure[9,97], it is possible to employ this particular montmorillonite as a novel environmentally benign and water based radical photoinitiator.[11]

3.1.3 *Organomodification of montmorillonite*

The hydrophobisation of montmorillonite by intercalation of amino compounds bearing tallow groups is well known and described by several authors.[70,72,98,99] The focus of this section is set on the immobilisation of functional groups by cation exchange reactions into the interlayer galleries of the layered clay using polar modification reagents.

Due to their highly polar and negatively charged interlayer gallery surface, the immobilisation of amino compounds by means of cation exchange reactions can be performed without difficulty. As montmorillonite clays exhibit a large surface area and a multiporous structure, they can be employed for filtration processes as well as absorbents for dyes from aqueous solutions.[83] Furthermore the absorption of methylene blue is an established method to determine the surface area of clay minerals and soil samples.[100]

The immobilisation of the amino acid glycine in the interlayer galleries of MMT is well studied, however this is mostly employed as precursor for the preparation of longer peptide condensates.[101–104] The adsorption of organic substances by montmorillonite leads to an increase of the layer-to-layer distance as well as to delamination of the clay platelets.

Organoclays with immobilised thiol moieties may find application for the removal of heavy metal ions from waste water by formation of coordination complexes with e.g. Hg^{2+} and Cd^{2+} [81,105,105–107] As thiols are employed for photochemical crosslinking of NR and XNBR[89], such clay minerals may be employed as solid state crosslinking aids, with the advantage that no leaching of the thiol can take place. The immobilisation of amino sulphonic acids by the

means of cation exchange has been performed and investigated by Kaufmann.[71] The sulphonic acid moiety can be employed in the field of cation donor/exchange materials and for heavy metal complexation.[108,109]

3.2   SURFACE FUNCTIONALISATION

The polarity tuning of inorganic surfaces and the immobilisation of functional groups by the means of silanisation is a well-established procedure[110,111], which provides the commercial availability of a variety of surface modified silicon dioxide particles. These are either available as colloidal particle dispersions such as Bindzil® or Levasil® from AkzoNobel (Amstdam, Netherlands) or as solid particles such as Actisil® by Hoffmann Mineral (Neuburg, Germany) with different functionalities (e.g. thiol, vinyl) attached onto the surface.

The immobilisation of alkoxysilanes onto surfaces bearing hydroxyl groups is a rather simple procedure, which is depicted in Fig. 4. Traces of water in the solvent (e.g. ethanol) lead to hydrolysis of the alkoxy moieties, leading to splitting off of alcohols. This is followed by condensation of the hydroxyl groups of the surface and the silane, leading to immobilisation of the functional groups that are attached to the silane. This reaction mechanism can also be catalysed by acids, which leads to increased reaction speed.[31–33]
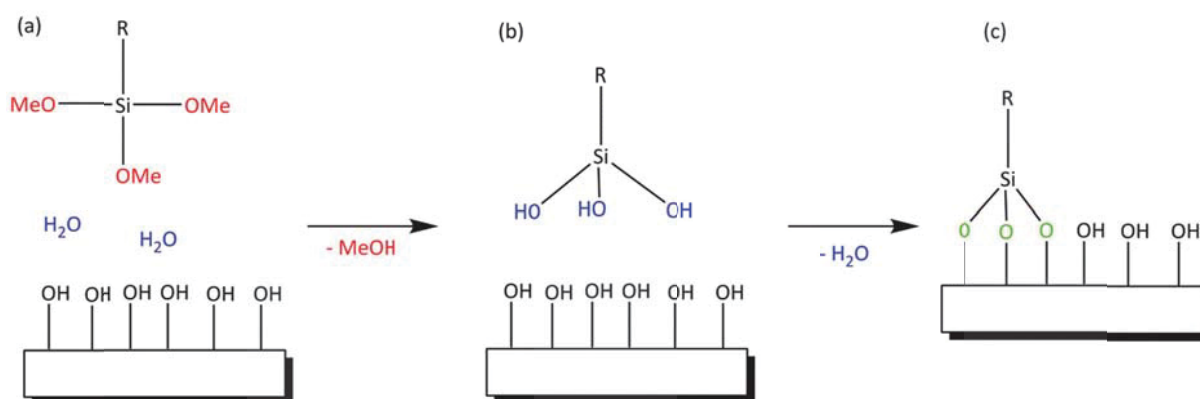
Fig. 4:   Reaction mechanism of immobilisation of an alkoxysilane onto a silicon surface; (a) traces of water in the solvent (e.g. ethanol) lead to hydrolysis and splitting off of methanol (b); condensation of hydroxyl groups (c). The structural representation has been simplified for clarity.

The surface modification of inorganic surfaces by the means of silanisation is also utilised for the introduction of thiols and sulphonic acids onto the surface of montmorillonite platelets by means of condensation reactions of the silanol groups.[112–114] It can additionally be

employed for the preparation of particles bearing photoactive groups such as azides[115] or for grafting of polymeric shells from the surface of silica particles.[116] Griesser et al. describe the self-assembly of photoactive monolayers with tuneable surface polarity onto silicate substrates which can be applied in the field of organic electronic devices.[117,118]

4.   ORGANIC-INORGANIC COMPOSITE MATERIALS

As this work is focused on preparation and investigation of water-based polymer solutions, particle suspensions and composite dispersions, the emphasis of this section of the literature review is set on composites comprising poly(vinyl alcohol), silica particles and layered platy clay minerals and the applications of such materials.

The incorporation of inorganic particles into a polymer matrix is employed to modify various properties of polymers such as flammability[119], solvent resistance[11], gas barrier properties and mechanical properties such as stiffness and heat deflection temperature.[72,99] In order to enhance the compatibility between the matrix and the inorganic particles, thus improving the modifying effect on the composite, additional modification steps can be performed on the additive surface.[70,71]

PVA silica composite materials are conveniently prepared by the sol-gel technique from aqueous solutions of PVA and tetraalkoxysilanes by acid catalysed condensation, which also leads to covalent bonding of the inorganic phase onto the polymer backbone as depicted in Fig. 1 as well as to formation of an inorganic silicon dioxide phase.[31,120,121] This leads to increased solvent stability and an increase of barrier properties against non-polar substances has been reported by Nishiuara.[31,35,122,123]
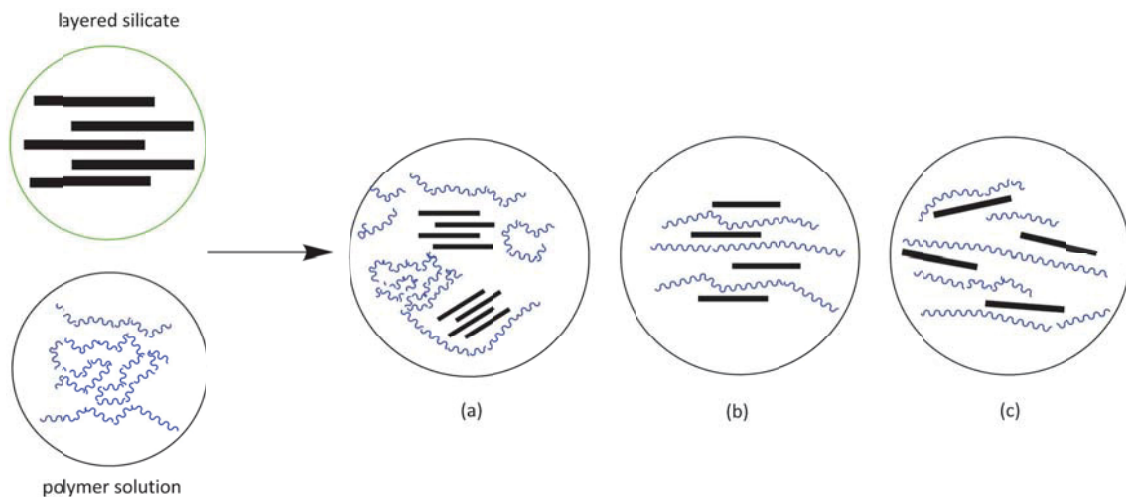
Fig. 5: Schematic representation of different types of clay particle formation in composite materials according to Alexandre and Dubois. (a) phase separation; (b) intercalation; (c) exfoliation.[99]

Melt processing is a convenient method to prepare micro- and nanocomposites comprising PVA, EVA, EVAl and layered silicates such as montmorillonites with improved fire resistance as well as gas barrier properties.[124,125]

Although Pavlidou mentions the disadvantages of polymer/platy clay composites prepared from solution due to the large solvent quantities, on the contrary it is stated by Grunlan that water based systems do not cause these problems.[70,126] Due to strong polymer-filler interactions in PVA-clay composites by intercalation of the clay by the polymer and hydrogen bonding between the silanol groups of the platelet surface, an improvement of the water stability of the composite material is the result.[127]

The preparation of highly disperse nanocomposites from aqueous solutions by the freeze/thawing technique, which leads to immobilisation of inorganic particles by precipitation of the matrix polymer is reported by Kokabi and Nho.[128,129] The obtained hydrogels may find application for wound dressing due to their biocompatibility.[128,130]

The implementation of organoclays bearing cetyl groups as functional filler for PVA composites is reported by Kokabi. This should lead to increased organophilic behaviour thus improving the polymer-filler interactions.[128] It has to be stated that no literature concerning the embedding of amino acid intercalated MMTs in PVA from aqueous solution has been published as yet.

III.   OBJECTIVES

The major goals of this thesis are investigations of alternative crosslinking methods for poly(vinyl alcohol), the preparation of novel types of water-based functional additives, and the characterisation of novel composite materials comprising PVA and highly functional additives.

As PVA was employed as matrix polymer, it was crucial to investigate the structural properties such as molar mass distribution, the degree of hydrolysis and the melting behaviour. Due to the fact that a number of different crosslinking techniques were performed, the swelling behaviour of thin solid neat PVA samples in deionised water was investigated. The determination of the optical properties such as UV absorption and the refractive index was of interest, hence doping of the polymer with photoactive agents was performed.

1.   ALTERNATIVE METHODS OF CROSSLINKING OF PVA

The aim was the investigation of alternative methods of crosslinking PVA using environmentally benign substances as crosslinking agents. Convenient crosslinking consisted condensation reactions of PVA with aldehydes (e.g. glutaraldehyde)[27,28], carboxylic acids (e.g. adipic acid)[22,29,30] or multifunctional silanes (e.g. tetraethyl orthosilicate)[31,32,35], which may exhibit cytotoxicity or may be leached out of the polymer due to swelling, have not been taken into consideration.

1.1   RADIATION ASSISTED METHODS

Electron beam. It is well known that ionising radiation exposure can be employed for the radical crosslinking of a number of polymers such as polyethylene, PVA/alginate copolymers and epoxide and acrylic resins.[37,131,132] Therefore it was assumed that PVA, which was doped with a crosslinking aid bearing vinyl moieties, could be crosslinked in a similar manner. The focus was set on the investigation of radiation induced changes of the solubility behaviour in deionised water of this novel PVA material.

UV crosslinking. UV assisted crosslinking of Fe^{3+} ion doped PVA has been well investigated by Kuncser, Filoti et al. for polymers with low molar mass.[42,45–51,53] However, no swelling

tests of irradiated samples or photolithography experiments followed by development of thin samples were performed by these authors.

The aim of this thesis was the preparation of an iron ion doped PVA with comparatively low iron content and to investigate UV related changes of the optical properties, the formation of crosslinks by swelling tests in deionised water and the preparation of resist materials that may be applied for photolithographic patterning by different methods. Doping with Fe^{3+} ions provides an environmentally friendly, water-based and non-toxic alternative to UV crosslinking of chromate doped PVA systems.[9,16,41]

1.2 AZOSULPHONATE DOPED PVA

Photoactive aryl azosulphonate dyes and their decomposition behaviour were investigated by Riess, Nuyken and Voit in the early 90s as resist materials and monomers for the preparation of UV active resins and polymers.[57,61,62,64] In accordance to Riess, two azosulphonate dyes with carboxylic moieties attached to the aromatic ring were prepared and purified, with the intention to prepare a novel photoreactive azosulphonate-doped PVA material that is water-based and considered eco-friendly.

The aim was to investigate the UV response of the azosulphonate-doped PVA solutions and the preparation of thin films. Further investigations concerning the immobilisation of the dopant by heat initiated condensation reactions were performed by spectroscopic methods as well as swelling tests. These doped PVA materials may be employed as resist coatings with UV tunable polarity and density, therefore the suitability for photolithography was investigated by phase contrast imaging. It has to be stated, that the decomposition products of the photoactive species are non-toxic and generally regarded as save by the European Commission[20].

2. FUNCTIONALISATION OF INORGANIC PARTICLES

The layered structure of phyllosilicates such as muscovite, vermiculite and montmorillonite result in negative surface charges, which are balanced by metal cations. [69,70]. In order to prepare modified functional additives, a number of montmorillonites were modified in accordance to various cation exchange methods. To immobilise azosulphonate moieties

onto particle surfaces, a surface silanisation of inorganic particles (SiO_2, montmorillonite) was performed. One main objective was the preparation of water-based functionalised particles, with an emphasis on the immobilisation of environmentally benign and non-toxic modification reagents.

2.1   CATION EXCHANGE

Activation. The treatment of sodium montmorillonite clays with hydrochloric acid was performed to improve delamination of the platelets as well as to exchange the interlayer sodium cations with protons to attain a precursor for further modification steps.[74,76,112,133] The activated H^+-MMT should have increased organophilic properties, therefore an increased amount of amino acids should be intercalated into the interlayer galleries and compatibility with polar polymers should have improved. As the acid treatment also leads to a decomposition of impurities[77], the H^+-MMT was employed for the immobilisation of azosulphonate dyes.

Metal cation exchange. As previously mentioned, the negative surface charge of the layered silicate facilitates cation exchange. Therefore it was intended to prepare transition metal exchanged montmorillonites by mixing the clay with the appropriate metal chlorides.[92–96] The aim was to immobilise multifunctional metal ions, which could be employed as crosslinking agents for aqueous polymer dispersions and solutions.

With the intention to substitute zinc oxide as crosslinking agent for XNBR latex dispersions[89], Mn^{2+} and Zn^{2+} cation exchanged MMTs were prepared. An UV reactive montmorillonite, bearing immobilised Fe^{3+} ions as photoactive species was prepared for UV assisted radical crosslinking of PVA.[9,11]

2.1.1   *Intercalation of organic cations*

In order to immobilise functional groups in the interlayer galleries of montmorillonite, amino acids were intercalated into the layered silicate. One aim was to investigate the influence of the foregoing acid activation of MMT on the amount of intercalated organic cations. The secondary main objective was the introduction of functional groups, such as sulphonic acid, mercapto and carboxylic acid moieties, which could be employed for condensation reactions with polar polymers such as PVA.[103,106,133] Further emphasis was set on the utilisation of

biologically compliant substances as well as a complete removal of excess modification reagents to prevent leaching out from polymer composites during application.

2.2   SURFACE FUNCTIONALISATION

The aim of the surface modification was the immobilisation of photolabile azosulphonate moieties on inorganic surfaces, thus preventing the leaching out or migration out of organic-inorganic polymer composite materials. The particles consisted of fumed silica and silica nanoparticles as well as different fractions of activated montmorillonite, thus providing a variety of sizes and particle geometries. Due to the different decomposition mechanisms, depending on the chemical environment (see Fig. 2), this new class of particles may act as radical initiator or anion donor by releasing SO_3^{2-} anions upon irradiation.[57,109]

3.   ORGANIC-INORGANIC COMPOSITES

In order to improve the solvent stability by physical strong polymer-filler interactions and the formation of covalent crosslinks, organic-inorganic composite materials were prepared, most of them based on poly(vinyl alcohol) as matrix polymer. The focus of composite preparation was on the employment of non-hazardous additives with immobilised functional centres, as well as the utilisation of water as solvent. As an add-on, the suitability of metal cation exchanged montmorillonites for XNBR crosslinking has been investigated.

UV reactive PVA-Fe^{3+}-MMT composites. Ferric ion exchanged montmorillonite was employed as photoactive filler to improve the swelling stability of PVA against deionised water. The emphasis was to characterise the UV instigated changes of the prepared composite samples and the determination of the particle distribution. The intention was to immobilise the iron ions onto the MMT surface to prevent leaching out by water uptake and to enhance the swelling behaviour in deionised water. Additionally the preparation of photolithographically patterned samples was investigated by phase contrast imaging to visualise density changes due to crosslinking.

Composite materials comprising PVA and organomodified MMT. A new class of composites comprising organomodified sodium montmorillonite (or activated and modified H$^+$-MMT) should exhibit improved swelling behaviour in comparison to the neat polymer. In order to

investigate condensation reactions between the matrix polymer and the filler material, a heat treatment was employed and the formation of covalent crosslinks between the polymer and the carboxylic moieties of the modification reagents was investigated. The main objective was to improve the swelling stability of PVA for the preparation of barrier materials for biomedical applications. Furthermore the preparation of composites was performed from solution, thus employing high speed dispersion tools.

Composite materials comprising PVA and surface modified particles. Here, the main aim was the determination of the UV instigated changes of the swelling behaviour due to the employment of photoreactive azosulphonate particles as functional additives. The particles should act as photoinitiator, thus facilitating radical photo crosslinking. Another aim was the immobilisation of the photoactive species on the particles to prevent leaching and migration, which would be pivotal for a variety of applications. Furthermore the photo cleavage mechanism of the immobilised dyes had to be investigated by spectroscopic methods.
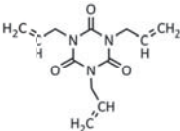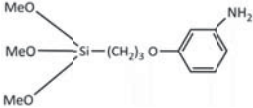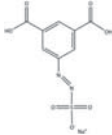
Electron beam crosslinking of organic-inorganic composites. The first objective was the preparation of PVA composites containing commercially available vinyl-terminated silica particles. Under electron beam irradiation covalent crosslinks between the particles and the PVA matrix are expected to be formed. The second goal was the improvement of the swelling behaviour of the PVA composite and complete conversion of the vinyl double bonds at the particle surface.

XNBR-Zn^{2+}/Mn^{2+}-MMT composites. The main aim was the substitution of zinc oxide as crosslinking aid for XNBR by cation exchanged montmorillonites (Zn^{2+}/Mn^{2+}) and the investigation of the influence on the swelling stability against chloroform and crude oil and the mechanical properties. Additionally the influence of subsequent UV crosslinking via the thiol-ene reaction on the material behaviour was investigated.[89]. The suitability of the prepared XNBR composites as sealants or protective coatings for applications concerning crude oil resistance was evaluated.
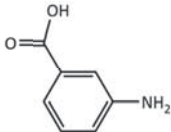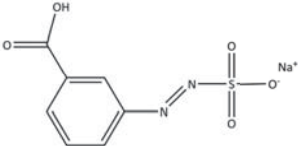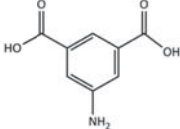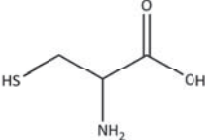
IV. MATERIALS AND METHODS

1. MATERIALS
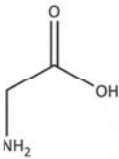
Table 1: List of employed substances

Compound	Structure	CAS-No.	Supplier
1,3,5-triallyl-1,3,5-triazine-2,4,6(1H,3H,5H)-trione (Triallyl isocyanurate (TAIC))		1025-15-6	Sigma-Aldrich Co. LLC (St. Louis, USA)
3-(m-aminophenoxy)propyltrimethoxysilane		71550-66-8	ABCR GmbH & Co. KG (Karlsruhe, Germany)
3,5-dicarboxyphenylazosulphonate sodium (AZOII)			synthesised
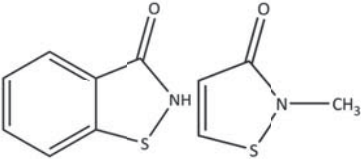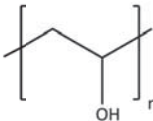
Compound	Structure	CAS-No.	Supplier
3-aminobenzoic acid		99-05-8	Sigma-Aldrich Co. LLC
3-carboxyphenyl azosulphonate sodium (AZOIII)			synthesised
5-amino isophthalic acid		99-31-0	Sigma-Aldrich Co. LLC
2-amino-3-sulfhydrylpropanoic acid (L-cysteine)		52-90-4	Sigma-Aldrich Co. LLC
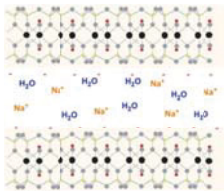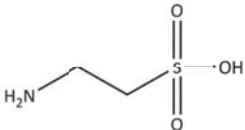
Compound	Structure	CAS-No.	Supplier
Ethanol	(structure: ethanol)	64-17-5	Carl Roth GmbH & Co. KG (Graz, Austria)
Aminoethanoic acid (glycine)	(structure: glycine)	56-40-6	Sigma-Aldrich Co. LLC
Hydrochloric acid	HCl (37 % solution)	7647-01-0	Carl Roth GmbH & Co. KG (Graz, Austria)
Iron(III)chloride	$FeCl_3$	7705-08-0	Sigma-Aldrich Co. LLC; Donauchemie AG (Vienna, Austria)
Manganese(II)chloride	$MnCl_2$	7773-01-5	Sigma-Aldrich Co. LLC
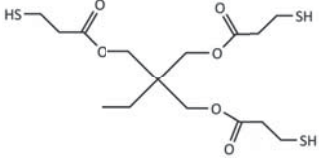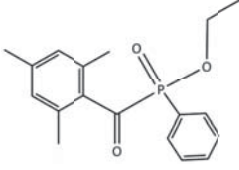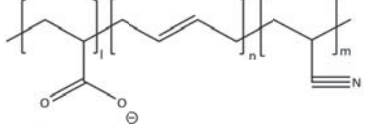
Compound	Structure	CAS-No.	Supplier
Petrosid MBZ biocide based on (benzoisothiazolinone / methylisothiazolinone)		2634-33-5 / 2682-20-4	Biomontan LC (Enns, Austria)
Potassium rhodanide (potassium thiocyanate)	KSCN	333-20-0	Sigma-Aldrich Co. LLC
Poly(vinyl alcohol) (Elvanol® 90-50)		9002-89-5	DuPont (Wilmington, USA)
Fumed silica (Wacker HDK N20)	SiO_2	7631-86-9	Wacker Chemie AG (Munich, Germany)
Silicon dioxide nanoparticles (10 – 20 nm)	SiO_2	7631-86-9	Sigma-Aldrich Co. LLC
Silver nitrate	$AgNO_3$	7761-88-8	Merck KGaA (Darmstadt, Germany)

Compound	Structure	CAS-No.	Supplier
Sodium carbonate	Na_2CO_3	497-19-8	Sigma-Aldrich Co. LLC
Sodium montmorillonite (Cloisite Na^{+})			Southern Clay Products Inc. (Gonzales, USA)
Sodium nitrite	$NaNO_2$	7632-00-0	Sigma-Aldrich Co. LLC
Sodium sulphite	Na_2SO_3	7757-83-7	Sigma-Aldrich Co. LLC
2-aminoethanesulphonic acid (Taurine)		107-35-7	Sigma-Aldrich Co. LLC

Compound	Structure	CAS-No.	Supplier
Trimethylolpropane-tris-3-mercaptopropionate (THIOCURE® ETTMP 1300)		33007-83-9	BRUNO BOCK Chemische Fabrik GmbH & Co KG (Marschacht, Germany)
Tin(II)chloride	$ZnCl_2$	7772-99-8	Sigma-Aldrich Co. LLC
Ethyl-2,4,6-trimethylbenzoylphenylphosphinate (Lucirin TPO-L)		282-810-6	BASF (Ludwigshafen, Germany)b
XNBR (40 wt.-% solids content)		9003-18-3	Zeon Ltd. (Sully, Great Britain)

2. EQUIPMENT

Table 2: Laboratory equipment

Device	Description
Analytical balances	Kern (Kern und Sohn GmbH, Balingen-Frommern, Germany) 770-13; weighing range: 0–220 g; weighing resolution: 0.1 mg; weighing accuracy; 0.1 mg; calibration: external weight. Kern ABT220-4M; weighing range: 0.01–220 g; weighing resolution: 0.1 mg; weighing accuracy; calibration: internal
High speed dispersion equipment	IKA (IKA GmbH, Staufen im Breisgau, Germany) UltraTurrax T18 equipped with S18N-19G steel dispersing element; dispersing speed range: 3000–25000 rpm; viscosity range: up to 5000 mPas.
Laboratory balance	AND EK2000i (A&D Company Ltd., Tokyo, Japan), weighing range: 0.1–2000 g; weighing accuracy: ± 0.1 g.
Magnetic stirrers	IKAMAG (IKA GmbH, Staufen im Breisgau, Germany) RCT Standard equipped with a PT1000 temperature probe; stirring speed range: 0–2000 rpm; Heat output 600 W; Heating range: 0–310 °C.
Convection oven	Binder (Binder GmbH, Tuttlingen, Germany) FD115; Temperature range: (RT + 5)–300 °C; Volume 158 l; Air changes per hour: 26–32; actual power output: 1600 W.
pH measurement	Thermo (ThermoFisher Scientific, Waltham, USA) Orion* 3-Star pH Benchtop meter equipped with an Orion* 9157BNMD Triode* 3-in-1 pH/ATC Probe; pH-range: -2.000–19.000; pH-resolution: 0.01; accuracy ± 0.002 pH; Calibration: 3-point calibration with DIN buffer solutions.
Stirring	Heidolph (Heidolph Instruments GmbH & Co. KG, Schwabach, Germany) RZR 2041 with radial flow impeller (d = 50 mm); stirring speed range: 40–2000 rpm; viscosity range: up to 100 000 mPas.
Sonification	Bandelin (Bandelin electronic GmbH & Co. KG, Berlin, Germany) Sonorex Digitec DT 102 H-RC; ultrasound peak performance: 480 W; temperature range: 20–80 °C.

Table 3:   Irradiation devices and spectrograph

Device	Description
E-beam	IBA (IBA Industrial, Louvain-La-Neuve, Belgium) Rhodotron® TT100 10MeV 35kW electron accelerator; scanning horn size: 100 cm; beam energy: 10 MeV (+ 0 KeV - 250 KeV).
Spectroradiometer	Solatell (Solatell Inc., Croydon, UK) SolaScope 2000: single grating spectrograph optimised for UV with 512 pixel UV enhanced detector array; Diffuser: Cosine response UV diffuser, d = 10 mm; wavelength range: 235–470 nm; spectral sampling: 0.5 nm; bandwidth 1nm (+ 0.5 nm /- 0 nm); sensitivity: < 10nWcm^{-2}nm^{-1}.
Flood exposure	FusionUV (Fusion UV Systems Inc., Maryland, USA) Light Hammer 6 conveyor belt irradiation device; light source(s): medium pressure mercury vapour lamp (no dopant, Ga or Fe doped); power output: variable; conveyor belt speed: 0.1–75 m/min.
Photolithographic patterning	Süss (Süss Microtec GmbH, Garching, Germany) MJB4 Mask Aligner; light source: medium pressure mercury vapour lamp with filters; wavelength range: 280–350 nm; intensity: 25 mWcm^{-2}.
Spot curing	Lumen Dynamics (Lumen Dynamics Group Inc., Mississauga, USA) OmniCure S1000 equipped with a flexible light guide; Light source: High Pressure 100 Watt Mercury Vapor Short Arc; no filters fitted; emitted wavelength: 250–500 nm.

Table 4: Spectroscopic and microscopic equipment

Device	Description
FTIR spectrometer	PerkinElmer (PerkinElmer Inc., Waltham, USA) Spectrum One; wavelength range: 7800–350 cm^{-1}; resolution: 0.5–64 cm^{-1}; wavelength accuracy: 0.1–1600 cm^{-1}.
MAXS	Hecus (HECUS X-Ray Systems GmbH, Graz, Austria) equipped with S3-Micro camera, Xenocs source (G-09) and FOX3D optics; X-rays: Cu-K$^{\alpha}$ (λ =1.54 Å); detector: 2D-Pilatus 100 K; power: 50 kV, 0.6 mA (30 W).

Device	Description
NMR spectrometer 400 MHz	Agilent (Agilent Technologies, Santa Clara, USA) NMR 400MHz resonance frequency; methods: ^{1}H / ^{13}C; various solvents.
Optical microscope	Olympus (Olympus Corp., Tokyo, Japan) BX 51, equipped with a CCD Camera; magnification: 10x, 20x, 50x 100x; phase contrast optics and polarisation filters.
Refractometer	Atago (Atago CO Ltd., Tokyo, Japan) Nar1T; light source: sodium D-Line (λ = 589 nm); measurement range: n^D = 1.3000 to 1.7000; accuracy: n^D ± 0.0002; temperature range: 0–50 °C.
SEM/EDX	Zeiss (Carl Zeiss GmbH, Oberkochen, Germany) Auriga 60 crossbeam workstation; accelerator voltage: 0.1–30 kV; detector system: InLens, CZ BSD.
UV/Vis spectrometer	Agilent (Agilent Technologies, Santa Clara, USA) Cary 50; wavelength range: 190–1100 nm; scanning speed: up to 24 000 nmmin^{-1}; optical system: dual beam; light source: Xenon flash lamp.

Table 5: Thermal analysis

Device	Description
Thermogravimetric analysis (TGA)	PerkinElmer (PerkinElmer Inc., Waltham, USA) Pyris 7; temperature range: RT–1000 °C; temperature precision: ±2 °C; balance accuracy: 0.02 %; balance sensitivity: 0.1 µg; sample pan: platinum.
Thermogravimetric analysis / Differential scanning calorimetry (TGA/DSC)	Mettler-Toledo (Mettler-Toledo AG, Greiffensee, Switzerland); TGA/DSC StarE System; temperature range: RT–1100 °C; temperature precision: 0.15 °C; temperature accuracy: 0.25 °C; sample pan: aluminium oxide.

3. EXPERIMENTAL

3.1 NEAT PVA – REFERENCE MATERIAL

3.1.1 *Determination of structural parameters*

To determine the molar mass distribution (MMD) of neat poly(vinyl alcohol) (PVA), size exclusion chromatography was performed at the Institute of Chemistry at the University of Graz (Graz, Austria). The polymer samples were dissolved in a highly purified aqueous sodium chloride solution (0.05 M NaCl), which was also employed as eluent fluid. Using a combination of refractive index detection (RI), laser light scattering (LS) and with an internal dextran standard, the MMD, the weight average (M_w) and the number average (M_n) molecular weight as well as the polydispersity index (PDI) were determined.

Nuclear magnetic resonance spectroscopy was performed to detect residual acetate groups of the PVA to quantify the degree of hydrolysis. An amount of 10 mg PVA was dissolved in 1 mL deuterated water (heavy water, D_2O) at a temperature of 80 °C in an ultrasonic bath for a duration of 2 hours, until a homogenous sample solution was obtained. ^{1}H and ^{13}C NMR measurements were conducted applying 1024 or 10 000 scans in accordance to the particular method.

3.1.2 *Preparation of solutions and solid PVA samples*

An aqueous PVA solution comprising 5 weight percent (wt.-%) polymer, with regard to the dry matter, was prepared by vigorously stirring appropriate amounts of PVA powder and deionised water at room temperature for 10 minutes, until a slurry was obtained. Subsequently the slurry was heated to a temperature of 85 °C and this temperature level was kept for at least 1 hour to prepare a homogenous solution, which was filtered through a MN 615 ¼ (Machery-Nagel GmbH & Co. KG, Düren, Germany) filter paper. To prevent fouling, caused by fungi and bacteria, an amount of 200 ppm of the biocide Petrosid® MBZ, which is based on benzoisothiazolinone and methylisothiazolinone, was added.

Calcium fluoride (CaF_2) platelets for FTIR and UV-Vis spectroscopy were coated by the drop coating method and dried under constant air flow. Thin solid films for investigations of the swelling behaviour and thermal analysis were obtained by the gravity settling method. An amount of 10 g PVA solution was cast onto polystyrene petri dishes with d = 85 mm (Greiner

Bio-One GmbH, Frickenhausen, Germany) and dried at room temperature (20 °C) under constant air flow.

3.1.3   *Optical methods*

FTIR measurements of PVA coated CaF_2 platelets in a wavenumber range of 4000–850 cm^{-1} with 8 scans and a resolution of 2 cm^{-1} were conducted to investigate the polymer composition, with emphasis on the degree of hydrolysis. To determine the light absorbing properties of PVA, absorption spectra of PVA (on CaF_2 platelets) were recorded at wavelengths ranging from 800 to 250 nm applying a medium scanning speed.

The refractive indices of liquid and solid PVA samples were determined with an Abbe refractometer using a sodium D-line light source (589 nm) at 20 °C. All measurements were performed triplicate.

3.1.4   *Thermal analysis*

Differential Scanning Calorimetry (DSC) measurements of thin PVA film samples were carried out to determine the melting point and investigate the thermal properties of the polymer. A four-step heating program was applied using a heating rate of 20 °Cmin^{-1}, starting from 25 °C to 250 °C, followed by cooling to 25 °C and repeated heating to 250 °C and cooling to 25 °C. The sample chamber was purged with nitrogen at a flow rate of 30 mLmin^{-1}.

3.1.5   *Solubility behaviour*

Thin PVA films were cut into 1 x 1 cm² pieces, weighed to obtain the initial sample weight (w_i) and immersed in deionised water at 23 °C for 48 h to obtain equilibrium swelling.[134,135] After this period the samples were withdrawn, dipped in chloroform to remove surface water and the weight of the swollen samples (w_s) was determined. Drying of the samples was done under steady air flow for approximately 24 hours at 60 °C. Subsequently the weight of the dried sample (w_d) was determined.

The swelling ratio was calculated according to equation (1):[127,132]

$$S\,(\%) = \frac{W_s}{W_i} * 100$$

(1)

The gel content was defined according to equation (2):[132]

$$Gel\ (wt-\%) = \frac{W_d}{W_i} * 100$$

$$(2)$$

All measurements were performed triplicate.

3.2 INVESTIGATION OF RADIATION CROSSLINKING MECHANISMS

3.2.1 *Doping*

e-beam PVA. To facilitate radical formation by electron beam (e-beam) irradiation and therefore improve the crosslinking density, PVA is doped with triallyl isocyanurate (TAIC), the general compositions and sample notations are listed in Table 6. The liquid systems were degassed by sonification in an ultrasound bath prior to thin film preparation and irradiation.

Table 6: Composition of PVA:TAIC formulations (with regard to the dry matter) for e-beam exposure

notation	PVA (wt.-%)	TAIC (wt.-%)
PVA	100	0
TAIC 1	97.5	2.5
TAIC 2	95	5
TAIC 3	92.5	7.5
TAIC 4	90	10

PVA:FeCl$_3$. An aqueous FeCl$_3$ stock solution was prepared to avoid aggregation of FeCl$_3$ powder, prior to the dispersion in the PVA solution. Appropriate amounts of both PVA and FeCl$_3$ solutions were thoroughly stirred on a magnetic stirrer at room temperature until a homogenous PVA:FeCl$_3$ solution with an FeCl$_3$ content of 5 wt.-% (with regard to the dry matter) was attained.

3.2.2 *Sample preparation - thin films*

Thin film preparation for swelling tests, FTIR and UV-Vis measurements and photolithographic pattering was conducted in accordance to the methodology described on page 27.

3.2.3 *Exposure*

Electron beam. E-beam exposure of thin films was performed at Mediscan GmbH (Kremsmünster, Austria) with an IBA Rhodotron TT-100 electron beam accelerator, applying collective radiation doses of 100, 150, 200, 250 and 300 kGy. Radicals are generated statistically in the prepared thin film and recombine, thus giving crosslinked polymer films with improved stability against deionised water.

UV irradiation. To achieve matching between UV absorption of the samples and the emitted UV light, an iron doped medium pressure mercury vapour lamp was applied. Its emission spectrum is depicted in Fig. 6. The samples (thin films and coated CaF_2 platelets) were exposed to UV light with an intensity of 55 $mWcm^{-2}$, for durations of 0, 10, 20, 30, 40 and 60 s.
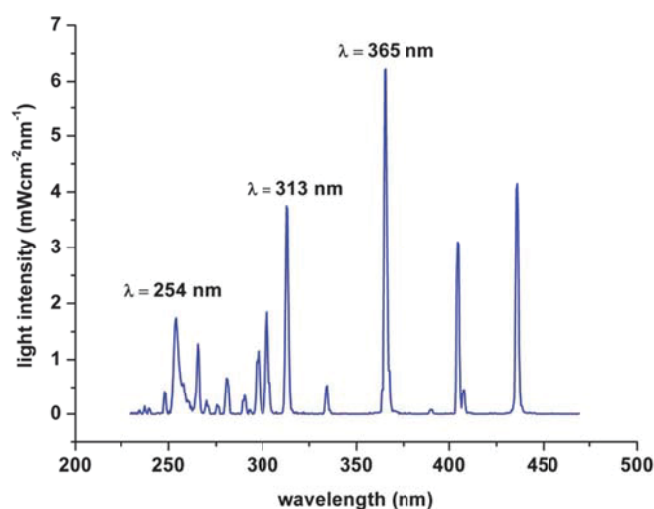

Fig. 6: Emission spectrum of the iron doped medium pressure mercury vapour lamp at an intensity of 55 $mWcm^{-2}$. The emission peaks at 254, 313 and 365 nm are relevant for the UV induced crosslinking of $PVA:FeCl_3$.

3.2.4 *Changes in polymer structure*

E-beam PVA. Thin PVA or TAIC films were analysed by the ATR-FTIR technique to determine changes of the polymer structure due to irradiation, especially the loss of the C=C units of the dopant at wavenumbers of 1680 and 813 cm^{-1} was investigated. Also the formation of C-O-C crosslinks and keto groups (1750–1690 cm^{-1}) was monitored (compare Fig. 7).
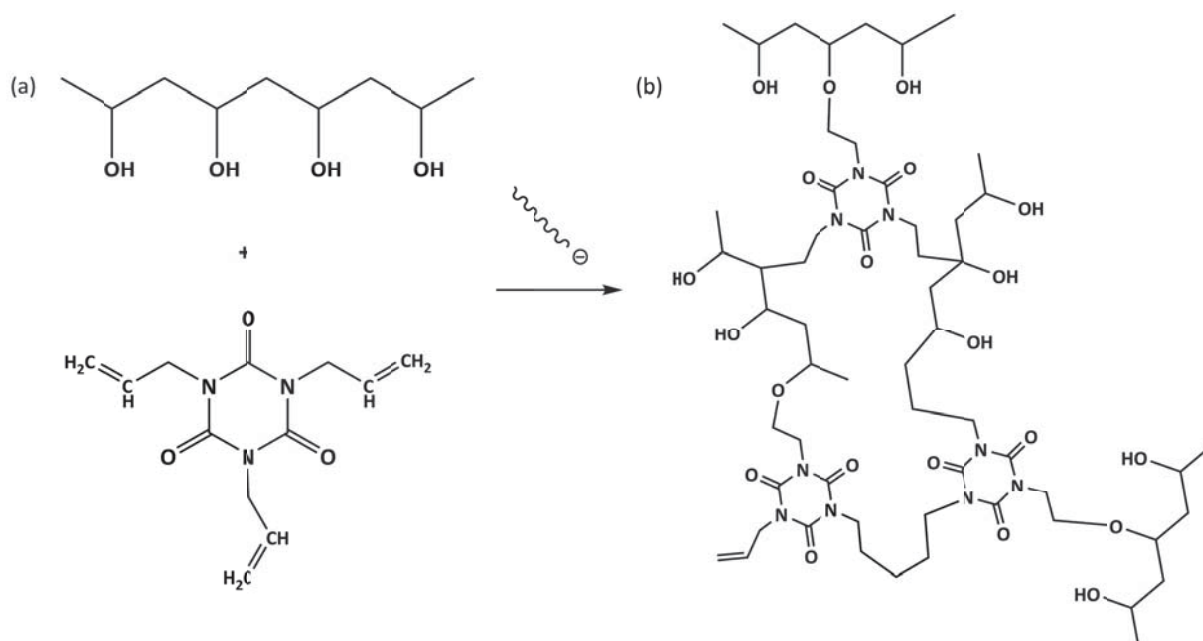
Fig. 7:   (a) Proposed crosslinking mechanism of PVA:TAIC samples; radicals are generated statistically upon e-beam exposure on the polymer backbone and the crosslinking aid; (b) recombination of the radicals and crosslink formation.

PVA:FeCl₃. In order to investigate the UV response of Fe(III) and the photoreduction reaction to Fe(II), liquid samples were filled into quartz cuvettes (3.5 mL, 1 x 1 cm). UV-Vis absorption spectra in a wavelength range of 650 to 250 nm were recorded applying medium scanning speed and the absorption at 360 nm was observed, which can be assigned to Fe(III).[45,136] The cuvettes were irradiated with a spot curing device (high pressure mercury vapour UV light source) with a power output of 9.25 mWcm⁻².
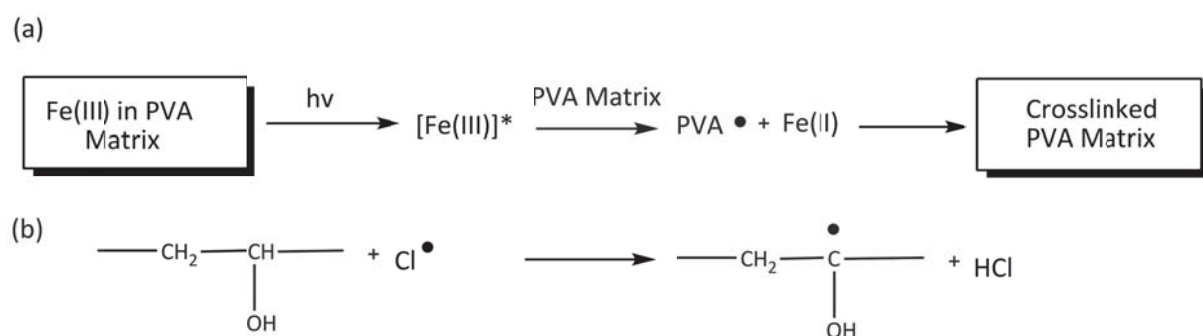

Fig. 8:   Proposed crosslinking mechanisms of PVA:FeCl₃ systems: (a) photoreduction of Fe(III) to Fe(II) and macroradical formation [44] (b) chlorine radical formation and transfer onto the polymer backbone.[51]

Changes of the optical absorption behaviour of thin PVA:FeCl₃ layers that were coated onto CaF₂ platelets were investigated in a similar manner. UV induced changes of the polymer backbone such as the formation of crosslinks or oxidation processes, were investigated by

recording FTIR transmission spectra of thin PVA:FeCl$_3$ layers. Additionally the refractive index (n^D) at the sodium D-line (λ = 589 nm) and its changes due to UV exposure were determined with an Abbe refractometer at 20 °C.

3.2.5 *Determination of swelling behaviour*

Changes of the swelling behaviour due to radiation induced crosslinking reactions (either e-beam on Fig. 7 or UV on Fig. 8) were determined in accordance to the described method at page 28.[127,132]

3.2.6 *Photolithographic pattering*

As the electron beam exposure was only performed in areal operating mode at the Mediscan plant, no lithographic patterning of the exposed samples could be conducted.

Two different methods were employed for photolithographic patterning of PVA:FeCl$_3$. The first method consisted of placing a silicon dioxide / chromium mask with 100 µm features directly onto thin film samples. The subsequent irradiation with an iron doped medium pressure mercury vapour lamp was performed with an exposure time of 20 s and an intensity of 55 mWcm^{-2}.[9]

The second method used a Süss MJB 4 Mask-Aligner (Süss Microtec, Garching, Germany; see Fig. 9), which is equipped with a medium-pressure mercury-vapour lamp and optical filters to provide UV light with wavelengths ranging from 270 to 350 nm and an intensity of 25 mWcm^{-2}. Samples were irradiated for 120 s in soft-contact imprinting mode, applying a patterned silicon dioxide / chromium mask and constant power lamp-operating mode. The exposed areas of the PVA:FeCl$_3$ films are crosslinked, thus reducing the solubility in water. The principle of the photolithographic patterning process is depicted in Fig. 10.[9,11]

Fig. 9:   Süss MJB4 Mask Aligner, which was used for photolithographic patterning experiments ([©] Technical University of Braunschweig, Germany).
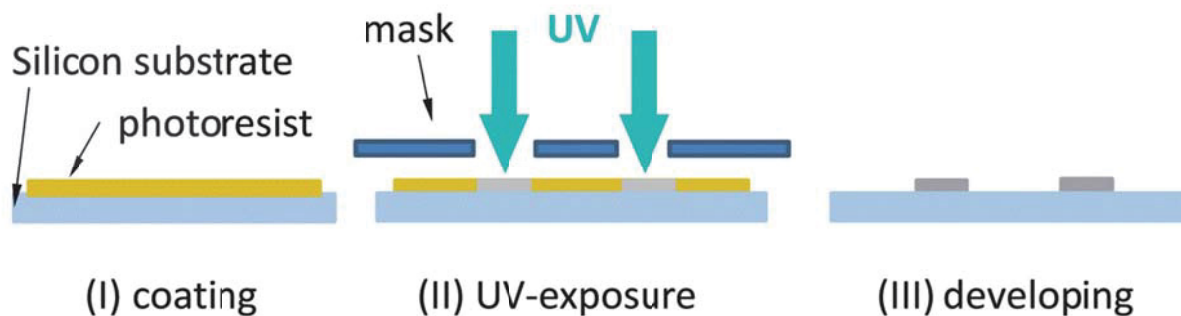

Fig. 10:   Principle of photolithographic patterning. (I) a silicon substrate is coated with a photoactive layer. (II) patterned illumination through a mask; the exposed areas are crosslinked (negative tone photoresist). (III) development step with an appropriate solvent and dissolution of the none-illuminated areas.

Polarised light and phase contrast microscopy of structured samples was performed to evaluate changes in material density and refractive indices. The development process is based on immersion in deionised water for 30 min at RT, which was followed by drying under constant air flow. Profilometric measurements were conducted at the Polymer Competence Center Leoben (PCCL GmbH) to visualise the topographical features of the patterned samples after development.

3.3 PREPARATION OF AZOSULPHONATE DOPED PVA

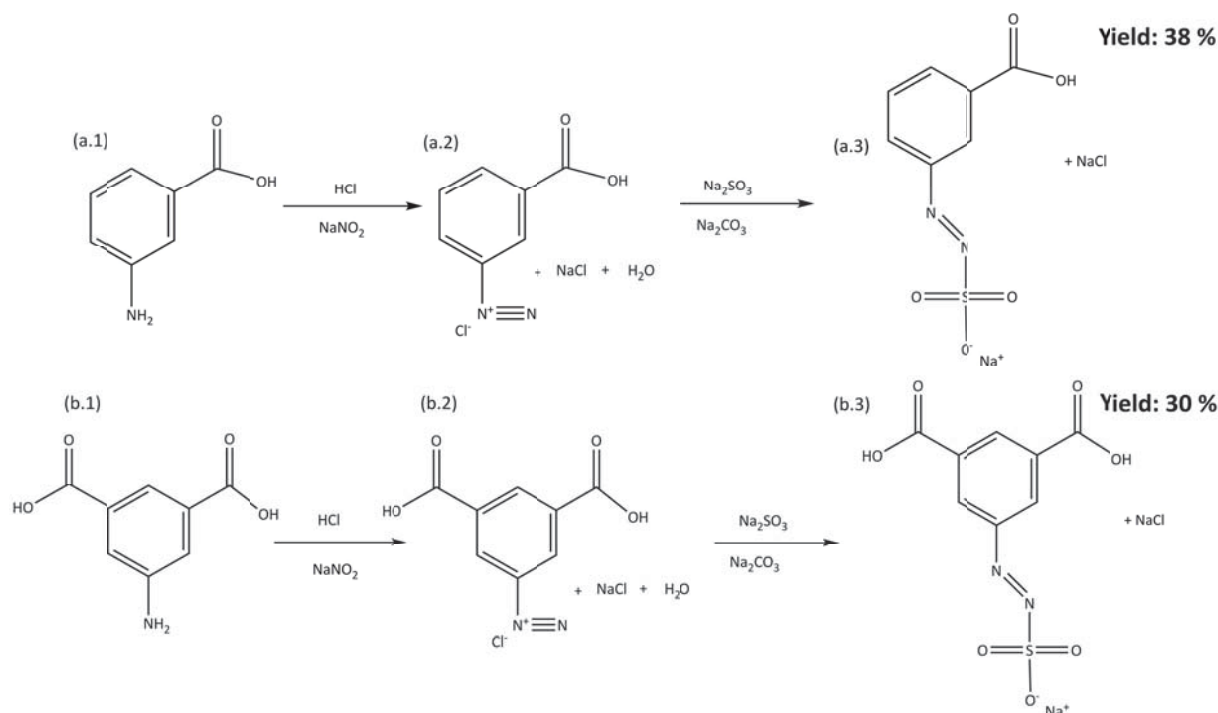### 3.3.1 *Synthesis of aryl azosulphonate compounds*

Fig. 11: Two step synthesis of water soluble aryl azosulphonates bearing carboxylic moieties on the aromatic ring. Nomenclature of compounds was defined in accordance to Riess (a) monofunctional azosulphonate sodium salt (AZO III); (b) difunctional azosulphonate sodium salt (AZO II). [61]
(a/b.1) 3-amino benzoic acid / 5-amino isophthalic acid dissolved in hydrochloric acid; diazotisation using sodium nitrite (a/b.2); (a/b.3) sulphonation, neutralisation and precipitation of appropriate aryl azosulphonate sodium salts.

3.3.1.1 Synthesis and purification

3.3.1.1.1 *Synthesis of 3,5-dicarboxyphenyl azosulphonate – sodium (AZOII)*

In a first step 200 mmol 3-amino isophthalic acid were dissolved in 100 mL hydrochloric acid solution (10 wt.-% in deionised water) and cooled to 0 °C. A pre-chilled sodium nitrite solution (200 mmol in 100 mL deionised water) was added drop wise to the acid solution to diazotise the amino groups (see Fig. 11a.2). As diazonium compounds tend to decompose at elevated temperature, the suspension was kept cooled and slowly added into a sodium sulphite (240 mmol) / sodium carbonate (300 mmol) solution at 0 °C (see Fig. 11a.3) with continuous stirring.

The resulting orange reaction mixture was stored in a refrigerator at 0–5 °C for 18 hours prior to the addition of concentrated hydrochloric acid solution until the pH reached a value of 2. This lead to the precipitation of the product, which was filtered, dried at 50 °C and ground to a fine powder in an agate mortar. [61] The product was purified by recrystallisation and a yield of 38 % (76 mmol) was attained.

3.3.1.1.2 Synthesis of 3-carboxyphenyl azosulphonate – sodium (AZOIII)

The synthesis was carried out in a similar manner as the synthesis of AZOII (see page 34) with 3-amino benzoic acid as precursor. The amount of sodium sulphite is reduced to 200 mmol and carbonate to 150 mmol. [57,61] Purification was performed by recrystallisation from warm water, achieving a total yield of 30 % (60 mmol).

3.3.1.2 Structure determination

^{1}H and ^{13}C nuclear magnetic resonance (NMR) measurements were conducted applying 1024 or 10 000 scans in accordance to the particular method to survey the structure of the synthesised azosulphonate salts, 10 mg of each were dissolved in 1 mL of D_2O.

3.3.1.3 Photolysis

To investigate the light induced decomposition reaction of the obtained azosulphonate compounds (see Fig. 2); FTIR and UV-Vis kinetics were recorded. Prior to the measurements aqueous solutions of AZOII and AZOIII were prepared. The samples were irradiated with a spot curing device (high pressure mercury vapour UV light source) with a power output of 9.25 mWcm^{-2}.

FTIR spectroscopy. Thin layers of azosulphonate were prepared by drop coating of CaF_2 platelets with the sample solutions and evaporation of the solvent. Transmission spectra were recorded in a wavenumber range of 2000–850 cm^{-1}, with emphasis on the Ar-N, -N=N- and -N-S- absorption bands. Also the formation of hydroxyphenyl groups, which could be formed due to the presence of aerial humidity, was investigated.

UV-Vis spectroscopy. 1 mL of the sample solution was filled into a quartz cuvette and diluted with 2.5 mL of deionised water. UV-Vis absorption spectra ranging from 800 to 200

nm wavelength were recorded and changes in the electron density of the aromatic ring system (with emphasis on the π-π* transition) were monitored.[61]

3.3.1.4 Thermolysis

To determine the thermal stability and the decomposition temperature of the prepared azosulphonate salts, thermogravimetric measurements were conducted. Samples were filled into aluminium oxide (Alox) crucibles and heated with a heating rate of 20 Kmin^{-1} using nitrogen as purge gas with a flow rate of 30 mLmin^{-1}.

3.3.2 *Preparation of azosulphonate doped PVA*

As a novel approach to prepare polymeric light sensitive compounds, poly(vinyl alcohol) was doped with different amounts of the obtained and purified azosulphonates. To avoid leaching out of the low molecular components, thin film samples were subjected to heat treatment, which should lead to the formation of ester bonds for AZOIII and crosslinks for AZOII (see Fig. 12).

Table 7:   Composition of PVA-AZO formulations (with regard to the dry matter)

notation	PVA (wt.-%)	AZO II (wt.-%)	AZOIII (wt.-%)
PAII.1	97.5	2.5	
PAII.2	95	5	
PAII.3	92.5	7.5	
PAII.4	90	10	
PAII.5	80	20	
PAIII.1	97.5		2.5
PAIII.2	95		5
PAIII.3	92.5		7.5
PAIII.4	90		10
PAIII.5	80		20

Liquid PVA-AZO samples were prepared by dissolving the calculated amount of azosulphonate in a 5 wt.-% aqueous PVA solution with a pH value of 3 by sonification and stirring at 60 °C. The solutions were cooled to 20 °C and stored in brown glass vials to prevent light induced decomposition of the azosulphonate compounds.

Thin film formation. Thin PA film samples were prepared by the gravity settling method, which has already been descripted at page 27. CaF$_2$ platelets were coated by the drop coating method for further investigation of the coupling reaction by FTIR measurements.

3.3.2.1 Annealing

Thin films and coated CaF$_2$ platelets were subjected to a heat treatment at 100 °C using a circulating air oven applying annealing times of 5, 10, 15, 30, 45 and 60 minutes. FTIR spectra of the cured samples were collected in a wavenumber range of 2000–850 cm^{-1}, with special regard to changes of the C=O vibration at 1750–1670 cm^{-1} and the C-O-C vibration 1200–1100 cm^{-1} to determine the anticipated formation of ester bonds.[137]
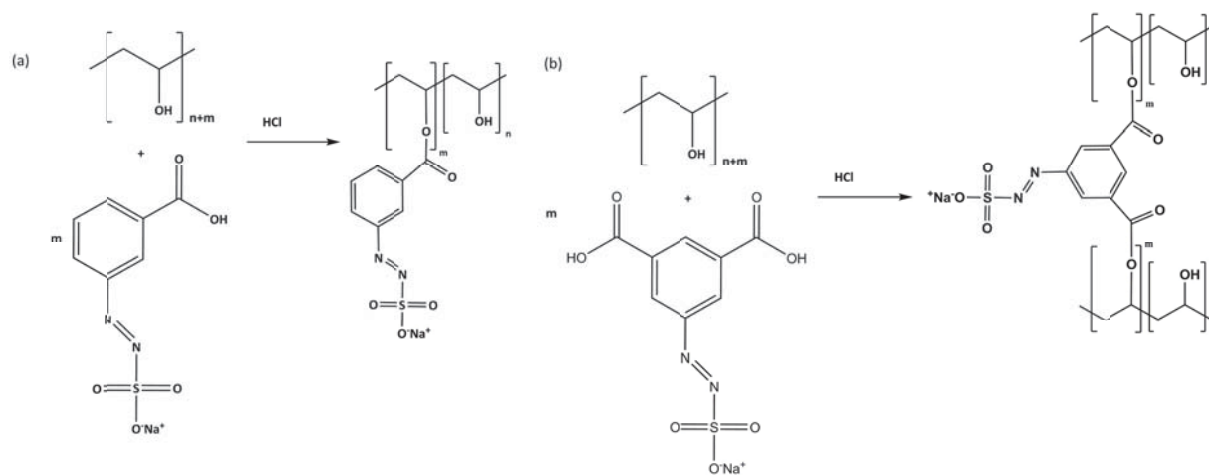
Fig. 12:   Proposed mechanism of coupling reaction of aryl azosulphonates onto PVA via polymer analoguous esterification reactions; (a) coupling of monovalent AZOIII; (b) crosslinking of PVA by coupling of AZOII.

In addition to this, one experiment with ^{13}C NMR measurements was conducted with PAII.5 and PAIII.5 samples. Of each composition non heat treated samples and thin films that had been subjected to 60 minutes of annealing were dissolved / swollen in deuterated water at 85 °C. Subsequently changes of the recorded NMR spectra were monitored.

3.3.2.2 UV exposure of thin films

Illumination of heat treated samples (coated CaF$_2$ platelets) was performed with the spot curing unit (light intensity: 9.25 mWcm^{-2}) and changes in UV-Vis absorption and FTIR transmission spectra were determined.
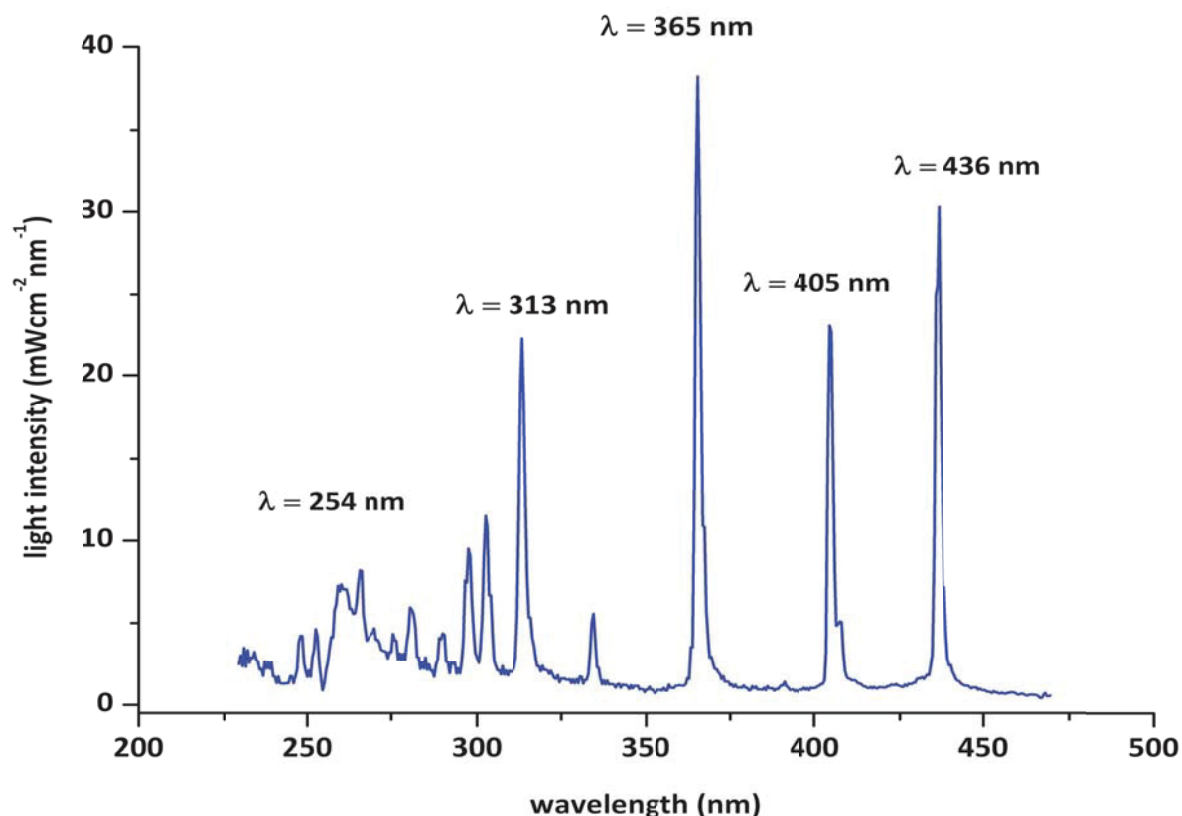
Fig. 13: Emission spectrum of the medium pressure mercury vapour lamp (integrated power output: 740 mWcm^{-2}), that had been applied for irradiation of self-supporting thin films of PVA.

3.3.2.3 Investigation of swelling behaviour

Prior to investigation of the solubility behaviour of the prepared thin films, the samples were subjected to annealing (60 minutes at 100 °C) and were subsequently exposed to UV light (30 and 60 s), see Fig. 13. Afterwards the effects on the swelling behaviour were investigated by the method described on page 28.[127,132]

3.4 FUNCTIONALISATION OF INORGANIC PARTICLES

3.4.1 *Preparation of cation exchanged montmorillonites*

3.4.1.1 Activated montmorillonite

An aqueous Na$^+$-MMT suspension (Cloisite® Na$^+$) containing 10 wt.-% dry matter was diluted with deionised water to reduce its solids content to 5 wt.%. This was carried out by vigorously stirring until a homogenous suspension was attained.

To exchange sodium cations, thus activating the MMT (see Fig. 14), an excess (ratio by weight = 2:1) of concentrated hydrochloric acid solution (with regard to the solid matter of montmorillonite) was added and further stirred at room temperature for at least 24 hours. The activation process was performed in a manner related to published work concerning the preparation of acid activated platy clays, but the direct activation with concentrated mineral acids is a new and convenient approach to obtain activated clays.[74,75,80,112]

Due to acid treatment a swelling of the montmorillonite clay occurred, therefore the suspension had to be further diluted with deionised water to keep it dispersible. Furthermore the acid activation process leads to decomposition of carbonates, impurities and biological contaminants such as algae and fungi and to improved delamination of the platelets, augmenting the accessibility of the interlayer galleries for subsequent modification steps.
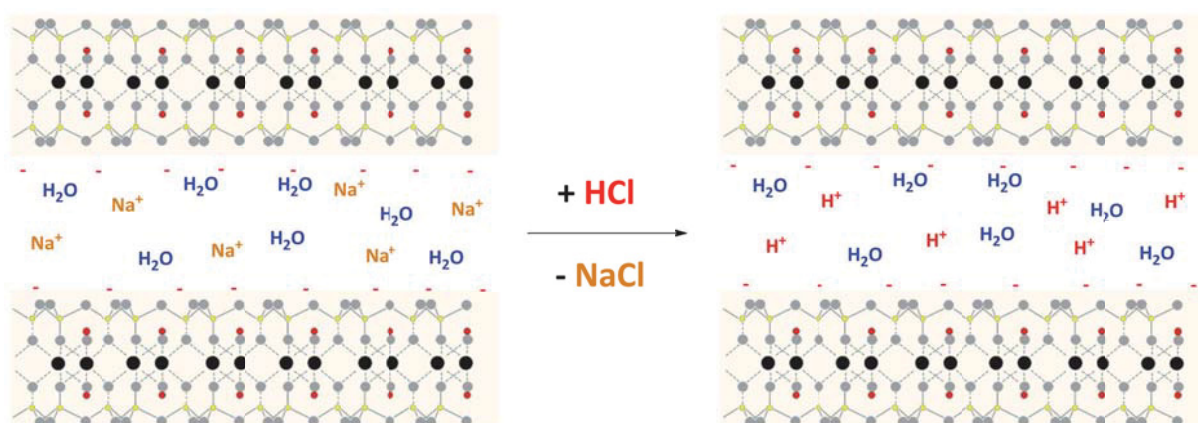
Fig. 14:   Principle of cation exchange reaction of sodium cations by protons due to acid treatment of pristine sodium montmorillonite with hydrochloric acid.

The obtained cation-exchanged H^+-MMT was filtered and rinsed with deionised water to wash off excess hydrochloric acid and NaCl until the rinsing water reached a pH-Value > 4 and no more chloride anions were detected by precipitation using $AgNO_3$.[93] The H^+-MMT was subsequently dispersed in deionised water to give a 10 wt.-% suspension for further characterisation and organic modification steps.

3.4.1.1.1 *Characterisation of H⁺-montmorillonite*

FTIR spectroscopy. Thin layers of activated MMT were cast onto CaF_2 platelets and dried under constant air flow. Transmission spectra in wavelength range of 4000–850 cm^{-1} were recorded with a resolution of 2 cm^{-1}.

EDX spectroscopy. Energy dispersive X-ray spectroscopy proved to be a versatile tool to determine the metal cation exchange. Changes of the sodium K_α line at 1.04 keV were monitored. Limit of detection: 0.1 wt.-% or elements with atomic number < 10.

XRF spectroscopy. X-ray fluorescence spectroscopy on powdered montmorillonite samples was performed to investigate changes of the elemental composition due to the activation step as well as to investigate leaching of the interlayer sodium cations. The measurements were performed at the Department of General, Analytical and Physical Chemistry at the University of Leoben (Leoben, Austria).

MAXS experiments. The activated MMT was dried at 80 °C, ground to a fine power and filled into 1 mm glass capillaries prior to the X-ray scattering measurements. The detector was calibrated with Ag-stearate (d = 48.68 Å) and Cu-K_α (λ =1.54 Å) radiation was employed for exposure times of 900 s. Scattering patterns between q-values of 0.04 < q < 1.06 $Å^{-1}$ were recorded and the d_{001} spacing of the montmorillonite was calculated out of the detected peak values.

Thermogravimetry. TGA measurements of dried and ground MMT powder samples were performed to investigate changes of interlayer water content and acid induced phenomena. A heating rate of 20 $Kmin^{-1}$ was employed and nitrogen was used as purge gas with a flow rate of 30 $mLmin^{-1}$. The samples were heated from 25 to 900 °C and the mass loss was evaluated (wt.-%) with regard to the initial mass.

These methods and the appropriate evaluation of the obtained data have been employed for all metal cation exchanged montmorillonites, except the MAXS measurements, which are more relevant for the investigation on changes of the basal spacing of organo-modified MMTs.

3.4.1.2   Transition metal cation exchange

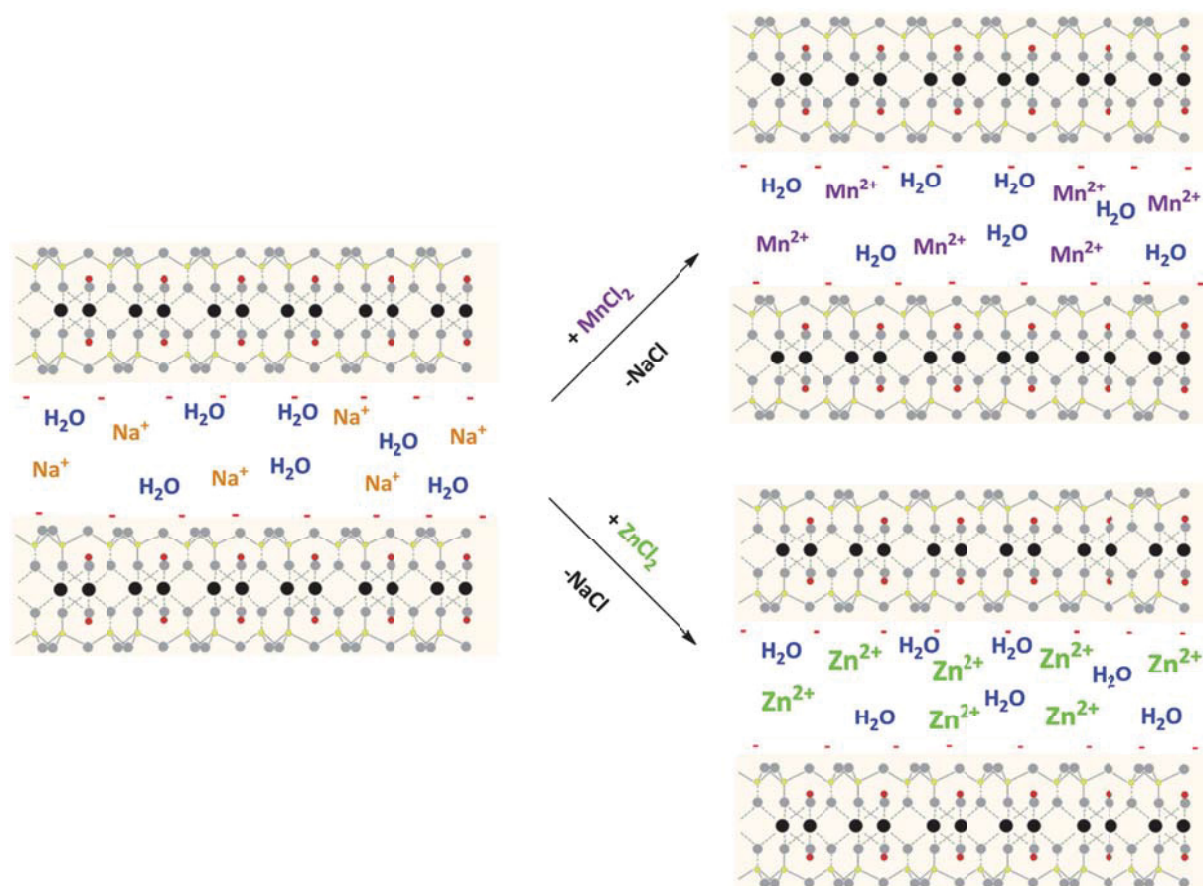*3.4.1.2.1 Preparation and characterisation of Me^{2+}-montmorillonite*

Fig. 15:   Principle of cation exchange of sodium with divalent transition metal cations to give either manganese montmorillonite (Mn^{2+}-MMT) or zinc montmorillonite (Zn^{2+}-MMT).

A highly diluted aqueous sodium montmorillonite suspension (approx. 2 wt.-% solids content) was vigorously stirred with an excess of the particular transition metal salt (either zinc or manganese chloride; ratio by weight = 2:1) for 48 hours at room temperature to facilitate complete exchange of sodium by the transition metal cations.

In a following step the montmorillonite suspensions were filtered through folded filters (MN 615 ¼) and the cation exchange products (sodium chloride) and excess MnCl$_2$ or ZnCl$_2$ were leached out with deionised water. The washing process was repeated, until no more chloride anions were detected by precipitation with AgNO$_3$.[93] In addition to this, the washing of Mn^{2+}-MMT was continued until no more manganese cations were detected by an alkaline precipitation reaction.[138]

The purified montmorillonite suspensions were diluted and stored at room temperature, while a portion of each was dried and ground to a fine powder for EDX spectroscopy measurements to investigate the cation exchange (see page 40).

The obtained montmorillonites may be employed in a novel process as crosslinking aids for XNBR lattices by acting as ion-donor materials. Due to ionic bonding onto the carboxylic moieties of the polymer as well as the presence of polymer-filler interactions, the solvent resistance of such composites should be enhanced. As the active species (Me^{2+}) is bound onto the MMT particle surface, no leaching out occurs; this would be crucial for biomedical applications.

3.4.1.2.2 *Preparation and characterisation of Fe^{3+}-montmorillonite*
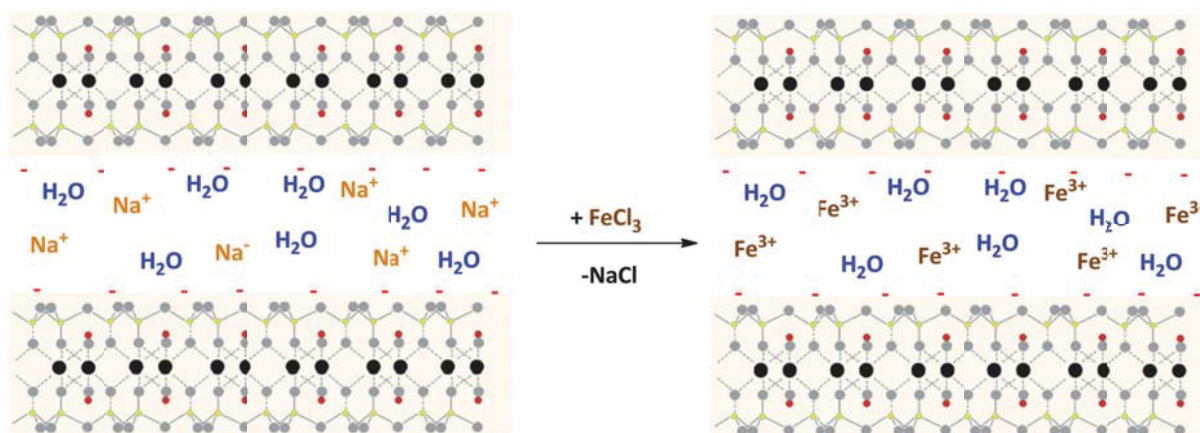
Fig. 16:   Cation exchange of sodium with iron (III) cations.

Cation exchange and purification. An aqueous Cloisite® Na^+ suspension (10 wt.-%) was dispersed with an excess (ratio by weight = 2:1) of 40 wt.-% $FeCl_3$ solution for the duration of 48 hours at room temperature. The resulting slurry was washed with deionised water and filtered to leach out excess iron(III) cations and sodium chloride. The leaching process was continued until no more Fe^{3+} ions could be detected in the rinsing water by the potassium thiocyanate complexation reaction (red colouration). As no precipitate of AgCl by the $AgNO_3$ test was formed, it was assumed, that chlorine anions are also leached out quantitatively.[93]

FTIR / EDX / XRF spectroscopy. Calcium fluoride platelets were coated by the drop coating method and dried under constant air flow. FTIR spectra of Fe^{3+}-MMT in a ranging from 4000 to 850 cm^{-1} were recorded. EDX and XRF measurements were conducted to investigate the cation exchange reactions as well as monitor structural changes of the layered clays.

UV-Vis spectroscopy. To investigate the UV response of the modified montmorillonite, a highly diluted and stable dispersion was prepared and filled into 3.5 mL quartz cuvettes. UV exposure was performed with a spot curing unit, with a UV light intensity of 9.25 mWcm^{-2}. The resulting changes of the absorption at 360 nm were monitored and compared to an aqueous FeCl$_3$ solution.

3.4.1.3 Amino acid intercalation

3.4.1.3.1 *Preparation of organo modified montmorillonites*

An aqueous montmorillonite suspension (either Na$^+$ or H$^+$-MMT) was dispersed in deionised water to reduce the solids content and the pH-value was adjusted to 3 by hydrochloric acid, which is needed to protonate the amino groups of the intercalating agents. This was followed by the addition of the selected amino acid (see Fig. 17a/b/c) resulting in a ratio of modification reagent to clay of 1:1 by weight. The reaction mixture was heated to 80 °C and vigorously stirred for 3 hours at this temperature.
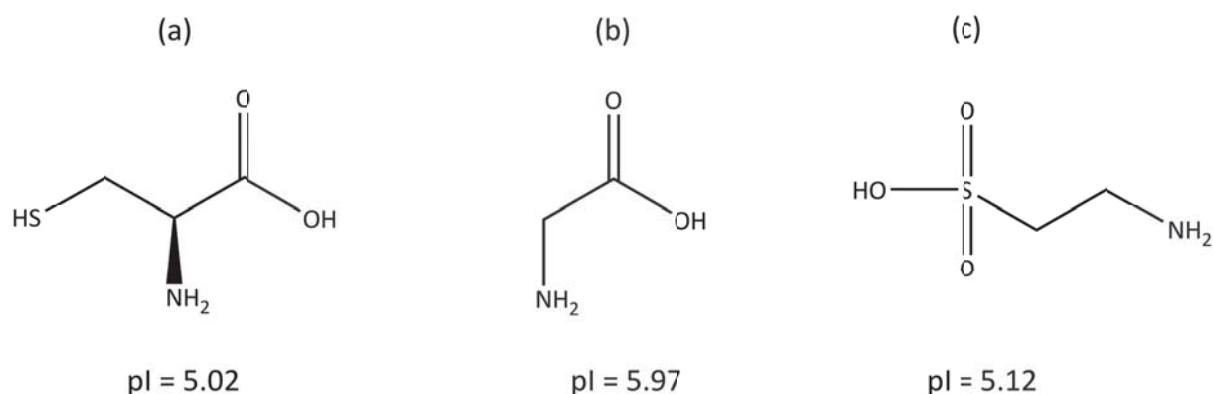
Fig. 17:   Amino acids with their isoelectric points that were utilized for the organic modification of montmorillonite. (a) L-cysteine; (b) glycine; (c) taurine.

After cooling to room temperature (20 °C), the suspensions were filtered and the filtrates were rinsed with deionised water, washing off excess modification reagents and hydrochloric acid, until no organic content was detected in the rinsing water by the means of FTIR spectroscopy. The purified products were dried at room temperature until a constant weight was attained. The terminology of the amino acid-intercalated clays is given in Table 8 and Fig. 19.
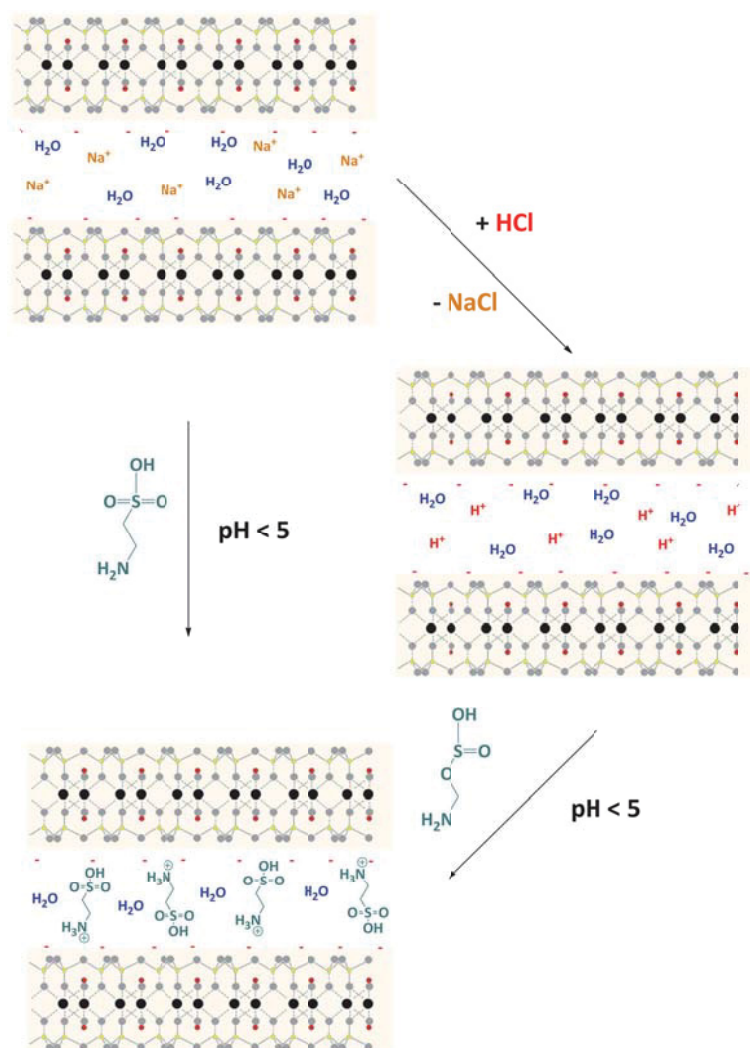
Fig. 18: Schematic representation of the functionalisation steps of montmorillonites by means of cation exchange using hydrochloric acid and taurine as modification reagents.

It has to be pointed out, that the organic modification of montmorillonites with taurine is a novel concept to immobilise sulphonic acid moieties, which may be applied as proton donors for catalytic purpose or as ion exchange materials. Furthermore the organic modification of H^+-MMT should lead to intercalation of higher quantities of amino acid compared to the one step method using Na^+-MMT (see Fig. 18).
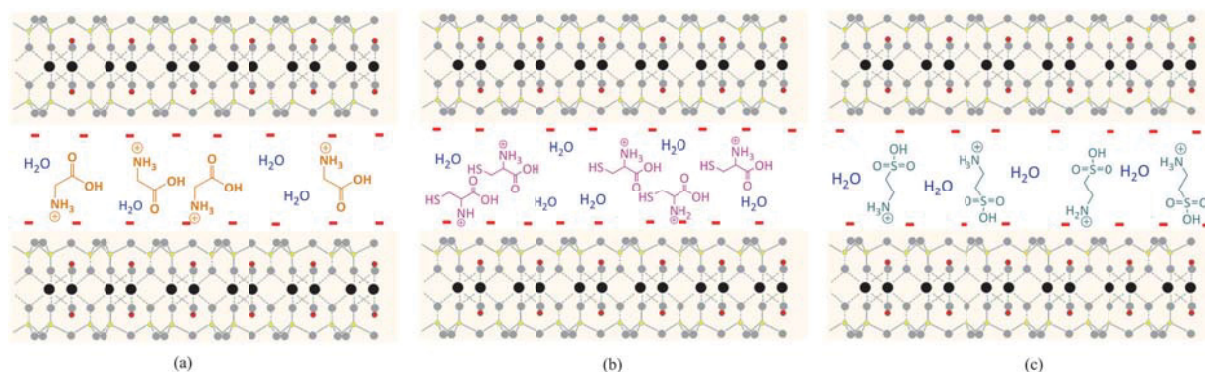
Fig. 19: Schematic representation of the interlayer galleries of amino acid intercalated montmorillonites bearing the protonated intercalates on the negative charged platelet surface: (a) glycine; (b) L-cysteine; (c) taurine.

Table 8: Notation of organo modified montmorillonite clays

sample	modification	sample	modification
Na$^+$-MMT	pristine	H$^+$-MMT	pristine
Na$^+$-MMT_C	L-cysteine	H$^+$-MMT_C	L-cysteine
Na$^+$-MMT_G	glycine	H$^+$-MMT_G	glycine
Na$^+$-MMT_T	taurine	H$^+$-MMT_T	taurine

3.4.1.3.2 *Characterisation*

FTIR spectroscopy. Thin layers of modified MMT were cast onto CaF$_2$ platelets and dried under constant air flow. Transmission spectra in wavelength range of 2000 to 850 cm^{-1} were recorded with a resolution of 2 cm^{-1}.

Thermogravimetry. TGA measurements of dried and ground MMT powder samples to determine the intercalated organic content were conducted in accordance to the noted parameters on page 40.

MAXS experiments. Organo modified H$^+$-MMTs were dried at 80 °C, ground to a fine power and filled into 1 mm glass capillaries prior to the X-ray scattering measurements. The principle and the experimental setup were described on page 40 and Table 5.

3.4.2 *Preparation of surface functionalised particles*

The immobilisation of photolabile aryl azosulphonate groups onto surfaces bearing hydroxyl groups would give the possibility to prepare UV reactive particles with a tuneable

decomposition mechanism depending on the chemical environment (see Fig. 2).[57,61] This novel class of photolabile particles may find use as radical initiators, photo acid generators or blowing agents, as nitrogen gas is generated upon decomposition. As the reactive sites are attached to the particle surface, leaching of the azo compound out of polymer-particle composite materials can be prevented.

3.4.2.1 Surface silanisation

In a first step fumed silica particles (Wacker HDK® N20), activated montmorillonite powder and silicon dioxide nanoparticles were dried and subsequently dispersed in ethanol by means of high speed dispersion tools to attain a homogenous distribution and disintegration of agglomerates. This was followed by sonification and addition of 3-(m-aminophenoxy) propyltrimethoxysilane. The resulting reaction mixture was stirred with a magnetic stirrer for 24 hours at RT to allow complete conversion of the alkoxysilane (see Fig. 20). Prior to the diazotisation reactions the surface modified particles were subjected to a purification step by osmosis in ethanol (48 hours, RT) to leach out non-conversed silane.
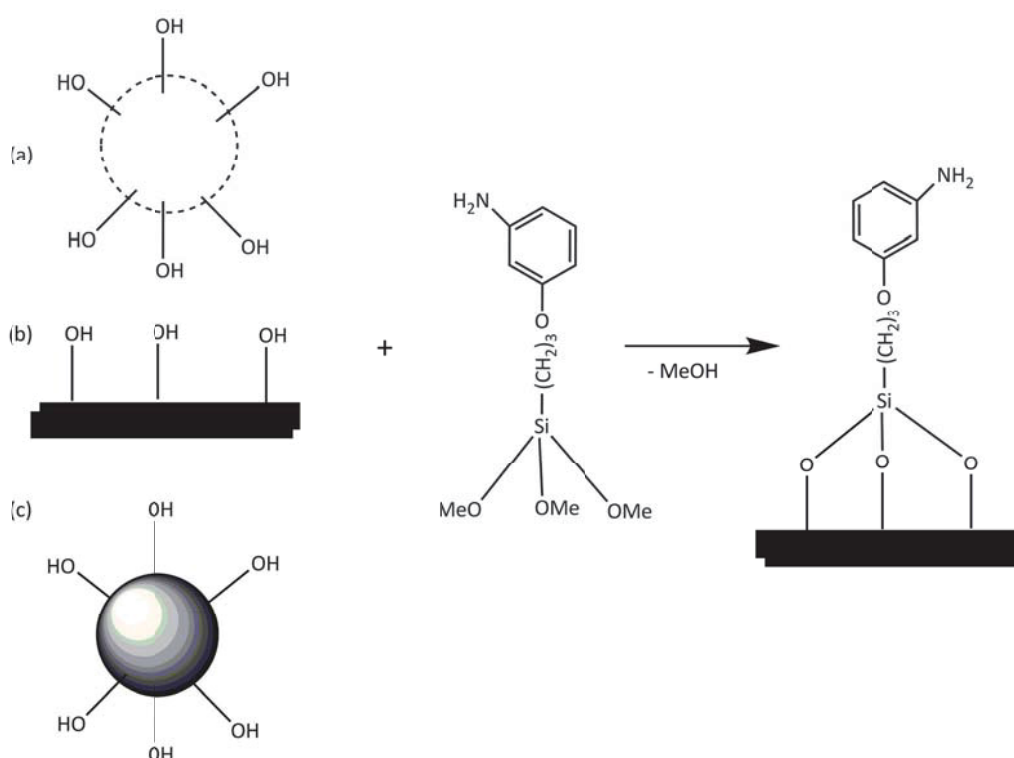
Fig. 20: Surface modification step for the preparation of UV reactive particles by immobilisation of 3-(m-aminophenoxy) propyltrimethoxysilane onto the particle surface. (a) fumed silica; (b) activated montmorillonite; (c) SiO_2 nanoparticles. The structural representation has been simplified for clarity.

In a further step the purified particle dispersions were diluted with deionised water and residual ethanol was evaporated at 185 mbar at 55 °C. After filling the dispersions into round bottom flasks, they were cooled to a temperature below 5 °C.

Table 9: Notation of surface functionalised particles; ratio of particle/silane;

notation	particle type	particle/silane (weight ratio)
P1	fumed silica	1:1
P2	fumed silica	1:2
P3	fumed silica	1:4
MMTa	H^+-MMT (filtrate 0.45 µm - Millipore)	1:1
MMTb	H^+-MMT (fine fraction)	1:1
MMTc	H^+-MMT (coarse fraction)	1:1
MMTd	H^+-MMT (no filtration)	1:1
NP	SiO_2 nanoparticles (10-20 nm)	1:1

Several montmorillonite fractions were prepared by different separation techniques to obtain a variation of particle sizes (MMTa-c) as well the original fraction (MMTd).

3.4.2.2   Diazotisation of particle surfaces

The modified particles (200 mmol -NH_2 groups) were acidified to a pH of 2 and an aqueous sodium nitrite solution (200 mmol) was added dropwise, while the reaction mixture was cooled to avoid decomposition of the thermally unstable diazonium stage (see Fig. 21b).
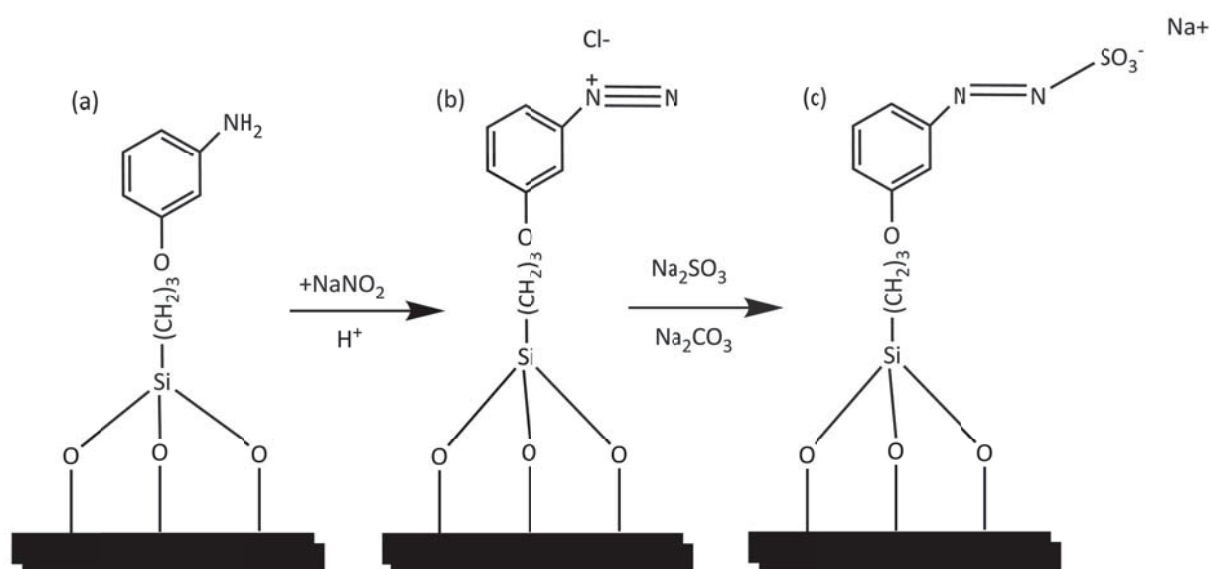
Fig. 21:   Synthesis of UV reactive particles; (a) surface modified particle(see Fig. 20); (b) diazotisation; (c) sulphonated photolabile particle.

In the next step, the diazotised particles were slowly poured into 50 mL of a pre-chilled sodium sulphite / sodium carbonate solution (200 mmol / 240 mmol) to perform sulphonation combined with neutralisation of the hydrochloric acid. After decomposition of sodium carbonate stopped, the orange coloured reaction mixture was filled into molecular porous membrane tubing and subjected to one final osmosis step in deionised water for 72 hours.

3.4.2.3   Characterisation

Thermogravimetry. TGA measurements of dried particle samples were conducted to determine the amount of azosulphonate groups that are immobilised on the surface. The analysis was performed in accordance to the parameters on page 40.

FTIR spectroscopy. CaF_2 platelets were coated with particle dispersion by the drop coating method and dried under constant air flow at RT. FTIR transmission spectra were collected in a wavenumber range of 2000–850 cm^{-1}. Furthermore photolysis kinetics were recorded by irradiation of the samples with a spot curing emitter, using an intensity of 9.25 Wcm^{-2}.

UV-Vis spectroscopy. Aqueous particle dispersions were filled into 3.5 mL quartz cuvettes and illuminated with UV light from the spot curing device with an intensity of 9.25 Wcm^{-2} and changes of the UV-Vis absorption spectra (λ = 800–200 nm) with emphasis on the aromatic ring (200–300 nm) were surveyed.

3.5   ORGANIC-INORGANIC COMPOSITE MATERIALS

3.5.1   *PVA-Fe³⁺-MMT nanocomposites*

3.5.1.1   Sample preparation

An aqueous PVA solution with a solids content of 5 wt.-% was stirred at room temperature with the appropriate amounts of Fe^{3+}-MMT suspensions to obtain the noted compositions (see Table 10). After 24 hours the obtained dispersions were subjected ultrasound treatment and were dispersed with an IKA UltraTurrax dispersing unit with rotation speeds of 20 000 rpm. One advantage of the employment of the high water content was that no local overheating of the composite dispersion can take place, hence the water acts as coolant.

Table 10: PVA-Fe^{3+}-MMT dispersion composition

sample	PVA* (wt.-%)	Fe^{3+}-MMT* (wt.-%)
PVA-Fe^{3+}-MMT_1	80	20
PVA-Fe^{3+}-MMT_2	70	30
PVA-Fe^{3+}-MMT_3	60	40
PVA-Fe^{3+}-MMT_4	50	50

*) with regard to dry matter

Thin composite films for SEM measurements, UV exposure experiments and swelling tests were prepared by casting defined amounts of the prepared dispersions into polystyrene petri dishes.

3.5.1.2 Investigation of UV reactivity

UV-Vis spectroscopy. To investigate the UV response of Fe(III) and the photoreduction to Fe(II), 1 mL of liquid PVA-Fe^{3+}-MMT dispersion was filled into quartz cuvettes (3.5 mL) and diluted with 2.5 mL of deionised water. UV-Vis absorption spectra in a wavelength range from 650 to 250 nm were recorded with medium scanning speed.[9,47] Additionally the samples were irradiated with a spot curing device (high pressure mercury vapour UV light source) with a power of 9.25 mWcm^{-2} and irradiation times up to 1500 s (see Fig. 8a).[11]
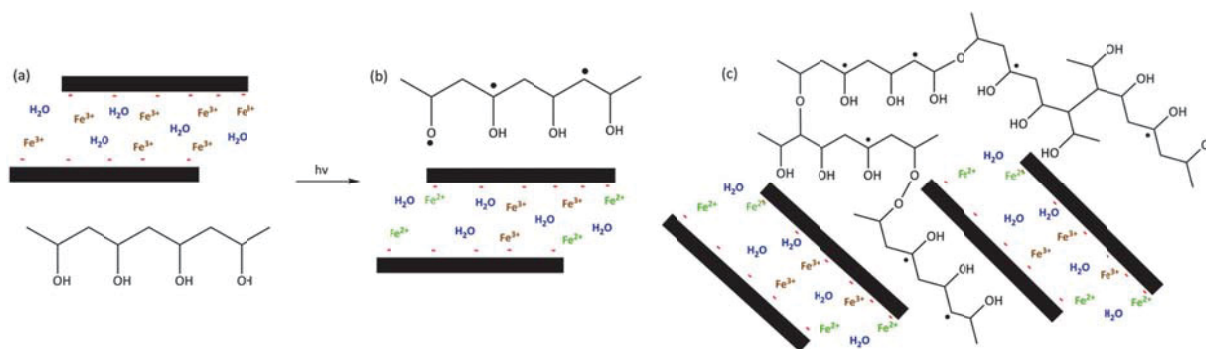
Fig. 22: Proposed mechanism of crosslinking of a PVA-Fe^{3+}-MMT composite (a); photoreduction of Fe(III) to Fe(II) and radical generation on the PVA matrix backbone (b); recombination and crosslink formation (c).[9,11]

Refractometry. Changes of the refractive index at the sodium D-line (λ = 589 nm) were determined by casting liquid dispersion samples directly onto the prism of the Abbe refractometer. After drying the films were irradiated with the spot curing device (intensity 9.25 mWcm^{-2}). The measurements were performed triplicate.

UV exposure. Thin films were irradiated with a Hg vapour medium pressure lamp with a light intensity of 530 mWcm^{-2} for 0, 30, 60, 90 and 120 s resulting in a radiation dose of 70 Jcm^{-2}.

3.5.1.3   Nanocomposite characterisation

3.5.1.3.1 *Filler particle distribution*

To determine the filler particle distribution, thin films were cryogenically broken using liquid nitrogen. SEM micrographs of the fracture surface and of the top view were recorded using an acceleration voltage of 20 kV and a backscatter electron detector to visualise material contrast.

3.5.1.3.2 *Swelling behaviour*

The equilibrium swelling behaviour was determined in accordance to the described method. Furthermore, the testing temperature of irradiated samples was elevated stepwise (23; 40; 60; 80 °C). The stability of the samples during contact with the aqueous phase was monitored.

3.5.1.3.3 *Photolithographic patterning*

Thin films were illuminated with an intensity of 740 mWcm^{-2} (Hg vapour medium pressure lamp; see Fig. 13) through a quartz / chromium mask bearing 100 µm patterns that was directly placed on the substrates (radiation dose of 90 Jcm^{-2}). After illumination and development by immersion in deionised water at 20 °C, the samples were observed under polarised incident light and with phase contrast optics

3.5.2   *Composite materials comprising PVA and organo modified montmorillonite*

3.5.2.1   **Sample preparation**

Although the organic modification of montmorillonite is well described, up to now, the application of amino acid intercalated MMTs as well as of the novel activated and organomodified MMTs as additives for poly(vinyl alcohol) has not been described in the literature.

A PVA stock solution with a solids content of 5 wt.-% was acidified to a pH of 3 by the addition of hydrochloric acid. Activated and organo modified montmorillonites, which were prepared in accordance to the described methods (see Table 8), were dispersed by means of high speed dispersion tools in the PVA solution to obtain composite dispersions with 5 and 10 wt.-% montmorillonite content.

Table 11: Sample notation for PVA montmorillonite composite samples. MMT contents of 5 and 10 wt.-% (with regard to the dry matter) are dispersed into PVA

sample	modification	sample	modification
PVA_Na$^+$-MMT	pristine	PVA_H$^+$-MMT	acid activated
PVA_Na$^+$-MMT_C	L-cysteine	PVA_H$^+$-MMT_C	L-cysteine
PVA_Na$^+$-MMT_G	glycine	PVA_H$^+$-MMT_G	glycine
PVA_Na$^+$-MMT_T	taurine	PVA_H$^+$-MMT_T	taurine

Self-supporting films for DSC and SEM measurements as well as the investigation of the swelling behaviour were obtained by adding 10 g of the prepared dispersions onto PS petri dishes with a diameter of 85 mm, followed by drying under constant air flow. CaF$_2$ platelets were coated by the drop coating method for FTIR measurements.

3.5.2.2 Composite characterisation

Determination of thermal properties. About 10 mg of PVA-MMT composite were deposited into an aluminium oxide ceramics crucible prior to the measurement. A four-step heating program was applied using a heating rate of 20 °Cmin^{-1}, starting from 25 °C to 250 °C, followed by cooling to 25 °C and repeated heating to 250 °C and cooling to 25 °C. Changes of the melting curve due to the utilisation of modified montmorillonites were observed.

SEM measurements. Thin composite samples were analysed by SEM measurements to determine particle distribution. To obtain conductivity a thin layer of gold is deposited on the sample surface.

Thermal treatment. The film samples and the coated CaF$_2$ platelets were subjected to thermal treatment to induce crosslinking reactions with the MMT surface and the organic intercalants. Annealing was performed at 100 °C, while treatment times of 5, 10, 15, 25 and 40 minutes were employed.
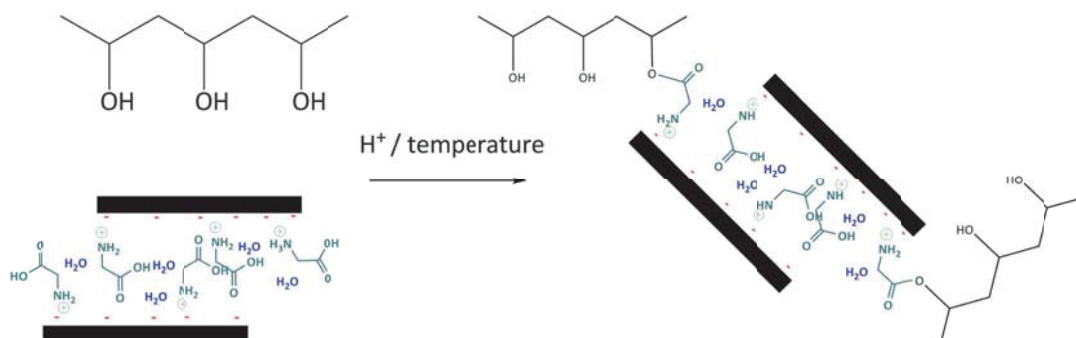
Fig. 23:   Proposed mechanism of covalent bonding of organo modified montmorillonites onto a PVA matrix backbone by thermally initiated esterification reactions; e.g. glycine intercalated MMT.

FTIR measurements. FTIR transmission spectra of thin composite layers that were deposited onto CaF_2 platelets are recorded, with special emphasis on changes of the carbonyl absorption due to heat treatment.

Swelling behaviour. Sol-gel analysis (see page 28) is performed to investigate changes of the solubility behaviour due to annealing at 100 °C.

3.5.3   *Use of UV reactive particles for the crosslinking of PVA*

3.5.3.1   Sample preparation

A PVA stock solution with a 5 wt.-% solids content was acidified to a pH of 3 by the addition of hydrochloric acid. UV reactive surface modified particles bearing azosulphonate groups (preparation and characterisation steps see page 45) were added and dispersed by alternating magnetic stirring and ultrasound treatment. Dispersion compositions and notations are listed in Table 12.

Thin films were prepared by casting the dispersions into polystyrene petri dishes and evaporating the water under constant air flow. CaF_2 platelets were coated by drop coating.

Table 12: Notation and composition of UV reactive PVA azosulphonate particle systems

notation	particle type (Table 9)	PVA (wt.-%)*	Particle (wt.-%)*
PP1.1	P1	97.5	2.5
PP1.2	P1	95	5
PP2.1	P2	97.5	2.5
PP2.2	P2	95	5
PP3.1	P3	97.5	2.5
PP3.2	P3	95	5
PMMTb1	MMTb	97.5	2.5
PMMTb2	MMTb	95	5
PMMTc1	MMTc	97.5	2.5
PMMTc2	MMTc	95	5
PMMTd1	MMTd	97.5	2.5
PMMTd2	MMTc	95	5
PNP1	NP	97.5	2.5
PNP2	NP	95	5

*) with regard to the dry matter

3.5.3.2 Determination of UV response

UV-Vis absorption spectra of diluted aqueous PVA-particle dispersions were collected as well as FTIR transmission spectra of coated CaF_2 platelets. The samples were irradiated with a spot curing device at a light intensity of 9.25 Wcm^{-2}.

3.5.3.3 Composite characterisation

To determine particle size and observe their distribution in the PVA matrix, SEM micrographs of thin films were recorded using a backscatter electron detector. Illumination experiments using a Light Hammer 6 conveyor belt irradiation device with an emission output of 740 $mWcm^{-2}$ for 30 and 60 s respectively. Changes in the swelling behaviour due to UV exposure were investigated in accordance to the described method (see page 28).

Furthermore the influence of thermal treatment and subsequent UV exposure was investigated. The samples were subjected to annealing at 100 °C with treatment times of 5, 10, 20, 30 and 60 minutes. Subsequent UV exposure was performed for samples that were treated 60 min with radiation doses of 22.2 and 44.4 Jcm^{-2}.

3.5.4   *Vinyl-modified particles for e-beam crosslinking of PVA*

3.5.4.1   Sample preparation

Silicon particles bearing reactive vinyl moieties on their surface (Actisil® VM56 from Hoffmann Minerals) were dispersed in a PVA stock solution (5 wt.-% solids content) by alternating magnetic stirring and ultrasound treatment (composition and sample notation see Table 13).

Table 13: Composition of samples for e-beam exposure

notation	PVA (wt.-%)*	Actisil® VM56 (wt.-%)*
VM1	97.5	2.5
VM2	95	5
VM3	92.5	7.5
VM4	90	10

*) with regard to the dry matter

Thin films were prepared by the gravity settling method, by pouring 10 g of the dispersion into PS petri dishes with a diameter of 85 mm. The samples were dried under constant air flow at room temperature for 24 hours and sealed in polyethylene zip lock sample bags. E-beam exposure was performed at the Greiner Mediscan Plant (Kremsmünster, Austria) with energy dosages of 100, 150, 200, 250 and 300 kGy.

3.5.4.2   Effects of e-beam exposure

ATR-FTIR spectroscopy of the samples was performed to investigate the depletion of the C=C double bond vibration at 1640 cm^{-1} and 813 cm^{-1} which should occur during exposure with ionising radiation (see Fig. 24).[137]
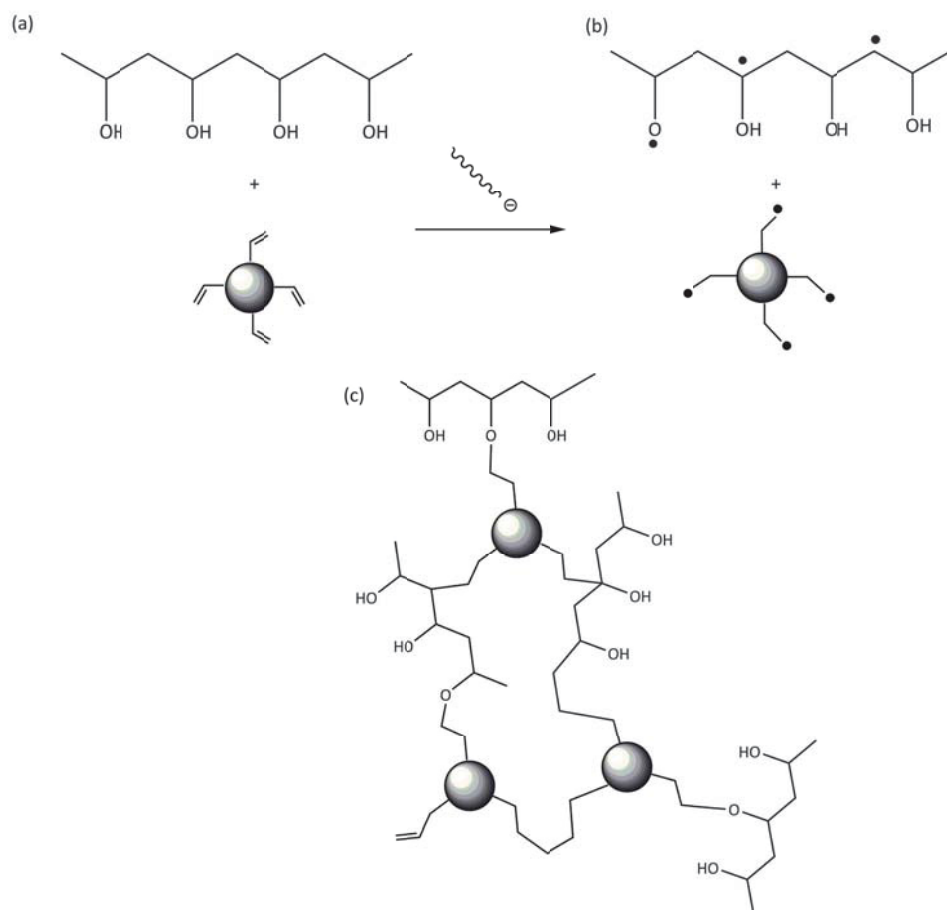
Fig. 24:   Proposed crosslinking mechanism of (a) PVA and particles with immobilised vinyl moieties on their surface; radical generation by e-beam exposure (b); statistic recombination of radicals leads to crosslinking and covalent bonding of particles on the PVA backbone (c).

Also the equilibrium swelling behaviour was investigated at room temperature in accordance to the described method.

3.5.5   *Improvement of solvent resistance of XNBR*

3.5.5.1   Sample preparation

Thin XNBR films comprising crosslinking chemicals and modified montmorillonites were prepared by coagulation of an aqueous XNBR latex dispersion onto porcelain formers, that were dipped (30 s) into a coagulation bath (60 °C) containing chalk, calcium salts and tensides (see Fig. 25). For subsequent UV crosslinking using a Ga-doped medium pressure mercury vapour lamp utilizing the thiol-ene reaction, 1 phr of THIOCURE® ETTMP 1300 and a photoinitiator were added to the latex dispersion.[89] The coagulation step is followed by drying of the porcelain formers at 120 °C for 15 minutes.

Fig. 25:   Porcelain former that is used for thin XNBR film formation by coagulation.

Three different methods for crosslinking of XNBR latex were employed. The first consisted of conventional ionic crosslinking of XNBR using ZnO as Zn^{2+} ion donor (see Fig. 26.I). The second was ionic crosslinking with ZnO, followed by dosing of cation exchanged Zn^{2+}-montmorillonite as passive filler material (Fig. 26.II). The third method implied ionic crosslinking the means of cation exchanged Zn^{2+}/Mn^{2+}-MMTs (Fig. 26.III).
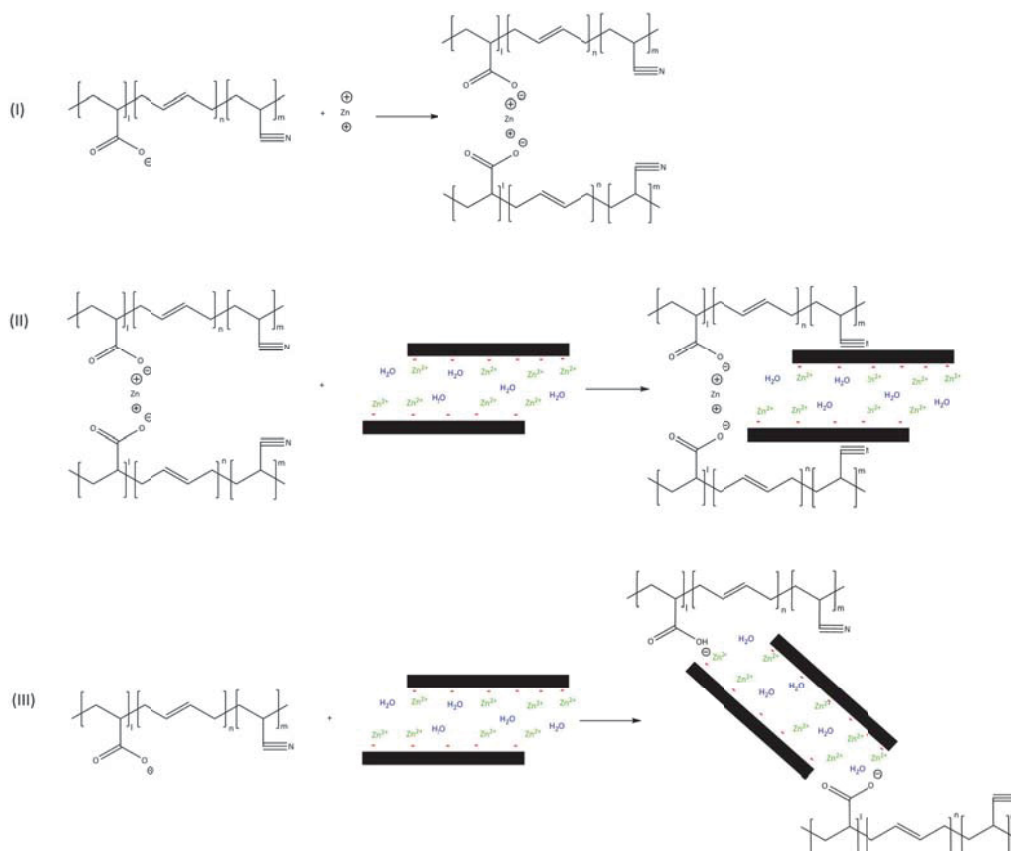
Fig. 26:   Mechanisms of crosslinking XNBR latex; (I) conventional crosslinking with Zn^{2+} ions (reference method); (II) ZnO crosslinking, with modified MMT as passive filler; (III) Zn^{2+}-MMT as crosslinking agent.

XNBR films that were prepared in accordance to method III (comprising 2 wt.-% of MMT) were crosslinked using a Ga-doped medium pressure mercury vapour lamp and exposure times to reach the noted radiation doses (see Fig. 27). This should lead to improved solvent resistance of the prepared samples.

Table 14: Notation of prepared XNBR samples in accordance to different methods of crosslinking. Composite samples comprising manganese cation exchanged montmorillonite are solely prepared in accordance to method III.

method	sample notation	UV irradiation
I	ZnO	
II	ZnO (5 wt.-% Zn^{2+}-MMT)	
II	ZnO (10 wt.-% Zn^{2+}-MMT)	
III	2 wt.-% Zn^{2+}-MMT	yes
	7 wt.-% Zn^{2+}-MMT	no
	2 wt.-% Mn^{2+}-MMT	yes
	5 wt.-%Mn^{2+}-MMT	yes
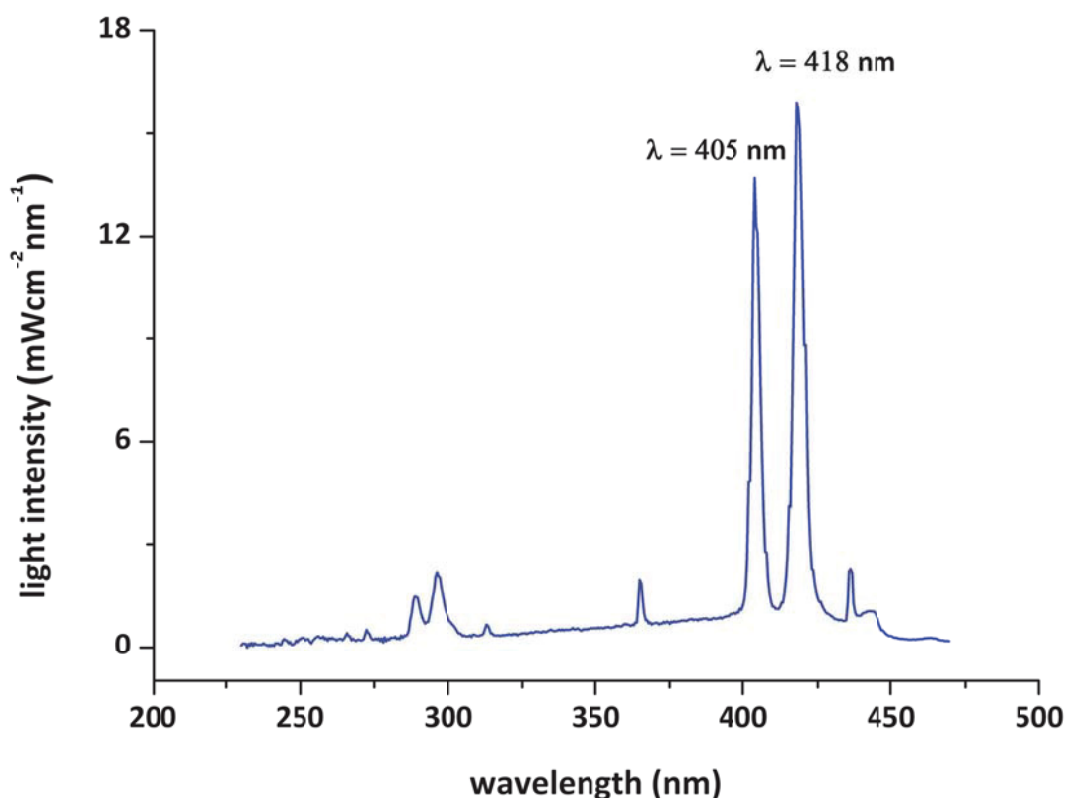
Fig. 27: Emission spectrum of the employed Ga-doped medium pressure mercury vapour lamp. UV radiation doses of 8.44; 10.37 and 12.66 Jcm^{-2} were administered to XNBR films that were prepared in accordance to method III (see Fig. 26 and Table 14).

3.5.5.2 Determination of mechanical properties

The obtained samples were characterised by tensile testing in accordance to EN 455-2:2009+A1:2011 using a Zwick Tensile tester Z010 (Herefordshire; United Kingdom) with testing speeds of 500 mmmin^{-1}. The Young's modulus (E_t), the stress (σ_B) and the strain at break (ε_B) were determined and compared to the ZnO crosslinked reference material [139]

3.5.5.3 Investigation of solvent resistance

Swelling resistance against crude oil was determined at room temperature in a similar manner to the described method at page 28. In addition to this, changes of equilibrium swelling of UV irradiated samples were determined in chloroform.[89,127,134]

V.   RESULTS AND DISCUSSION

1. NEAT PVA – REFERENCE MATERIAL

1.1   DETERMINATION OF STRUCTURAL PARAMETERS

The determination of the molar mass distribution of neat poly(vinyl alcohol) reveals a high M_w of 130 800 gmol^{-1}, which strongly affects the mechanical properties such as tensile strength as well as the solvent stability and thermal properties.[16] Given that and a M_n of 98 200 gmol^{-1}, a PDI of 1.32 is calculated.[140] Furthermore the anticipated narrow distribution is found by SEC (see Fig. 28).
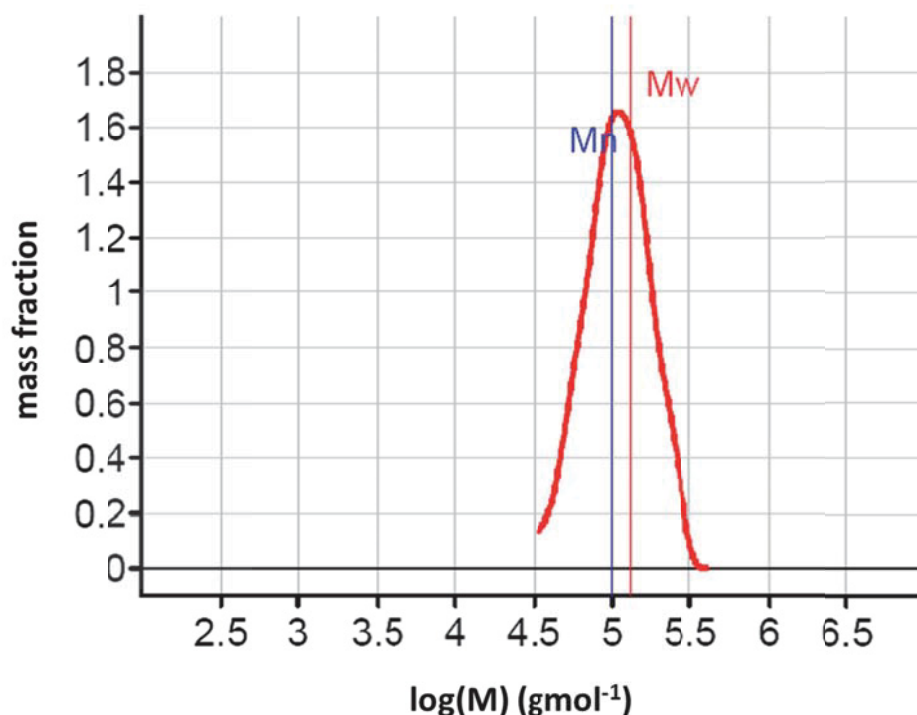
Fig. 28:   Molar mass distribution of neat Elvanol® 90-50 (PVA), which was determined by SEC with a highly purified aqueous sodium chloride solution (0.05 M NaCl) as eluent.

^{1}H and ^{13}C NMR spectroscopy was performed on PVA samples that were dissolved in deuterated water (D_2O) with focus on the detection of residual vinyl acetate groups to determine the degree of hydrolysis.
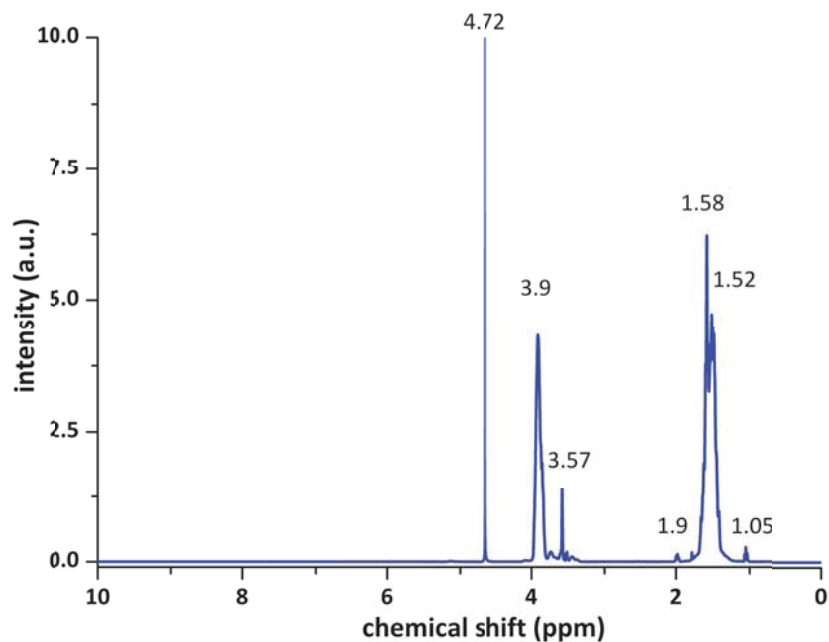
Fig. 29: ^{1}H NMR spectrum of neat PVA to determine the degree of hydrolysis. The sharp peak at 4.72 ppm originates from deuterated water.

The ^{1}H NMR spectrum in Fig. 29 displays the hydrogen atoms of the polymer backbone. The chemical shift at 3.9 ppm can be attributed to the -CHO- units of the PVA, whereas the broad peak at 1.58 is assigned to the $-CH_2-$ units of the main chain.[137] An additional peak at 3.57 ppm can be assigned to the $-CH_3$ end groups of the polymer. The weak signal at 1.9 ppm is caused by $-CH_3$ groups of residual vinyl acetate units, resulting in a peak area value of 0.0025. This leads to the conclusion that the polymer is almost fully hydrolysed with a degree of hydrolysis higher than 99 mol%.[15]
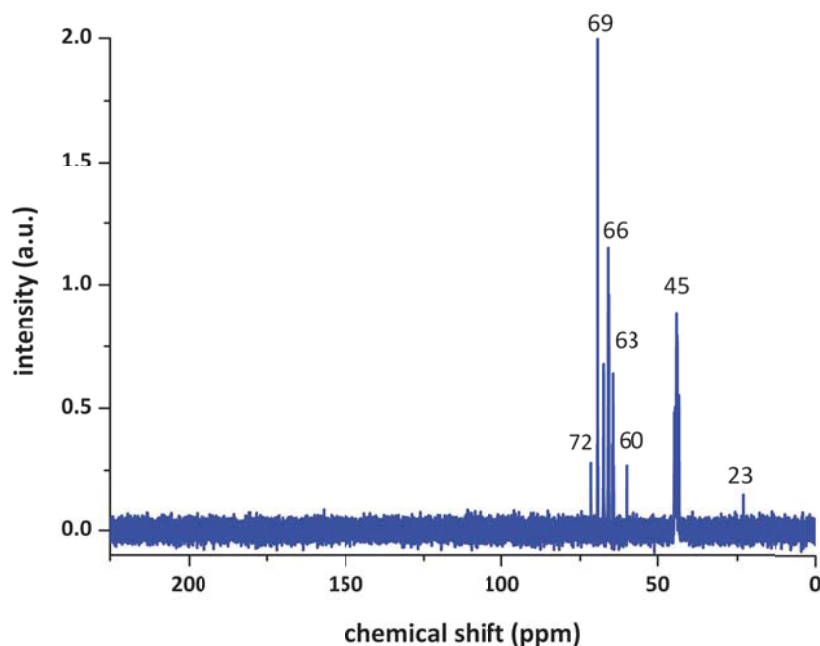
Fig. 30: ^{13}C NMR spectrum of neat PVA, dissolved in D_2O.

The ^{13}C NMR spectrum of the neat polymer displays the -CHO- and the -CH2- groups at chemical shifts of 72 to 60 ppm and 45 ppm. No acetate units are detected, which would give a carbonyl signal at a chemical shift of 170 ppm, but additionally a faint signal at 23 ppm is found, which is caused the -CH$_3$ end groups.[15,137]

The obtained results lead to the conclusion that the neat PVA is fully hydrolysed with a very high molar mass and a narrow molar mass distribution (MMD). These structural parameters have a strong impact on properties such as crystallinity, solvent resistance, gas barrier and mechanical properties. Also the solubility in water is affected, hence the polymer starts dissolving at temperatures higher than 80 °C.[15,141,142]

1.2   OPTICAL METHODS

The FTIR transmission spectrum of a thin film of neat PVA, which had been coated onto CaF_2 platelets, is depicted in Fig. 31. Besides strong -OH bending vibrations, hydrogen bonding between the polymer chain occurs, which leads to a strong and broad peak with a maximum at 3350 cm^{-1}.[137,143] At a wavenumber of 2940 cm^{-1} the -CH$_2$ valence vibration of the PVA backbone contributes to the absorption of IR.

The very faint absorption in the carbonyl region at wavenumbers ranging from 1750 to 1690 cm^{-1} can be assigned to residual vinyl acetate units. However the content of carbonyl groups is very low.[137,144]
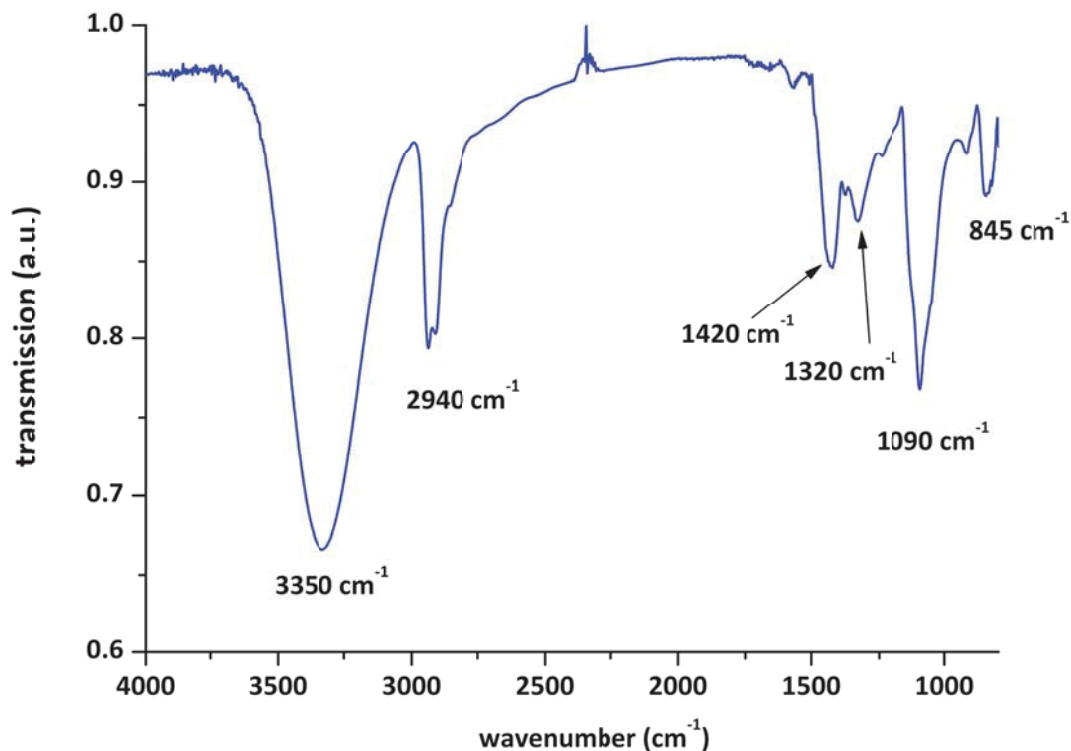
Fig. 31:   FTIR transmission spectrum of a thin PVA film coated onto CaF_2.

In the fingerprint area, the -CH deformation vibration of the CHOH units of the polymer contribute to the peak at 1420 cm^{-1}, while the absorption at 1320 cm^{-1} is a result of the -OH deformation vibration. The peak at 1090 cm^{-1} can be assigned to the -C-O- valence vibration and the absorption band at 845 is a result of the -C-C- stretching.[137,143–146]
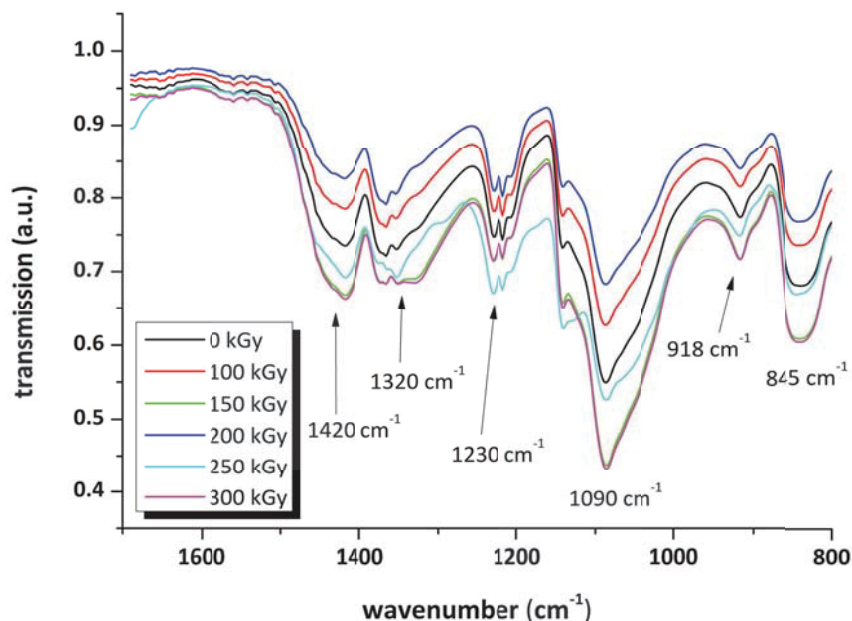
Fig. 32:   Attenuated total reflection (ATR) FTIR spectrum of e-beam exposed PVA films

As e-beam exposure is performed on self-supporting thin films at an external facility, ATR-FTIR spectra are collected instead of transmission spectra of coated CaF_2 platelets. Neat PVA exhibits no significant changes in the FTIR spectrum as a result of exposure to ionising irradiation (Fig. 32). The formation of the small shoulder at a wavenumber of 1140 cm^{-1}, at an exposure dose of 250 kGy may be contributed by changes of the C-O valence vibration, as a result of oxidation or statistic recombination of radicals (compare Fig. 7).[137]
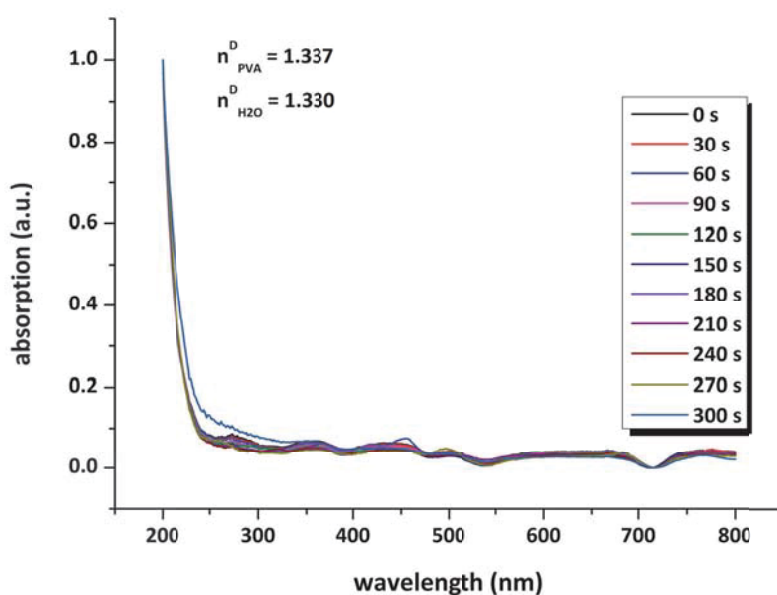
Fig. 33:   UV-Vis spectrum of neat PVA solution upon exposure with an EXFO spot curing emitter with a power output of 9.25 Wcm^{-2}. The refractive indices of PVA and H_2O at the sodium D-Line are plotted as well.

Pristine PVA does not exhibit a significant optical absorption. The samples are transparent and show no turbidity. However, slight absorption bands at 275 nm and 350 nm occur, that can be assigned to residual carbonyl groups and therefore are caused by the π-π* and the n-π* electronic transitions of the chromophores.[42,147,148]

1.3 THERMAL ANALYSIS

Differential scanning calorimetry (DSC) measurements were conducted to determine the melting temperature of the neat polymer, which is influenced by the degree of hydrolysis. In a temperature range of 80 to 170 °C the evaporation of intermolecular water takes place during the first heating cycle, whereas during the second heating step no changes in this temperature range are detected. In both cycles a melting temperature of 230 °C is determined, which is - according to published work - related to fully hydrolysed poly(vinyl alcohol).[16,127,145,149]
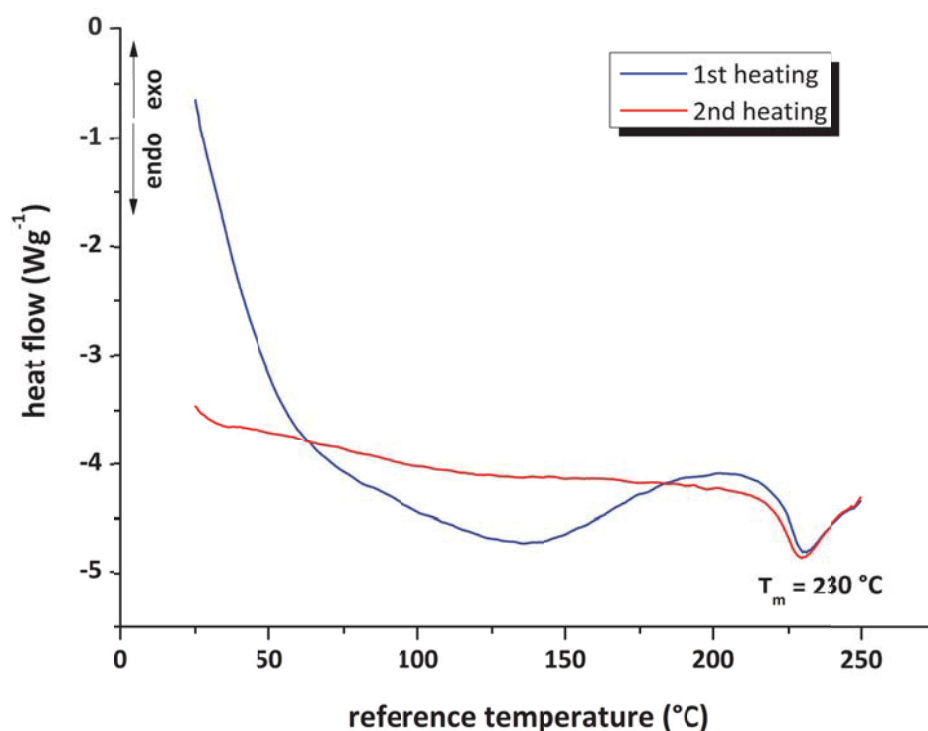
Fig. 34: DSC curves of neat PVA; heating rate 20 Kmin[-1]; purge gas: nitrogen.

1.4 SOLUBILITY

The influence of heat treatment (or annealing), e-beam exposure and UV irradiation on the solubility behaviour of neat PVA films in deionised water is investigated in this section.

Annealing. Untreated PVA films exhibit gel contents of 21 wt.-% as a result of the high molar mass and the very high degree of saponification, which lead to increased intermolecular interactions as well as higher crystallinity.[16] Annealing at 100 °C results in gel contents of up to 77 wt.-% after treatment times of 30 minutes, which stay constant for increasing annealing time (see Fig. 35). The degree of swelling shows an almost exponential decay over the thermal treatment time, with a slight increase after 30 minutes, as a result of cracking of the samples, which lead to an increase of water uptake. This results are in good agreement with the work published by Finch, which states that fully hydrolysed PVA exhibits improved solvent stability due to crystallisation as a result of heat treatment.[16]
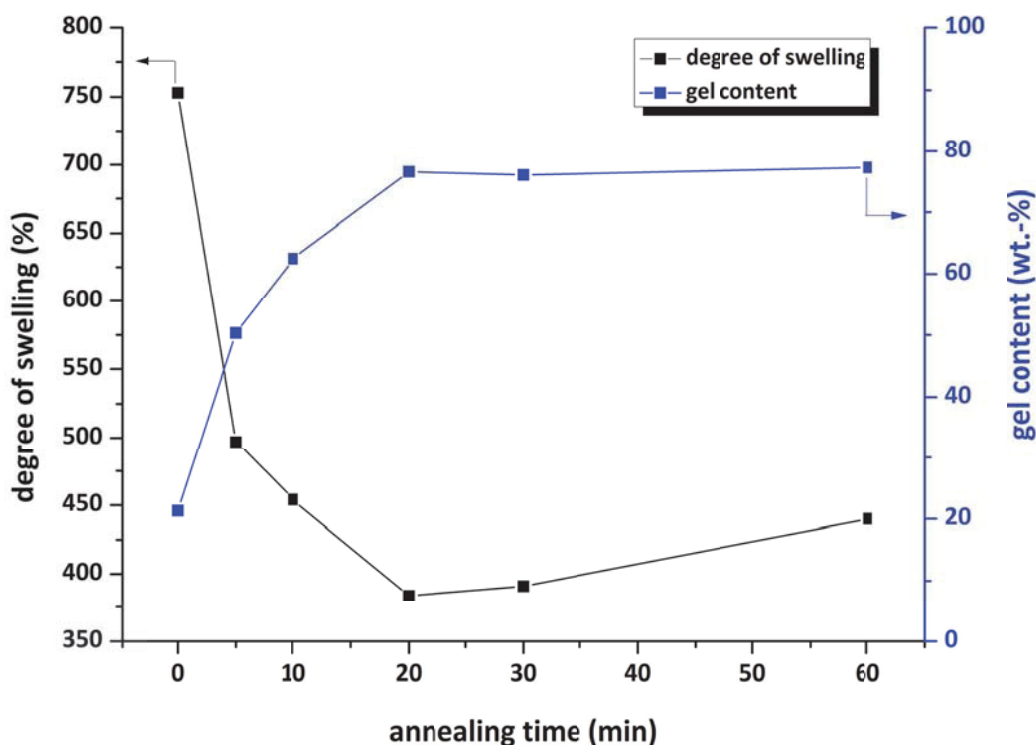
Fig. 35: Degree of swelling in water and gel content over the annealing time at 100 °C. The testing is performed at 20 °C. The lines are a guide to the eye.

Radiation exposure. UV exposure with a medium pressure mercury vapour lamp under air (corresponding emission spectrum see Fig. 13) does not lead to covalent crosslinking of neat PVA, hence the polymer exhibits no significant absorption in the area of the UV emission

(see Fig. 33). The gel content of thin films is increased (while the degree of swelling is decreasing) due to heating, as a result of the high energy density of the employed lamp, but reaches almost constant value after doses of 22 Jcm^{-2}. The increase of the degree of swelling of about 200 % may be a result of UV induced oxidation and chain scission, or the formation of surface cracks due to embrittlement of the samples.

Table 15: Degree of swelling and gel content of neat PVA in relation to UV exposure with a medium pressure Hg lamp (under air).

irradiation dose (Jcm^{-2})	degree of swelling (%)	gel content (wt.%)
0	750	21.3
22.2	310	55.5
44.3	550	52.9
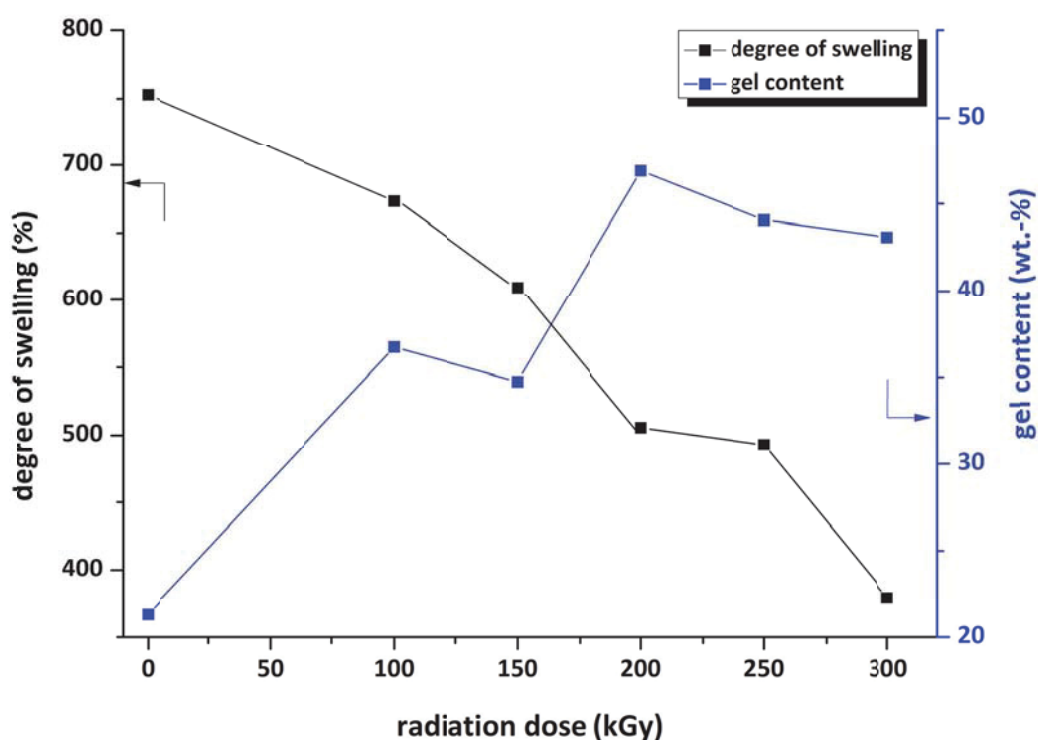
Fig. 36: Degree of swelling and gel content of neat PVA as a function of e-beam radiation dose in deionised water at 20 °C. The lines are a guide to the eye.

Electron beam exposure under air leads to statistic formation of radicals as well as heating of the samples due to the high energy density of the employed radiation source, which leads to recombination of the radicals and crystalline formation. An increase of the gel content to 45 wt.-% is observed, while the degree of swelling is reduced from 750 % to 380 %.

2. ALTERNATIVE METHODS FOR THE CROSSLINKING OF PVA

2.1 E-BEAM CROSSLINKING OF PVA

2.1.1 *Doping of PVA*

As both the PVA solution and triallyl isocyanurate (TAIC) are clear and colourless liquids, no UV-Vis absorption experiments on the liquid systems are performed. As the e-beam exposure was performed at an external facility (Greiner BioOne, Kremsmünster, Austria), self-supporting thin films of PVA:TAIC are prepared and subsequently investigated by ATR-FTIR measurements and sol-gel analysis.

2.1.2 *Radiation induced structural changes*

In order to alleviate peak identification of PVA:TAIC samples and the structural changes upon e-beam exposure, TAIC has been deposited on CaF_2 platelets and a transmission spectrum of the TAIC reference in a wavenumber range from 2000 to 850 cm^{-1} was collected (see Fig. 37). The carbonyl groups of the cyclic molecule result in the strong absorption at 1692 cm^{-1}, which is superposed by the R-CH=CH$_2$ stretching vibration of the vinyl groups resulting in a peak at 1646 cm^{-1}. The broad absorption band from 1510 to 1380 cm-1 can be attributed to the -CH- scissor vibration, the C-NR$_2$ vibration and the N-CH$_2$- deformation vibration. The peaks in the fingerprint area at 990 cm^{-1} are a result of the R-CH=CH2 out-of-plane vibration and the R_2N-CH$_2$-CH=CH$_2$ vibration at 930 cm^{-1}.[137,144]
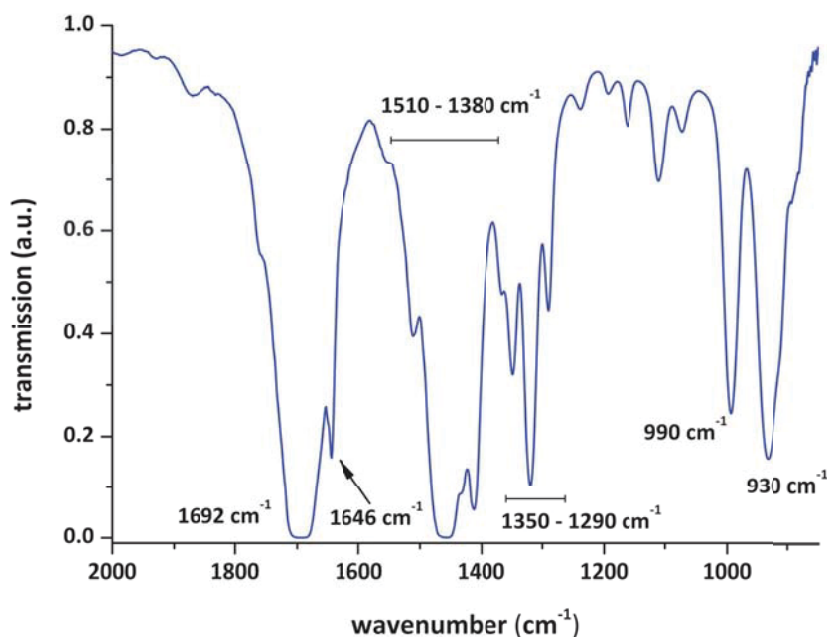
Fig. 37:   FTIR spectrum of a thin layer of triallyl isocyanurate (TAIC) deposited onto CaF_2 and peak identification

ATR-FTIR spectra of irradiated solid samples were collected in a wavenumber range of 2000-800 cm^{-1} and are depicted in Fig. 38. Changes in the carbonyl region are caused either by an oxidation of the PVA backbone, or by the ring opening of the triallyl isocyanurate due to the high energy density that was employed during exposure. No significant changes compared to neat PVA were detected for a system comprising 2.5 wt.% of crosslinking agent (TAIC) by the means of IR spectroscopy.[137,144]

The changes in the spectra in Fig. 38 suggest that a portion of the double bonds of the crosslinking agent undergoes conversion (1680 cm^{-1}), as well as -C-O-C- links are generated (1430–1470 cm^{-1}). Conversion of the double bonds can be observed and the formation of crosslinks, which are not cleaved upon further radiation exposure, is found for the doped PVA. However, these results provide insight of radiation-resulted changes only at the surface of the sample films. The film surface appears to be greasy, which may be caused by migration of the crosslinking agent out of the polymer film due to rapid heating that occurs during the crosslinking step.
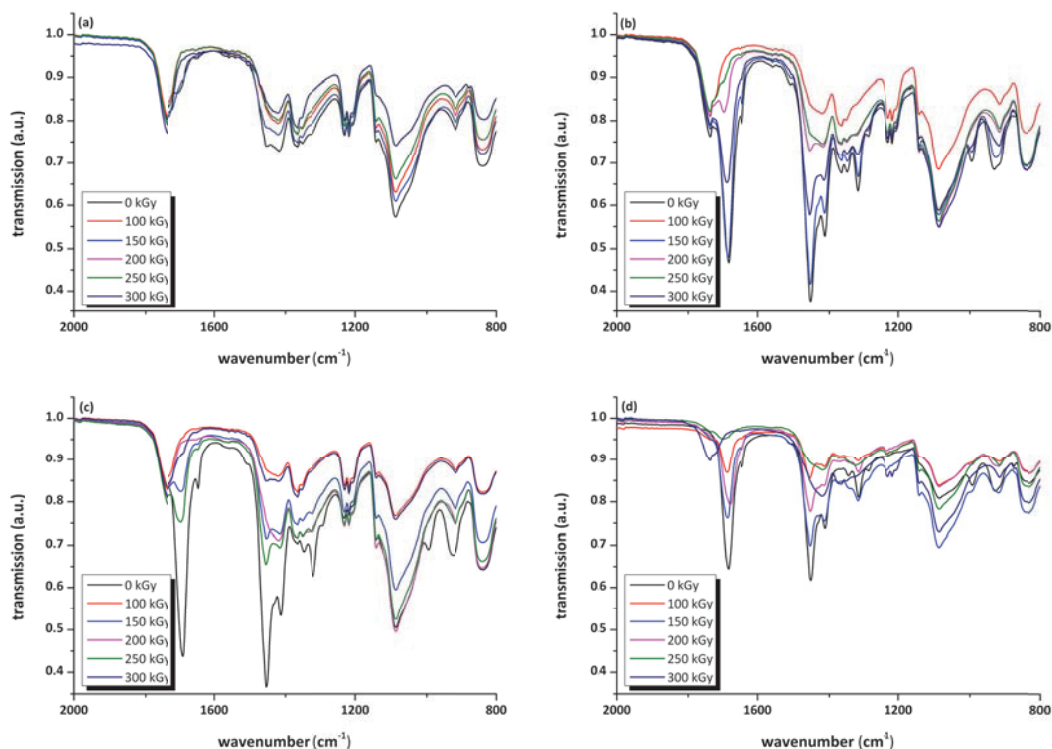
Fig. 38: ATR-FTIR spectra of self-supporting PVA:TAIC films (a) 2.5 wt.%; (b) 5 wt.-%; (c) 7.5 wt.% and (d) 10 wt.-% TAIC content.

2.1.3 *Determination of swelling behaviour*
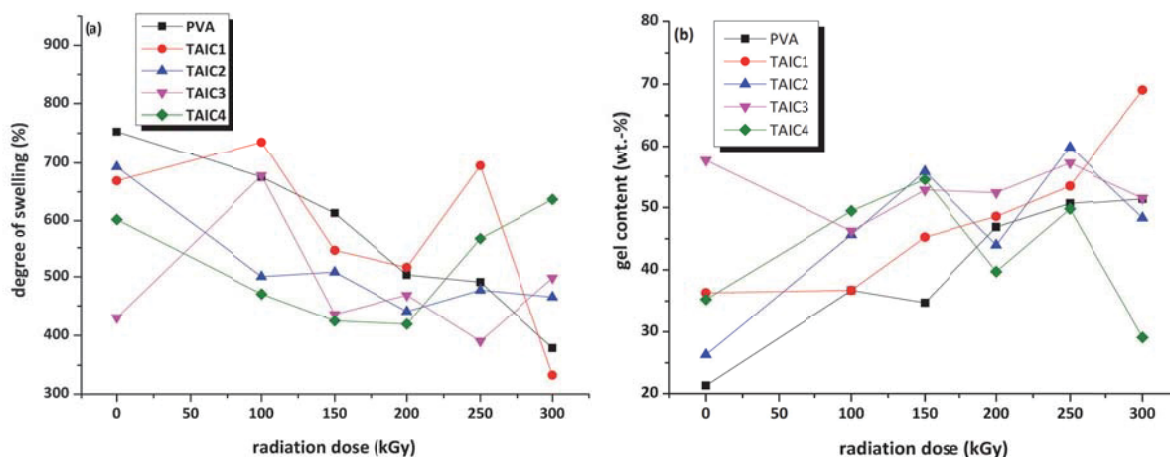
Fig. 39: Swelling behaviour of PVA:TAIC formulations in dependence of the radiation dose ; (a) degree of swelling; (b) gel content. Testing fluid: deionised water at room temperature. The lines are a guide to the eye.

The effects of electron beam exposure on the swelling behaviour of self-supporting PVA films that have been doped with triallyl isocyanurate as crosslinking agent, are depicted in Fig. 39. The swelling behaviour tends to decrease by the addition of 10 wt.-% of TAIC (TAIC4 in Fig. 39a), which may be caused by leaching out of non-conversed crosslinker and by chain

69

scission caused by the ionising radiation. As the gel content tends to increase as well, it is concluded, that the crosslinking agent is leached out and radiation resulted chain scission occurs. Solely the formulation comprising 2.5 wt.% TAIC exhibits both an increased gel content as well as a degree of swelling lower than 350 %. This may be caused by heating as a result of the high energy density of the e-beam exposure, which leads to crystallisation thus giving improved water resistance.[16]

Summing up, the e-beam irradiation of PVA:TAIC does not lead to enhanced solubility behaviour in deionised water by crosslink formation. Due to incompatibility of PVA and TAIC, the crosslinking aid migrates onto the surface ("bleeding"), thus resulting in greasy sample surfaces.

2.2 UV CROSSLINKING OF PVA

2.2.1 *Investigation of UV-response*

In a first control experiment, the change of the UV-Vis absorption spectrum of an aqueous $FeCl_3$ solution upon irradiation with a spot curing unit is determined and compared to the neat PVA solution (see Fig. 40a and Fig. 33). The strong decrease of the absorption in the range of 290 to 450 nm can be attributed to the photoreduction reaction of Fe^{3+} to Fe^{2+} ions, which leads to photobleaching and the formation of •OH radicals. While neat PVA does not exhibit any UV absorption.[97,150,151]

An aqueous PVA:$FeCl_3$ solution displays a similar UV response as the $FeCl_3$ reference solution (see Fig. 40a/b), leading to photoreduction and bleaching. This would facilitate the UV assisted crosslinking of comparatively thick solid substrates.[9]
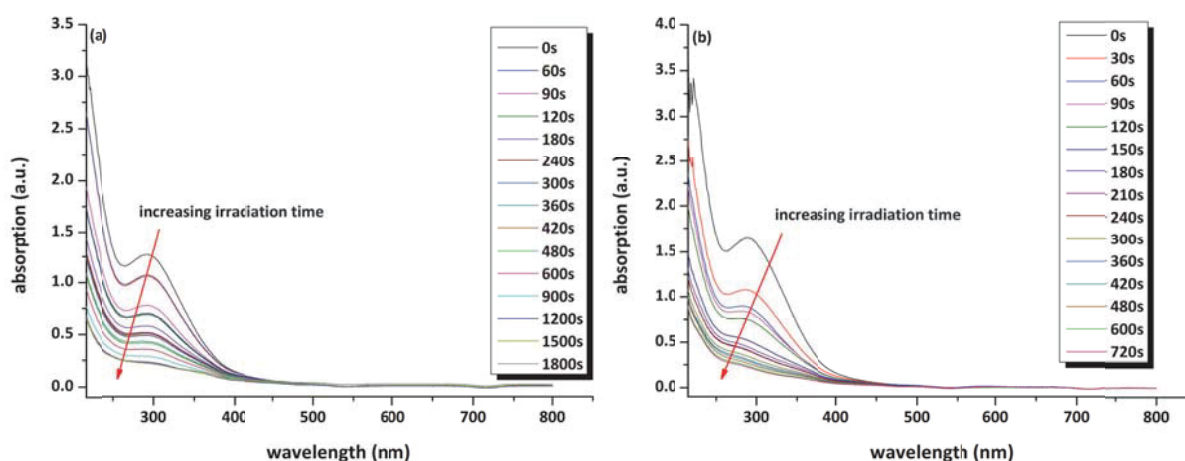
Fig. 40: Change of the UV-Vis absorption spectra of both highly diluted aqueous $FeCl_3$ (solids content: 1 wt.-%) (a) and $PVA:FeCl_3$ solution (solids content: 1.5 wt.-%) (b) upon exposure with an EXFO OmniCure spot curing unit with an emitter intensity of 9.25 Wcm^{-2}.

2.2.2 UV exposure

FTIR transmission spectra of drop coated PVA/Fe^{3+} films on CaF_2 platelets were collected and the carbonyl absorption area at 1750–1680 cm^{-1} is surveyed as well as the fingerprint region was analysed. Hydrogen bonds resulting from intermolecular interactions and residual water content in the samples are detected at a wavenumber of 1660 cm^{-1}. At 1430 cm^{-1} the absorption band corresponds to the $-CH_2-$ deformation vibration of the polymer backbone, while at 1090 cm^{-1} the -C-O- valence vibration can be observed.[137,143,144,144]

Upon doping with $FeCl_3$ a slight shoulder in the carbonyl region at 1705 cm^{-1} arises (see Fig. 41b) that increased in intensity upon irradiation with UV light. It is therefore concluded that main chain keto groups are formed on the PVA backbone due to UV exposure. Simultaneously the photoreactive species Fe^{3+} is reduced to Fe^{2+}, which has been reported by Changkakoti, Kowalonek and David, and is confirmed by our experimental data as well (see Fig. 40 and Fig. 42).[49,51,97,150]
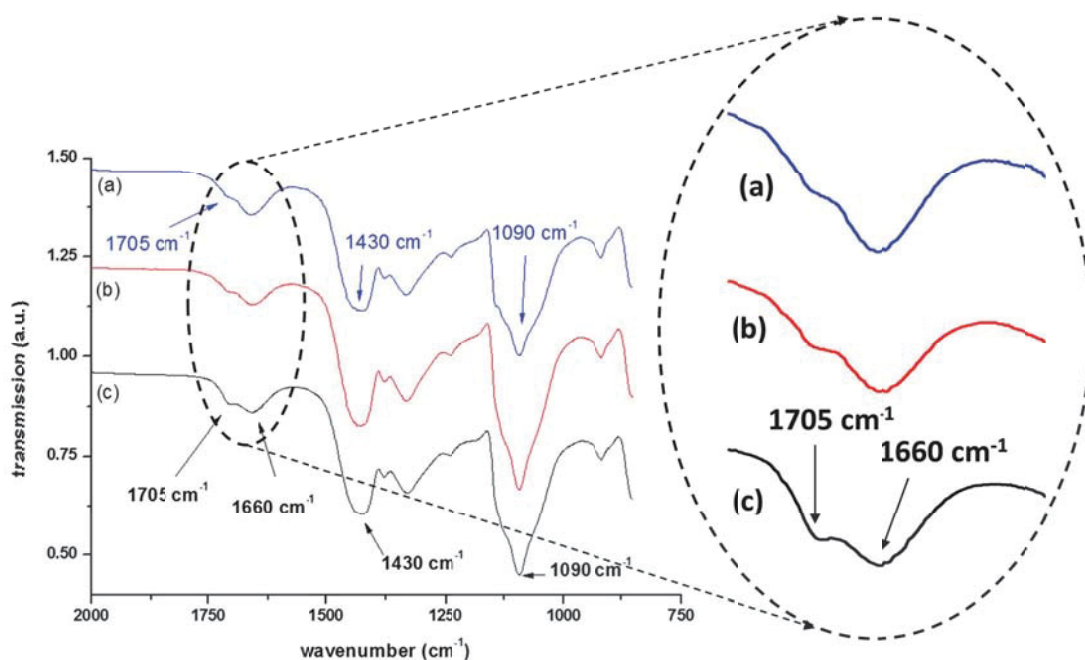
Fig. 41: FTIR spectra of thin films of PVA deposited onto CaF_2 platelets. (a) neat PVA and PVA:$FeCl_3$ before (b) and after UV illumination (c) with a dose of 3.37 Jcm^{-2}.

As neat PVA does not give significant absorbance in the wavelength range of 250 to 800 nm, the doping process leads to strong increase of absorption below wavelengths of 500 nm, thus giving susceptibility for UV induced reactions (Fig. 33 and Fig. 42). The strong absorption in this region is caused by Fe^{3+} cations that are reduced upon exposure (photobleaching). The absorption at 360 nm can be assigned to iron(III) and is decreasing almost exponentially (see detail in Fig. 42).[44,46]
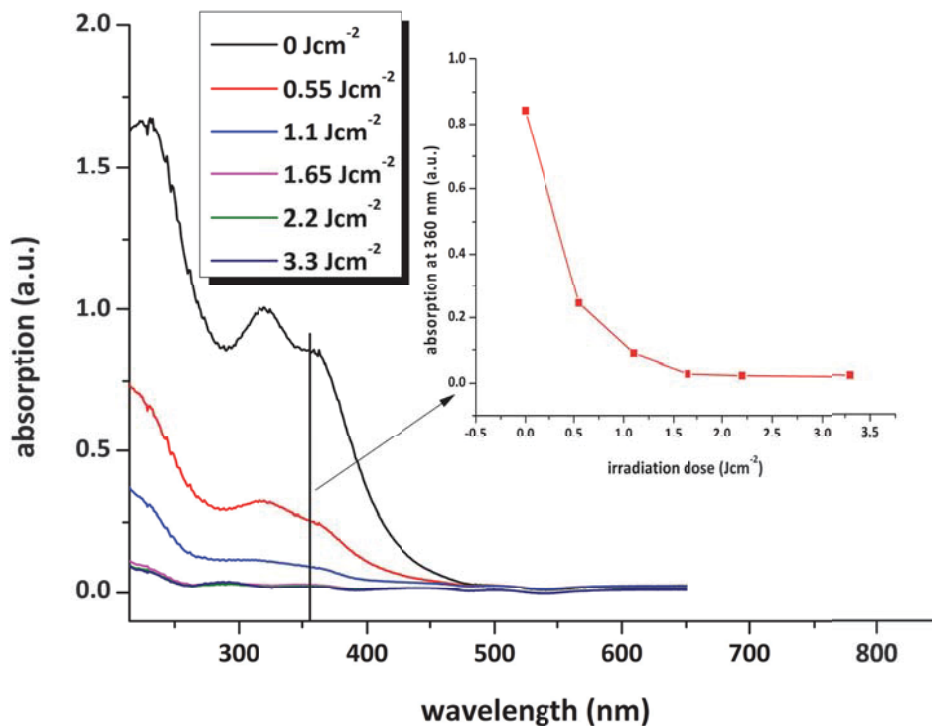
Fig. 42: Change of the UV-Vis absorption of thin layers of PVA:FeCl$_3$ coated onto CaF$_2$ platelets. The absorption at 360 nm results from Fe^{3+} ions, and follows an almost exponential decay upon UV-exposure (see picture insert).

Refractive index measurements using an Abbe refractometer that is equipped with a sodium D-line light source (λ = 589 nm) reveal that the refractive index changes rapidly due to UV exposure. After employing a radiation dose of 2.2 Jcm^{-2} the n^D is significantly reduced by Δn^D = -0.09 (see Fig. 43). To explain these experimental results, the refractive indices of aqueous solutions of both FeCl$_3$ and FeCl$_2$ (each 10 wt.-% solids content), as well as of neat PVA and deionised water, are determined and compared. For the FeCl$_3$ solution n^D is found to be 1.355, whereas the refractive index of the FeCl$_2$ solution is 1.338, which is similar of the index of neat PVA (n^D = 1.337).

Therefore it is concluded that the negative refractive index change of PVA:FeCl$_3$ as a result of UV exposure is caused by a change of the oxidation state of the iron ions.[49,97] As the wavelength for determination of the refractive index is outside the optical absorbance of Fe^{3+}, anomalous dispersion can be ruled out in this case. It should be noted, that crosslinking of polymers usually leads to an increase of the refractive index. For the PVA:FeCl$_3$ system however, this effect is overruled by the bleaching effect of the photoreduction of Fe^{3+} to Fe^{2+}.[9,10,45–47,49]
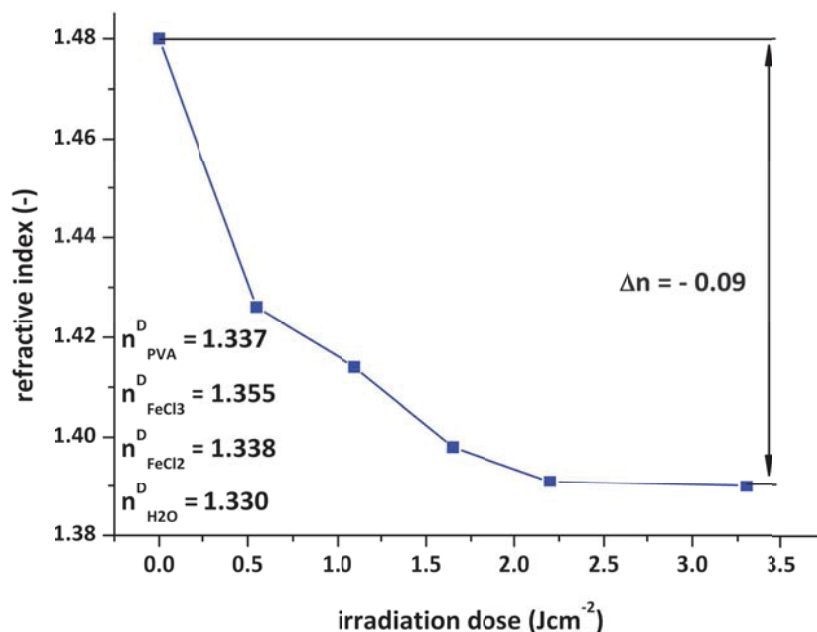
Fig. 43: Change of the refractive index (at λ = 589 nm) of PVA:FeCl$_3$ films as a function of the UV irradiation dose. The lines are a guide to the eye.

Furthermore, the strong decrease of the refractive index could be utilised to prepare flexible polymer waveguides, which has been investigated in the early 90s by Trepanier et al. using low molar mass PVA.[10] The photobleaching effect makes crosslinking of comparably thick substrates of PVA:FeCl$_3$ feasible.

2.2.3   *Determination of the swelling behaviour*

It is evident that Fe^{3+} doped PVA can be crosslinked by UV irradiation with relatively low energy doses. Employing 2.25 Jcm^{-2} causes an increase of the gel content by about 20 wt.-%, while the degree of swelling is reduced to almost one third of the original value (see Fig. 44). This leads to the further conclusion that the iron ions do not distort the intricate network of hydrogen bonds (inter- and intramolecular), but are well integrated into the PVA matrix, probably by formation of a coordination complex as reported by Manivannnan.[44]
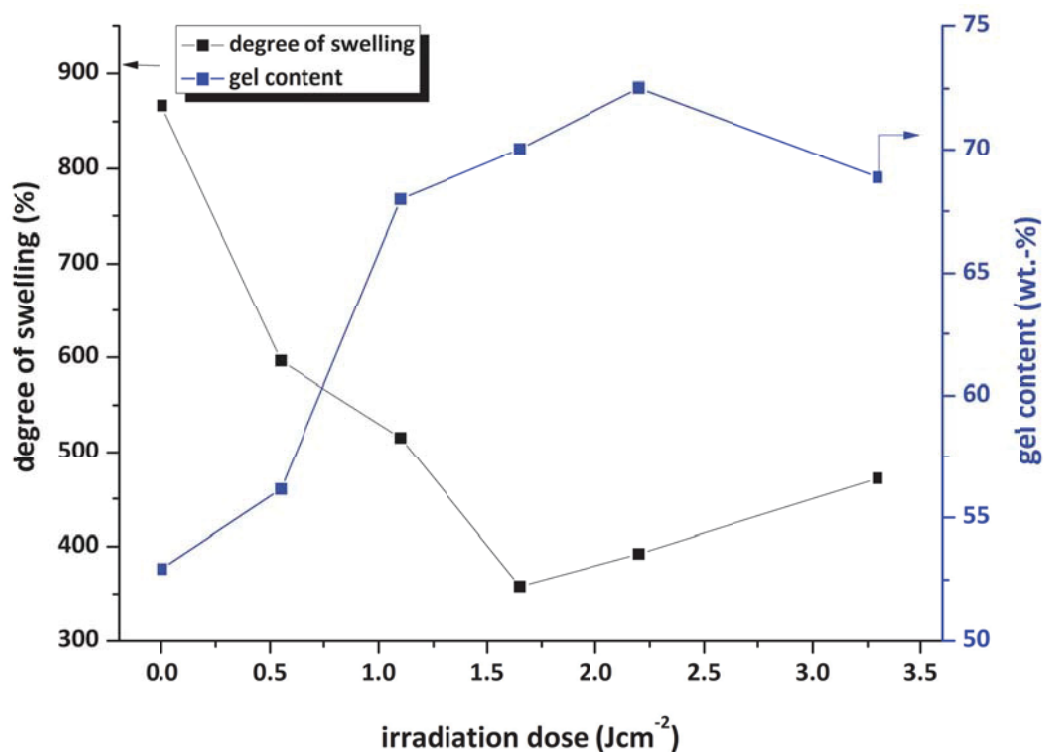
Fig. 44: Solubility behaviour of PVA:FeCl$_3$ as a function of the UV irradiation dose. The lines are a guide to the eye.

Further exposure of the doped PVA leads to a slight decrease of the swelling behaviour and the gel content as well, which may be caused by chain scission as a result of statistic radical formation.

2.2.4 *Photolithographic pattering*

The patterned illumination through a quartz/chromium mask bearing 100 μm features leads to excellent pattern contrast behaviour after illumination (see Fig. 45a). After a development step in deionised water for 30 min, followed by subsequent drying under constant air flow, the pattern contrast is still discernible.
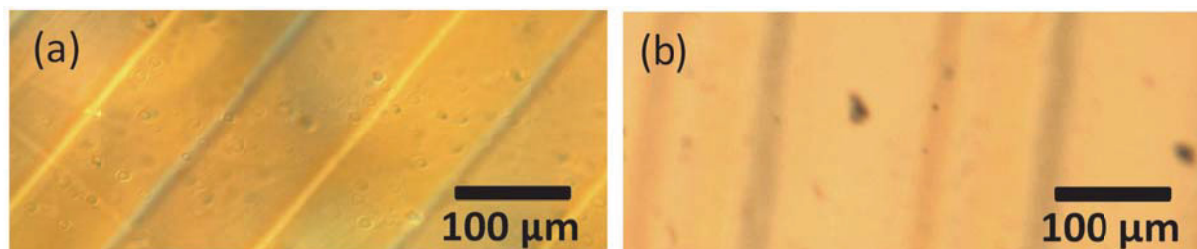
Fig. 45: Self-supporting PVA:FeCl3 films that were illuminated through a quartz/chromium mask with a UV intensity of 55 mWcm^{-2} for 20s (radiation dose of 1.1 Jcm^{-2}); (a) post exposure; (b) after development in deionised water and drying under constant air flow.[9]

The second method of patterning employs a Süss MJB 4 mask aligner in soft-contact imprinting mode silicon wafers that are coated with PVA:FeCl$_3$ are irradiated, applying an intensity of 25mWcm^{-2}, but longer exposure times of 120 s. After successful patterning, development and a drying step, the silicon platelets are examined by incident polarised light microscopy and profilometric measurements to analyse the surface topography of the patterned and developed areas.

The outstanding pattern contrast of a developed sample of PVA:FeCl$_3$ is depicted in Fig. 46a, each pattern exhibits the size of approximately 250 x 250 µm. The illuminated areas display topographical features (see Fig. 46b) after the development step, leading to the conclusion that these areas were crosslinked. Therefore the result is improved resistance against dissolution and swelling.
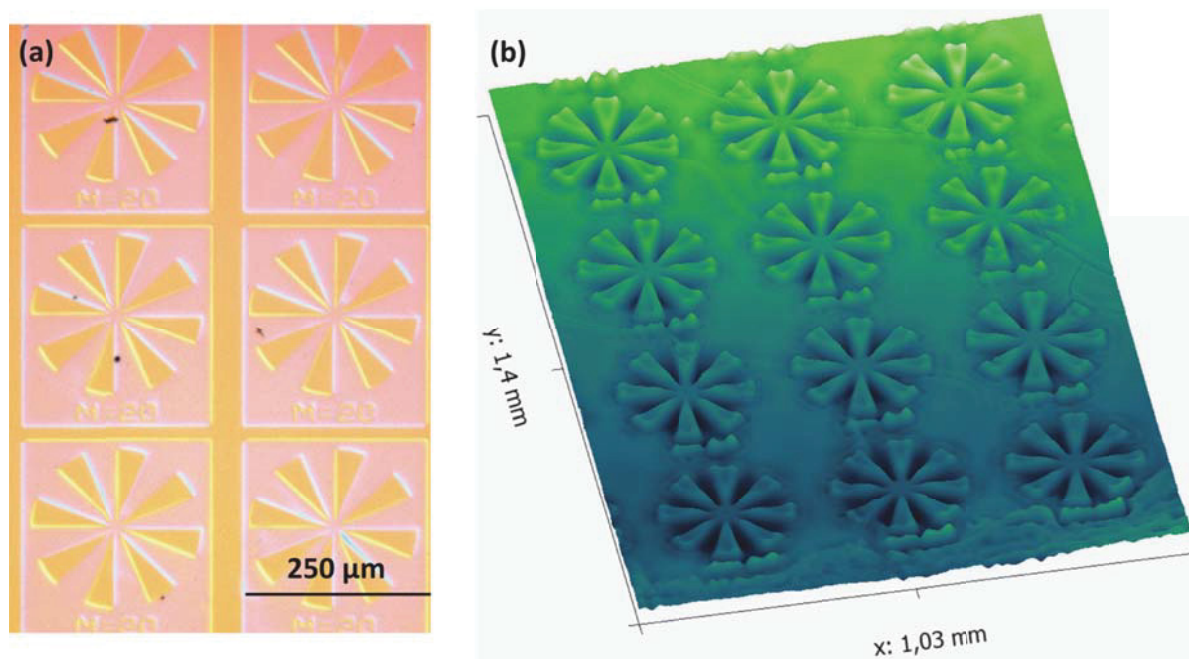
Fig. 46:   PVA:FeCl$_3$ coated silicon wafers after 120 s of exposure and development in deionised water (Süss MJB 4 mask aligner) (a) coated silicon platelets under polarised light; (b) profilometric imaging of a developed sample. Different areas of the samples were observed for this visualisation.

2.3   CONCLUSION

Electron beam exposure of thin films comprising PVA and triallyl isocyanurate (TAIC) under air causes oxidation of the polymer chains and conversion of the vinyl groups of the

crosslinking agent. ATR-FTIR data leads to the conclusion that the crosslinks and the polymer chains are cleaved upon further irradiation. This is confirmed by swelling measurements.

The resistance against water is deteriorated by e-beam exposure, also in the presence of the crosslinking agent. The TAIC molecules may disturb the formation of hydrogen bonds between the PVA molecules; therefore the crystallinity is decreased, which leads to a decrease of the gel content. Furthermore non-converted TAIC tends to migrate out of the matrix, thus giving an oily film surface. Desorption of the crosslinking agent takes place, which is potentially noxious and hazardous to water organisms. These effects as well as the chain scission caused by the ionising radiation do not lead to improved solvent stability of the prepared PVA specimens.

On the other hand, doping of PVA with $FeCl_3$, gives a photocurable system, which exhibits decisive changes of its optical properties by exposure due to photoreduction of Fe^{3+} to Fe^{2+}. This leads to oxidation of the polymer backbone, forming main chain keto groups as well as strong changes in the optical absorption and the refractive index.[10,46,49,97]

These changes in the optical properties are accompanied by a photobleaching effect that is caused by the reduction of the iron ions. Photolithographic patterning gives excellent pattern contrast after development with topographical features that contribute to the contrast pattern. These results and the findings of Schauberger et al. lead to the conclusion that PVA:$FeCl_3$ would be suitable for water-soluble and water-developable photoresist materials for rapid curing applications employing high UV irradiation intensities.[9] The combination of both an environmentally benign polymer and the non-organic photoactive reagent provides suitability for food packaging and medical products. Moreover, the application as base material for flexible polymer waveguides, high temperature coatings or electrochromics has to be considered.[10,42,43,146,152,153]

2.4 AZOSULPHONATE DOPED PVA

2.4.1 *Synthesis of aryl azosulphonate compounds*

2.4.1.1 Synthesis and purification

Two aryl azosulphonate sodium salts bearing carboxylic moieties (see Fig. 47) attached to the aromatic ring were prepared in a two-step synthesis, which has already been described (see chapter 3.3.1.1 and Fig. 11). The obtained azo dyes are purified by recrystallisation from deionised water at elevated temperatures, according to Riess.[61]
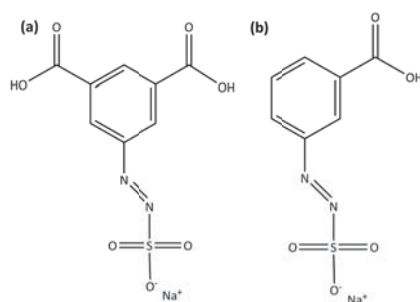
Fig. 47: Structural formulae of water soluble arylazosulphonate dyes.
(a) 3,5-dicarboxyphenyl azosulphonate - sodium (AZOII)
(b) 3-carboxyphenyl azosulphonate - sodium (AZOIII)

2.4.1.2 Structure determination

Nuclear magnetic resonance (NMR) spectroscopy proves to be a very versatile tool to determine the structure of the synthesised compounds. Both AZOII and AZOIII were dissolved in deuterated water (D_2O) followed by ^1H and ^{13}C NMR measurements. The spectra for AZOII are depicted in Fig. 48 and for AZOIII in Fig. 50 respectively.
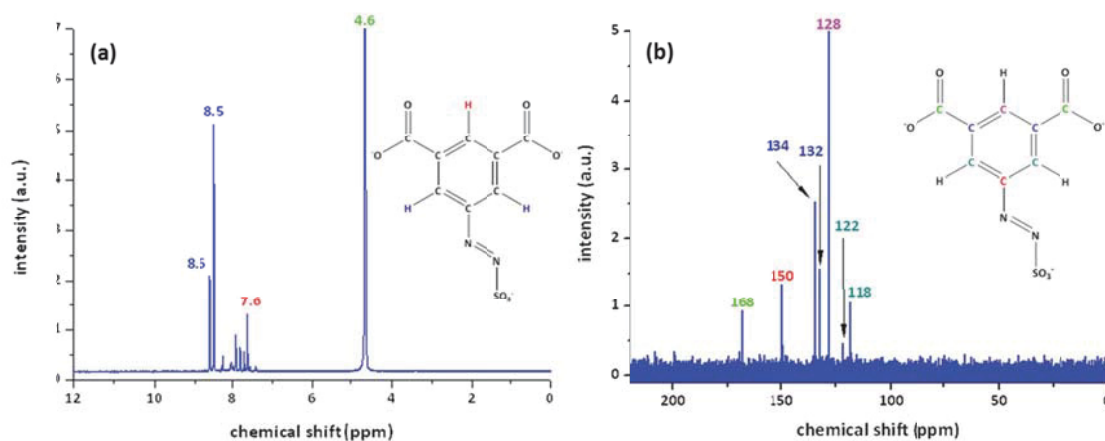
Fig. 48: ^1H (a) and ^{13}C (b) NMR spectra of AZOII dissolved in deuterated water.

The protons of the aromatic ring of AZOII can be assigned to the peaks at 8.6 and 8.5 ppm, which are marked blue and are assigned to the meta position. The remaining hydrogen atom is therefore related to the peak at 7.6 ppm. The peak at 4.6 ppm is attributed to the solvent D_2O (see Fig. 48a).

As additional chemical shifts between 7.6 and 8.5 ppm are detected, it is assumed that the obtained azo dye is contaminated with byproducts of the synthesis, although the product had been purified by recrystallisation and precipitation. Spectral simulation using ChemBioDraw reveals that these additional peaks are a result of partial deprotonation of the carboxylic moieties, by changing the dipole moment of the molecules (compare Fig. 48a with Fig. 49a/b).[61,137] As the simulation and the measurement concur, it is therefore concluded, that the carboxylic moieties of AZOII are almost completely deprotonated upon dissolution in D_2O.

The ^{13}C NMR spectrum of AZOII is not affected by the deprotonation, each of the carbon atoms can be assigned to a specific peak. The carboxylic acid groups can be attributed to the peak at 169 ppm, while the $-C-N=N-SO_3^-$ shift is detected at 150 ppm. The remaining five carbon atoms of the aromatic ring can be assigned to the chemical shifts between 134 and 118 ppm and are colour coded in Fig. 48b.
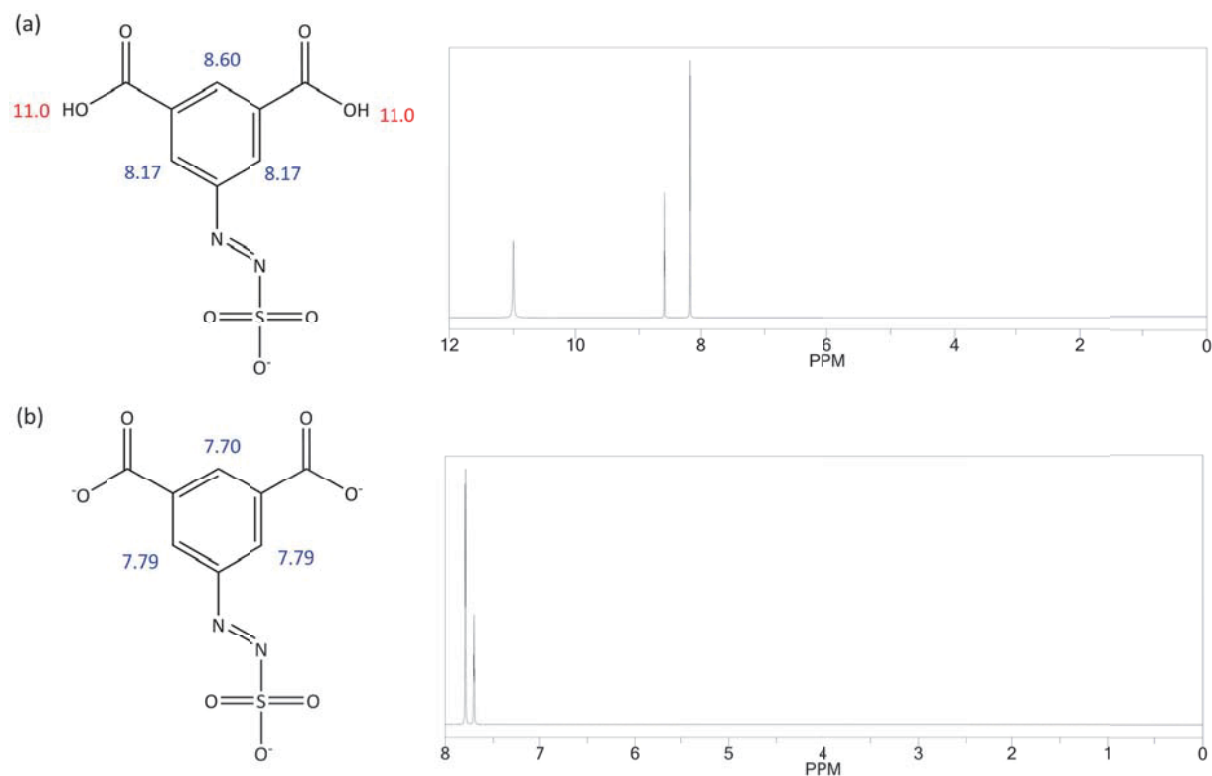
Fig. 49:   ^{1}H NMR peak prediction of AZOII, visualising the effect of deprotonation of the carboxylic acid moieties on the chemical shift in the spectra.

In accordance to the results for AZOII, the ^{1}H NMR spectrum of AZOIII reveals that the carboxylic moiety of the azo dye is deprotonated, otherwise a signal at a chemical shift of 11 ppm would be detected and the peaks of the protons of the aromatic ring would be shifted as mentioned previously. Hence only one carboxylic moiety is attached to the aromatic ring, the shift caused by changes of the dipole moment, as a result of deprotonation, is not as strong as found for AZOII. Proton NMR peak prediction and the determined spectra exhibit good correlation and it is possible to assign each of the hydrogen atoms of the aromatic system to a specific chemical shift (compare Fig. 50a with Fig. 51).[61,137]
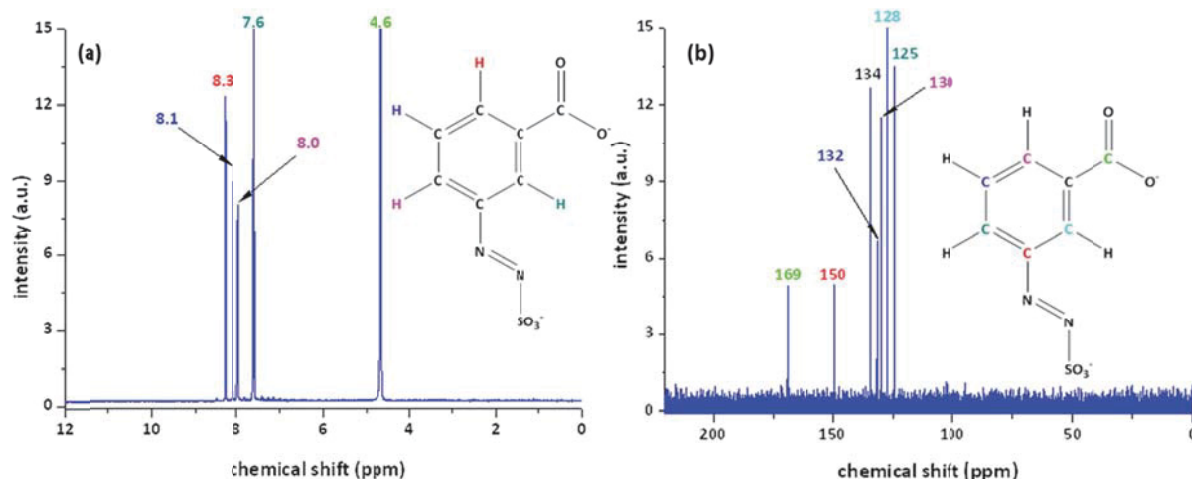
Fig. 50: ^{1}H (a) and ^{13}C (b) NMR spectra of AZOIII dissolved in deuterated water.

The ^{13}C NMR spectrum of AZOIII exhibits a strong signal of the carboxylic moiety at 169 ppm as well as the Ar-N=N-SO$_3^-$ shift at 150 ppm. The position of the carbon atoms of the aromatic ring is colour coded in the range of 134 to 125 ppm (see Fig. 50b).[137]
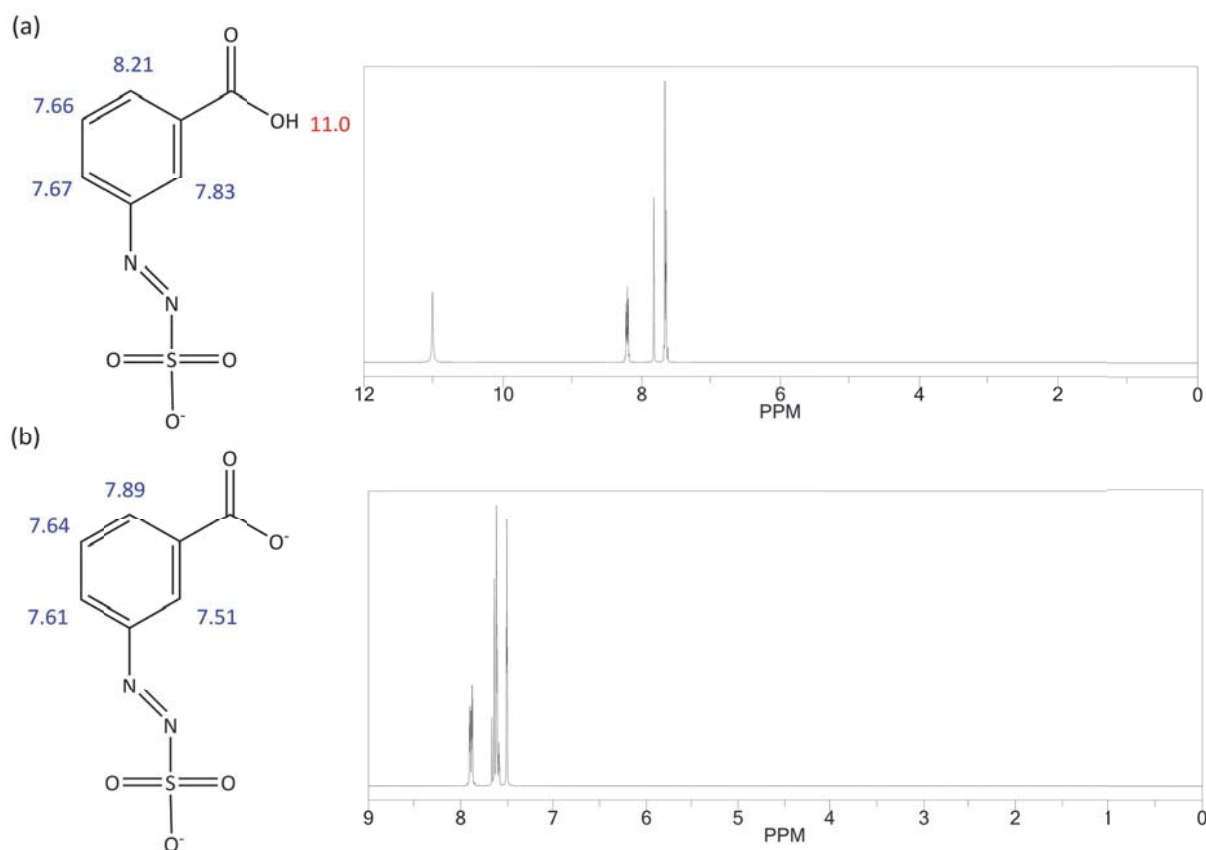
Fig. 51: ^{1}H NMR peak prediction of AZOIII, visualising the effect of deprotonation of the carboxylic acid moieties on the chemical shift in the spectra.

2.4.1.3 Photolysis

In a first attempt photolysis experiments of the prepared and purified azo dyes were performed in diluted aqueous solutions by irradiating quartz glass cuvettes with an EXFO spot curing emitter. The change of the UV-Vis absorption spectra at a wavelength of 224 and 227 nm of both azo dyes can be assigned to changes in the electron density of the aromatic system as a result of UV induced decomposition (see Fig. 52a/b). As photoinduced decomposition takes place, diminishing of the π-π* transition occurs, which can be attributed to the absorption at 285 nm (Fig. 52a) for AZOII and AZOIII (Fig. 52b). The n-π* transition of the chromophore azosulphonate group should occur around a wavelength of 400 nm, due to the small absorption coefficient it is not discernible.[57,60,63]
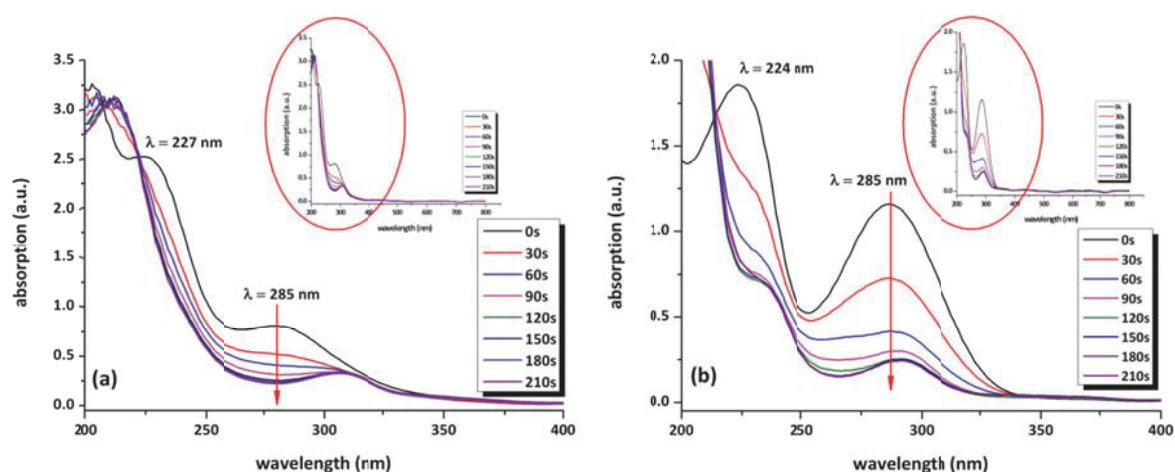
Fig. 52: Change of the UV-Vis absorption spectra of aqueous solutions of AZOII (a) and AZOIII (b) upon exposure with a high pressure mercury vapour emitter with an intensity of 9.25 mWcm[-2].

As the prepared azo compounds exhibit changes in their UV-Vis absorption in aqueous solution during UV irradiation, thin layers of these dyes were deposited on CaF_2 platelets by the drop coating method to determine UV light induced structural changes by means of FTIR spectroscopy (see Fig. 53 and Fig. 54).
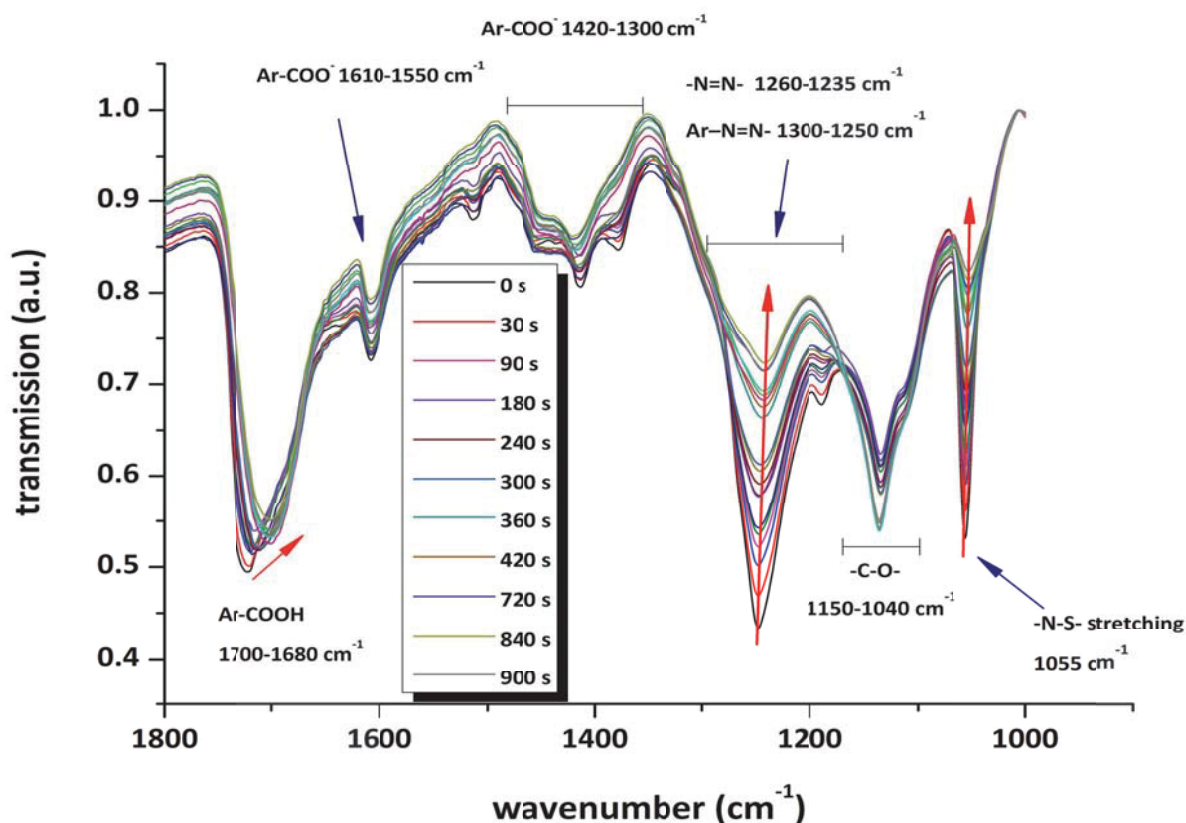
Fig. 53: Photolysis of solid AZOII on CaF_2 platelets using a high pressure mercury emitter with an intensity of 9.25 mWcm^{-2}.

In contrast to the dissolved substance, the carboxylic moieties of solid AZOII are partly deprotonated, which can be observed by the formation of absorption bands at 1610–1550 cm^{-1} and 1420–1300 cm^{-1} as well as by the change of the strong signal of the -COOH groups at 1700 cm^{-1}(see Fig. 53 and Fig. 54). This is resulted by the precipitation step, hence a large part of the carboxylic moieties is protonated, while a residue of carboxylates is left. This is found for both azo dyes.[137,144,151]

Due to irradiation of the thin layers, the Ar-N=N- and the -N=N- stretching vibration, which contribute to the absorption from 1300 to 1235 cm^{-1}, are strongly decreasing as well as the -N-S- stretching vibration at 1055 cm^{-1} (see Fig. 53 and Fig. 54). As the para substituent of the aromatic systems is decomposed, the dipole moment of the whole molecule is changed, which also explains the shift of the Ar-COOH vibration for AZOII from 1700 cm^{-1} to lower wavenumbers.

Additionally a slight increase of the -C-O- valence vibration at 1150 to 1040 cm^{-1} is observed, which may me a result of hydroxyphenyl formation according to Nuyken and Voit (compare with Fig. 2).[57]
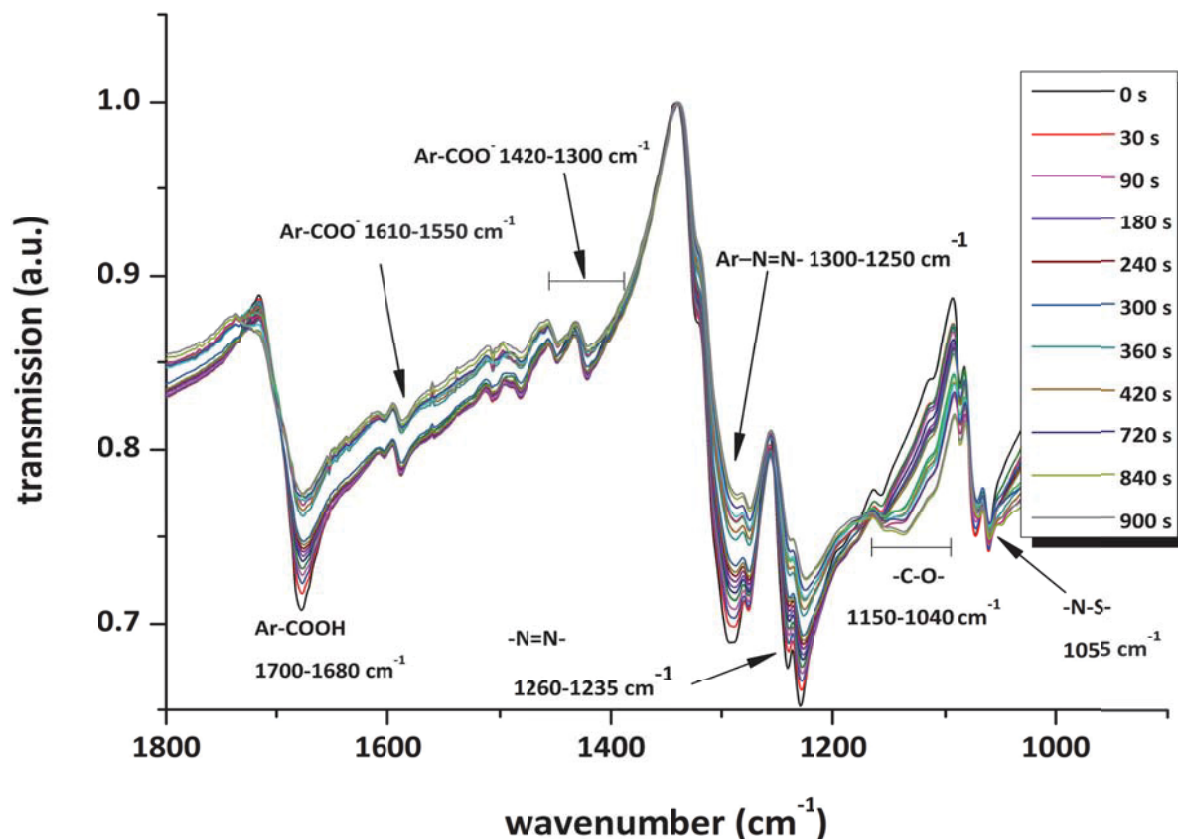
Fig. 54: Photolysis of AZOIII upon irradiation of coated CaF_2 platelets using a high pressure mercury emitter with an intensity of 9.25 $mWcm^{-2}$.

As a result of UV irradiation the azo groups of both synthesised azo dyes are decomposed, which leads to nitrogen gas release and splitting off of the sulphonic acid moiety. This proposed decomposition mechanism is confirmed by the obtained FTIR kinetics and can also be followed by UV-VIS measurements, as the electron density of the aromatic system is altered due to UV induced decomposition of the chromophore groups.

2.4.1.4 Thermolysis

As 3,5-dicarboxyphenyl azosulphonate - sodium exhibits high hygroscopy, it takes up aerial water, which can be observed as a mass loss of 2.5 wt.-% up to 150 °C in the thermogravimetric curve as well as an endothermic heat flow (see Fig. 55a). The monoacid AZOIII on the other hand, does not exhibit such behaviour, but it displays a higher thermal

stability, with the decomposition starting at 240 °C, while AZOII shows an onset of decomposition at 170 °C (compare Fig. 55a/b).

This first decomposition temperature can be related to fragmentation of the azo groups, which leads to nitrogen gas emission.[154] The cleavage is very rapid for AZOIII, with a first sample weight loss of about 37 wt.-%, while AZOII shows a weight loss of 25 wt.-% (compare Fig. 55a/b). It is also evident that the monoacid AZOIII is thermally more stable than AZOII.
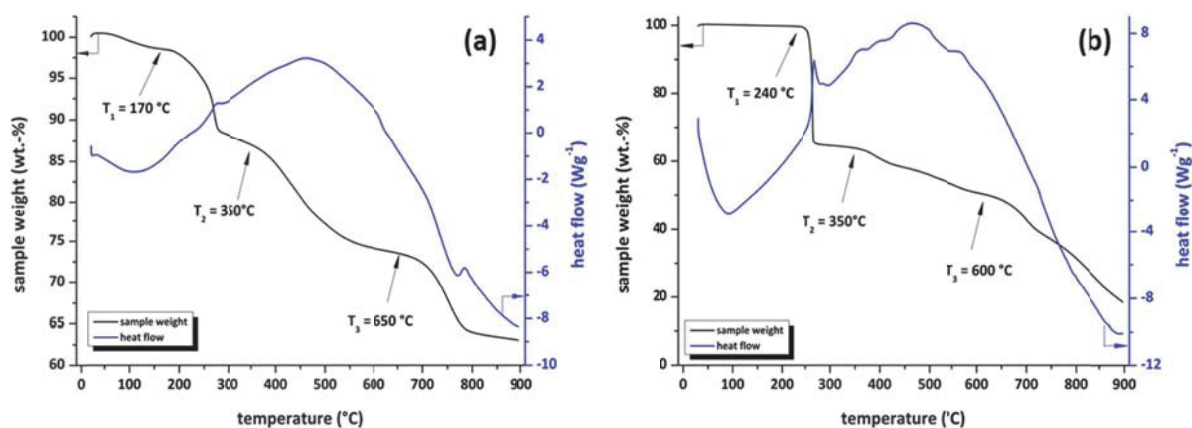
Fig. 55: Thermogravimetric curves (weight loss in relation to the initial sample weight) and the corresponding heat flow of AZOII (a) and AZOIII (b) upon heating under nitrogen atmosphere with a heating rate of 20 Kmin^{-1}.

The first decomposition step is followed by decarboxylation and the decomposition of the aromatic ring up to a temperature of 650 °C, which leads to a further mass loss of 15 wt.-% for AZOII and of 10 wt.% for AZOIII.[61] Finally, thermal decomposition of the residual sulphonic acid groups takes place at temperatures ranging up to 800 °C for AZOII and 750 °C for AZOIII.[155]

The overall weight loss is higher for AZOIII (81.5wt.-%), leading to the conclusion that the decomposition products of this substance are more volatile, whereas AZOII exhibits a residual value of 60 wt.-%. Furthermore the thermal decomposition of AZOIII leads to blowing of the solid substance, resulting in a lift-off of the crucible cover. This could give the feasibility for the application of thermal induced blowing agent. AZOII on the other hand, is pyrolised to ash, not exhibiting any expansion due to thermolysis under nitrogen atmosphere.

2.4.2 Characterisation of azosulphonate doped PVA

2.4.2.1 Annealing

The effects of heat treatment of thin films of AZO-doped PVA (sample notation in accordance to Table 7) are investigated by spectroscopic methods such as ^{1}H and ^{13}C NMR and FTIR spectroscopy. Due to limit of detection (LOD) issues solely ^{13}C NMR spectra of PAII.5 and PAIII.5 were obtained, to investigate the formation of ester groups by heat induced condensation reactions. The FTIR spectra of the samples are collected in the figure appendix (see and compare P 1 to P 5 for PAII.1–5 and P 6 to P 10 for PAIII.1–5). The allocation of pivotal absorption bands (shift of C=O; formation C-O-C) is exemplarily presented for PAII.5 and PAIII.5.
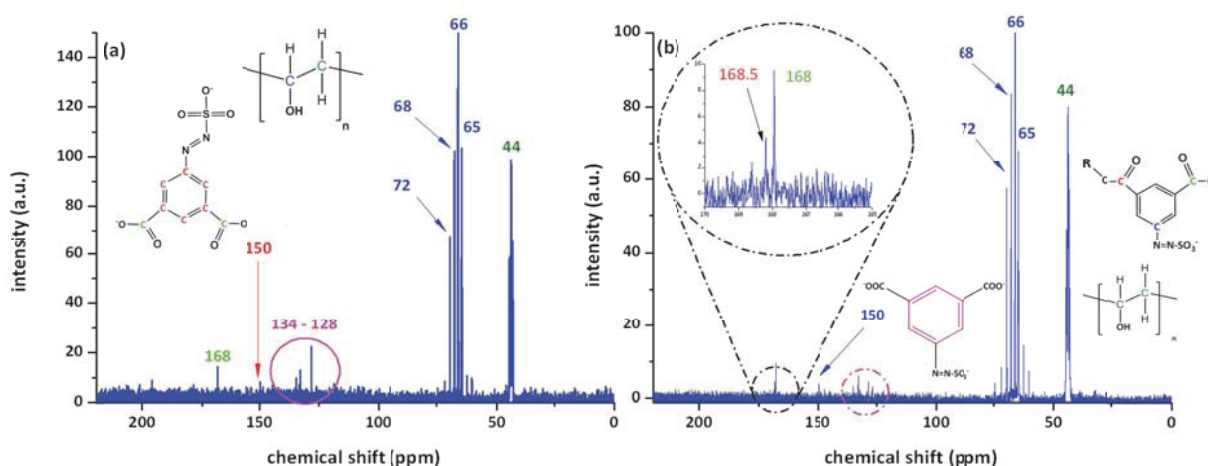
Fig. 56: ^{13}C NMR of PAII.5 (comprising 20 wt.-% of AZOII) before (a) and after (b) annealing at 100°C for 60 min.

A sample of PAII.5, which was not subjected to heat treatment, gives a superposition of the ^{13}C NMR spectra of the source materials (see Fig. 56a, compare with Fig. 30 and Fig. 48b). It is evident that the detection of specific C-atoms reaches the detection limit of the measurement system; however it is possible to determine the structural elements, which are colour coded in Fig. 56.

Upon heat treatment, the formation of aromatic ester linkages can be evidenced by the splitting of the carbonyl shift at 168 ppm into two different signals (see detail in Fig. 56b).[137] As this signal is very faint, additional FTIR measurements were conducted on thin films to ascertain these findings.
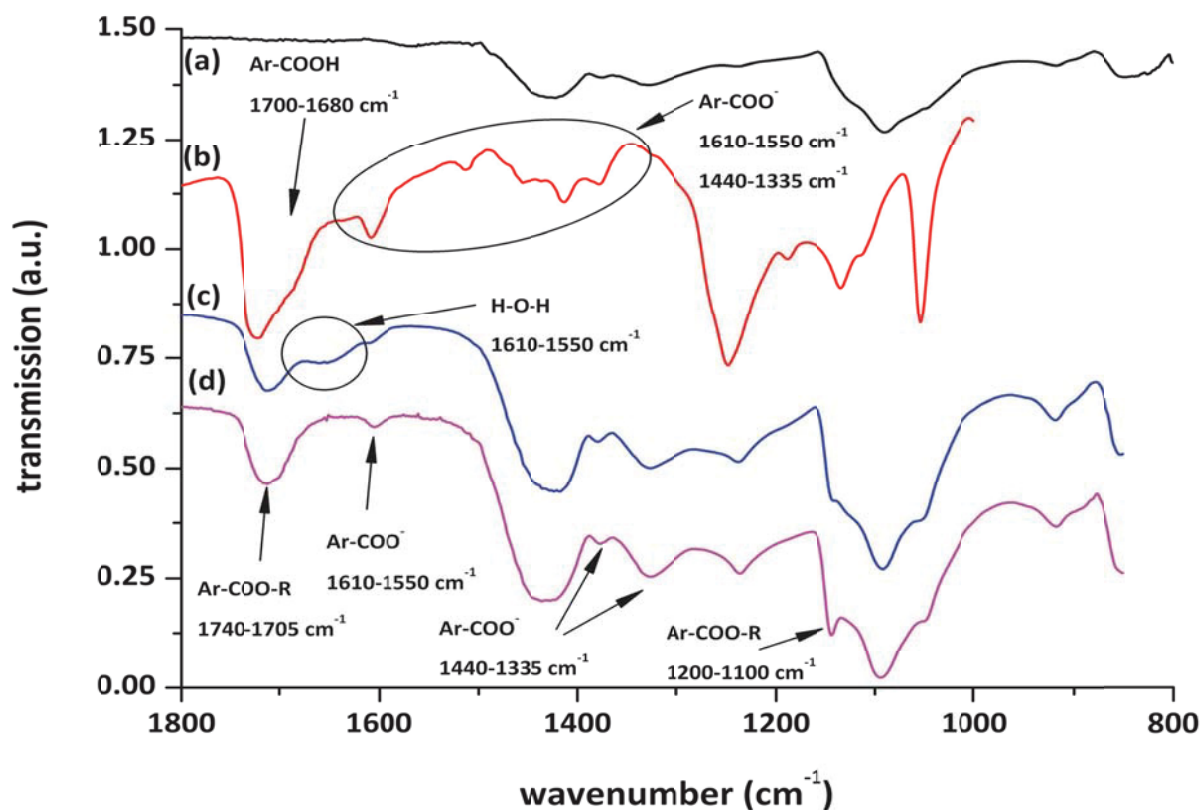
Fig. 57: FTIR spectra of (a) neat PVA; (b) AZOII; (c) PAII.5 containing of 20 wt.-% AZOII; (d) PAII.5 after 60 min of annealing at 100°C.

Upon heat treatment, the evaporation of intermolecular water takes place, which leads to vanishing of the H-O-H bending vibration from 1610 cm^{-1} to 1550 cm^{-1} as well as the formation of aromatic ester groups, resulting in a shift of the carbonyl area from 1700 cm^{-1} to 1715 cm^{-1} (see Fig. 57c and d).[156] Furthermore a C-O-C stretching signal emerges at 1150 cm^{-1} that can be attributed to ester crosslink formation by condensation of PVA and AZOII.[144]

The carboxylic groups of AZOII are partially deprotonated for the pristine azosulphonate, as well as for the doped PVA films and the heat treated samples. Spectroscopic methods give insight that the carboxylic moieties are sluggish in reaction, therefore leaching out of the low molecular photoactive species may occur due to swelling by appropriate solvents. However, the dicarboxylic acid could lead to the formation of crosslinks, thus affecting the solubility behaviour of PVA.
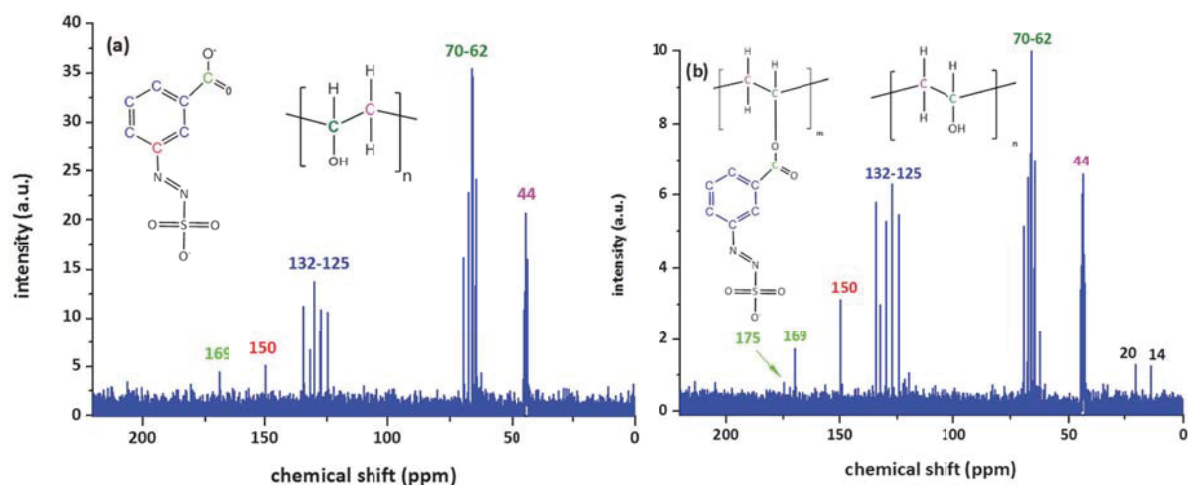
Fig. 58: ¹³C NMR of PAIII.5 (comprising 20 wt.-% of AZOII) before (a) and after (b) annealing at 100°C for 60 min.

The coupling reaction of the monovalent acid AZOIII can also be followed by CNMR spectroscopy, however, the formation of ester groups by FTIR spectroscopy is only discernible for PVA films comprising at least 10 wt.-% azosulphonate (see P 6–P 10 in the appendix). The emerging of a second carbonyl signal at 175 ppm (see Fig. 58b) can be attributed to an aromatic ester and the signal at 169 ppm stems from non-converted carboxylic groups.[137]
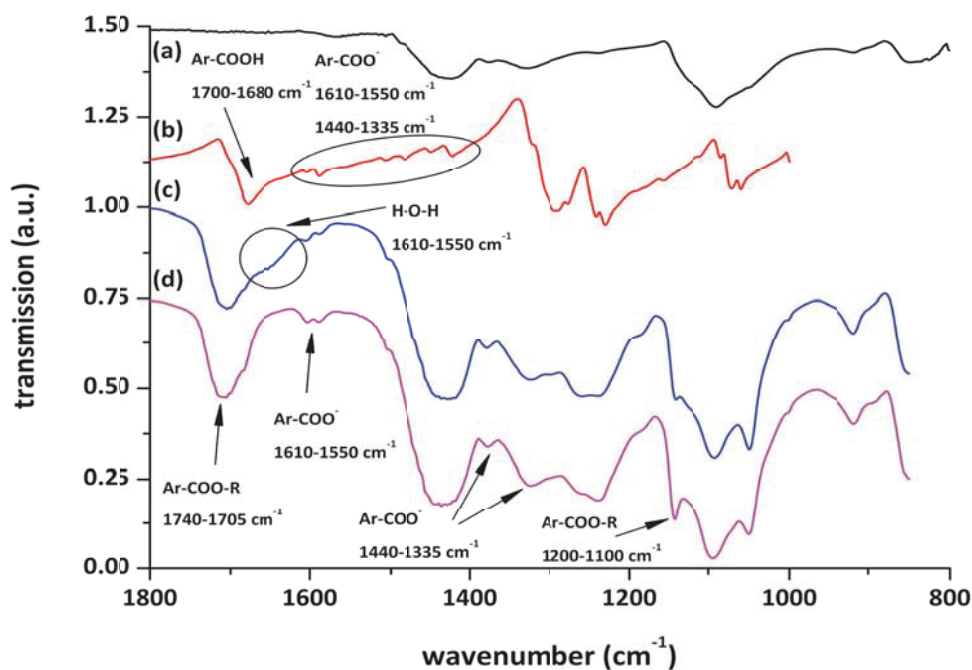
Fig. 59. FTIR spectra of (a) neat PVA; (b) AZOIII; (c) PAIII.5 comprising of 20wt.-% AZOIII; (d) PAIII.5 after 60 min of annealing at 100°C.

Infrared spectroscopy allows the identification of aromatic esters as well as the existence of non-converted acid groups and carboxylic acid salts after annealing at 100 °C, besides the depletion of the H-O-H bending vibration by evaporation of water (see Fig. 59c/d). The non-converted azosulphonates may be leached out of the prepared solid films by appropriate solvents, also as a result of swelling of the matrix polymer.

2.4.2.2   Photolysis

The annealing step of azosulphonate doped PVA is followed by investigation of the photolysis kinetics by FTIR and UV-Vis spectroscopy upon irradiation with UV light with an intensity of 9.25 mWcm^{-2}. The obtained spectra are collected in the figure appendix (P 11–P 20). Due to concentration issues, only faint changes in the FTIR spectra can be discerned (P 11a–P 20a), however the corresponding UV-Vis spectra exhibit strong changes that can be assigned to the aromatic ring and the decomposition of the photoactive azosulphonate substituent. As an example, the photolysis behaviour of PAII.5 and PAIII.5 is illustrated and discussed in this section.
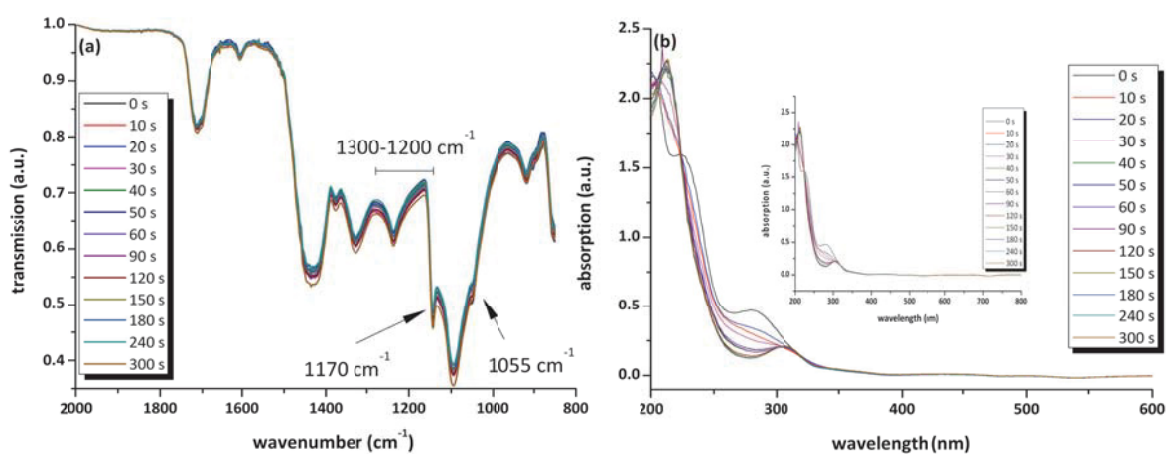
Fig. 60:   UV irradiation kinetics of FTIR transmission (a) and UV-Vis absorption spectra (b) of annealed thin PAII.5 films coated onto a CaF$_2$ substrate. UV light is emitted by a high pressure Hg lamp with an intensity of 9.25 mWcm^{-2}.

Due to UV exposure, decomposition of the azosulphonate dyes is caused, regardless of the conversion of the carboxylic groups by annealing. This can be followed by the depletion of the IR absorption at a wavenumber of 1055 cm^{-1} that is attributed to the -N-S- stretching vibration as well as slight changes in the spectral region of 1300–1200 cm^{-1} (-N=N- and Ar-N=N- absorptions). As superposition of the IR absorption bands of the azo dye and the

PVA matrix occurs, it is very difficult to determine these changes, especially for concentrations below 10 wt.-% of photoactive species (see P 11a–P 13a). However changes of the peak at 1170 cm^{-1} occur, which may be a result of the formation of hydroxyphenyl (-C$_6$H$_5$OH) residue groups (see Fig. 60a and Fig. 61a).[137,144]

These results, however, are in contrast to the decomposition mechanism published by Nuyken, which states that in the presence of alcohols phenyl (-C$_6$H$_5$) residue groups are generated by UV induced cleavage.[57] It is therefore concluded, that in heat treated films either residual water is present or most likely the decomposition of the azo dye in the doped films follows an ionic pathway.
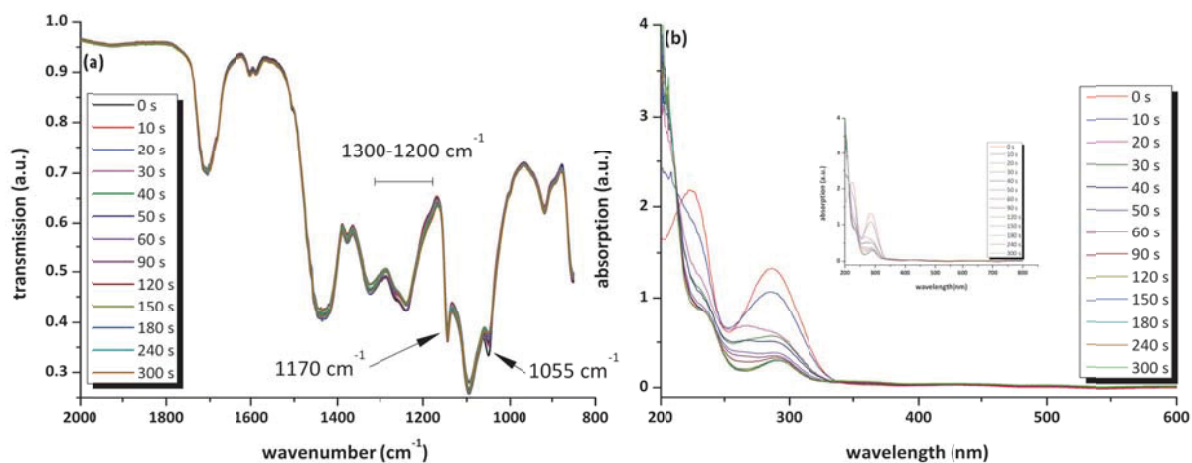
Fig. 61:   UV irradiation kinetics of FTIR transmission (a) and UV-Vis absorption spectra (b) of annealed thin PAIII.5 films coated onto a CaF$_2$ substrate. UV light is provided by a high pressure Hg lamp with an intensity of 9.25 mWcm^{-2}.

Due to the improved sensitivity, UV-Vis spectroscopy is more appropriate to investigate UV induced decomposition of the azo dye in the doped PVA films. As the electron density of the aromatic ring is altered by the cleavage of the azo group, the absorption at 227 nm is diminishing and shifting towards 215 nm for PAII.5 (Fig. 60b), while PAIII.5 shifts towards 206 nm and a residual absorption at 230 nm.[61,62,157] The decrease of the second absorption maximum at 282 nm can be directly attributed to the π-π* transition. This leads to a bathochromic shift of the absorption to 290 nm for PAIII.5 and to 305 nm for PAII.5. As the azosulphonic moieties are decomposed, nitrogen gas and sulphite anions (SO$_3^{2-}$) are generated.

2.4.2.3 Investigation of swelling behaviour

For investigations of the solubility behaviour self-supporting thin films of azosulphonate-doped PVA are prepared by the gravity settling method. To achieve an advantageous depth-dose distribution for the illumination, a high intensity medium pressure mercury vapour emitter (emission spectrum see Fig. 13) was employed.

As the formation of ester crosslinks by annealing is difficult to detect by the means of FTIR and CNMR spectroscopy, sol-gel analysis can give additional information concerning this thermally induced condensation reactions. The addition of an azosulphonate bearing two carboxylic moieties and subsequent heat treatment leads to a strong decrease of the degree of swelling (see Fig. 62a), reaching lower values than neat PVA even without any heat treatment. However the insoluble fraction is increasing due to the heat treatment, but no significant improvement compared to neat PVA can be discerned. This may be a result of leaching out of non-bound AZOII, which exhibits very good water solubility (see Fig. 62b).
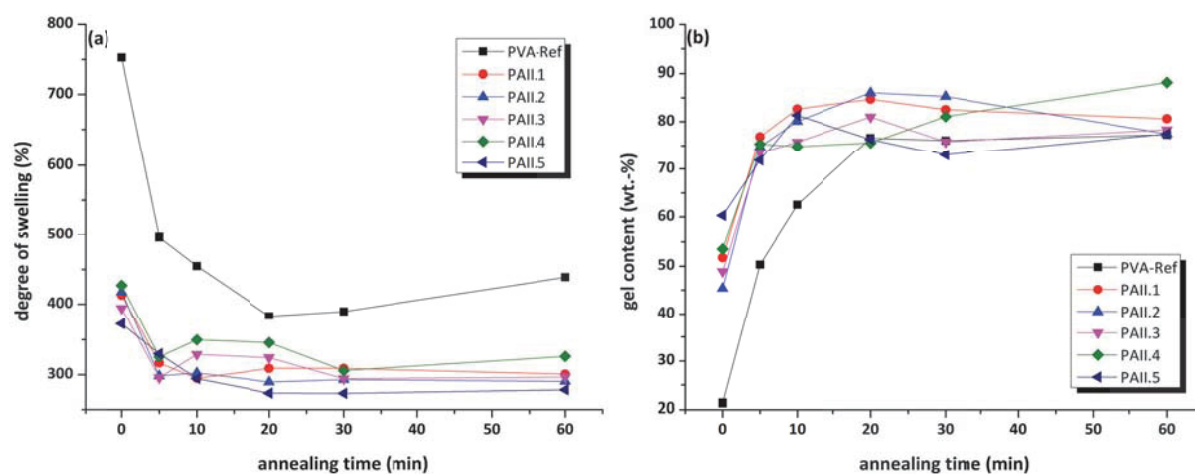
Fig. 62: Influence of annealing on the degree of swelling (a) and the gel content (b) of neat PVA and PAII films after immersion for 48 hours at room temperature. The lines are a guide to the eye.

Subsequent UV exposure of PVA-AZOII films leads to a slight increase of the degree of swelling; the deviation of PAII.2 and PAII.4 may be caused by surface water or fragmentation of samples. The gel content is not increased by further UV exposure after annealing except for PAII.2 (see Fig. 63). As previously mentioned, this may be the result of leaching out of the azosulphonate. The UV induced decomposition of the photoactive species does not lead to

deterioration of the crosslink density, therefore exhibiting no adverse effects on the solubility behaviour.
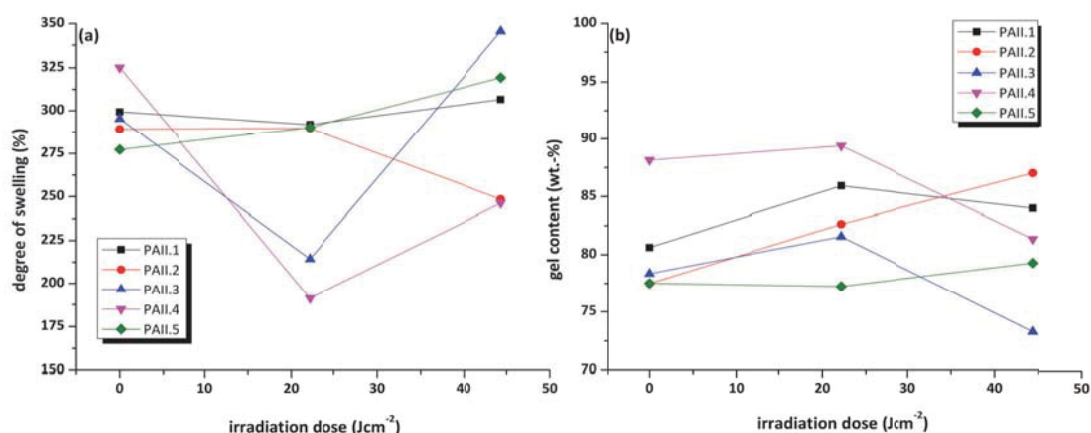
Fig. 63: Influence of subsequent UV exposure using a medium pressure Hg lamp (Fig. 13) with a power output of 740 mWcm^{-2}. (a) degree of swelling and (b) gel content of PAII films. The lines are a guide to the eye.

While the difunctional carboxylic acid improves the swelling behaviour of PVA upon annealing by forming ester links, the addition of the monovalent AZOIII leads to an increase of the degree of swelling (see Fig. 64a). The coupled azosulphonate acts as spacer, inhibiting the formation of intermolecular hydrogen bonds and acts as imperfection that prevents heat induced crystallisation. Furthermore, lower gel contents compared to neat PVA are determined, which is a clue that a portion of the unattached AZOIII is leached out (see Fig. 64b).
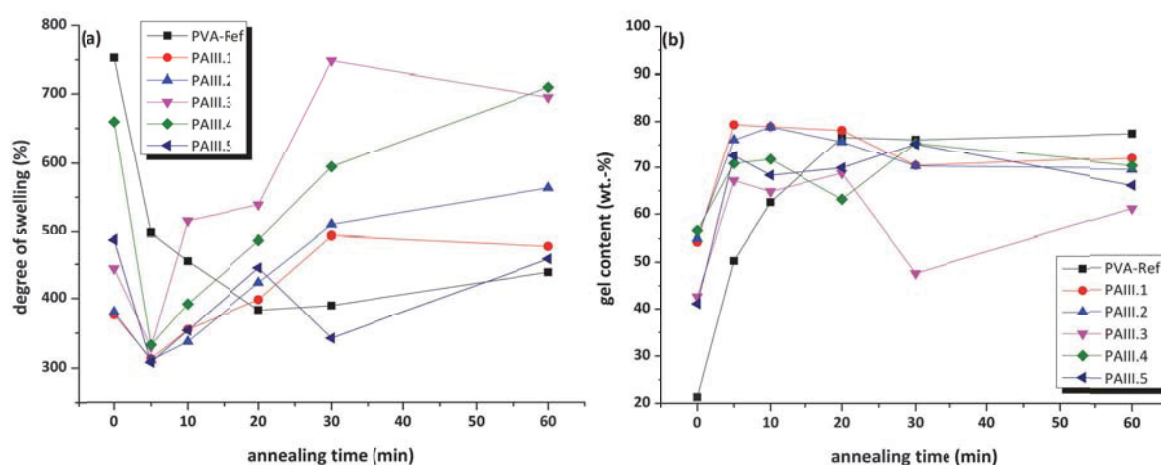
Fig. 64: Influence of annealing on the degree of swelling (a) and the gel content (b) of neat PVA and PAIII films. The lines are a guide to the eye.

While an adverse effect of the monovalent AZOIII on the solubility behaviour of heat treated azosulphonate-doped films was found, subsequent UV exposure does not lead to further deterioration of the swelling behaviour. The gel content shows a slight decrease, which may be caused by heat induced crystallisation of the polymer chains due to the high power intensity of the employed emitter (see Fig. 65).
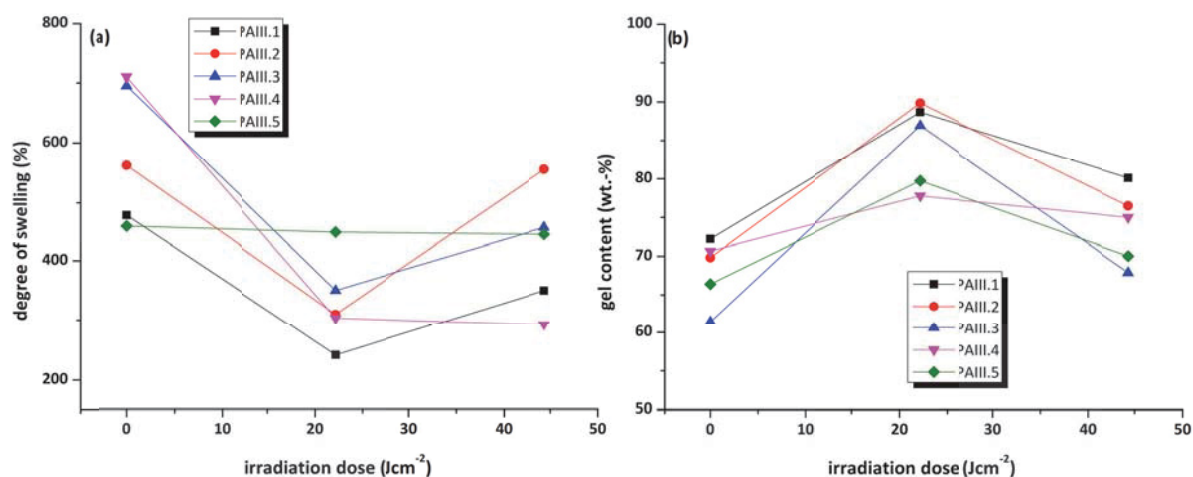
Fig. 65: Influence of subsequent UV exposure using a medium pressure Hg lamp (Fig. 13) with a power output of 740 mWcm^{-2}. (a) degree of swelling and (b) gel content of PAIII films. The lines are a guide to the eye.

2.4.2.4 Photolithographic patterning

Photolithographic patterning is performed by placing a quartz / chromium mask with 100 micron features onto thin PVA-AZO films, followed by illumination with a medium pressure mercury vapour emitter with an intensity of 740 mWcm^{-2} for 60 s. To enhance the visualisation of the pattern contrast, caused by decomposition of the azo dyes, a combination of phase contrast imaging (PCI) and polarised light imaging is employed. Images after patterning and after development in deionised water were recorded.

Films containing 2.5 wt.-% of azo dye exhibit excellent contrast behaviour under phase contrast (see Fig. 66a). After development the pattern contributes to topographical features, which can be visualised by polarised light (Fig. 66b). Some difficulties occur for visualising the phase contrast of PAII.2 after development (see Fig. 66b), the increased surface roughness of the illuminated areas may be a result of the release of nitrogen and leaching of non-coupled azo dye.

Polarised light imaging shows the sharp boundaries of the imprinted features in PAII.3, which persist the development in deionised water very well (see Fig. 66e/f). PAII.4 exhibits distinct topographical features after development, as well as an increased surface roughness. Films comprising 20 wt.-% of azosulphonate show good patterned contrast, however they seem to be grainy. It is evident, that upon development gas bubbles lead to surface cracking of the swollen polymer matrix (Fig. 68a) and leaching out of non-coupled azo dye occurs, resulting in the rough surface areas.
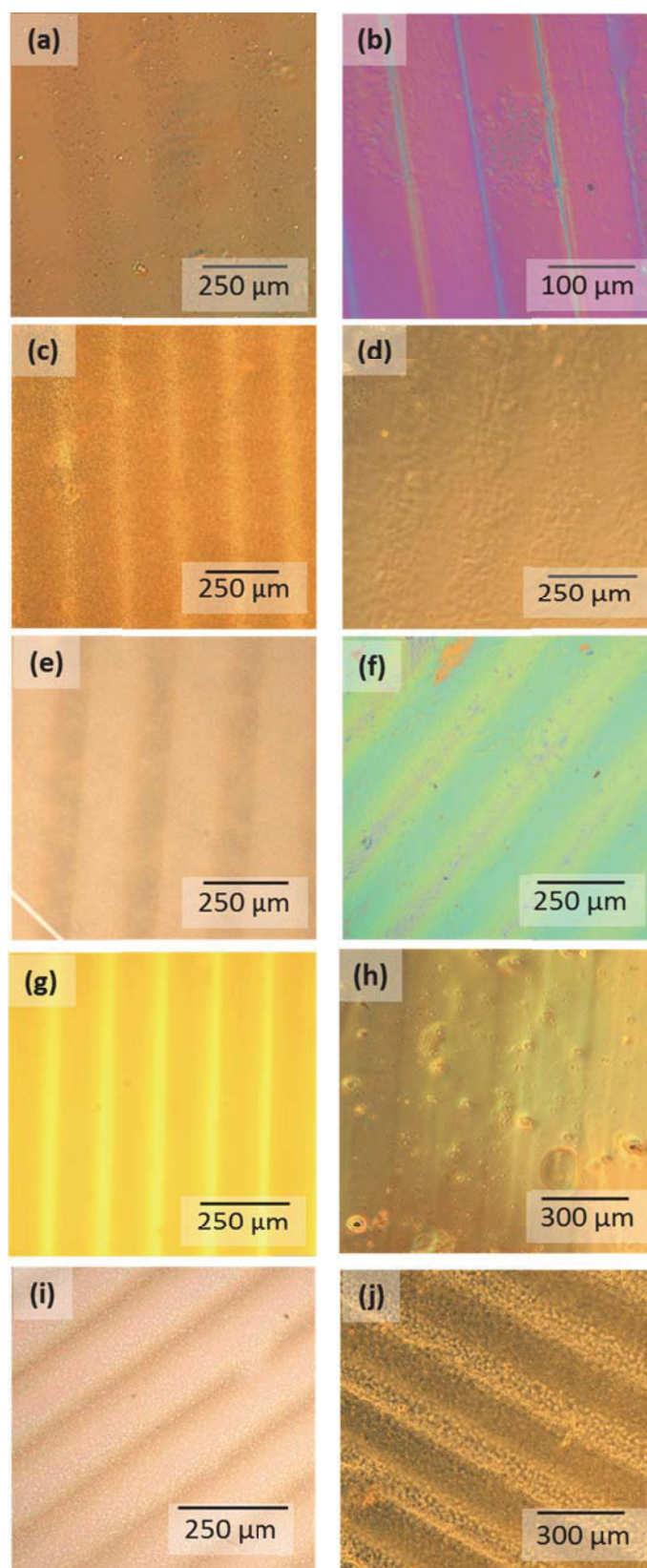
Fig. 66: Phase contrast images of thin patterned PVA-AZO films (left column) and after development in deionised water (right column); PAII.1 (a/b); PAII.2 (c/d); PAII.3 (e/f); PAII.4 (g/h); PAII.5 (i/j).

Although PVA films containing the carboxylic acid AZOIII exhibit a deterioration of the swelling behaviour compared to the difunctional dye, the photoactivity of the material leads to outstanding contrast behaviour of the patterned samples. It is evident that with increasing dye content the number of surface defects increases after development, which is caused by outgassing of cleavage products (nitrogen gas) and leaching out of non-coupled azosulphonate (see Fig. 67b/d/f/h/j).

The addition of comparatively small amounts of AZOIII (2.5 wt.-%) leads to well resolved linear patterns with sharp boundaries, which give topographical features after development (Fig. 67a/b). Samples comprising 20 wt.-% of photoactive species, seem to be grainy, which may be caused by phase separation during the drying step (Fig. 67i). During development of such samples (PAIII.5) extensive gas bubble formation occurs after short time in deionised water (see Fig. 68b).
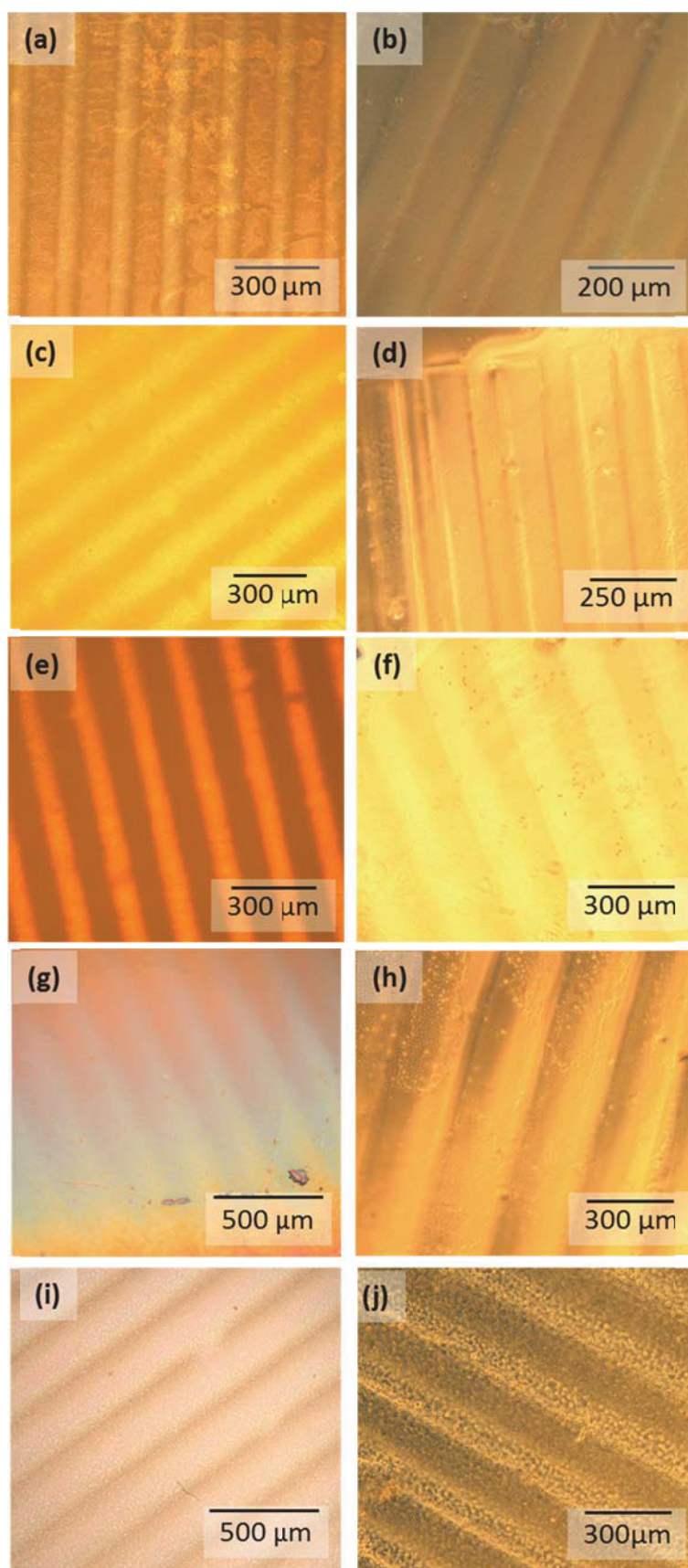
Fig. 67: Phase contrast images of thin patterned PVA-AZO films (left column) and development in deionised water (right column); PAIII.1 (a/b); PAIII.2 (c/d); PAIII.3 (e/f); PAIII.4 (g/h); PAIII.5 (i/j).

The obtained structures are a result of decomposition of the chromophore azo groups and nitrogen gas release. During the development step gas bubble formation, most likely nitrogen gas due to UV induced cleavage of the azosulphonate dyes, takes place. The bubbles are formed in the illuminated areas (bright lines, see Fig. 68), thus giving further evidence, that the patterning step is the origin of this effect.
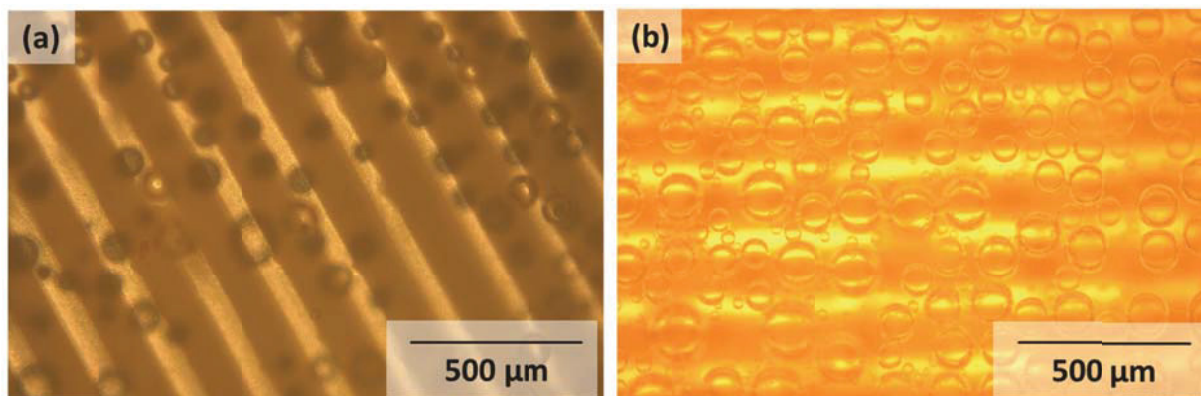
Fig. 68:   Gas bubble formation upon development of patterned samples (100 μm features; dose: 45 Jcm^{-2}) in deionised water using phase contrast imaging mode. (a) PAII.5; (b) PAIII.5.

2.4.3   *Conclusions*

Water soluble aryl azosulphonate dyes with carboxylic moieties attached to the aromatic ring (AZOII/ZOIII) have been prepared in accordance to published work (see Fig. 47).[57,61] The photolytic behaviour of AZOII and AZOIII has been investigated by decomposition in aqueous solution, providing information that the electron density of the aromatic ring is changed by UV induced cleavage of the -N=N-SO$_3^-$ group. These results are confirmed by FTIR spectroscopy of thin films on CaF$_2$ platelets, by the depletion of the –C-N=N- and -N=N- absorption bands as well as the -N-S- absorption. Thermolysis exhibits high temperature stability of the prepared photoactive dyes, with decomposition temperatures higher than 240 °C for AZOIII and 170 °C for the dicarboxylic acid AZOII.

In a novel approach a water based photoresist material comprising the prepared aryl azosulphonate compounds and poly(vinyl alcohol) has been prepared. The coupling between the photoactive carboxylic acids and the polymer by heat induced esterification has been studied. Due to detection limit issues, it is difficult to prove the coupling reaction of the carboxylic moieties and the hydroxyl groups of the polymer. At least 10 wt.-% of

azosulphonate is required to detect the formation of ester groups unambiguously by the means of FTIR and ^{13}C NMR spectroscopy.

These concentration limits also pose a problem for the investigation of the photoactivity by FTIR spectroscopy. Therefore UV-Vis spectroscopy has been employed due to the enhanced sensitivity to visualise UV induced changes for the prepared materials. As neat PVA exhibits no UV absorption, changes in the absorption spectra result from photolytic cleavage of the azosulphonate units, which can be attributed to the π-π* transition, whereas the n-π* transition is not discernible due to the low absorption coefficient.

While a heat treatment leads to crystallisation of neat PVA and therefore increased stability against dissolution in deionised water, additional condensation of the azo dyes onto the polymer backbone occurs.[16] Annealing of PVA films containing AZOII, results in the formation of additional crosslinks, thus leading to a decrease of swelling, compared to the neat polymer. In contrast to this, the monofunctional carboxylic acid AZOIII increases the distance between the polymer molecules, thus diminishing the density of the hydrogen bonding network and therefore resulting in increased solubility. Additionally the non-coupled azosulphonates are leached out of the polymer matrix by the immersion fluid (deionised water).

These novel UV reactive materials exhibit outstanding contrast behaviour after photolithographic patterning, which can be visualised by polarised light and phase contrast imaging (see Fig. 66and Fig. 67). This leads to the conclusion, that changes of the optical contrast of the thin films are a result of the cleavage of the azosulphonate groups. Strong gas bubble formation of irradiated samples is observed during the development step (see Fig. 68).

As leaching of the photoactive species occurs, the obtained materials may not be feasible for biomedical applications; hence the azo dyes are not evaluated for their biocompatibility and cytotoxicity. The decomposition products of the synthesised azosulphonates may comprise benzoic acid (E210) or isophthalic acid for radical cleavage, and m-hydroxybenzoic acid or 5-hydroxyisophthalic acid for the ionic splitting mechanism.

Due to the thermal stability of both the azosulphonate compounds and PVA, applications for high temperature coatings with tuneable polarity depending on the chemical environment (see Fig. 2) would be possible. Further adaptions concerning the coupling process of the azosulphonates onto the polymer backbone could lead to full conversion of the carboxylic moieties, thus preventing leaching of the possibly hazardous photoactive species. Another alternative to prevent leaching would be the immobilisation of the azosulphonate groups onto inorganic particle surfaces.

2.5   SUMMARY

Electron beam irradiation of PVA containing a low molecular organic crosslinking aid does not lead to improvement of the solubility behaviour. On the one hand, triallyl isocyanurate tends to migrate to the surface the samples and is leached out. Furthermore it acts as impurity, thus preventing the formation of a hydrogen bonding network and crystallite formation, which would enhance the swelling stability. As the crosslinker is considered to be noxious, no further use of this material for biomedical and food packaging applications is considered.

The preparation of UV curable metal ion doped systems such as $PVA:FeCl_3$ is considered as a viable alternative to ionising radiation curing, as the crosslinking aid is environmentally benign and leaching out does not result in cytotoxicity and irritation of sensitive tissue. Furthermore UV crosslinking leads to strong changes of the refractive index, thus giving the possibility to prepare flexible polymer waveguides. This has been investigated by Trepanier et al. by the means of prism-film coupler techniques.[10] The utilisation of Fe^{3+} ion doping for UV crosslinking would be a non-hazardous alternative for chromates, which are highly toxic and carcinogenic. To prevent leaching out of the iron salt, the preparation and utilisation of ion carrier materials such as cation exchanged alumosilicates (montmorillonite or zeolite) is investigated.

Two aryl azosulphonate dyes bearing carboxylic acid moieties attached to the aromatic ring, have been synthesised. A monovalent (AZOIII) and a difunctional acid (AZOII) are obtained, purified and the photoactivity as well as the thermal stability is determined.[57,61]

In a novel approach, PVA is doped with these azo compounds and thin films are annealed at elevated temperature to thermally induce condensation reactions between the carboxyl moieties and the hydroxyl groups of the PVA. Due to superposition of the relevant IR absorptions, it is difficult to clearly prove the formation of ester links between the dye and the matrix polymer, especially for low azosulphonate concentrations. It is observed, that the difunctional AZOII leads to an improvement of the swelling behaviour, resulting in lower degrees of swelling compared to neat PVA, but a portion of the azo dyes is leached out. After patterned illumination, the formation of gas bubbles is observed during the development steps in the exposed areas.

It is remarkable that the employment of monovalent AZOIII leads to a deterioration of the swelling properties in deionised water. This is probably caused by distortions of the hydrogen bonding network by the azo dye, therefore leading to decreased crystalline areas, which results in a deterioration of the swelling behaviour.

As previously mentioned, the preparation of modified particles, bearing azosulphonate groups on their surface would prevent leaching out of the potentially noxious compounds.

3. FUNCTIONALISATION OF INORGANIC PARTICLES

3.1 PREPARATION OF CATION EXCHANGED MONTMORILLONITES

3.1.1 *Activated montmorillonite*

Acid treatment of sodium montmorillonite clay leads to decomposition of accessory minerals (e.g. gypsum and carbonates) as well as to a warding off of biological contaminants such as bacteria, algae and fungi. Furthermore delamination of the platelets occurs, thus increasing the specific surface area of the platy clay.[69] This facilitates interlayer cation exchange and allows almost complete replacement of the sodium cations with protons. The decomposition of impurities and biological contaminants also leads to a bleaching of the montmorillonite clay resulting in an almost white clay suspension (see Fig. 69).
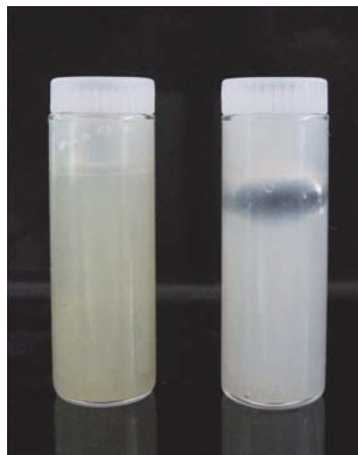
Fig. 69:   Pristine sodium MMT suspension (left) and H$^+$- MMT suspension (left). Bleaching is caused by decomposition of impurities and leaching out of the reaction products.

Due to the activation step additional silanol groups are formed, which act as hydrogen bonding sites.[77] Additionally this effect would be beneficial for the intercalation of polar organic intercalates (e.g. amino acids) as well as for the preparation of composite materials with highly polar polymers such as poly(vinyl alcohol).

EDX spectroscopy. Pristine sodium montmorillonite exhibits the typical peaks of aluminium, silicon and oxygen in the EDX spectrum (see Fig. 70a) and traces of gold, which originates out from the sample preparation by deposition of a thin film to keep the sample surface electrically conducting during the investigation. Due to treatment with HCl, the sodium cations are exchanged with protons resulting in the disappearance of the sodium K_α line at 1.04 keV (see Fig. 70a/b). Additionally no chloride (K_α = 2.6 keV) was detected with EDX spectroscopy, thus proving that the leaching and purification process was sufficient.
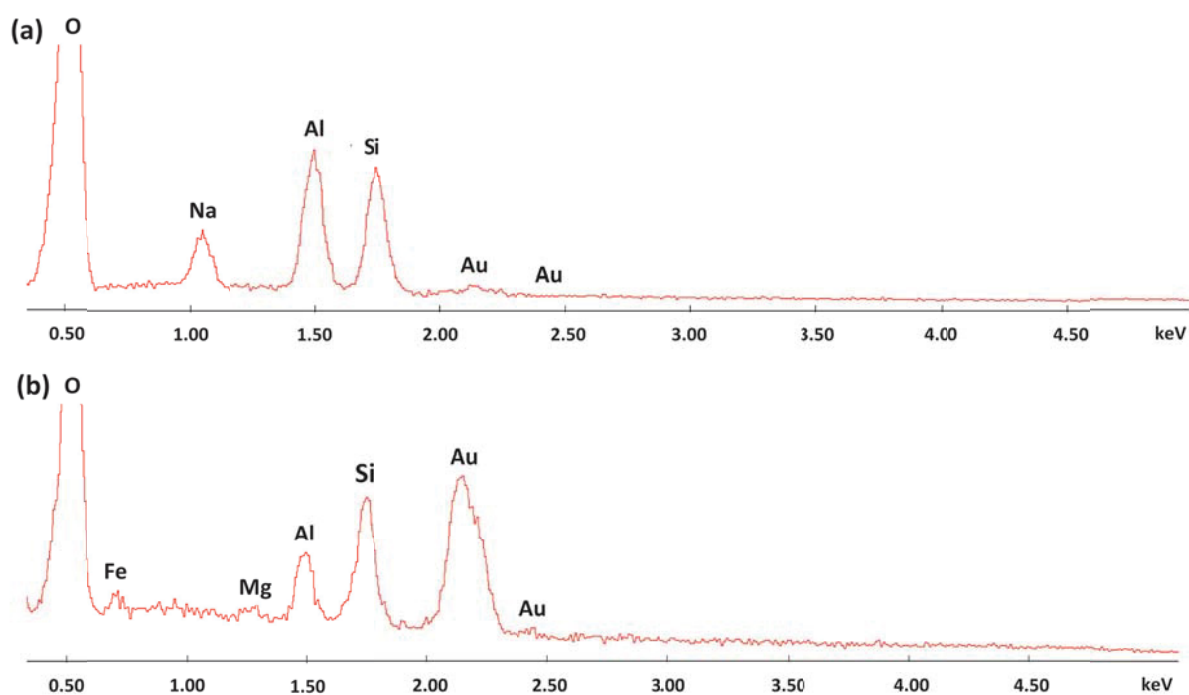
Fig. 70:   EDX spectra of pristine montmorillonite (a) and HCl activated MMT (b).

XRF spectroscopy. The elemental composition of pristine sodium montmorillonite is depicted in Fig. 71a, which resembles the findings of the EDX measurements. Additionally faint amounts of structural magnesium and iron are detected by X-ray fluorescence spectroscopy. The activation procedure with hydrochloric acid does not result in structural changes, as the elemental composition of activated montmorillonite resembles that of neat MMT. Only the sodium cations of the layered silicate are leached out and thus replaced by protons, which can be discerned in Fig. 71b by vanishing of the sodium peak.
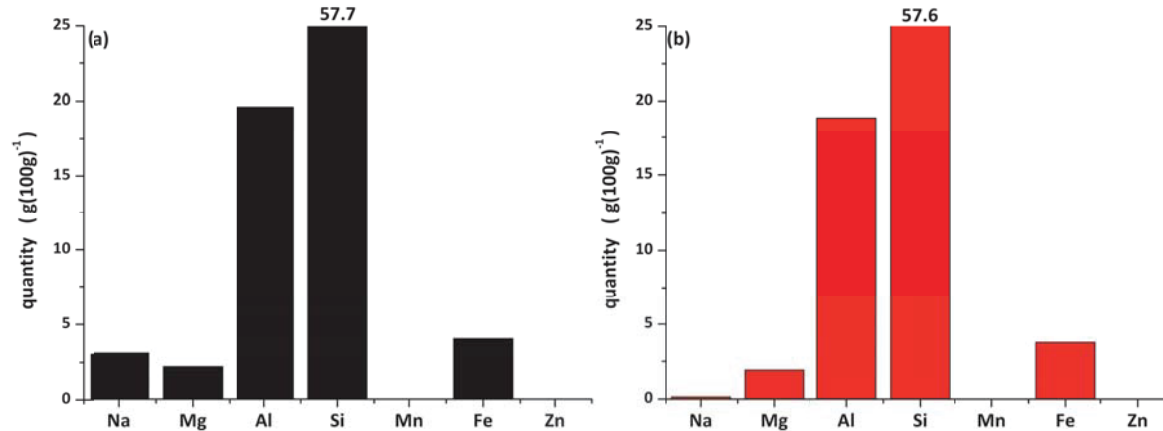
Fig. 71:   Elemental composition of (a) pristine sodium montmorillonite and (b) H$^+$-MMT

It is therefore concluded, that acid activation leads only to purification of the montmorillonite and leaching out of sodium cations from the interlayer galleries, while the structural composition of the layered silicate is not affected.

FTIR spectroscopy. FTIR spectroscopy of thin layers of MMT deposited onto CaF_2 platelets reveals a strong and sharp absorption at 3630 cm^{-1} that can be attributed to free -OH groups of the silicon platelets. Crystal water can be determined at 3220 cm^{-1} and hydrogen bonds as well between the surface and the water are detected at 3417 cm^{-1} (see Fig. 72a/b).[137,144]
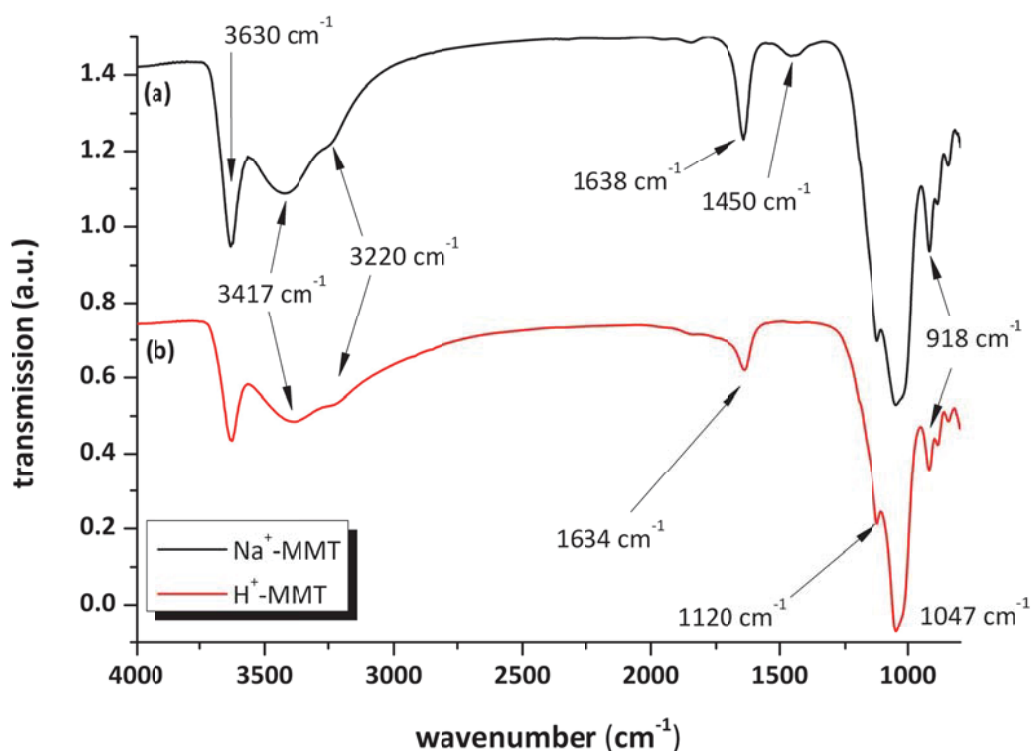
Fig. 72:   FTIR transmission spectra of thin layers of montmorillonite deposited onto CaF_2 platelets. (a) pristine Na$^+$-MMT; (b) activated H$^+$-MMT.

Due to interlayer and surface water a weak absorption band at 1634–1638 cm^{-1} arises as a result of the H-O-H bending vibration.[143,158] The montmorillonite specific Si-O absorption bands are visible at 1120 cm^{-1} and 1047 cm^{-1}, at which the former is orientation related and can be attributed to a perpendicular vibration.[159,160] Structural -OH groups of the silicate platelets can be observed in the fingerprint area at 918 cm^{-1} as the absorption band of the -O-H deformation vibration.[73,106,143,161]

Thermogravimetric analysis. As the thermal decomposition of a variety of montmorillonites has been investigated by a number of authors, different models of evaluation are employed to interpret the obtained data [101,162,163]:

In accordance to Greene-Kelly the thermogram of pristine MMT can be separated into two regions: The free water and interlayer water region to temperatures up to 300 °C and the structural water region in the range of 300 to 1000 °C[164,165], where structural -OH undergoes dehydroxylation. [101,162]

As later on some of the prepared MMTs will be subjected to organic modification, the model of Xie et al. seems more appropriate for the evaluation of the thermogravimetric curves, in which four regions of decomposition are identified: (I) the free water region up to 200 °C, followed by (II) the decomposition region of organic substances from 200 to 500 °C; (III) the structural water region up to 800 °C[101,166]; and (IV) a region where a reaction of organic carbon takes place in a not yet determined mechanism.[163] Xie's model is employed for the evaluation of the thermograms of modified particles.
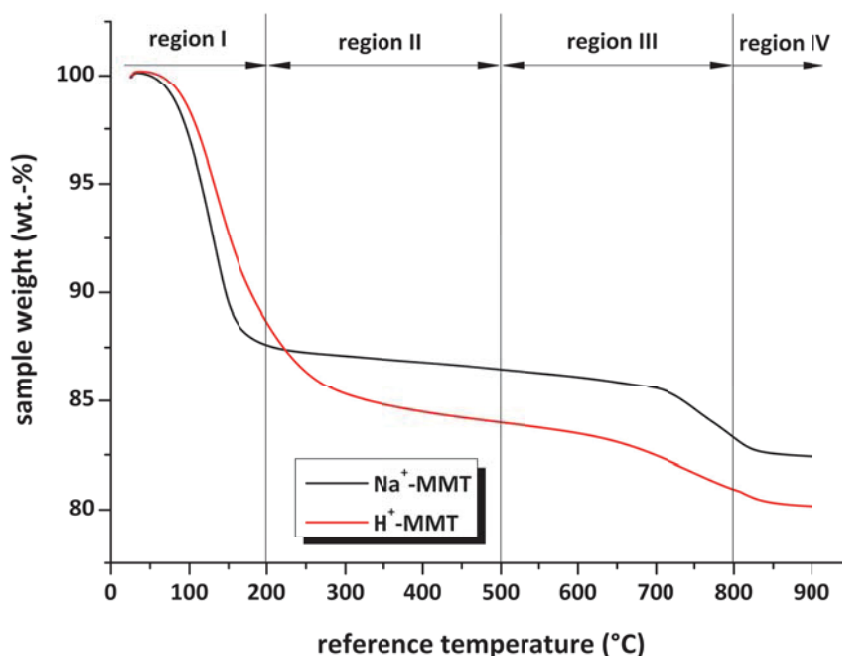
Fig. 73: Thermogravimetric curves of pristine sodium montmorillonite (black) and hydrochloric acid treated MMT (red); The curves are divided into four regions in accordance to Xie et al.[163]

In region I a total free water content for Na^+-MMT and H^+-MMT ranging between 11.5 and 12.4 wt.-% is determined (see Fig. 73). As no organic intercalates are used, the weight loss in region II is marginal for sodium MMT, whereas activated clay exhibits a weight loss of 4.5 wt.-%. This may be caused by decomposition of aluminium chloride, which is formed as byproduct of the activation by hydrochloric acid. In the temperature range of 500 to 800 °C structural hydroxyl groups are dehydrated. Additionally Xie et al. describe the formation of carbon dioxide in this region by a combination of TGA-FTIR measurements.[101,162,163,166] The shoulder at 700 °C is flattened out for acid activated MMT, which is caused by the decomposition of carbonates and organic matter.

Medium angle X-ray scattering (MAXS). The X-ray scattering patterns of dried and powdered samples, as depicted in Fig. 74, exhibit 001 reflections that can be assigned to basal spacings of 12.0 Å for pristine sodium MMT. Due to Na^+ cation exchange by protons during the acid treatment, the d_{001} spacing is reduced by 0.8 Å, which has also been found by Kwon et al. using a differing method of activation.[77] As the scattering peak does not change its form significantly it is assumed that the triple-layer structure of the silicate platelets is preserved as well as the orientation of the platelets.
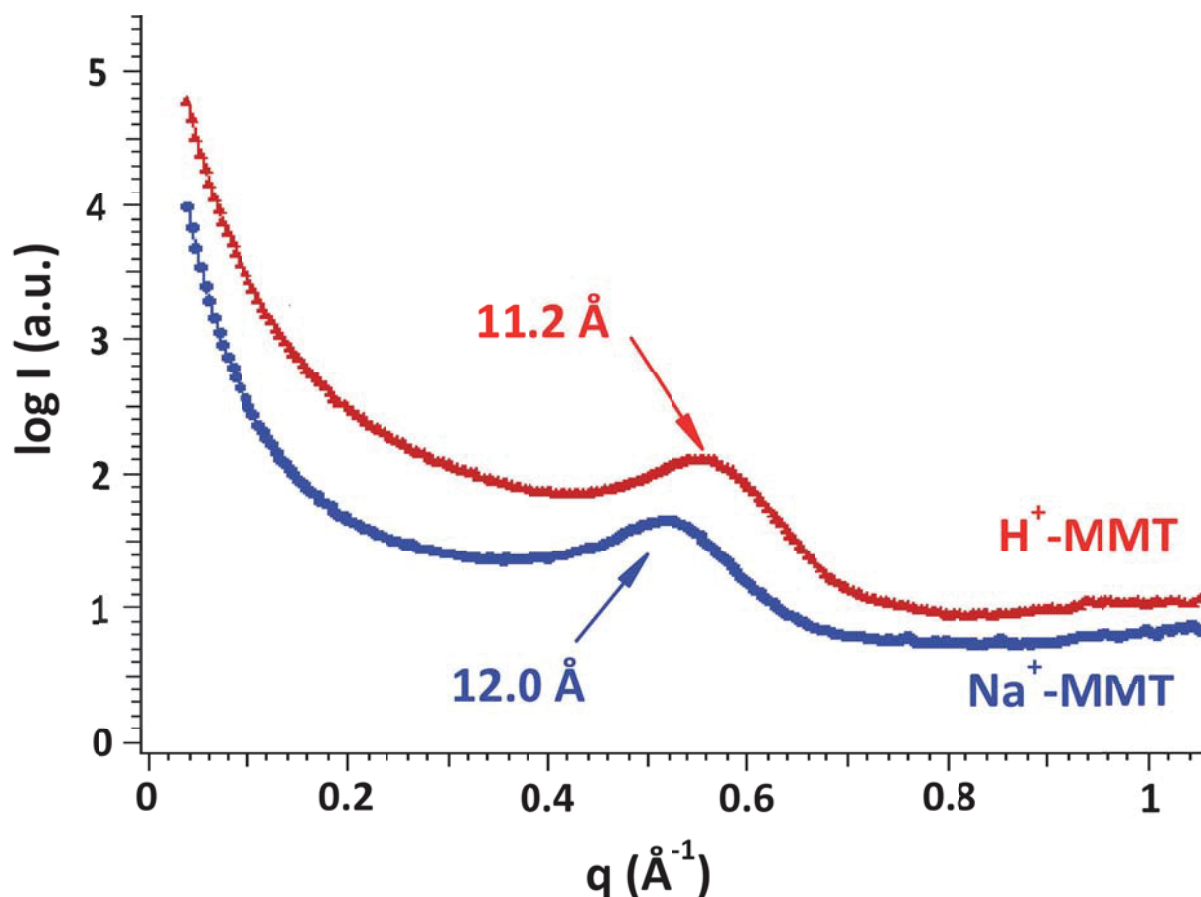
Fig. 74: Logarithmic MAXS intensity plot versus scattering vector q of pristine sodium MMT (blue) and activated H$^+$-MMT (red).

3.1.2 *Transition metal cation exchanged montmorillonites*

The preparation and purification of transition metal exchanged montmorillonites (either $Zn^{2+}/Mn^{2+}/Fe^{3+}$) is performed until no modification reagents and chloride anions are leached out. To detect successful cation exchange and replacement of interlayer sodium cations, EDX spectroscopy on solid samples is performed.

The cation exchange reaction leads to a significant colour change of the layered silicate suspensions, which is depicted in Fig. 75. As zinc intercalation leads to a whiting of the product, the manganese cations are partly oxidised to manganese dioxide resulting in a light brown colour. As Fe^{3+} cations exhibit a strong yellow to brown colour, the obtained iron(III) intercalated MMT suspension appears yellowish.
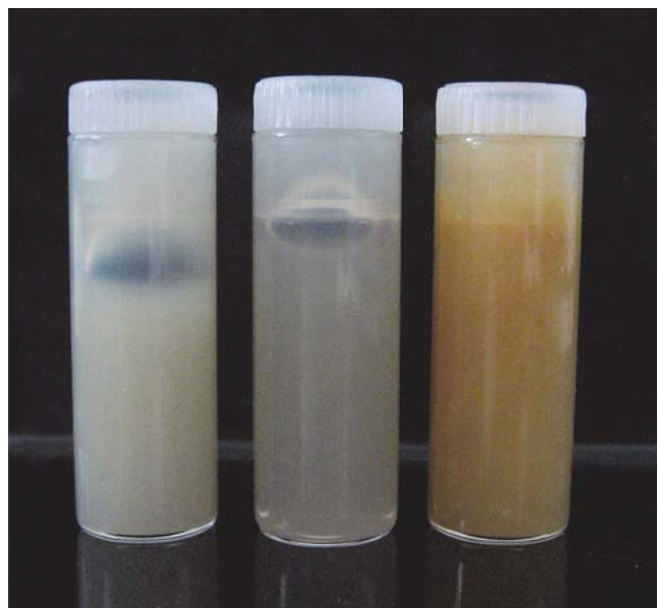
Fig. 75:   Sealed glass vials containing aqueous montmorillonite suspensions; Zn^{2+}-MMT (left); Mn^{2+}-MMT (middle) and Fe^{3+}-MMT (right).

EDX spectroscopy. Due to the cation exchange reactions and the thorough purification process, resulting in leaching out of excess modification reagents and sodium chloride, no sodium K_α line at 1.04 keV (compare Fig. 76 with Fig. 70) as well as no chlorine K_α line at 2.6 keV are detectable. Each of the obtained metal-cation exchanged MMTs exhibits the typical spectrum of the particular transition metal atoms. As the interlayer cations are exchanged, no effect on the skeletal structure lines (Si, O, Mg, Al) ranging up to 2 keV is observed (Fig. 76a/b/c).
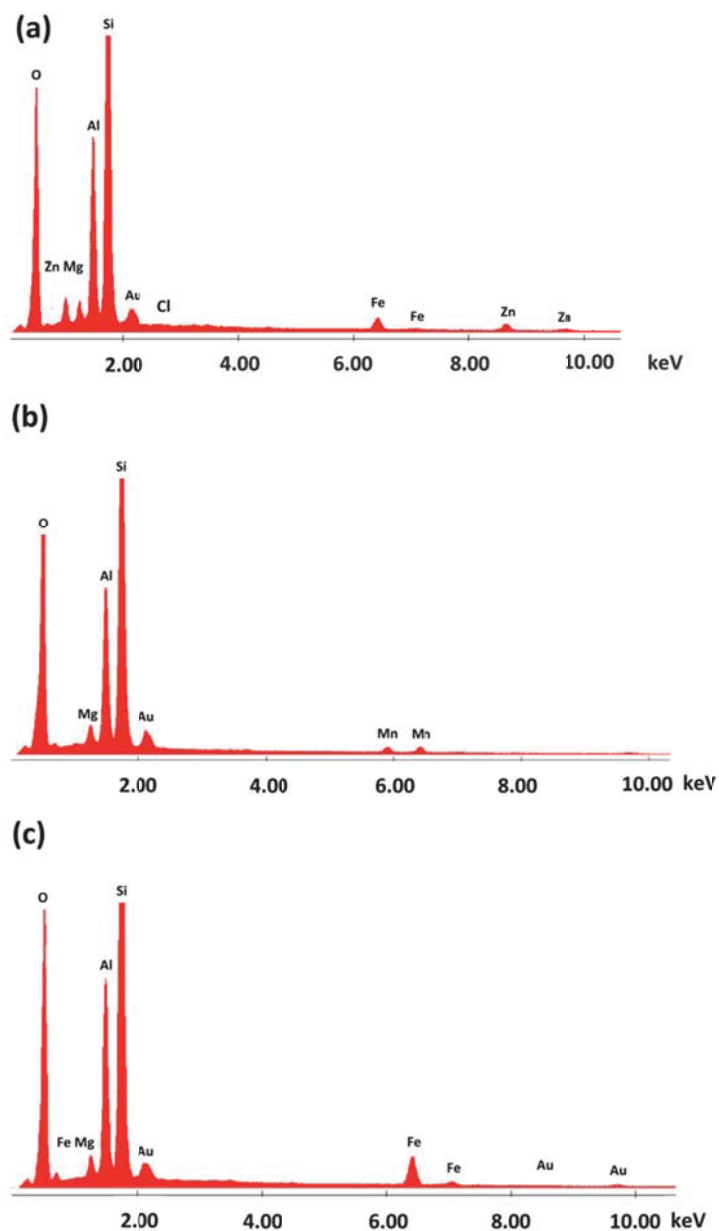
Fig. 76:   EDX spectra of transition metal cation exchanged montmorillonites: (a) Zn^{2+}-MMT; (b) Mn^{2+}-MMT; (c) Fe^{3+}-MMT.

XRF spectroscopy. The exchange of interlayer sodium cations with transition metal cations results in diminishing of the sodium content of the layered silicate, while no changes of the structural magnesium, silicon and aluminium peaks are observed (compare Fig. 77a-d). Additionally elemental specific signals arise due to successful intercalation of the particular transition metal cations as observed for Zn^{2+}- and Mn^{2+}-MMT (see Fig. 77b/c). Due to adsorption of Fe^{3+} ions onto the negatively charged surfaces, the iron content of the layered silicate almost doubles (see Fig. 77d).
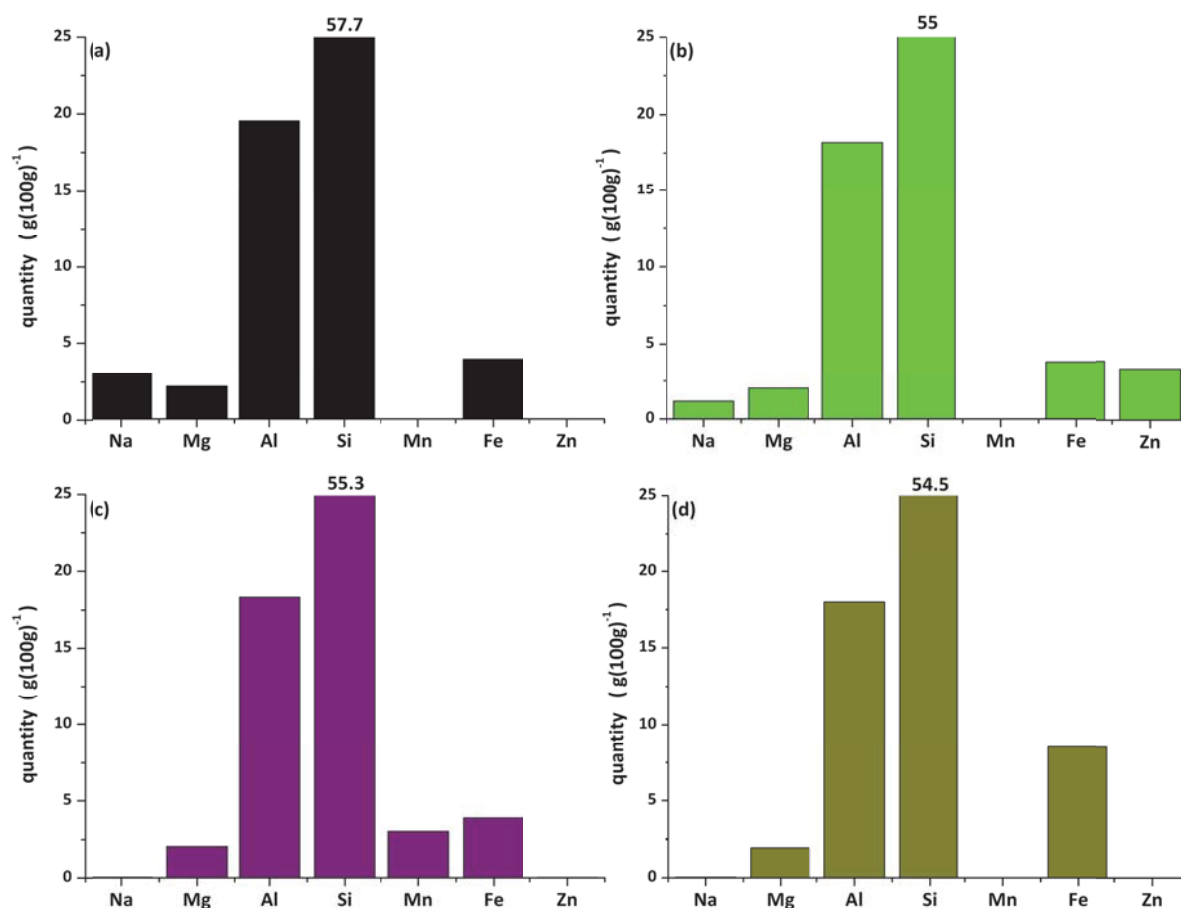
Fig. 77: Elemental composition of interlayer cation exchanged montmorillonites; (a) Na^+-MMT; (b) Zn^{2+}-MMT; (c) Mn^{2+}-MMT; (d) Fe^{3+}-MMT

FTIR spectroscopy. As no organic intercalates are incorporated into the interlayer galleries of transition metal cation exchanged MMTs, the FTIR spectra exhibit the typical montmorillonite structures, which have already been described in Fig. 72. Surface and crystal water (3220 cm^{-1}) as well as H-O-H bending vibrations (1638 cm^{-1}) resulting from free water and hydrogen bonding (3417 cm^{-1}) are detected. Structural -OH groups contribute to the sharp absorption at 3630 cm^{-1}.[73,106,143,161] The structural absorptions of Si-O and Si-O-H at wavenumbers of 1120–918 cm^{-1} do not undergo changes[159,160], leading to the conclusion that the skeletal structure of the obtained montmorillonites is not affected by the cation exchange reactions.
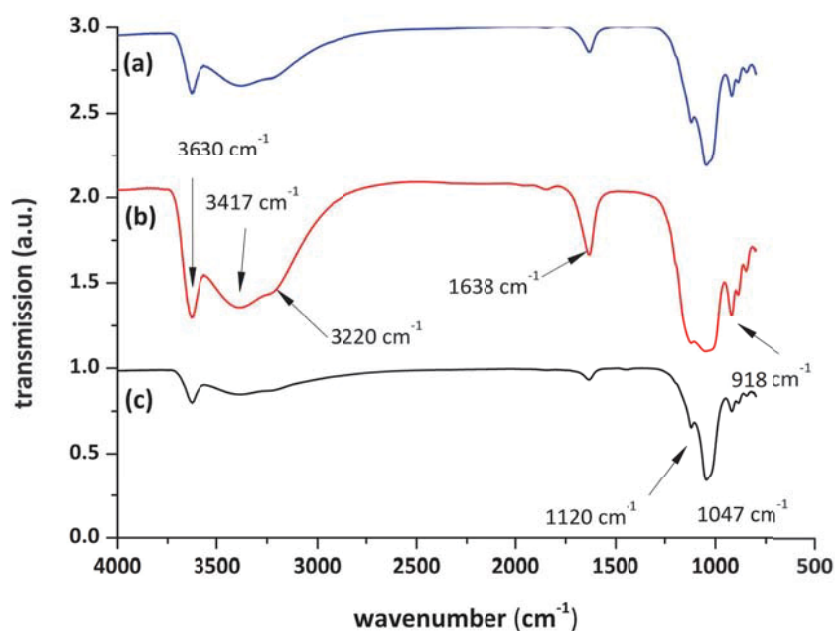
Fig. 78: FTIR spectra of thin layers of metal-cation exchanged montmorillonites deposited onto CaF_2 platelets; (a) Zn^{2+}-MMT; (b) Mn^{2+}-MMT; (c) Fe^{3+}-MMT.

Thermogravimetry. Thermogravimetric measurements of the transition metal cation exchanged montmorillonites reveal that only minor differences in the free water region (region I) occur. At temperatures above 200 °C the curves are almost parallel and exhibit no unexpected weight loss phenomena.
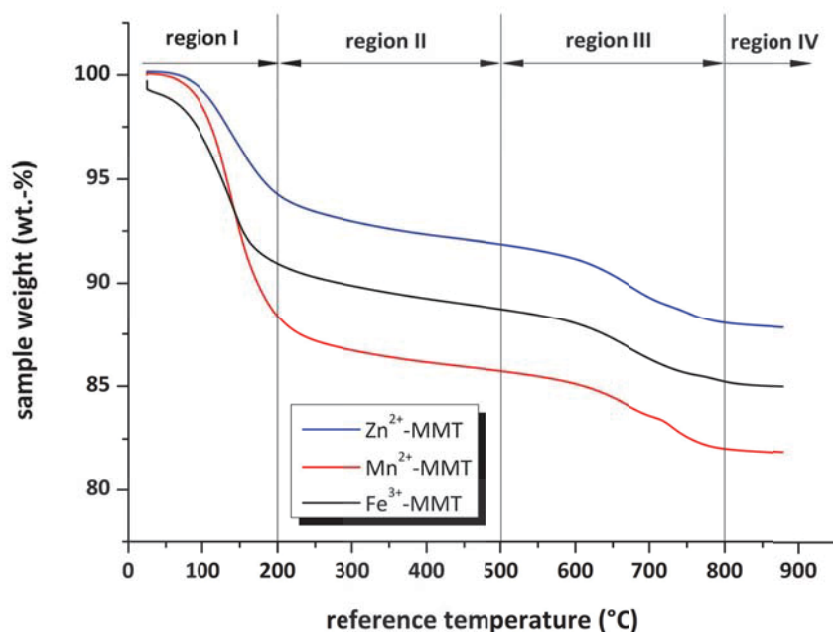
Fig. 79: Thermogravimetric curves of metal cation exchanged montmorillonite clays; purge gas: nitrogen; heating rate: 20 Kmin^{-1}.

The characterisation of metal cation exchanged MMTs reveals the limitations of TGA and FTIR methods, which are more suitable for the detection of organic intercalates. It has to be stated, that none of these methods was employed in scientific literature in this context. Otherwise, it is demonstrated that the prepared MMTs are free of organic or biological impurities and no unexpected decomposition mechanism are found by thermogravimetry.

UV-Vis spectroscopy. As the obtained Fe^{3+}-MMT is intended for the use as carrier material for the photoactive species Fe^{3+}, UV-Vis absorption kinetics were collected upon irradiation with a spot curing unit. Due to UV exposure slight changes of the UV-Vis spectrum in a wavenumber range of 320 to 380 nm occurs (see Fig. 80a), following an almost exponential decay for increasing exposure times (see Fig. 80b). The absorption can be assigned to the photoactive species Fe^{3+}, the depletion to the photoreduction to Fe^{2+}.[9,11,47]. The Fe^{3+} ions are immobilised at the montmorillonite surface, leaching of the interlayer cations by water and highly polar organic solvents (e.g. DMSO) is hampered.
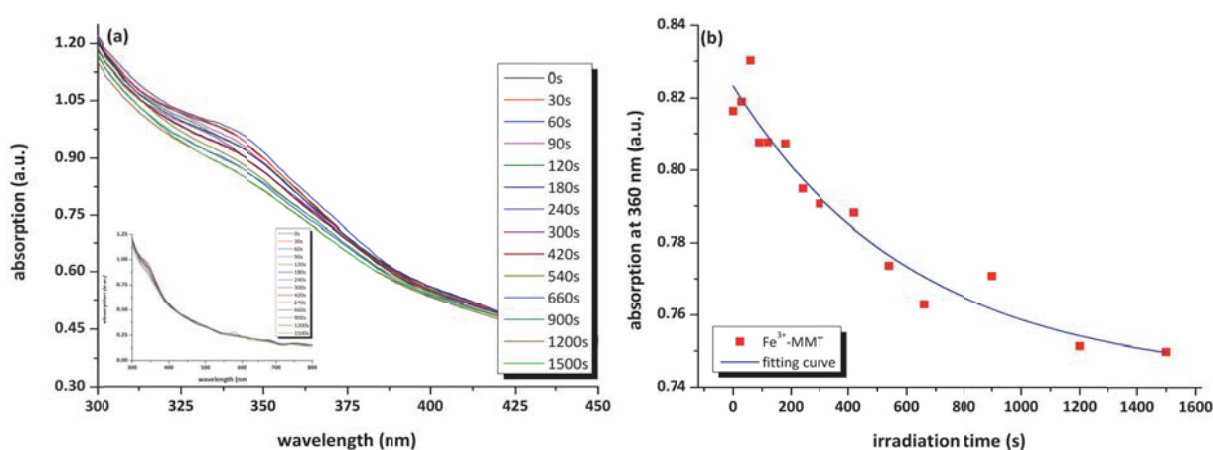
Fig. 80:   Detail UV-Vis absorption spectra of an aqueous Fe^{3+}-MMT suspension (a) with its changes due to irradiation with a spot curing unit with an intensity of 9.25 $mWcm^{-2}$. (b) absorption at 360 nm plotted versus irradiation time.

Conclusions. The successful exchange of interlayer sodium cations by transition metal ions is detected by EDX spectroscopy, proving that sodium is entirely leached out of the montmorillonites. Furthermore no chloride anions are detected by precipitation with $AgNO_3$ and EDX spectroscopy, proving that exchange reaction product NaCl and excess modification reagent are removed thoroughly. It is further demonstrated that thermogravimetry and FTIR spectroscopy are no suitable methods for characterisation of metal cation exchanged MMTs.

Montmorillonites containing bivalent metal cations (Zn^{2+}/Mn^{2+}) are intended for the application as crosslinking aids for XNBR latex, to substitute conventional crosslinking chemicals such as ZnO. As the active species is immobilised on the negatively charges platelet surface, leaching of the active sites should be prevented. The obtained minerals are considered to be biocompatible, which would make the application for biomedical rubber products feasible. Additionally strong polymer-filler interactions can lead to an improved solvent resistance against crude oil or chloroform.

The photoactivity of Fe^{3+}-MMT paves the way to a dual crosslinking of PVA, by either physical polymer-MMT surface interaction and UV induced radical crosslinking as reported by Schauberger, Kuncser and Manivannan.[9,44,46] The particular MMT is considered environmentally benign with the advantage that the transition metal ions cannot be released into water or leached out of a polymer-MMT composite. This would be most beneficial for the preparation of biocompatible UV-crosslinked PVA hydrogels and materials for food packaging applications. Furthermore Fe^{3+}-MMT may be applied as aqueous based radical photoinitiator for a number of applications such as resin curing or for additional UV crosslinking of rubbers by the radical thiol-ene reaction.[89]

3.1.3 *Amino acid intercalation*

Amino acid intercalated montmorillonites are prepared in accordance to the methodology described on page 43. Montmorillonites that have been modified with L-cysteine are marked with "_C" as suffix; glycine modified MMTs with "_G" and taurine intercalated clays with "_T" as suffix.

FTIR spectroscopy. As infrared spectroscopy is very sensitive to detect organic substances it is employed in a first attempt to determine the successful intercalation of amino acids into the interlayer galleries of the obtained MMTs. As the typical absorptions of pristine sodium and activated montmorillonite have been displayed and evaluated in detail in Fig. 72, the focus of the recent investigation is set on the detection of intercalated organic amino compounds.

The amino acid treated MMTs exhibit an absorption peak at 1635 cm^{-1}, which is not solely caused by the H-O-H bending vibration, but also by the protonated amino groups of the

intercalates. A weak absorption arises at 1445 cm^{-1}, which can be attributed to the -CH deformation vibration.[73,106,158]

The C=O absorption at a wavenumber range of 1750-1700 cm^{-1} is weak, due to the intercalation of the amino acid between the montmorillonite sheets. This effect is also observed on the second absorption band of -NH$_3^+$-groups at 1490 cm^{-1} that should appear on the spectra.[106] Though the IR measurements clearly show, that the intercalation reaction is feasible, the amount of intercalated modification reagents cannot be quantified by means of infrared spectroscopy.
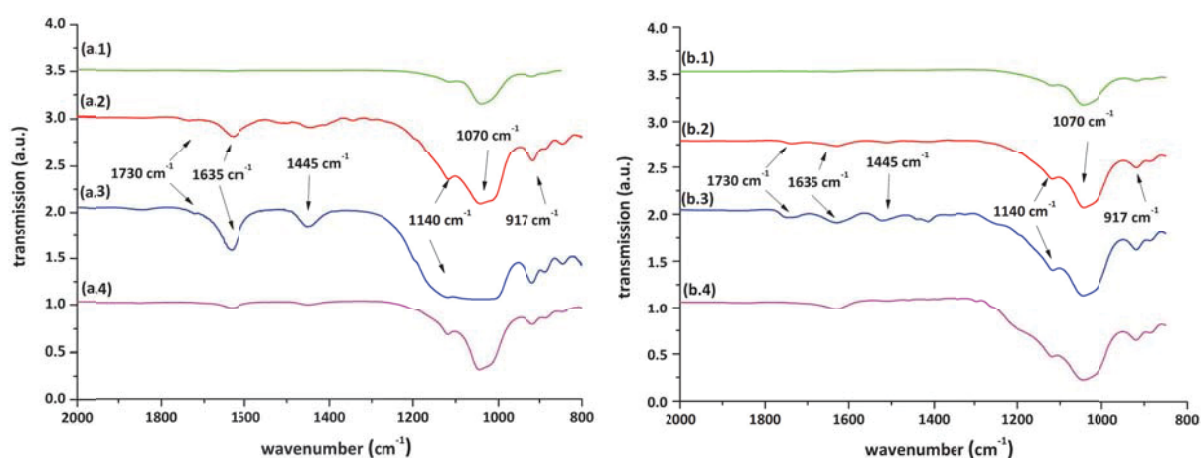
Fig. 81:   FTIR spectra thin films of amino acid intercalated montmorillonite, which are deposited onto CaF$_2$ platelets: (a.1) Na$^+$-MMT, (a.2) Na$^+$-MMT_C, (a.3) Na$^+$-MMT_G, (a.4) Na$^+$-MMT_T; (b.1) H$^+$-MMT, (b.2) H$^+$-MMT_C, (b.3) H$^+$-MMT_G, (b.4) H$^+$-MMT_T.

Thermogravimetric analysis. TGA measurements of dried functionalised montmorillonite samples are conducted in accordance to the described parameters and evaluated based on Xie's method.[163]. The thermograms of the clays are depicted in Fig. 82, while the calculated weight loss in the appropriate regions is noted in Table 16.

Region I: Sodium MMT and acid-activated MMT exhibit a total free water content between 11.5 and 12.4 wt.-%, while the organo modified clays show water contents ranging from 3.5 to 9.1 wt.-%. It is remarkable that the activated and subsequently organo-modified clays show lower free water content than organo modified sodium montmorillonites. This may be caused by the displacement of interlayer water due to intercalation of amino compounds and a more organophilic nature of the particles.[101,166]

Region II: The intercalated organic content of the amino acid-modified montmorillonite clays is defined as the weight loss in the range of 200-500 °C. Pristine sodium MMT exhibits a weight loss of about 1 wt.-% in this region and H$^+$-MMT of 4.5 wt.-% resulted by the decomposition of aluminium chloride, which is formed as byproduct of the activation by reaction with hydrochloric acid.

While the organo modified sodium montmorillonite clay exhibits organic contents up to 7.8 wt.-%, the preliminary activation step with hydrochloric acid leads to increased delamination of the platelets, therefore facilitating the cation exchange reaction.[77,81] This leads to organic contents ranging from 10.9 wt.-% for L-cysteine intercalated silicate up to 15.5 wt.-% for glycine-modified H$^+$-MMT, and a taurine content of 12.2 wt.-%. The thermal stability of taurine is at about 100 °C higher compared to the amino acids, which start to decompose at temperatures ranging from 228 to 235 °C (compare with Fig. 82b.5 and Table 16).
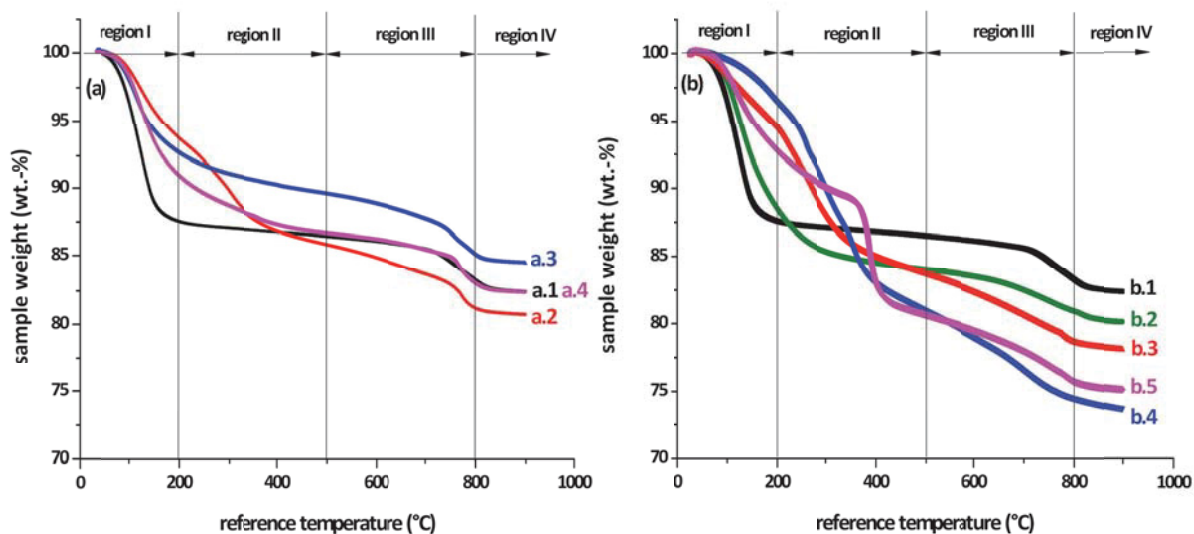
Fig. 82: Thermograms of clay samples: (a.1) Na$^+$-MMT, (a.2) Na$^+$-MMT_C, (a.3) Na$^+$-MMT_G, (a.4) Na$^+$-MMT_T; (b.1) Na$^+$-MMT (b.2) H$^+$-MMT, (b.3) H$^+$-MMT_C, (b.4) H$^+$-MMT_G, (b.5) H$^+$-MMT_T. Heating rates of 20 Kmin^{-1} under dynamic nitrogen atmosphere were applied.

Region III and IV: In the temperature range of 500 to 800 °C the hydroxyl groups, which are covalently incorporated in the crystal structure are dehydrated. In addition to this, Xie et al found out by combined TGA-FTIR measurements, that CO_2 is generated in this region, which could be the result of decomposition products of organic matter or carbonates and oxygen of the crystal structure of the MMT.[101,162,163,166]

Table 16: Weight loss in the identified decomposition regions of pristine and amino acid modified montmorillonite clays according to Xie et al.[163]

sample	region I	region II	region III	region IV
	T < 200 °C (wt.-%)	200 – 500 °C (wt.-%)	500 – 800 °C (wt.-%)	800 – 900 °C (wt.-%)
Na⁺-MMT	12.4	1.1	3.2	0.8
Na⁺-MMT_C	6.3	7.8	4.7	0.5
Na⁺-MMT_G	7.3	3.1	4.4	0.6
Na⁺-MMT_T	9.1	4.2	3.7	0.6
H⁺-MMT	11.5	4.5	3.1	0.8
H⁺-MMT_C	5.4	10.9	5.1	0.5
H⁺-MMT_G	3.5	15.5	6.5	0.8
H⁺-MMT_T	7.2	12.2	4.9	0.6

MAXS measurements. Fig. 83 shows the MAXS patterns of pristine sodium montmorillonite, activated MMT and amino acid intercalated H⁺-MMTs. Clays that are prepared by the one step process from sodium MMT are not evaluated, due to their comparatively low organic content. According to Khan et al. the basal spacing of organomodified montmorillonite is depending on the chain length of the intercalates and their orientation. They may be arranged as monolayer or bilayers.[104,167,168]

The obtained patterns provide evidence that the d_{001}-spacing is altered by either the activation step (Fig. 83a/b) as well as the intercalation reaction of organic cations (Fig. 83c/d/e). The decrease of the basal spacing by exchange of sodium by protons during the activation step is described in chapter 3.1.1. The intercalation of amino acids into the interlayer galleries leads to an increase of the layer-to-layer distance. Cysteine intercalated MMT exhibits a layer-to-layer distance of 13.7 Å, while glycine modified MMT shows a spacing of 12.6 Å.

The intercalation of taurine leads to a remarkable scattering profile, which is depicted in Fig. 83e. A broad peak with maxima at q-values of 3.8 Å⁻¹ and 4.8 Å⁻¹ arises, which suggests the existence of monolayers and bilayers of the aminosulphonic acid clay compound.[167,168] These peaks can be attributed to d_{001}-spacings of 17.2 Å and 13.0 Å, which corresponds to the findings of Lagaly, concerning mono- and bilayers of alkyl ammonium ions that are bound onto the clay surface.[168]
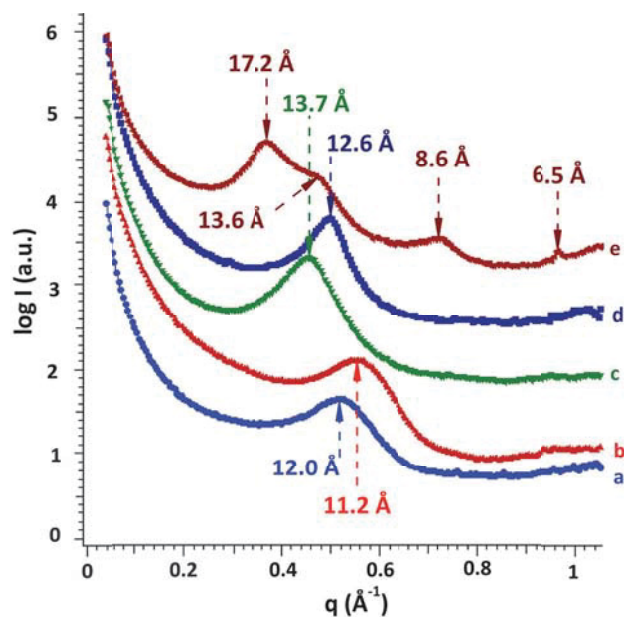
Fig. 83: MAXS patterns of powdered montmorillonite clay samples. (a) Na^+-MMT, (b) H^+-MMT, (c) H^+-MMT_C, (d) H^+-MMT_G, (e) H^+-MMT_T.

Conclusions. It is demonstrated that the treatment of sodium montmorillonite with hydrochloric acid results in activated surface areas that are more accessible to modification with amino acids under acidic conditions than pristine Na^+-MMT. Infrared spectroscopy reveals successful intercalation of organic compounds qualitatively, while thermo gravimetric measurements show that activated MMTs exhibit a significant increase of organic content compared to organo modified Na^+-MMT (compare Table 16, region II). Furthermore the expulsion of intercalated water molecules is observed upon the modification procedure.[101]

The d_{001}-spacings of MMT are decreasing due to exchange of Na^+ by H^+, which leads to an increased organophilic behaviour of the modified clay minerals. The interlayer distance of glycine and L-cysteine intercalated H^+-MMT suggests that a monolayer of the modification reagent is formed. The intercalation of taurine into the interlayer galleries leads to the formation of two diffraction peaks that can be attributed to bilayer and monolayer arrangement.

Since the prepared clay minerals were purified until no more excess modification reagents are leached out, these modification reagents are considered to be fully immobilised. Modified clay minerals could be implemented as functional additives for crosslinking of water soluble polar polymers such as poly(vinyl alcohol). Further advantages of such

prepared materials would be the biocompatibility and recyclability as well as the water solubility.

The immobilisation of the thiol moiety of cysteine in the interlayer galleries gives the feasibility for the employment as sequestrant to precipitate heavy metals such as Hg and Cd or for covalent bonding of the clay onto double bonds by the thiol-ene reaction.[82,89,169,170] The free carboxylic acid groups of the glycine and L-cysteine intercalated montmorillonite may be used for acid catalysed esterification reactions with polymers bearing hydroxyl functionalities such as poly(vinyl alcohol), poly(ethylene-co-vinyl alcohol) and poly(p-hydroxy-styrene).[171] As the sulphonic acid moiety is well known for its cation exchange ability and its catalytic properties, the taurine intercalated clay may be applied in such a manner.[108,109]

3.2   PREPARATION OF SURFACE FUNCTIONALISED PARTICLES

Inorganic particles bearing aryl azosulphonate moieties on their surface have been prepared in accordance to the multi-step process, which is ascribed in section 3.4.2. After proper purification steps by osmosis using deionised water, a fraction of the obtained dispersions was dried for further characterisation steps, except MMTa, which exhibits a very low particle yield (see Table 17). Therefore no thermogravimetric measurements to determine the amount of immobilised organic substance on the surface could be conducted for this particular montmorillonite fraction.

Table 17: Notation of prepared surface modified particles, the particle type and the particle to silane ratio.

notation	particle type	particle/silane (weight ratio)	remarks
P1	fumed silica	1:1	
P2	fumed silica	1:2	
P3	fumed silica	1:4	
NP	silicon nanoparticles (10-20 nm)	1:1	
MMTa	H^+-MMT (filtrate 0.45 µm - Millipore)	1:1	low yield; only suitable for determination of photoactivity
MMTb	H^+-MMT (fine fraction)	1:1	
MMTc	H^+-MMT (coarse fraction)	1:1	
MMTd	H^+-MMT (no filtration)	1:1	

3.2.1   *Surface silanisation*

By a three step synthesis, a photoreactive azo dye has been immobilised onto the surface of inorganic particles, which should exhibit similar decomposition behaviour upon UV exposure as the already described aromatic azosulphonate dyes.

As FTIR spectroscopy is a very sensitive method to confirm the presence organic compounds it is employed in a first attempt to prove successful surface modification of the obtained silicon dioxide particles. This is followed by thermogravimetric analysis to quantify the amount of immobilised organic substance on the surface.

Fumed silica particles. Pristine fumed silica particles exhibit very strong absorption at wavenumbers ranging from 1250 to 950 cm^{-1}, as a result of the Si-O absorption as well as the structural -OH groups. [73,106,143,161] A faint signal at 1650 cm^{-1} is caused by the H-O-H bending vibration from residual water.[158]

Surface modified particles on the other hand show several absorption regions, which can be attributed to the immobilised aryl azosulphonate moieties. The water absorption at 1650 cm^{-1} is superposed by the -C=C- valence vibration and a new absorption band arises at 1490–1430 cm^{-1}, which is caused by the aromatic =CH and the -C=C- stretching vibration.[137,144] The azosulphonate moiety contributes to the absorption region at 1300–1190 cm^{-1}, resulting from the Ar-N=N- absorption and the -N=N- stretching vibration. The -N-S- stretching vibration at 1055 cm^{-1} is superposed by strong Si-O- and -O-H signals from the particles themselves (see Fig. 84a). No differences of the IR spectra of P1 to P3 were evidenced, although different weight ratios silane / particles were employed during the modification step.
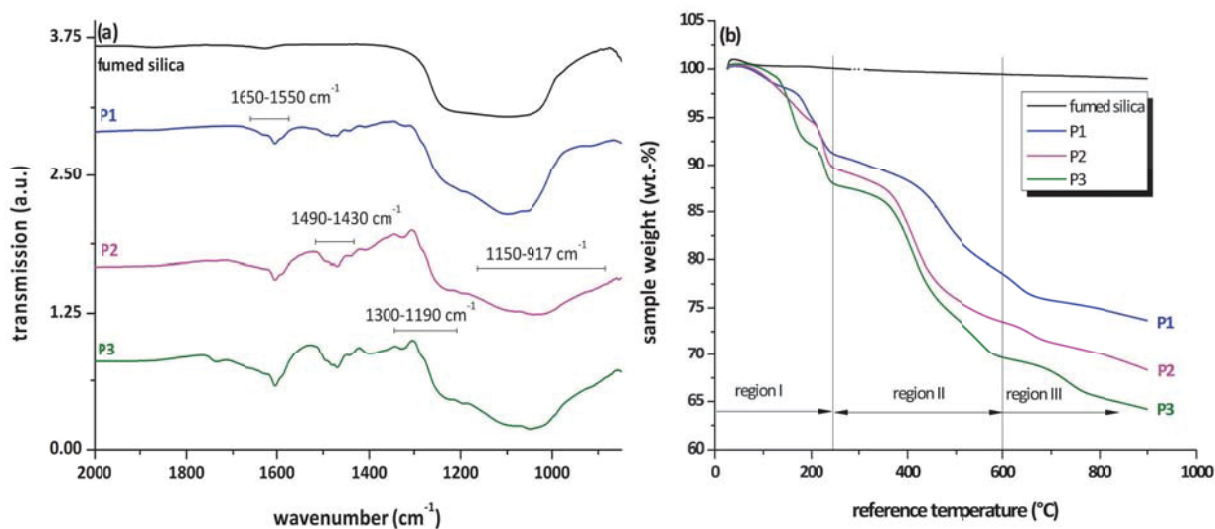
Fig. 84: (a) FTIR spectra of surface modified fumed silica particles (thin layers on CaF_2 platelets); (b) thermogravimetry curves of the obtained particles.

Thermogravimetric analysis shows that the neat fumed silica particles exhibit about 1.6 wt.-% mass loss, hence no organic substance is attached to the surface. The TGA curves recorded for surface modified particles are divided into three decomposition regions, and evaluated in accordance to this method. In the first region (up to 250 °C) the evaporation of water takes place, as well as the thermal decomposition of the azo groups.[154] Region II contributes to the decomposition of the propyl group of the modification reagent (see Table 1) and of the aromatic ring.[61] At temperatures higher than 600 °C the residual SO_3 groups tend to decompose, also dehydroxylation of the structural -OH groups occurs as reported by Holt, Shuali, Khan and Xie. [101,155,163,166]

Besides a high mass loss in region I, resulting from water release up to 150 °C (see Fig. 84b), followed by the decomposition of the azo groups, the modified particles exhibit strong weight losses in region II. This weight loss can be correlated with the weight ratio particle / silane. As for the modification of P3 the highest amount of functional silane was employed, these particles exhibit the highest weight loss in this region. The weight loss in region III is nearly identical for P1-P3 thus indicating that the immobilised azosulphonate groups are decomposed at temperatures up to 600 °C. In contrast to the report of Holt the main portion of SO_3^{2-} is split of at lower temperatures.[155]

Table 18: TGA weight loss fumed silica particles

sample	region I	region II	region III	Δm_{total}
	Up to 250 °C (wt.-%)	250 – 600 °C (wt.-%)	600 – 900 °C (wt.-%)	(wt.-%)
fumed silica	0	0.6	1	1.6
P1	8.8	12.8	5	26.6
P2	10.4	15.5	5.2	31.1
P3	12.3	18.5	5.5	36.3

Silicon nanoparticles. The infrared spectrum of neat SiO_2 nanoparticles (size: 10–20 nm) resembles the spectrum of fumed silica particles (compare Fig. 84a and Fig. 85a). Surface modification leads to a faint signal of an aromatic system in the areas of 1650–1550 cm^{-1} and 1490-1430 cm^{-1}. The absorption bands of the azo groups is obscured by the SiO_2 absorption bands.
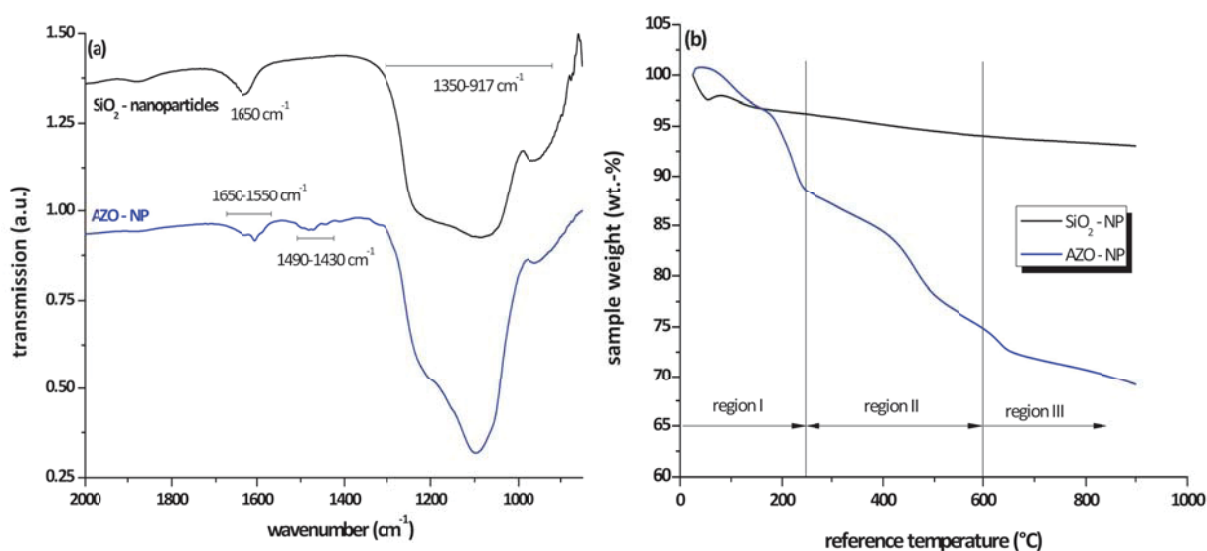
Fig. 85: (a) FTIR spectra of surface modified silica nanoparticles (thin layers on CaF_2 platelets); (b) thermogravimetry curves of the obtained particles.

The thermogravimetric curve of the neat nanoparticles exhibits a weight loss of 2.5 wt.-% in the low temperature region (up to 80 °C), which is caused by displacement of particles by the purge gas flow. Besides this effect an overall mass loss of 3.5 wt.-% is determined in the temperature range from 80 °C to 900 °C. The modified particles exhibit a high mass loss of 11 wt.-% in region I, followed by the decomposition of the main part of immobilised organic substance from 250 to 600 °C (region II), resulting in a loss of about 14 wt.%. As previously discussed, the weight loss in region III is relatively low (5.5 wt.-%), leading to the conclusion

that the sulphonic groups undergo decomposition at lower temperatures. The overall mass loss of the modified particles of about 31 wt.-% provides evidence that the nanoparticle modification was performed successfully.

Montmorillonites. Four different montmorillonite fractions have been obtained by the means of different separation techniques and have been subjected to immobilisation of azosulphonate moieties on the surface. MMTa has been obtained by filtration through a Millipore syringe filter with particle sizes below 0.45 µm; MMTb and MMTc were prepared by sedimentation, where MMTb is the fine fraction and MMTc the coarse fraction. MMTd has not been subjected to separation techniques.

The infrared spectra of activated H^+-MMT and the modified MMT fractions (MMTa-d; see

Table 17) show the typical aryl azosulphonate absorptions, as previously discussed in detail. The absorption bands at 1650–1550 cm^{-1} and 1490–1430 cm^{-1} are attributed to the aromatic ring, whereas the azo-groups are discernible at a wavenumber range of 1300–1290 cm^{-1}. The structural absorption bands of the montmorillonite structure are described in detail in section 3.1.1 and Fig. 72.
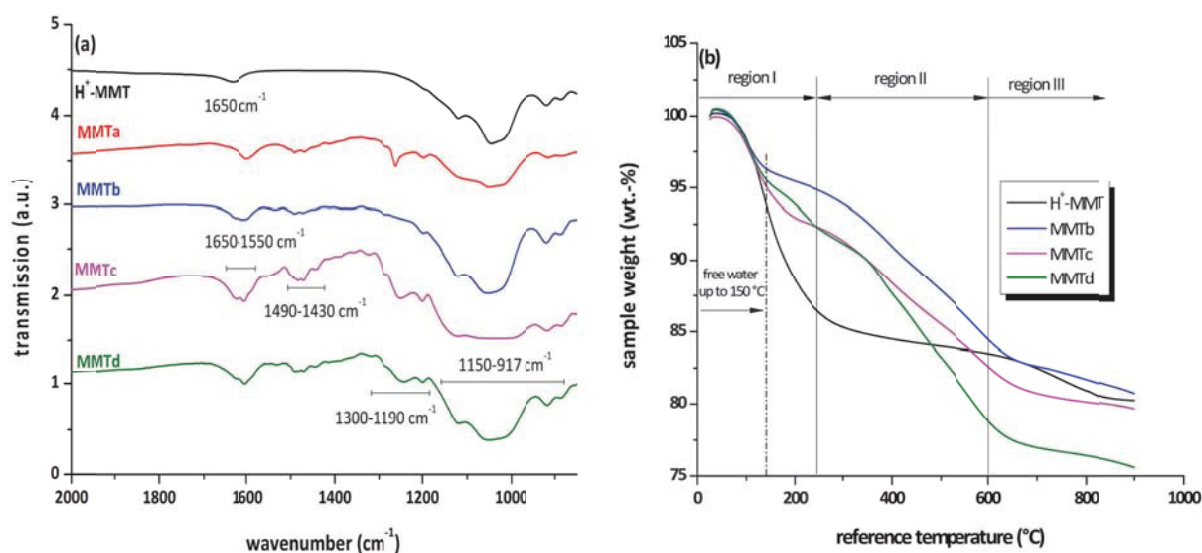
Fig. 86: (a) FTIR spectra of surface modified montmorillonites (thin layers on CaF_2 platelets); (b) thermogravimetry curves of the obtained MMTs.

Due to the low yield of particles the fraction MMTa could not be investigated by means of thermogravimetry. These particular TGA curves of modified montmorillonite are not

evaluated in accordance to Xie's method, as the modification affected the surface and not the interlayer galleries.[163] As activated MMT exhibits a very high weight loss in the low temperature region of 13.5 wt.-%, caused by evaporation of interlayer water and decomposition of $AlCl_3$, region II will be of mutual interest, concerning the decomposition of the azosulphonate moieties (see Fig. 86b). The modified MMTs show the main portion of the overall weight loss in this region, ranging from 10 to 14.5 wt.-%. As described by Riess in the early 90s, this is caused by the decomposition of the aromatic system and the propyl chain of the modification reagent.[61] The highest amount of immobilised organic substance can be detected for the non-filtrated montmorillonite fraction MMTd (see Table 19)

The decomposition of the azo groups is superposed by the evaporation of residual surface and interlayer water, and the low weight loss in the high temperature region can be attributed to the dehydroxylation and decarboxylation reported by Xie.[163] As the montmorillonites show strong hygroscopy, a total fraction of 10 wt.-% attributes to both free and interlayer water and decarboxylation reactions (see Table 19; regions I and III).

Table 19: TGA weight loss of the prepared particles as well as of the neat silicon dioxide particles.

sample	region I	region II	region III	Δm_{total}
	Up to 250 °C (wt.-%)	250 – 600 °C (wt.-%)	600 – 900 °C (wt.-%)	(wt.-%)
H^+-MMT	13.5	2.9	3.4	19.8
MMTa*	-	-	-	
MMTb	5.1	10.4	3.8	19.3
MMTc	7.2	10.5	2.9	20.6
MMTd	7.2	14.6	2.9	24.7

3.2.2 *Investigation of the photolysis of coupled azo compounds*

To investigate the UV reaction of the surface modified particles, samples were irradiated with a spot curing unit with a power output of 9.25 Wcm^{-2}. To obtain FTIR transmission spectra, thin layers of particles were deposited onto CaF_2 platelets by the drop coating method. UV-Vis absorption spectra of particle dispersions that had been filled in 3.5 mL quartz cuvettes were recorded to investigate changes of the chromophore by UV light induced decomposition.

Fumed silica. Exemplarily the FTIR and UV-Vis kinetics are depicted for the surface modified fumed silica particle type P1 (see Fig. 87). The photolysis kinetics of particles P2 and P3 are collected in the figure appendix (see P 21and P 22). As superposition of the structural IR absorptions of the silicon dioxide particles and the Ar-N=N- as well as the -N=N- absorption occurs, it is difficult to obtain FTIR photolysis kinetics (see Fig. 87a). However the change of the slope of the absorption at 1250 cm^{-1} can be attributed to the cleavage of the azo groups (compare with section 2.4.2.2). The faint change at 1055 cm^{-1} can be definitely assigned to the depletion of the -N-S- stretching vibration.[61,144]
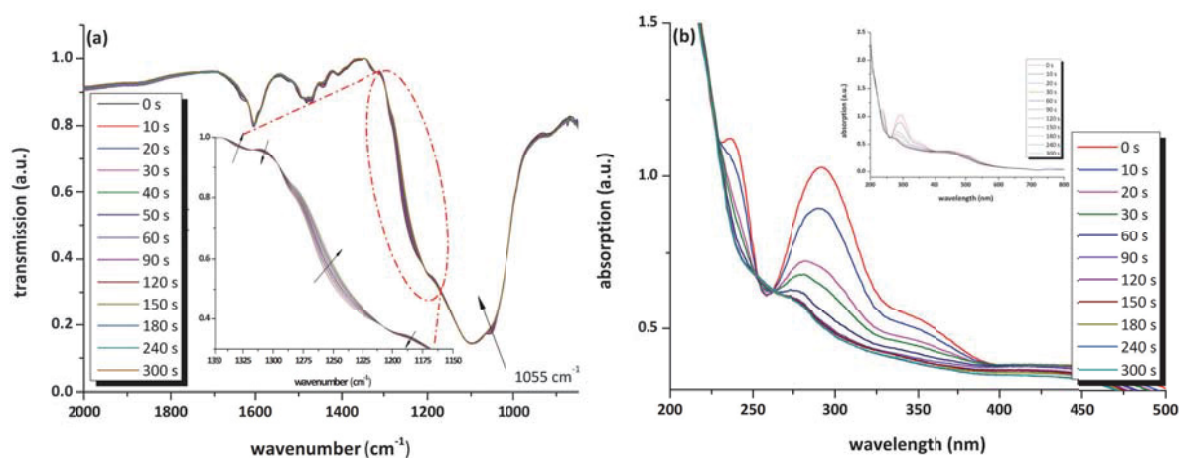
Fig. 87: (a) FTIR spectra of thin layers of surface modified silica particles **P1** deposited on CaF$_2$ platelets. (b) UV-Vis absorption spectra of an aqueous **P1** particle dispersion upon irradiation with a spot curing emitter with an intensity of 9.25 mWcm^{-2}.

In contrast to FTIR measurements, UV-Vis spectroscopy reveals significant changes of the immobilised photoactive species due to irradiation, due to the fact that silicon dioxide does not exhibit any absorption peaks. The absorption maximum at 293 nm can be attributed to the π-π* transition of the aromatic ring, while the n-π* transition (400 nm) of the azo groups is very faint and cannot be discerned distinctively.[60,63,137] As a result of increasing irradiation time, UV induced cleavage of the azo groups occurs, which leads to a rapid decrease of the absorption peak at 293 nm and a hypsochromic shift of the absorption to 273 nm (Fig. 87b).

Silicon dioxide nanoparticles. Since surface modified silicon dioxide nanoparticles exhibit the same chemical composition as fumed silica particles; both the FTIR and UV-Vis kinetics show the appropriate signals of the chromophore groups and structural SiO$_2$ absorption bands (compare Fig. 87 and Fig. 88). As described previously, the IR absorption of the azo groups is obscured by the strong absorption of the particles themselves, whereas the SiO$_2$

groups do not contribute to the UV-Vis spectra. Therefore it is concluded, that UV-Vis spectroscopy is the preferred method to determine changes of the immobilised photoreactive azosulphonate moieties.
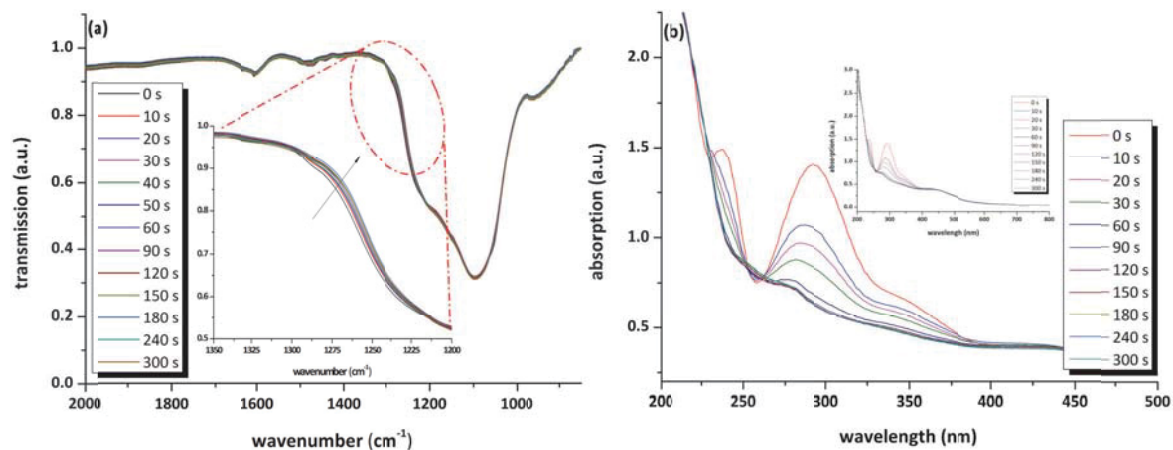
Fig. 88: (a) FTIR spectra of thin layers of surface modified **silica nanoparticles** deposited on CaF$_2$ platelets. (b) UV-Vis absorption spectra of an **aqueous nanoparticle dispersion** upon irradiation with a spot curing emitter with an intensity of 9.25 mWcm^{-2}.

Due to UV irradiation the particle dispersions are destabilised due to polarity changes of the particle surface caused by decomposition of the chromophore groups. This leads to phase separation and is exemplarily depicted in Fig. 89 for surface modified nanoparticles. Due to decomposition of the photoactive species, nitrogen gas is formed.
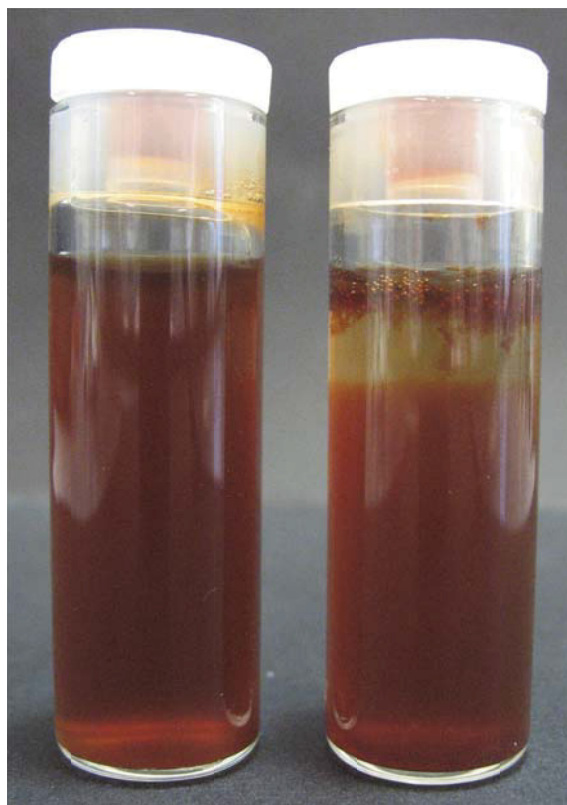
Fig. 89:   Stable nanoparticle dispersion before exposure (left); after 300 s exposure with a high pressure mercury vapour emitter using an irradiation intensity of 9.25 Wcm².

Montmorillonites. Photoreactive particles based on different montmorillonite fractions display the typical decomposition of the azo groups which results in a change of absorption at wavenumbers of 1300–1200 cm^{-1} (see Fig. 90a and Fig. 91a). In contrast to this, the fine fraction MMTa does not exhibit the strong UV-Vis absorption bands of aromatic azosulphonate compounds, as reported before (compare Fig. 88b and Fig. 90). But the UV-Vis spectra of MMTa show that irradiation leads to destabilisation of the dispersion due to irradiation, which results in an overall loss of absorption with increased irradiation time. This is probably a result of UV induced decomposition of the photolabile azosulphonate groups. Another reason that both fine fractions (MMTa/b; see P 23b) do not exhibit the strong absorptions of azo compounds may be the strong dilution (solids content of 0.4 wt.-%) of the dispersions as well as scattering of the transmitting light and a relatively low content of immobilised azosulphonic moieties.
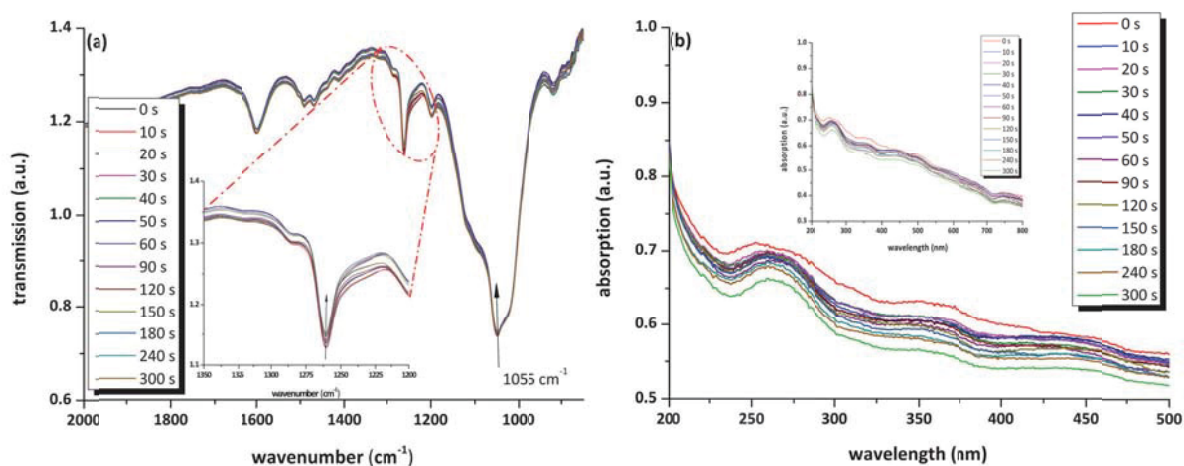
Fig. 90: (a) FTIR spectra of thin layers of surface modified montmorillonite (**MMTa**) deposited on CaF_2 platelets. (b) UV-Vis absorption spectra of an aqueous MMT dispersion upon irradiation with a spot curing emitter with an intensity of 9.25 mWcm^{-2}.

In contrast to this, the coarse montmorillonite fractions (MMTc/d) exhibit both significant changes in the azo-absorption region of the FTIR spectra (see Fig. 91a; picture detail) and in the UV-Vis spectra. The absorption maxima of the π-π* transition are diminished by UV exposure and a hypsochromic shift of the transition from 293 nm to 273 nm occurs. Moreover a slight parallel translation of the spectra is observed, which may be caused by destabilisation of the particle dispersion and the resulting sedimentation of the MMT particles (see Fig. 91b, Fig. 89 and P 24b).
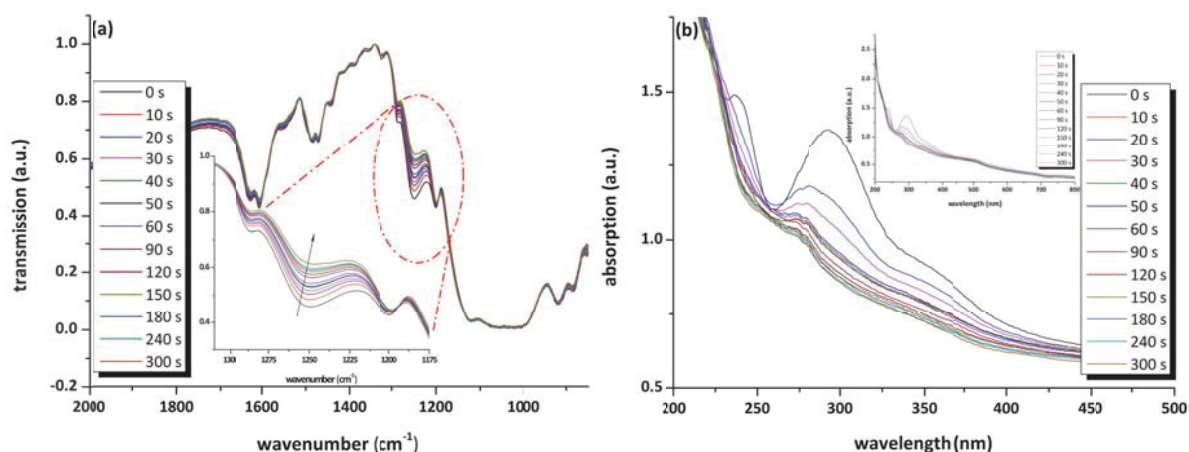
Fig. 91: (a) FTIR spectra of thin layers of surface modified montmorillonite (**MMTc**) deposited on CaF_2 platelets. (b) UV-Vis absorption spectra of an aqueous MMT dispersion upon irradiation with a spot curing emitter with an intensity of 9.25 mWcm^{-2}.

3.2.3 *Conclusions*

It is demonstrated that a number of different inorganic particles can be employed for the immobilisation of aromatic azosulphonic moieties by an innovative new three step process to prepare UV reactive particles. As the photosensitive units are immobilised onto the particle surface, no leaching out of the reactive groups, which may be noxious, can take place. This gives the possibility to employ these particles as proton donors or solid state radical photoinitiators. Due to nitrogen gas formation as a result of decomposition of the azosulphonate groups, a further application as blowing agents for microcellular foaming applications may be possible.

Due to the fact that the prepared particle dispersions are water based and the decomposition products are not classified as harmful these novel types of photoreactive particles are considered environmentally benign. Further investigations concerning the preparation of water-based photoresist materials comprising poly(vinyl alcohol) and organomodified particles are instigated in section 4.3.

4. ORGANIC-INORGANIC COMPOSITE MATERIALS

4.1 UV REACTIVE PVA – Fe^{3+}-MMT NANOCOMPOSITES

The use of Fe^{3+} cation exchanged montmorillonite as iron ion donor material for UV initiated crosslinking of PVA, in a similar way as doping with $FeCl_3$, is investigated in this section. As the photoactive species is immobilised onto the negatively charged MMT surface, no leaching out by solvents such as water will occur. Several novel concepts are employed: (a) the preparation of a nanocomposite based on aqueous solutions and suspensions by the means of high dispersion tools (see experimental section page 48); (b) the employment of cation exchanged montmorillonite as solid state crosslinking agent for covalent and physical crosslinking of PVA and (c) the preparation of translucent composite films with inorganic contents of up to 50 wt.-% with regard to the solid matter.[11]

Prior to the preparation of self-supporting thin films for UV crosslinking experiments and swelling tests, the UV response of aqueous sample dispersions is investigated by means of UV-Vis spectroscopy and refractometry. The UV response of $FeCl_3$ doped PVA and Fe^{3+} cation exchanged montmorillonites has been described in section 2.2.1 and section 3.1.2,

respectively. As the photoreduction mechanism of Fe^{3+} to Fe^{2+} is also investigated, the results of this section can be compared to previously discussed results.

4.1.1   *Investigation of UV-response*

As anticipated, each of the prepared PVA-Fe^{3+}-MMT dispersions exhibits strong changes of the Fe^{3+} absorption at 360 nm upon UV exposure with comparatively low intensities. The depletion of the absorption follows almost an exponential decay, which is a result of the photoreduction of Fe^{3+} to Fe^{2+} (Fig. 92).[11,47,48]

It is assumed that the photoreduction leads to radical formation, which would result in additional crosslink formation by recombination in the PVA composite material. At montmorillonite contents lower than 20 wt.-%, no photo reactivity can be determined by the means of UV-Vis spectroscopy, as the concentration of the UV absorbing is too low.
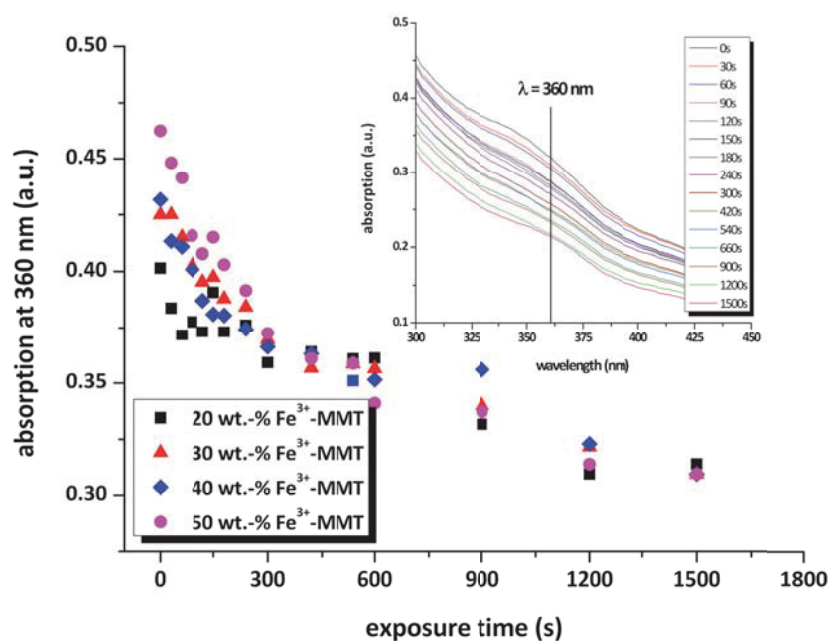
Fig. 92:   Change of UV-Vis absorption of aqueous PVA-Fe^{3+}-MMT dispersions upon irradiation with a spot curing unit with an intensity of 9.25 $mWcm^{-2}$. The picture insert shows the relevant absorption that can be attributed to the Fe^{3+} cation of a dispersion comprising 50 wt.-% iron montmorillonite.[9]

Due to photoinduced crosslinking reactions an increase of the refractive index of aqueous dispersion samples with increasing exposure times is observed (see Fig. 93). Dispersions containing 20 and 50 wt.-% of Fe^{3+}-MMT show a refractive index change of n^D of 0.029 and 0.025 respectively, while composites comprising of 30 and 40 wt.-% of modified clay exhibit

a change of Δn^D of 0.015. Upon 300 s of irradiation time the refractive indices reach a constant value, thus indicating that the photoreaction is completed.

The refractive index is increased by UV induced crosslinking reactions, which result in changes of the material density. In contrast to this is the strong decrease of n^D for $FeCl_3$ doped PVA samples, which is caused by a photobleaching effect as a result of charge transition of Fe^{3+} to Fe^{2+}.[9,47,97,150]
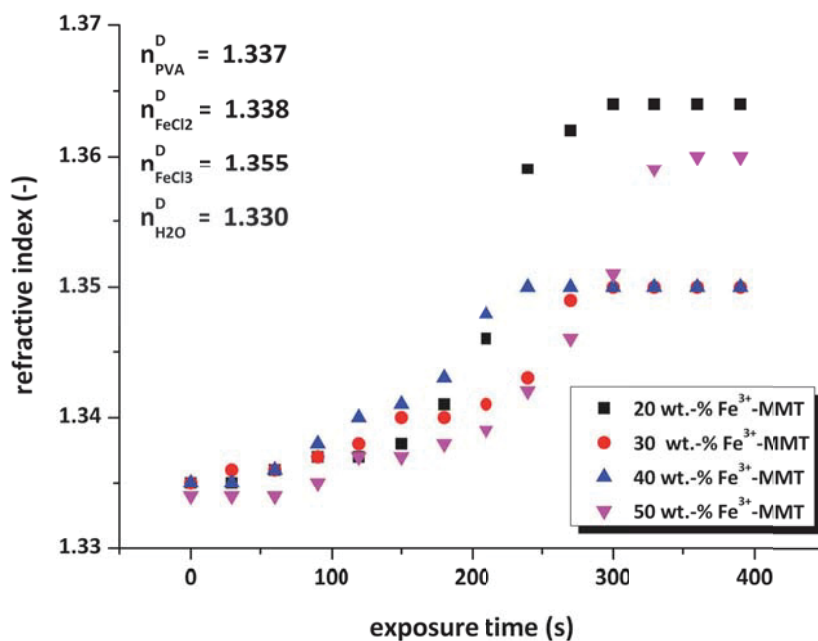
Fig. 93:   Increase of the refractive index n^D of aqueous PVA-Fe^{3+}-MMT dispersions upon irradiation with a UV spot curing unit with an intensity of 9.25 mWcm^{-2}.

Given that the investigation of the UV response of the prepared PVA-Fe^{3+}-MMT dispersions was fruitful, self-supporting thin films for the determination of particle distribution and swelling tests as well as for photolithographic patterning are prepared by the gravity settling method (see page 50).

4.1.2   *Nanocomposite characterisation*

In order to detect particle distribution along the cross section of thin composite films, the samples were cryogenically cracked, and the SEM images were recorded by the means of a backscatter electron detector to enhance the material contrast. As inorganic particles exhibit higher densities than polymers, a higher amount of electrons is scattered back, which leads to increased brightness.
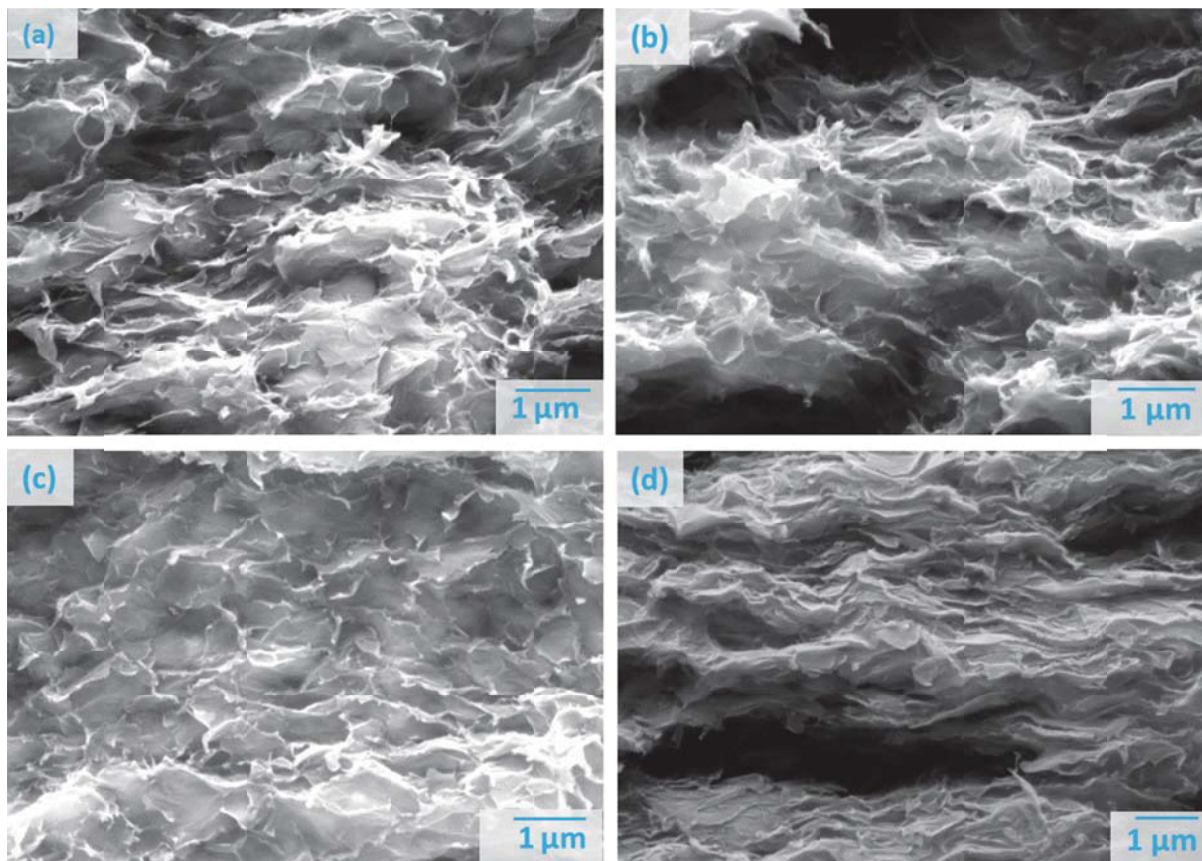
Fig. 94: SEM micrographs of the cross section of self-supporting thin films of PVA-Fe^{3+}-MMT composite films using a backscatter electron detector to enhance the material density contrast. (a) 20 wt.-% Fe^{3+}-MMT; (b) 30 wt.-% Fe^{3+}-MMT; (c) 40 wt.-% Fe^{3+}-MMT; (d) 50 wt.-% Fe^{3+}-MMT.

The SEM micrographs reveal a very homogenous and almost parallel orientation of the particles over the cross section of the obtained samples. Particles with sizes ranging from 15 to 100 nm are discernible at the edges of the scale-shaped structures (especially Fig. 94c). As the clay particles are delaminated and very well dispersed, it is assumed that strong polymer-filler interactions occur, which should lead to improved stability against deionised water and aerial humidity. It has to be stated, that self-supporting thin films with very high montmorillonite content (> 40 wt.-%) exhibit increased brittleness.

4.1.3   *Determination of swelling behaviour*

As the montmorillonite platelets are delaminated and partly exfoliated (see Fig. 94), PVA is intercalated into the interlayer galleries, which leads to strong polymer-filler interactions by hydrogen bonding. As neat PVA exhibits a gel content of 21 wt.-% upon swelling in deionised water, the addition of Fe^{3+}-MMT leads to gel contents of composite materials ranging from 68 wt.-% up to 93 wt.-% without any UV exposure (see Table 20). Therefore it is concluded,

that physical crosslinking as well as crystalline area formation lead to improved swelling behaviour with increasing montmorillonite content. These strong interactions also result in a decrease of the degree of swelling with increasing filler content.
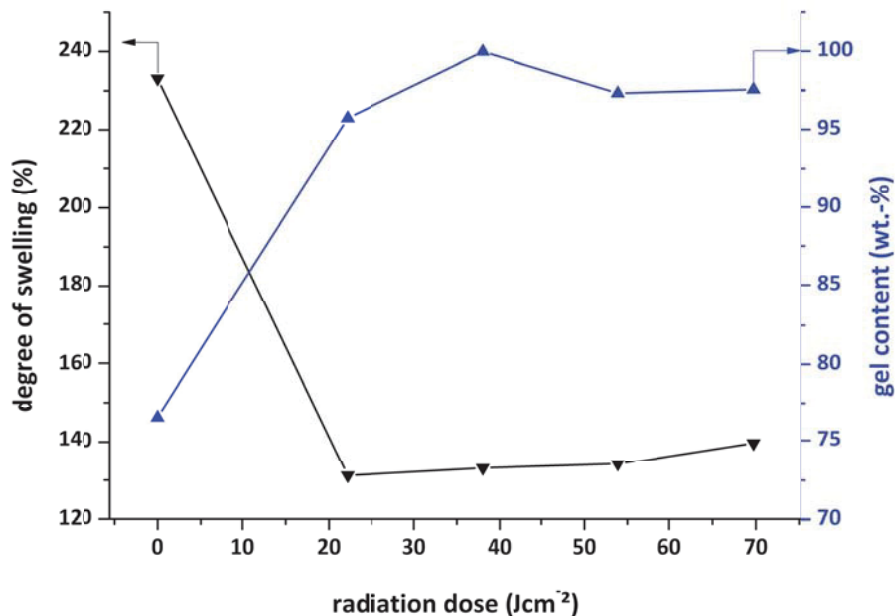
Fig. 95:   UV induced modulation of the swelling behaviour of a PVA composite comprising a total of 40 wt.-% of Fe^{3+}-MMT. Testing fluid: deionised water. The lines are a guide to the eye.

Additional UV exposure of the samples leads to an exponential decay of the degree of swelling, whereas the gel content reaches values higher than 95 wt.-%. Exemplarily this is depicted in Fig. 95 to visualise the rapid crosslinking mechanism and the strong influence of the additional crosslink formation on the solubility behaviour of a composite material comprising 40 wt.-% of cation exchanged montmorillonite. The slight decrease of the gel content for the composite with 50 wt.-% MMT content may be a result of sample fragmentation due to embrittlement, but no negative influence on the degree of swelling is found (see Table 20).

Table 20: Swelling behaviour of PVA-Fe^{3+}-MMT composite films in dependence of the UV irradiation dose

sample	degree of swelling (%)		gel content (wt.-%)	
	UV-exposure		UV-exposure	
	0 Jcm^{-2}	70 Jcm^{-2}	0 Jcm^{-2}	70 Jcm^{-2}
20 wt.-% Fe^{3+}-MMT	247	193	68	94
30 wt.-% Fe^{3+}-MMT	234	193	75	99
40 wt.-% Fe^{3+}-MMT	233	140	77	98
50 wt.-% Fe^{3+}-MMT	205	184	**93**	**91**

4.1.4   *Photolithographic patterning*

Irradiation of thin composite films through a quartz / chromium mask bearing 100 μm features leads to photobleaching of the exposed areas, which is caused by the photoreduction of Fe^{3+} to the colourless Fe^{2+} cation, as already determined by UV-Vis measurements with aqueous dispersions (see Fig. 92). The photobleaching results in an excellent pattern contrast under polarised incident light after immersion in deionised water as depicted in Fig. 96a.
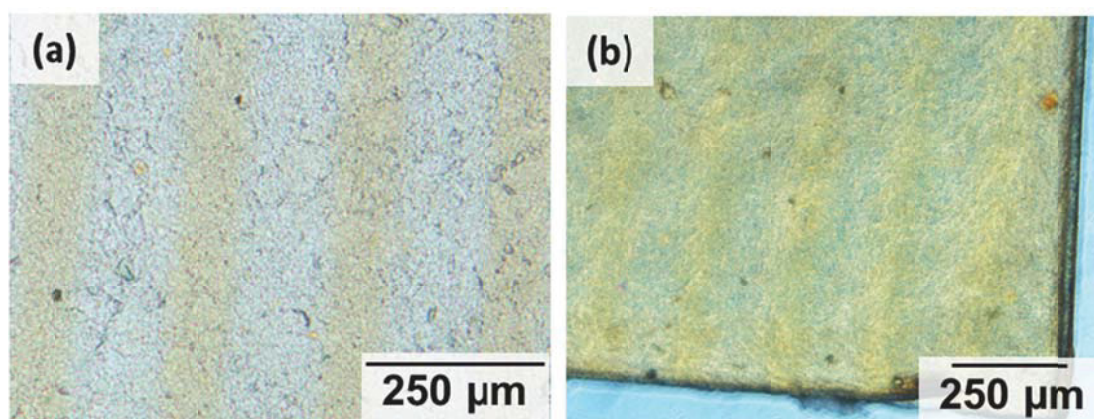
Fig. 96:   (a) a thin film of PVA-Fe^{3+}-MMT_20 wt.-% after patterning and immersion in deionised water for 24 hours at RT; (b) phase contrast image of developed sample containing of 50 wt.-% Fe^{3+}-MMT.

In an attempt to visualise the density contrast that is caused by UV instigated radical crosslinking, which results in an increase of the refractive index, phase contrast imaging

microscopy is employed. The pattern contrast as a result of patterned illumination followed by development in deionised water is depicted in Fig. 96b.

4.1.5   *Conclusions*

It is demonstrated that PVA-Fe^{3+}-MMT composite materials exhibit a similar mechanism of crosslinking as $FeCl_3$ doped PVA. This is a result of photoinduced reduction of Fe^{3+} to Fe^{2+}, which leads to PVA radical formation and crosslinking by recombination of the radicals.[9,11,44,97]

The montmorillonite particles are highly disperse and homogenously distributed over the cross section of self-supporting films, thus leading to the conclusion that delamination and exfoliation occurred. This leads to strong polymer-filler interactions and therefore to reduced swelling in deionised water. Further UV exposure results in highly crosslinked composite materials with gel contents higher than 95 wt.-%. It is also possible to selectively crosslink areas by patterned illumination, which can be visualised by polarised light microscopy as well as phase contrast imaging.

These novel composite materials are of potential interest for the preparation of environmentally benign photoresist materials or for biomedical applications. Hence the photoactive species is effectively immobilised onto the MMT surface (see section 3.1.2), no leaching out of iron ions nor migration out of the composite material can occur. This would make the manufacturing of barrier layers in the field of food packaging feasible, where the elimination of migration of crosslinking agents and contaminants is pivotal.[8] Due to the high crosslinking density improved water resistance is the result, which would avoid the deterioration of the outstanding barrier properties of PVA against non-polar organic substances.[172,173]

4.2   COMPOSITE MATERIALS COMPRISING PVA AND ORGANO MODIFIED MONTMORILLONITE

Composites of PVA and montmorillonite have been investigated by a number of authors, however the preparation and the properties of composites with amino acid intercalated clay have not been reported yet.[127,174,175] As the modification reagents are immobilised on the clay particles, no leaching out of the organic-inorganic composite will occur. It is assumed

that a fraction of the intercalated acid moieties of the organo modified montmorillonite can be crosslinked with the PVA matrix by heat induced crosslinking reactions, thus further immobilising the particles.

4.2.1   *Determination of thermal properties*

Differential scanning calorimetry measurements did not reveal significant changes of the melting temperature (T_m) of PVA-MMT-composites comprising 5 wt.-% of neat and organomodified Na^+-MMT, compared to pure PVA. The employment of glycine- and taurine-modified Na^+-MMT as filler material leads to a slight increase of T_m, while 10 wt.-% of L-cysteine-modified MMT lead to a significant decrease of the melting temperature (see Fig. 97b).

It is obvious that no additional phase formation occurs when incorporating 5 wt.-% MMT into a PVA matrix, otherwise a second melting temperature would be detected. The changes in the melting temperature that are found for Na^+-MMT content of 10 wt.-% could be caused by disturbance of the semi-crystalline PVA structure by hydrogen-bonding onto the MMT-surface OH-groups. Due to the comparatively low organic content of the modified filler particles (see Fig. 82 and Table 16) the effect on the melting temperature is negligible.
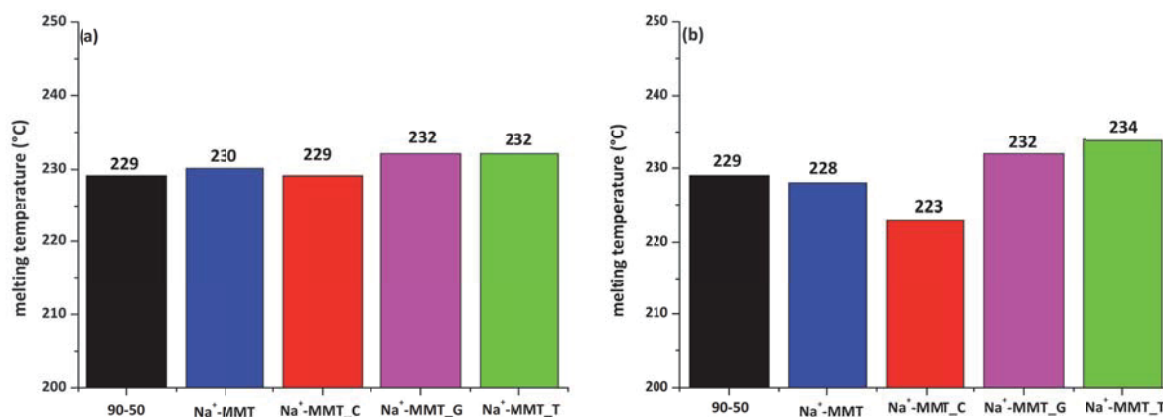
Fig. 97:   Melting temperatures (T_m) of PVA and PVA-Na^+-MMT composites, which are determined by DSC measurements during the second heating cycle in dynamic nitrogen gas atmosphere. (a) 5 wt.-% MMT content; (b) 10 wt.-% MMT content.

In contrast to these findings, the employment of 10 wt.-% activated and organomodified montmorillonite (H^+-MMT) results in the disappearance of the melting temperature in the second heating cycle (see Table 21 and Fig. 98). This effect also occurs for composites

comprising organomodified H^+-MMTs at contents of 5 wt.-%. Also a lower melting temperature is determined during the first heating cycle for these composite films, which is probably a result of evaporation of interlayer water or the formation of reaction water due to condensation reactions between the matrix polymer and the intercalated compounds.
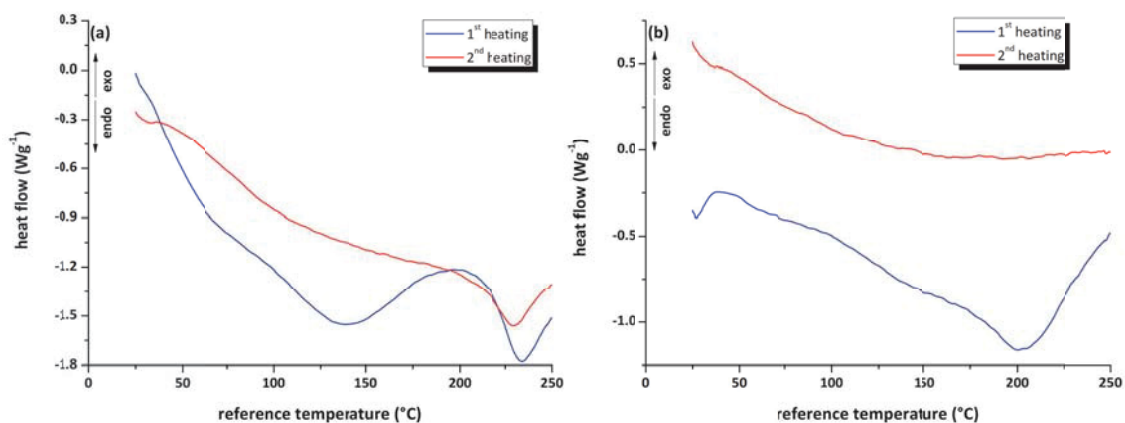
Fig. 98:   Exemplary representation of the vanishing of the melting peak during the second heating cycle. Composites comprising of (a) 5 wt.-% H^+-MMT and (b) 10 wt.-% H^+-MMT are depicted.

As incorporated or reaction water acts as plasticising agent for PVA, the melting temperature of composite materials comprising 10 wt.-% activated and organo modified MMT is lowered in the first heating cycle. This is exemplarily depicted in Fig. 98b, while during the second heating cycle no evaporation of water and melting of the composite can be detected.

Table 21: Melting temperatures of PVA and its composites with MMT. T_{m1} = melting temperature determined in the first heating cycle; T_{m2} = melting temperature measured at the second heating cycle.

5 wt.-% MMT	T_{m1} [°C]	T_{m2} [°C]	10 wt.-% MMT	T_{m1} [°C]	T_{m2} [°C]
pristine PVA	230	229	pristine PVA	230	229
PVA_Na$^+$-MMT	230	230	PVA_Na$^+$-MMT	233	232
PVA_H$^+$-MMT	234	229	PVA_H$^+$-MMT	200	n.d. [*)]
PVA_H$^+$-MMT_C	219	n.d. [*)]	PVA_H$^+$-MMT_C	199	n.d. [*)]
PVA_H$^+$-MMT_G	226	n.d. [*)]	PVA_H$^+$-MMT_G	224	n.d. [*)]
PVA_H$^+$-MMT_T	199	n.d. [*)]	PVA_H$^+$-MMT_T	204	n.d. [*)]

4.2.2   *Particle distribution*

To determine the particle distribution and the embedding in the PVA matrix, SEM measurements of thin composite films are performed, using a backscatter electron detector, which makes detection of density contrast feasible. Exemplary micrographs of composites containing of 5 wt.-% modified Na$^+$-MMT and 10 wt.-% of H$^+$-MMT are shown in Fig. 99 and Fig. 100 respectively.
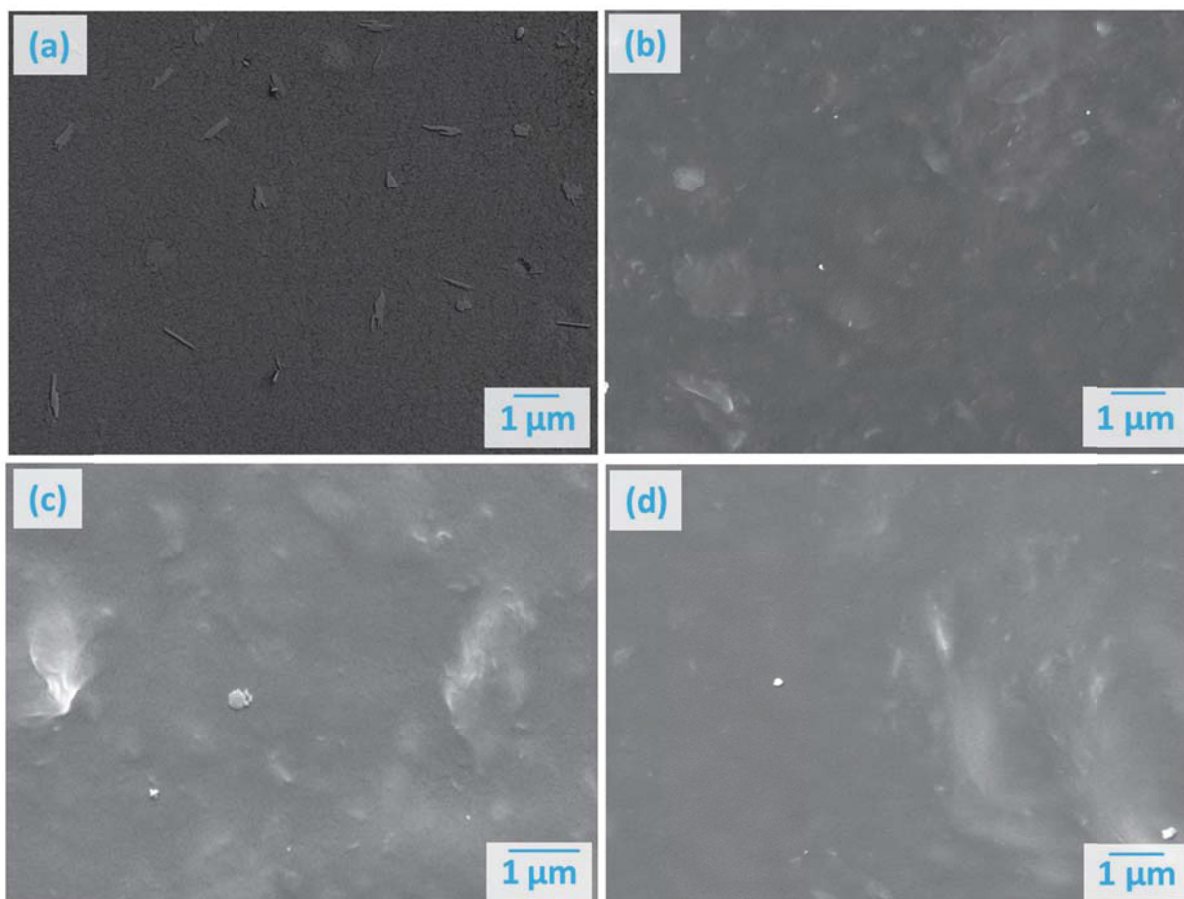
Fig. 99:   SEM micrographs of PVA-MMT composite films containing 5 wt.-% of (a) Na^+-MMT; (b) Na^+-MMT_C; (c) Na^+-MMT_G and (d) Na^+-MMT_T.

Composites containing neat sodium MMT begin to crack due to local overheating caused by the electron beam cess (see Fig. 99a) and relatively large agglomerates of the platy clay are discernible. The organomodified Na^+-MMT clays exhibit an improved dispersibility in comparison to the relatively large particles of the neat MMT (see Fig. 99b-d). Particle sizes ranging from 1 µm to less than 100 nm can be detected, while the distribution is not as homogenous as found for PVA-Fe^{3+}-MMT composites.
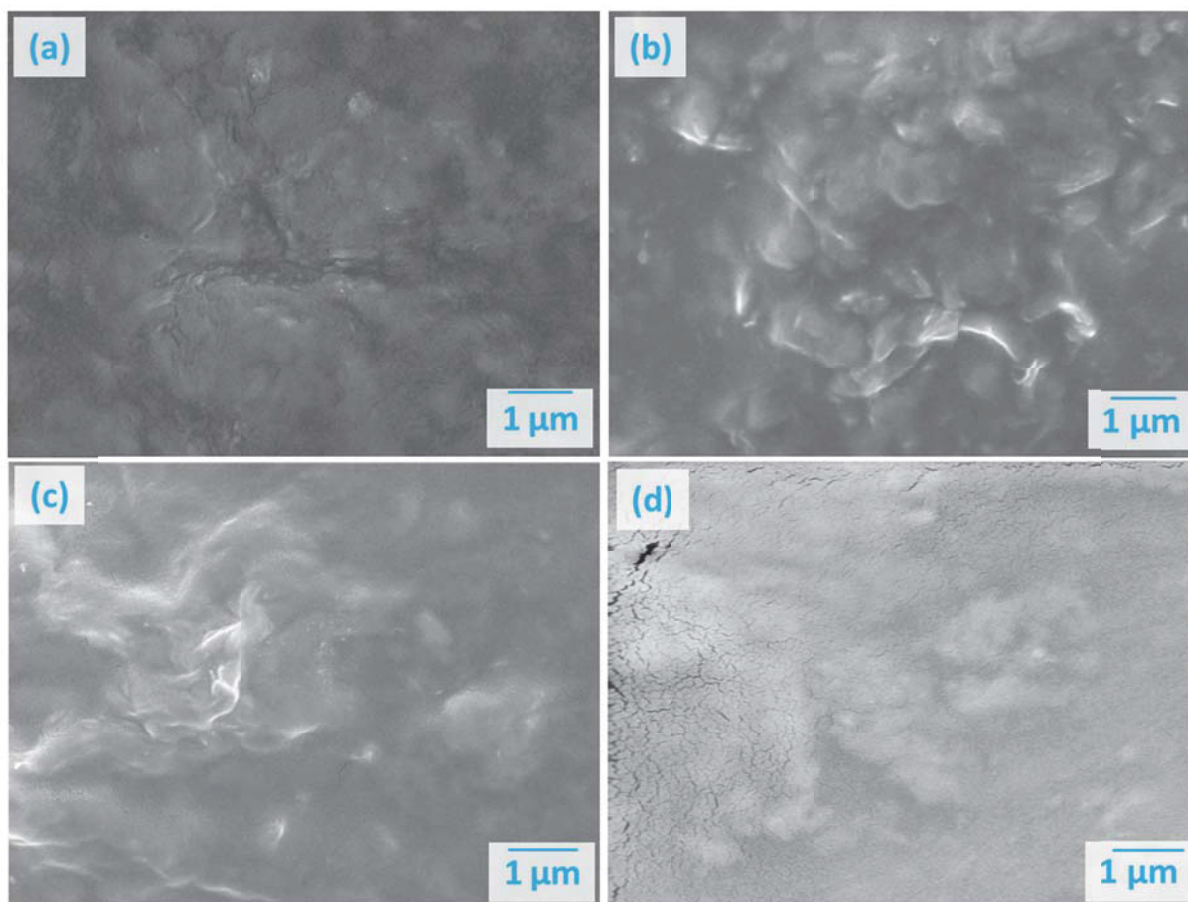
Fig. 100: SEM micrographs of PVA-MMT composite films containing 10 wt.-% of (a) H^+-MMT; (b) H^+-MMT_C; (c) H^+-MMT_G and (d) H^+-MMT_T.

The H^+ activation of montmorillonite leads to an improvement of the dispersibility of the non-modified particles compared to neat sodium MMT. Organomodified H^+-MMTs exhibit good compatibility with the matrix polymer and are well embedded, which can especially be discerned for taurine intercalated MMT (see Fig. 100d). Due to heating during the scanning process, crack formation as a result of evaporation of incorporated water occurs. To counter this effect, the acceleration voltage of the electron beam is decreased, which lead to a deterioration of the backscattering contrast.

As both montmorillonite and the polymer are highly polar, strong polymer-filler interactions are anticipated, which should further increase the water resistance of the obtained composite samples.

4.2.3   *Investigation of heat induced crosslinking*

In a first attempt to investigate potential heat induced crosslinking reactions thin layers of PVA-MMT composites were deposited onto CaF_2 platelets and were subjected to annealing

at elevated temperature. The measurements have been performed with special emphasis on the carbonyl region, but it has to be stated that it is difficult to discern the formation of ester groups. Hence the main portion of the organic content of the modified MMTs is located in the interlayer galleries, only a low number of carboxylic or sulphonic acid groups are accessible for heat induced condensation with the PVA. As the organic content of the layered silicates results only in very weak absorptions (see Fig. 81), these are obscured by the absorption bands of the PVA matrix.

On the other hand, slight changes of the FTIR spectra are detected, which may be a result of esterification reactions of a fraction of the carboxylic acid groups. This is exemplarily depicted in Fig. 101 for a composite containing of 10 wt.-% of cysteine intercalated H^+-MMT. As the intermolecular water is evaporated, the H-O-H bending vibration at 1650 cm^{-1} diminishes rapidly, while the residual absorption can be assigned to protonated amino groups.[137,144]

Furthermore the shape of the carbonyl absorption exhibits a shoulder at 1732 cm^{-1}, which can be attributed to aliphatic ester formation, while still carboxylic acid moieties are present leading to the absorption maximum at 1700 cm^{-1}. Besides the strong and broad peak of the structural C-O-H absorption of the polymer backbone, a new C-O-C absorption band at 1143 cm^{-1} arises, as a result of heat induced condensation reactions.
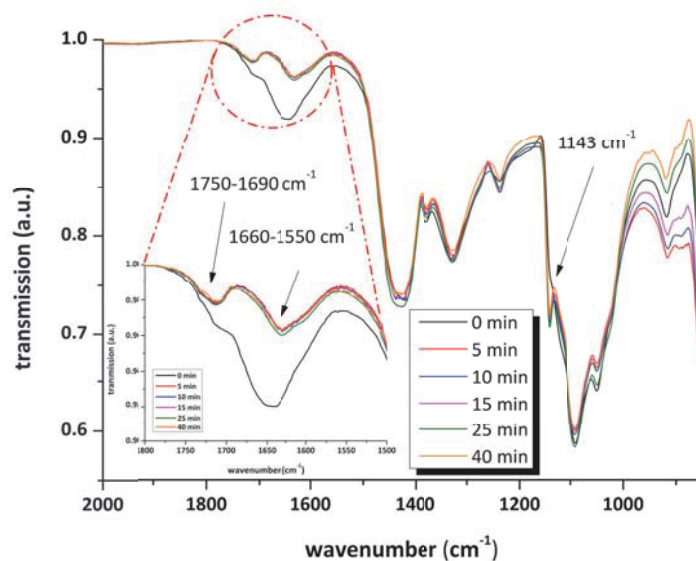
Fig. 101: Influence of heat treatment on FTIR spectra of a thin composite film containing 10 wt.-% H$^+$-MMT_C, deposited onto CaF$_2$. The picture detail depicts the carbonyl absorption region and the water and amino group absorption.

Dispersing pristine sodium montmorillonite clay into PVA changes the solubility of the composite in deionised water significantly (see Table 22). After 40 minutes of annealing the gel content doubles, which can be attributed to the evaporation of bound and surface water from the film, and the resulting changes of packing density due to formation of hydrogen bonds between the PVA molecules themselves and with the montmorillonite surface (see Fig. 102).
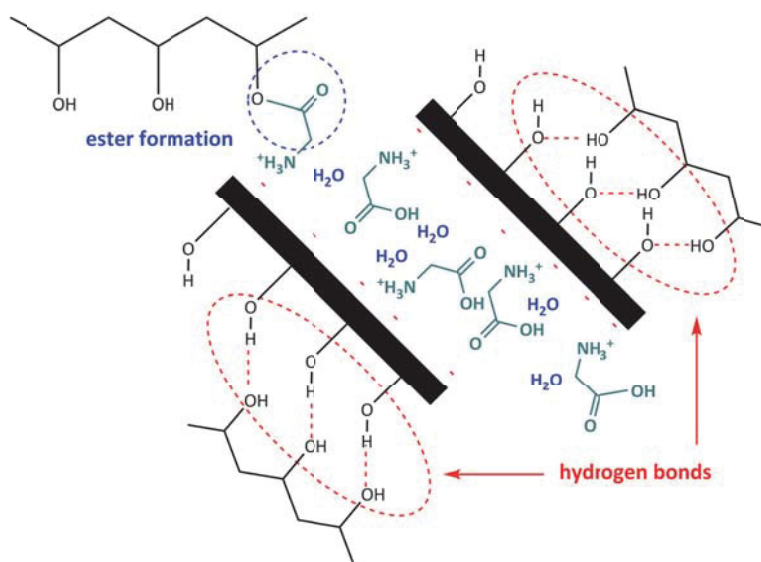
Fig. 102: Exemplary representation of dual crosslinking mechanism between PVA and organomodified montmorillonite (glycine). Covalent crosslink formation due to heat induced esterification reactions and physical interactions between the matrix polymer and particle surface (hydrogen bonding).

The incorporation of amino acid modified Na$^+$-MMT into PVA leads to gel contents (prior to annealing) in the range of 34 to 45 wt.-%, and reaches values higher than 70 wt.-% for 5 wt.-% of MMT, and 81 wt.-% for 10 wt.-% of the modified filler material due to heat treatment. As a result of organic modification the active surface area of MMT is increased, which leads to stronger interactions between the polymer and the filler material, thus improving the swelling behaviour. It is evident that a higher amount of montmorillonite content leads to a significant increase of the gel contents compared to composites comprising 5 wt.-% of MMT, except for neat Na$^+$-MMT.

Table 22: Gel content of PVA-MMT composites comprising organomodified sodium montmorillonite

	gel content (wt.-%)			
	5 wt.-% MMT		**10 wt.-% MMT**	
	annealing time		**annealing time**	
	0 min	40 min	0 min	40 min
Na$^+$-MMT	35.0	73.4	35.4	71.1
Na$^+$-MMT_C	40.2	76.0	44.0	81.0
Na$^+$-MMT_G	37.6	72.2	44.8	81.5
Na$^+$-MMT_T	34.0	71.4	44.2	80.6

Exemplarily the change of the gel content of PVA-MMT composites due to heat treatment is depicted Fig. 103a for a composite comprising of Na$^+$-MMT_C. This increase of the insoluble fraction is a further hint that condensation reactions between the matrix and a portion of the intercalated amino acids occur.
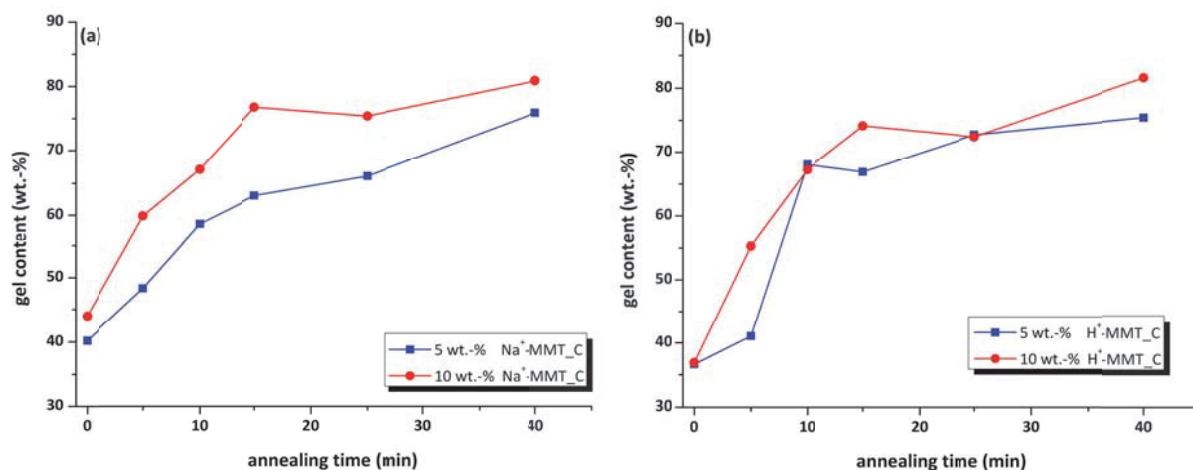
Fig. 103: Change of gel content of PVA-MMT composites due to annealing at 100 °C; (a) composite containing cysteine intercalated sodium MMT; (b) composite comprising activated and cysteine modified MMT. The lines are a guide to the eye.

The use of acid activated MMT as functional additive for PVA leads to a strong improvement of the solubility behaviour, which results in gel contents of 66 wt.-% prior annealing for a composite comprising 10 wt.-% MMT. It is evident that heat treatment leads to a higher gel content of the composite with non-modified H$^+$-MMT, possibly a result of the increased surface area caused by the activation step.

Due to the high polarity of the modified filler material the gel contents of composites containing amino acid intercalated MMT are decreased due to the strong affinity to water. Gel-contents of 81 wt.-% after annealing can be observed for composites bearing 10 wt.-% of cysteine modified H$^+$-MMT and taurine modified H$^+$-MMT (see Table 23). At 5 wt.-% filler content gel contents ranging from 75 to 77 wt.-% are observed for all composite films.

The lower gel content for composites containing of organo-modified H$^+$–MMT compared to composites bearing non-modified H$^+$-MMT is probably caused by the high polarity of the intercalated compounds and therefore increased affinity to water.

Table 23: Gel content of PVA-MMT composites comprising organomodified activated montmorillonite

	gel content (wt.-%)			
	5 wt.-% MMT		**10 wt.-% MMT**	
	annealing time		**annealing time**	
	0 min	40 min	0 min	40 min
H$^+$-MMT	44.5	75.5	65.8	92.6
H$^+$-MMT_C	36.6	75.4	36.9	81.6
H$^+$-MMT_G	41.3	76.8	58	75.2
H$^+$-MMT_T	47.5	77.8	44.9	81.8

The employment of activated and subsequently organo modified MMT as functional filler, leads to slightly higher gel contents compared to modified sodium MMT. This is caused by the increased amount of intercalated amino compounds into the interlayer galleries of the activated MMTs.

4.2.4 *Conclusions*

The activation of montmorillonite leads to increased delamination of the clay platelets, thus resulting in a higher particle surface area as well as higher intercalated organic content compared to sodium MMT. This leads to covalent crosslink formation, which results in the vanishing of the melting point during the second heating cycle of DSC measurements. Furthermore PVA-H$^+$-MMT composite films exhibit higher gel contents compared to sodium MMT composites. As the functional moieties are immobilised onto the additive, no leaching or migration out of the composite takes place.

As both types of clays lead to an improvement of the water resistance of PVA-clay composite films and the utilisation of non-toxic and non-irritating compounds for the modification, the obtained composites would be suitable for the usage as gas barrier and encapsulation materials. Also the application in the field of food packaging and biomedical products would be possible.[81–83] As cysteine can form complexes with heavy metals [82,169], this novel types of composite may act as hydrogel for the removal of Hg^{2+} or Cd^{2+} from water.

4.3   USE OF UV REACTIVE PARTICLES FOR THE CROSSLINKING OF PVA

Aqueous PVA-particle dispersions were obtained by mixing both a PVA solution and azosulphonate particle suspensions (see page 118) by means of high speed dispersion tools (sample notation see Table 12). As MMTa exhibits a low particle yield, it was not possible to prepare the appropriate composite dispersion.

4.3.1   *Investigation of UV reactivity*

In an attempt to investigate UV induced decomposition of the aryl azosulphonate groups, UV-Vis absorption spectra of aqueous PVA-particle dispersions are recorded. As FTIR kinetics of thin composite films do not exhibit strong changes of the azosulphonate absorption bands (1300–1100 cm^{-1}), because of superposition by the PVA backbone and the Si-O-Si absorption bands (1100–980 cm^{-1}) as well, further FTIR measurements with emphasis on the photo decomposition are not conducted (compare Fig. 90 and Fig. 104a).

The photoreactive groups on the particle surface undergo decomposition upon UV irradiation, which leads to destabilisation of the composite dispersions containing surface modified montmorillonite. This is discernible in Fig. 104b-d as a parallel translation of the absorption curves to lower absorbance values. Due to changes of the electron density of the aromatic system, the absorption peak at 290 nm shifts to lower values, which is a clue that phenol groups are formed [137]. The appropriate UV-Vis spectra of composite dispersions containing 2.5 wt.-% of modified particles are presented in the figure appendix (see P 25).
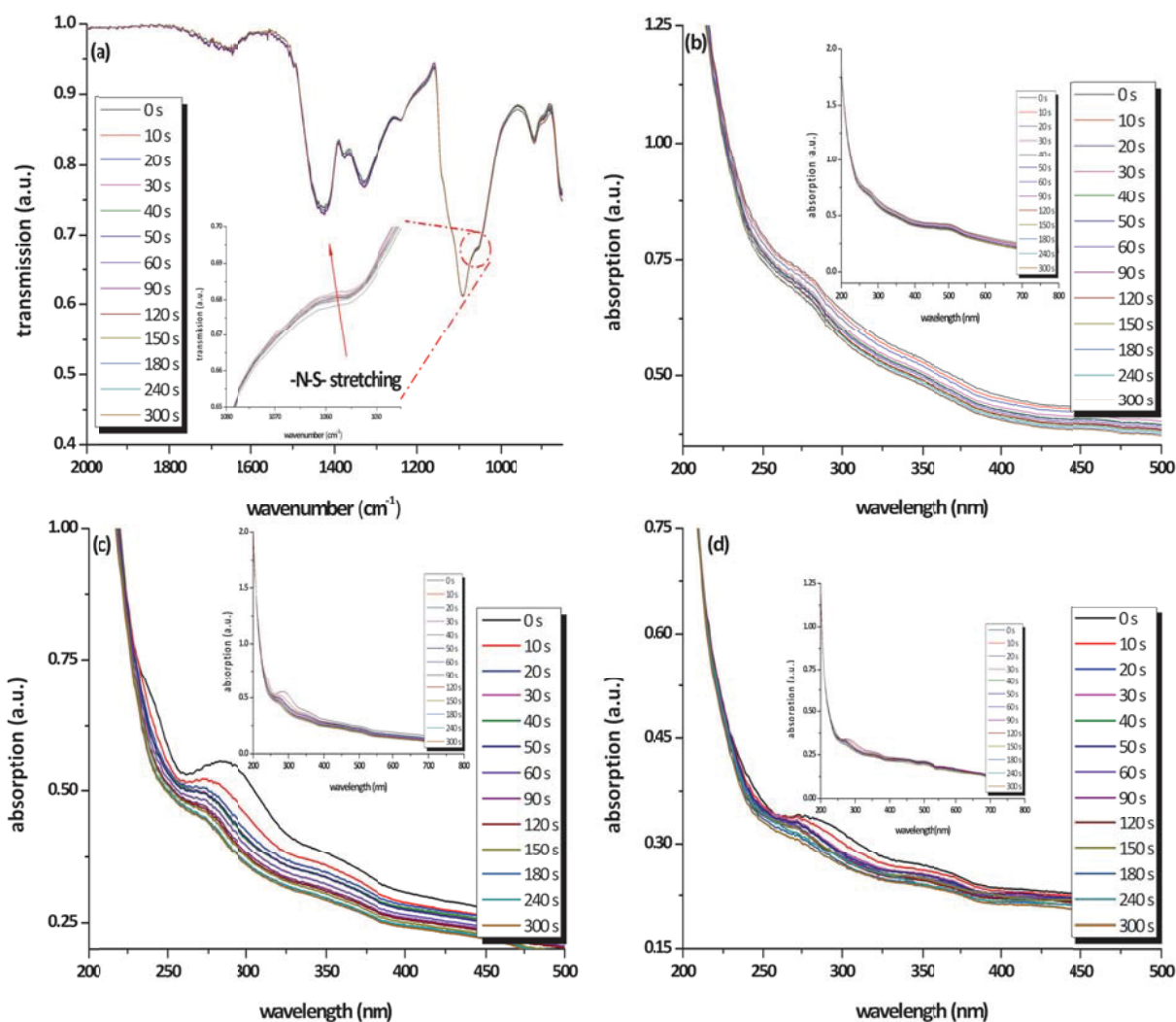
Fig. 104: UV exposure kinetics of PVA composites comprising of 5 wt.-% surface modified montmorillonite. (a/b) FTIR and UV-Vis spectra of PMMTb_2; (c) PMMTc_2; (d) PMMTd_2. Irradiation is performed with a high pressure mercury vapour lamp with an output intensity of 9.25 Wcm^{-2}.

Composite dispersions containing fumed silica based modified particles exhibit strong UV response, as a result of photoinduced decomposition of the azo groups.[61] The sample PP1_1 not only shows a decrease of the absorption caused by the chromophore, but also a hypochromic shift towards lower absorption values, thus indicating that destabilisation and sedimentation of the particles are caused by UV exposure (see Fig. 105a and compare with Fig. 89).

In contrast to these findings, the particle dispersions PP2_1 and PP3_1 (Fig. 105b/c) are stable upon irradiation, during which the chromophore is decomposed. Additional photolysis kinetics for dispersions containing 5 wt.-% of photoactive particles are collected in the figure

appendix in P 26, showing that PP2_2 is destabilised by UV irradiation in a similar manner as depicted in Fig. 89.
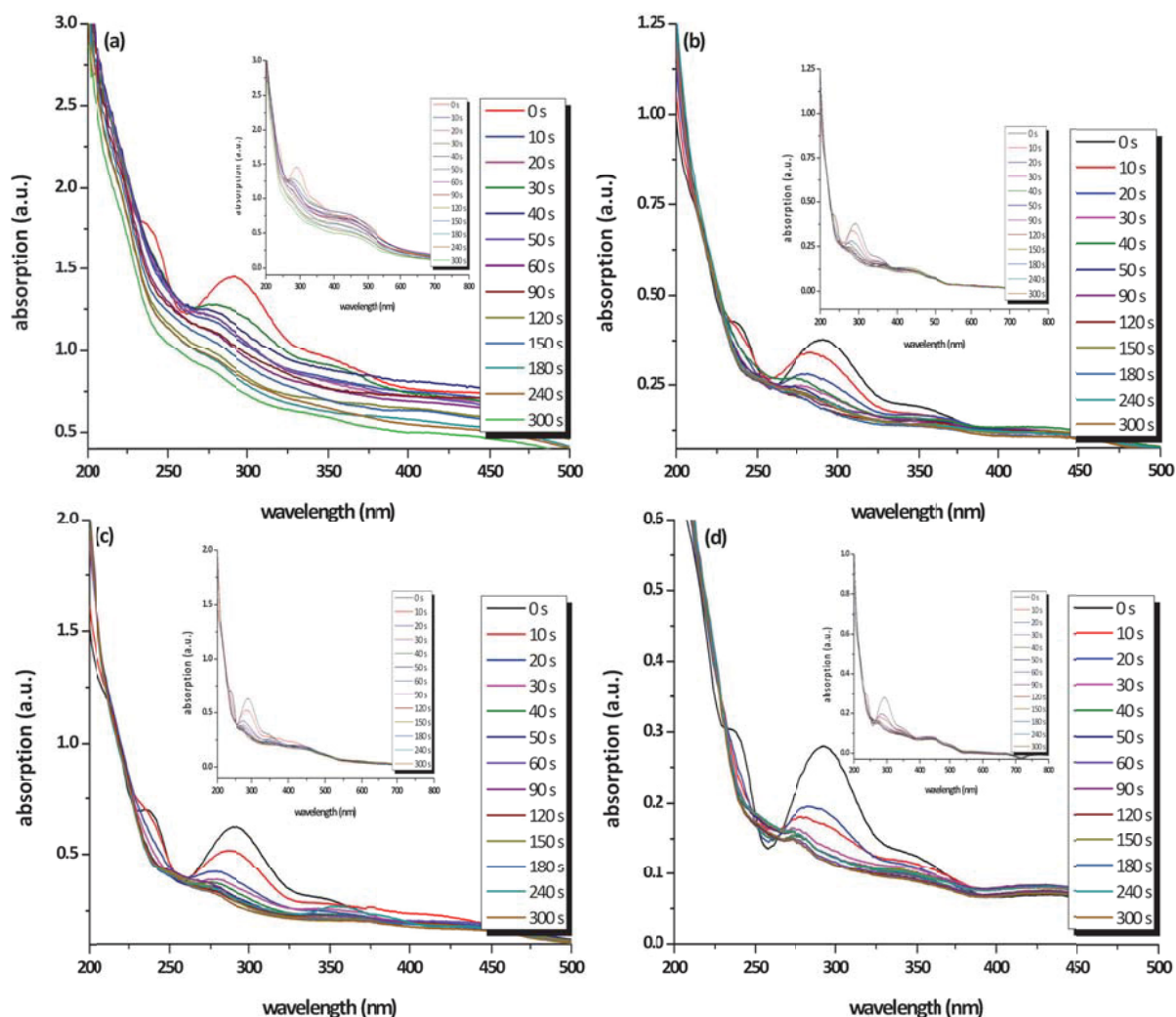
Fig. 105: UV exposure kinetics of PVA composites containing 2.5 wt.-% of surface modified silica particles: (a) PP1_1; (b) PP2_1; (c) PP3_1 and (d) nanoparticles PNP1. Exposure is performed using a high pressure mercury vapour emitter with an output intensity of 9.25 Wcm^{-2}.

The obtained PVA-nanoparticle dispersions PNP1 and PNP2 (see Fig. 105d and P 26d respectively) exhibit two isobestic points at wavelengths of 251 nm and 263 nm due to the photodecomposition of the chromophore. As a slight hypochromic shift of the spectra is observed, it is assumed that the dispersions are destabilised as a result of UV exposure.

4.3.2   *Composite characterisation*

SEM micrographs were recorded to visualise particle distribution and the embedding of the modified particles in the PVA matrix. As the inorganic particles feature a higher density than

the matrix, more electrons are emitted in the direction of the detector, thus giving brighter contrasted areas on the micrographs.
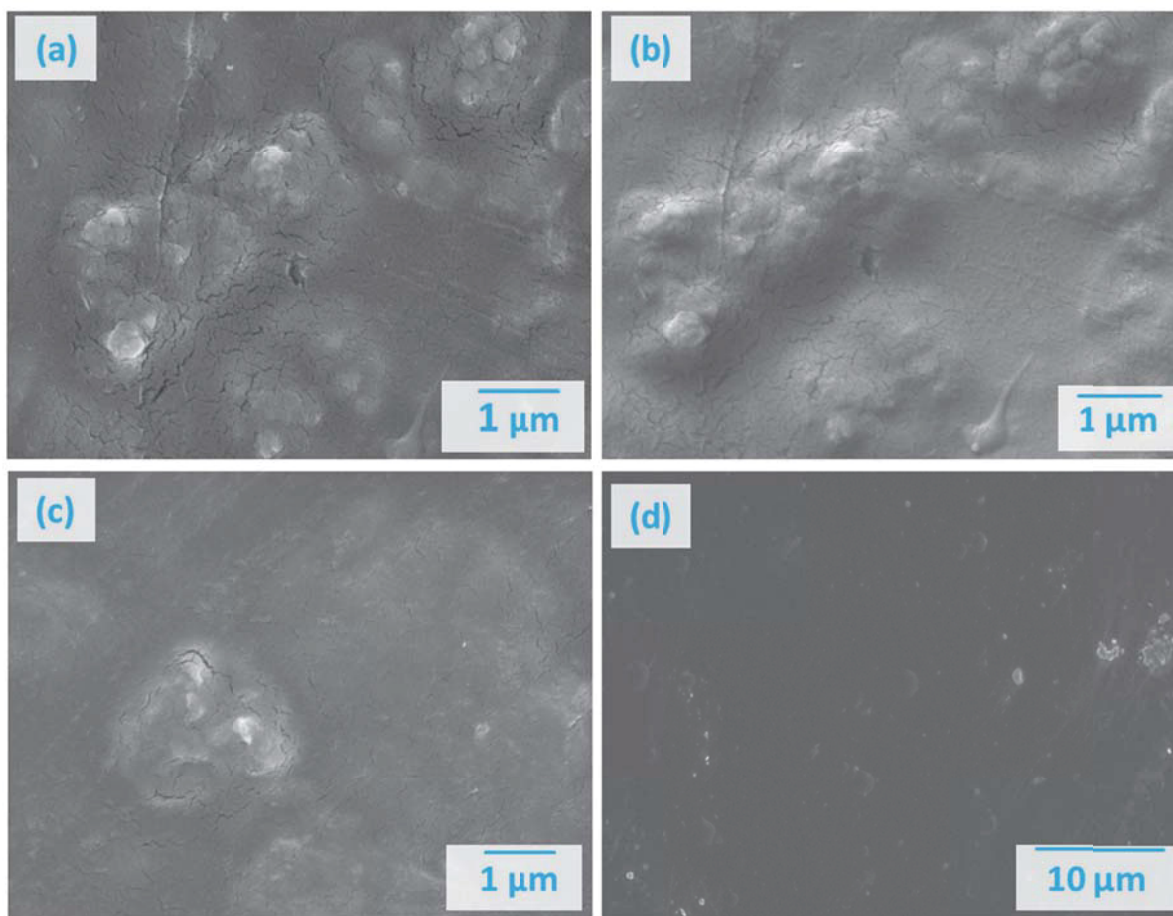
Fig. 106:   SEM micrographs of PVA composite films comprising 5 wt.-% of surface modified montmorillonite.(a/b) MMTb_2 observed with different detectors (a) inlens detector (b) combined secondary electron/secondary ion detector (SESI); (c) PMMTc_2; (d) PMMTd_2.

As the composite samples tend to form cracks during to scanning with the electron beam, as a result of local overheating, the accelerator voltage of the electron source has to be reduced. This renders the employment of a backscatter electron detector for determination of material contrast obsolete, therefore it is attempted to obtain micrographs of embedded particles with the standard inlens detector. The outcome is depicted in Fig. 106a, and compared to the topography that is recorded with a SESI detector (Fig. 106b). The employment of the inlens detector reveals embedded inorganic particles with higher contrast than the secondary ion detector. It is possible to discern montmorillonite structures below the sample surface with sizes ranging from 30 nm to 250 nm. MMTc exhibits higher

dispersibility with a higher number of particles smaller than 100 nm (see Fig. 106c). Because the polymer is very unstable under the scanning electron beam it was not possible to obtain micrographs for PMMTd_2 with higher magnification as depicted in Fig. 106d. On the other hand, this overview shows that only a small portion of the surface modified MMT is agglomerated, while the largest is very well embedded in the PVA matrix.
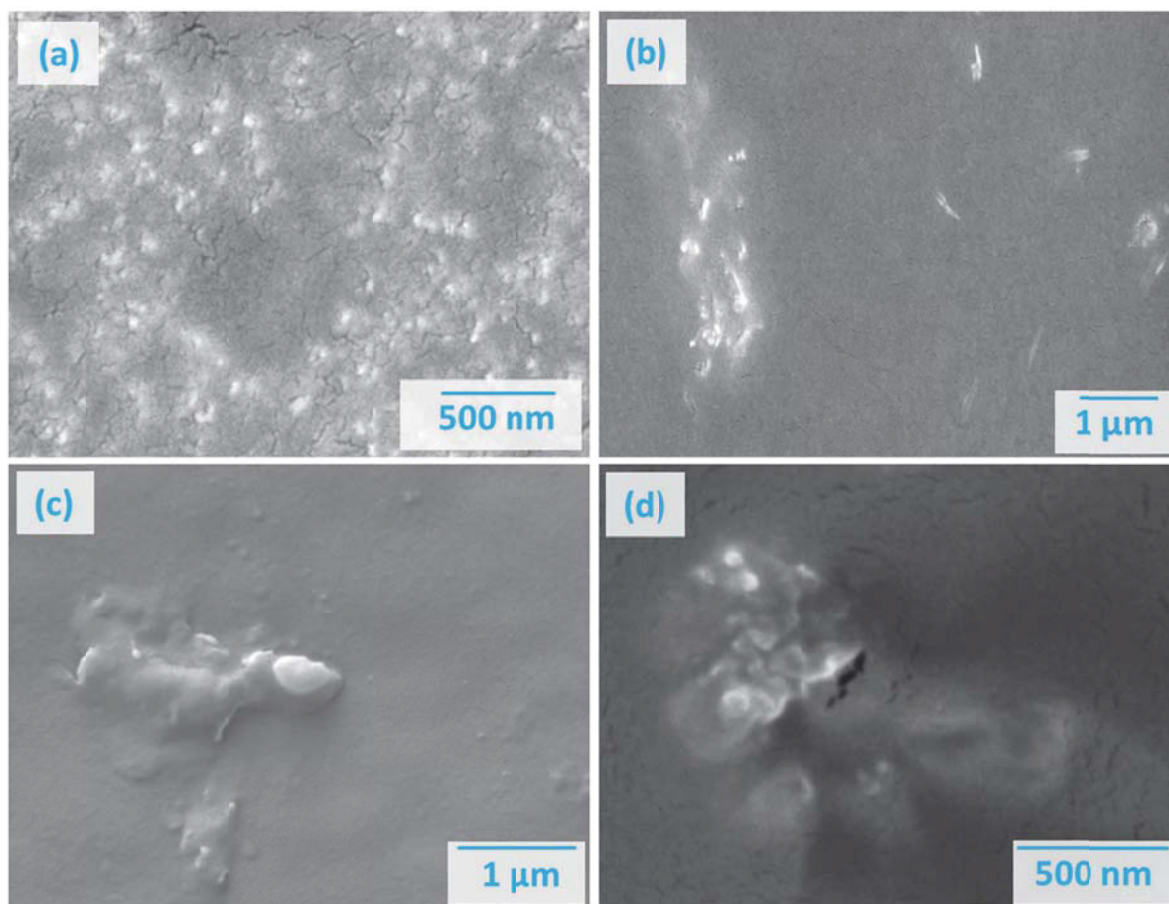
Fig. 107: SEM micrographs of PVA composite films containing 5 wt.-% of surface modified silica particles. (a) PP1_2; (b) PP2_2; (c) PP3_2 and (d) PNP2.

Photoreactive particles based on fumed silica exhibit small particle sizes below 100 nm (see Fig. 107a) with homogenous distribution. The sample PP2 shows needle-like agglomerates with a length of 150 nm (see Fig. 107b), which may be a result of the surface modification or the preparation of the fumed silica particles. Due to the very broad particle size distribution of fumed silica, single particles of about 250 nm diameter are determined, but in the vicinity of the agglomerate very small particles ten times smaller are found (see Fig. 107c).

Silicon dioxide nanoparticles are very well embedded in the PVA matrix, but they tend to agglomerate, thus forming aggregates with a size of 100 nm. Several single particles are discernible in Fig. 107d, while the matrix begins to decompose due to local overheating, which can be seen from crack formation.

SEM measurements reveal that the prepared surface modified particles are well embedded into the polymer matrix, although aggregate formation is found for montmorillonites as well as for fumed silica particles. Due to the high dispersibility of the photoreactive silica particles, strong polymer-filler interactions should occur, which should also lead to improved swelling resistance of the composite material.

Swelling behaviour of MMT/PVA composites. Due to polymer-filler interactions, the degree of swelling of PVA composites containing surface modified montmorillonite particles is decreased, in comparison to neat PVA. As a result of UV exposure, heating of the samples as well as decomposition of the azosulphonate moieties on the particle surface is caused. This leads to improved swelling behaviour of neat PVA, reaching gel contents of 55 wt.-%.[16,176–178] The composite systems, however, exhibit gel contents in the ranging from 70 to 80 wt.-%, except MMTd with 55 wt.-% (see Fig. 108). To further improve the swelling behaviour of the composite materials, annealing at 100 °C in a convection oven is performed.
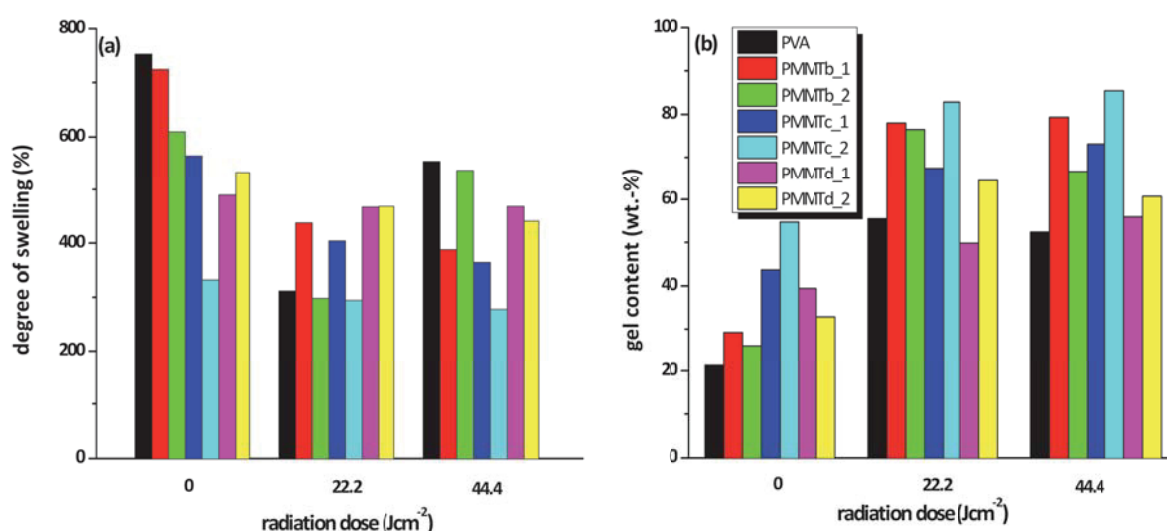
Fig. 108: Change of the degree of swelling (a) and the gel content (b) of PVA composite films comprising of surface modified montmorillonites. Irradiation is performed with a medium pressure mercury vapour emitter with an intensity of 740 mWcm^{-2}.

Heat treatment leads to an almost exponential decay of the degree of swelling for neat PVA and montmorillonite composite samples as well. As interactions between the highly polar organic phase and the silanol groups of the particle surface occur, the swelling behaviour of composite samples is improved, even with a relatively low MMT content of 2.5 wt.-% (see Fig. 109a). A further increase of the MMT content to 5 wt.-% leads to a degree of swelling of 300 % and a gel content higher than 80 wt.-% for composites of MMTc. (see Fig. 109c/d). This particular type of MMT exhibits a very high dispersibility (see Fig. 106c), therefore the particle surface and stronger interactions are the result. The heat treatment of composites is followed by subsequent UV irradiation.
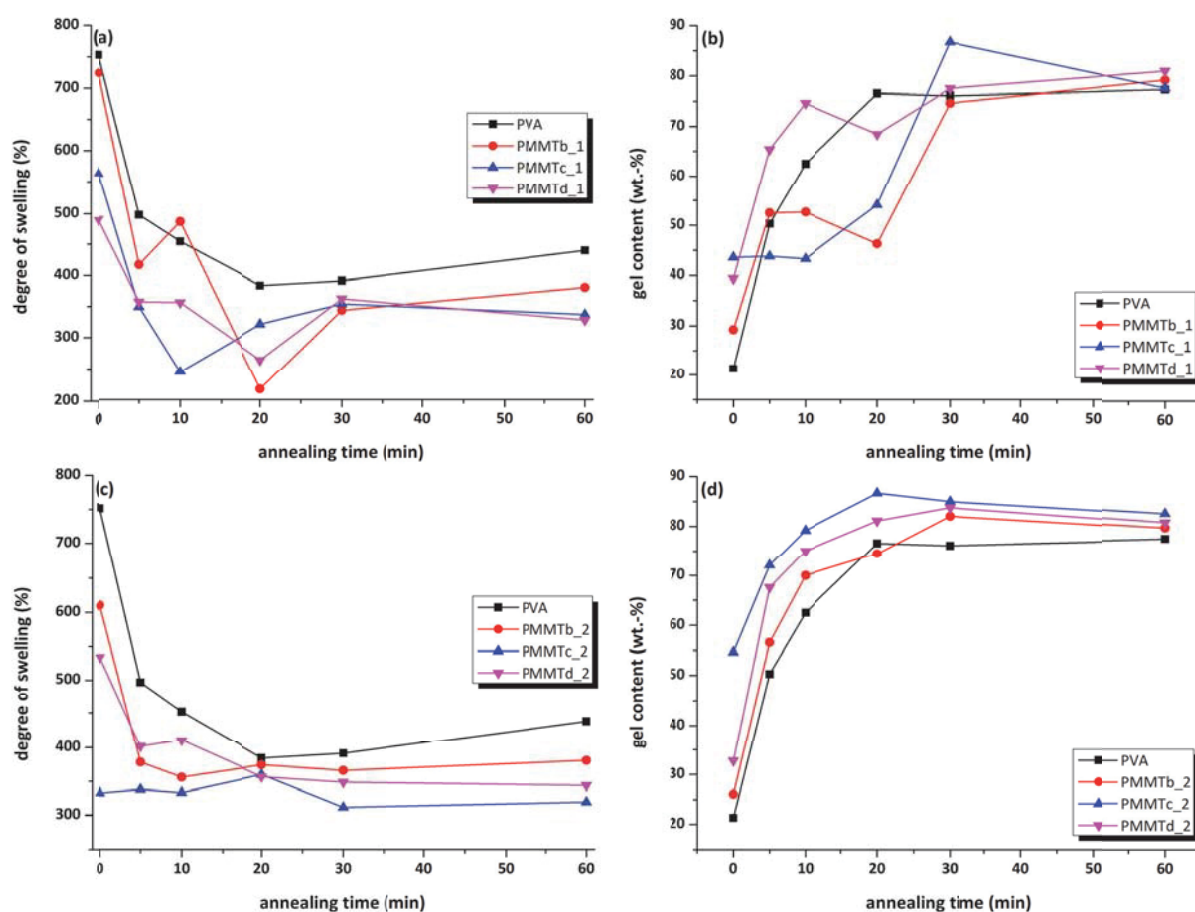
Fig. 109: Change of the degree of swelling (a) and the gel content (b) of PVA composite films containing surface modified montmorillonites. Changes of swelling behaviour of PVA-montmorillonite composite films due to thermal treatment. (a/b) 2.5 wt.-% MMT content; (c/d) 5 wt.-% MMT. The lines are a guide to the eye.

Subsequent UV irradiation after 60 min of heat treatment results in gel contents higher than 85 wt.-%, for all prepared composite materials and even neat PVA. This may be caused by radical formation and additional heating of the samples (see Fig. 110). Compared to the non-

heat treated samples, a significant improvement of the swelling behaviour as a result of this combined method of crosslinking is observed.
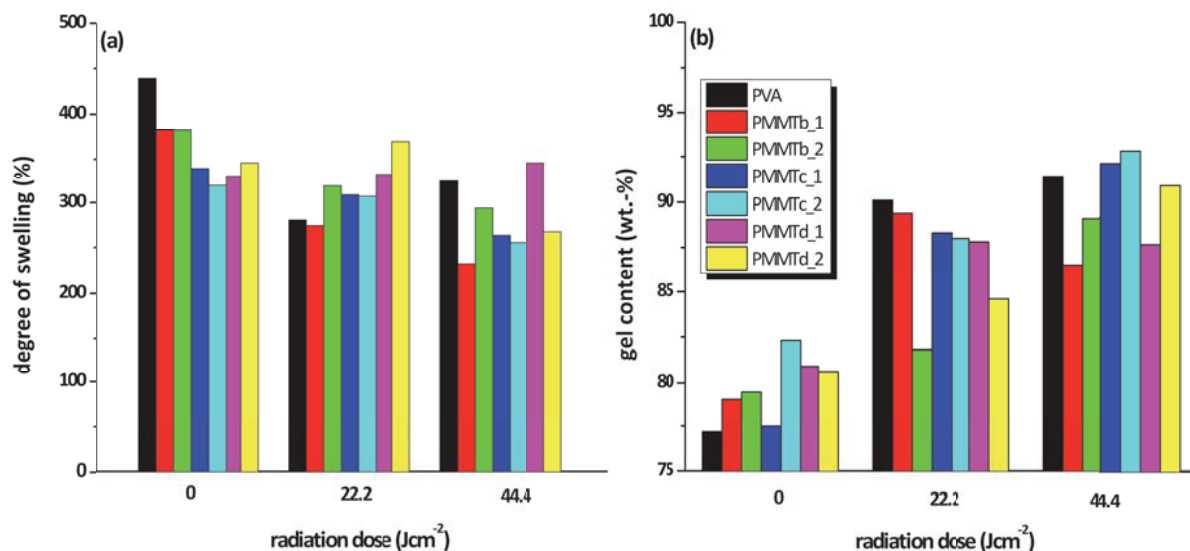
Fig. 110   Sol-gel analysis of heat treated (1 hour at 100°C) PVA-MMT composite films, which were UV irradiated with a medium pressure mercury vapour lamp with an output intensity of 740 mWcm^{-2}. (a) degree of swelling; (b) gel content.

It is evident that the employment of surface modified montmorillonite particles leads to an improvement of the swelling behaviour of PVA composites in deionised water, even without any UV exposure or heat treatment. Annealing followed by UV exposure, with a target dose of 44.4 Jcm^{-2} results in very high gel contents for neat PVA as well as the photoreactive particles. The decomposition of the UV reactive surface groups results in increased interactions between particles and the PVA matrix, either by the formation of covalent crosslinks or hydrogen bonding (see Fig. 111) . Annealing also leads to the formation of additional crystalline zones, which hamper the dissolution of the matrix polymer in water (see Fig. 35).
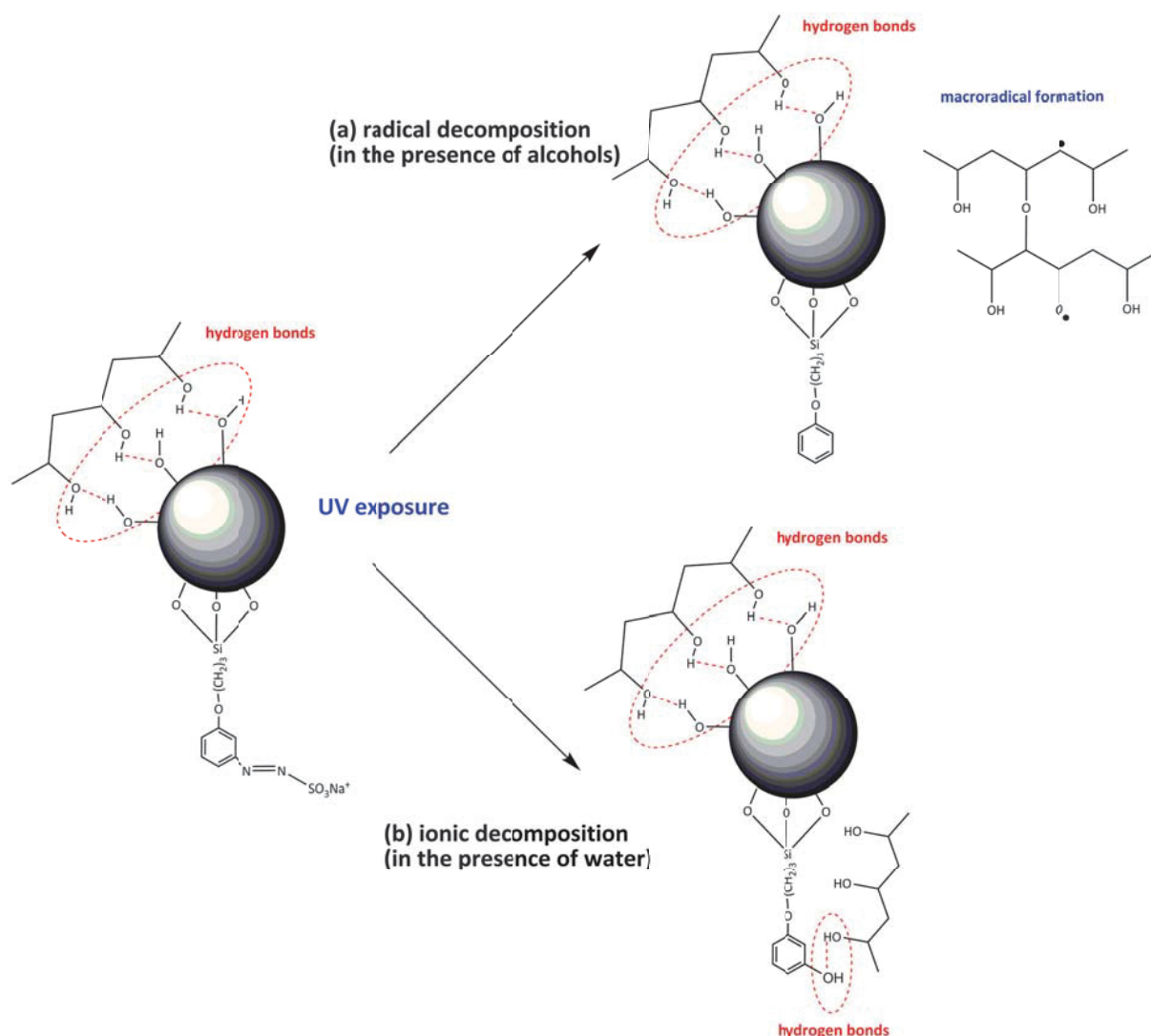
Fig. 111: Schematic representation of possible interactions between the PVA matrix and surface modified particles, bearing azosulphonate moieties on their surface. (a/b) represent the different pathways of decomposition after UV irradiation.

Swelling of silica/PVA composites. The UV exposure of composite samples containing of PVA and UV reactive silica particles results in a general decrease of the swelling behaviour as well as a strong increase of the insoluble fraction. While neat PVA exhibits a gel content of 55 wt.-%, silica composite samples (PP1_1, PP2_2, PP3_1/2) and nanoparticle composites show significantly higher values (see Fig. 112b). This is either resulted by the photodecomposition of the reactive groups, which leads to formation of crosslinks, as well as an increase of the crystalline fraction of the polymer due to heating.[16,177,178]

Whilst a composite comprising 5 wt.-% nanoparticles is dissolved prior UV exposure, the swelling behaviour is improved after a radiation dose of 22 Jcm^{-2}. Further irradiation leads to slight deterioration of the gel content, which is probably caused by chain scission.
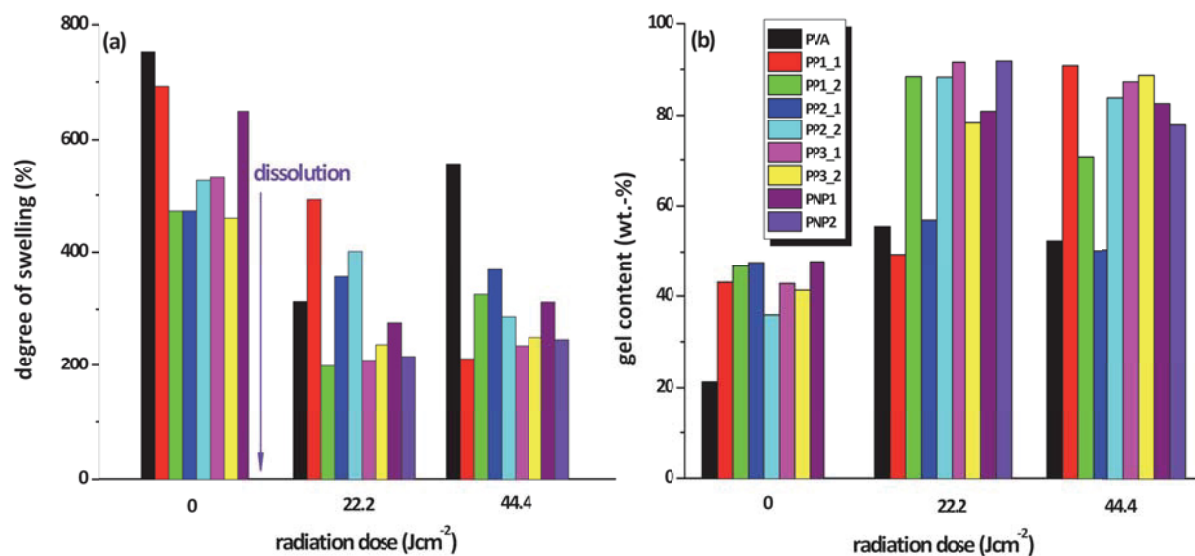
Fig. 112 Swelling behaviour of PVA composites comprising photoreactive silica particles; UV exposure is performed with a medium pressure mercury vapour lamp with an output intensity of 740 mWcm^{-2}.

Heat treatment of thin solid composite films leads to improved swelling resistance, however no advancement compared to the neat polymer can be observed. The nanoparticle composite PNP2 exhibits lower gel contents and a higher degree of swelling, which indicates that the polymer filler interactions are not as strong as in composites comprising fumed silica particles. This may be caused by the higher surface area of the fumed silica particles that leads to improved swelling behaviour. The influence of the heat treatment on the swelling behaviour of PVA composites is shown in the figure appendix (see P 27)

Additional UV exposure after heat treatment leads to an improvement of the swelling behaviour, but it has to be stated, that non-annealed samples reach similar stability against water uptake. It is evident, that UV exposure of thin composite films leads to both covalent crosslink formation and increased physical interactions, such as an increase of the crystallinity of the PVA matrix.

4.3.3 *Conclusions*

The preparation of a novel type of organic-inorganic composites containing of different photoreactive particles and PVA leads to improved swelling behaviour of the matrix polymer, even without any UV exposure or heat treatment. It is found that the polymer-particle dispersions are destabilised by UV irradiation resulting from decomposition of the chromophore on the particle surface. The photolysis behaviour and the resulting hypochromic shift can be easily followed by UV-Vis spectroscopy.

UV exposure of thin films leads to an improvement of the swelling stability, thus providing evidence that covalent crosslinks are formed and strong physical interactions between the organic matrix and the inorganic particles are present. A combination of heat treatment and UV irradiation leads to almost insoluble composites comprising surface modified montmorillonites; while silica based particles do not exhibit such behaviour.

As the photoactive species is immobilised on particle surfaces, neither leaching of the chromophore out of composite or migration onto the surface can take place. This would be crucial for the fabrication of coatings for biomedical applications or hydrogels.[8,17,179–180] As the composite materials exhibit improved stability against dissolution by water, the application as advanced barrier materials with phototuneable properties may be feasible. Furthermore the application as resist material or protective water based coating should be considered, because a dual crosslinking mechanism consisting of heat treatment and UV light can be employed.

4.4 VINYL-MODIFIED PARTICLES FOR E-BEAM CROSSLINKING OF PVA

In order to avoid leaching or migration of crosslinking chemicals, as identified in section 2.2.3 (see page 74), PVA composites containing surface modified silica particles with immobilised vinyl moieties have been prepared. The sample notation and the particle content are given in Table 13.

4.4.1   *Crosslink formation*

To investigate changes of the polymer structure and to identify crosslink formation as well as conversion of the vinyl groups of the silica particles, ATR-FTIR spectra of exposed samples are recorded. It is evident that at least 5 wt.-% of particles are necessary to detect radiation induced changes in the spectra (compare Fig. 113a-d). As a result of electron beam exposure the faint absorption at 936 cm^{-1} is diminished, which can be assigned to the C-H out-of-plane deformation vibration of vinyl groups. This indicates that at least a fraction of the vinyl terminated moieties are converted upon exposure to ionising radiation. An additional absorption of the vinyl CH$_2$ groups should be discernible in a wavenumber range of 905–856 cm^{-1}, but they are obscured by structural absorptions resulting from PVA.[137,144]
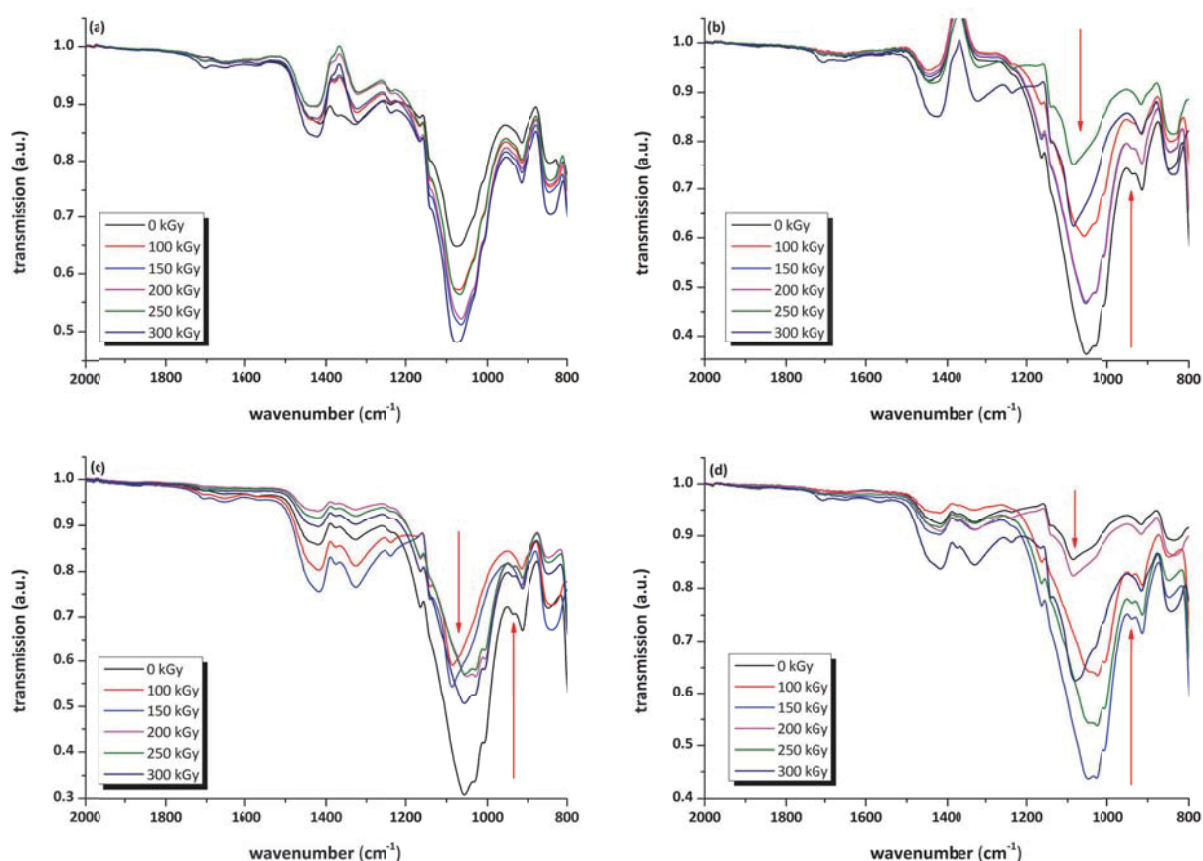
Fig. 113:   ATR FTIR spectra of PVA composites comprising vinyl-modified silica particles. (a) VM1; (b) VM2; (c) VM3 and (d) VM4. The arrows indicate certain areas that undergo changes upon electron beam exposure.

As the vinyl moieties undergo conversion, the formation of ether groups, as a number of -COH groups of the polymer backbone recombine with other formed radicals, is found. This is

indicated by the red arrows in Fig. 113c-d, marking the shift of the structural -COH absorption peak at 1056 cm^{-1} to lower wavenumbers that can be assigned to -C-O-C-deformation vibration.
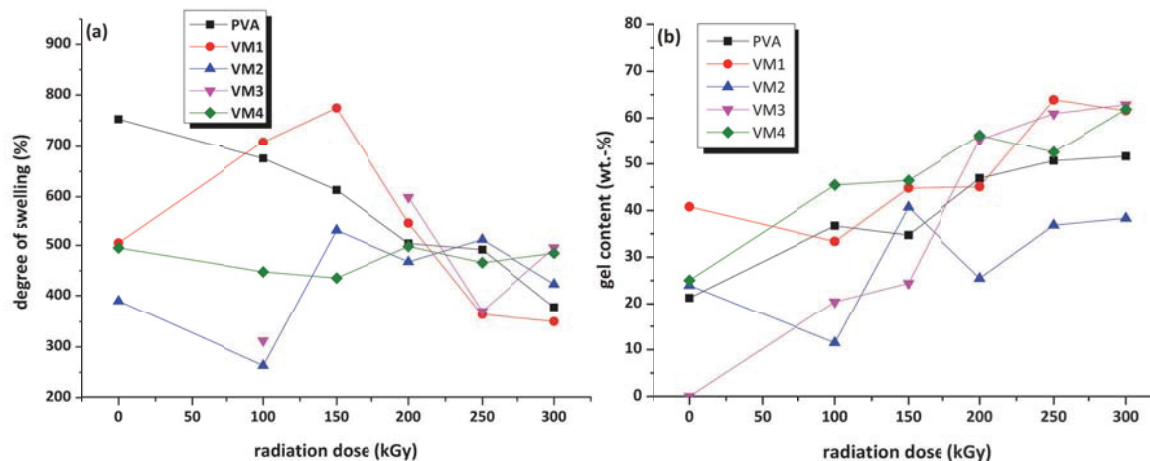
Fig. 114: Swelling behaviour of PVA composite films over applied radiation dose. (a)degree of swelling; (b) gel content. The lines are a guide to the eye.

As the exposure with ionising radiation should lead to radical formation and crosslink build-up by recombination of these radicals, no general improvement of the swelling stability of the prepared PVA-particle composite samples in deionised water can be found. It is evident that the degree of swelling is decreased and the gel content is increasing, but this is mainly caused by heating of the sample during the exposure.

Conclusions. The addition of commercially available vinyl-modified particles would have been a novel way to facilitate e-beam assisted crosslinking of PVA. FTIR measurements reveal that crosslinks are formed as well as a portion of the vinyl groups are converted. As the vinyl groups are of low reactivity, alternative particles with an acrylate or methacrylate moieties on their surface, which are more reactive, should be employed as solid crosslinking agents. Further addition of non-irritant radical initiators such as Lucirin® TPO-L could lead to improved crosslinking densities. On the other hand the initiator may migrate out of the composite material. It has to be stated that the addition of a number of alternatively prepared additives leads to improved swelling behaviour without the employment of ionising radiation or radical initiators. E-beam assisted crosslinking of PVA is therefore considered to be inferior to UV-light instigated crosslinking and heat induced methods.

4.5   IMPROVEMENT OF SOLVENT RESISTANCE OF XNBR

4.5.1   *Determination of particle distribution in XNBR matrix*

In order to investigate the montmorillonite particle distribution in XNBR, thin composite films, which were prepared in accordance to method III (see page 55), were cryogenically cracked to evidence the particle distribution over the cross section of the samples. The results of this investigation are depicted in Fig. 115, giving a survey of the crack surface as well as of the particle distribution (SEM micrographs). A backscatter electron detector is employed to visualise differences of material density thus alleviating the determination of incorporated montmorillonite platelets.

Composite films containing of 2 wt.-% either Zn^{2+} or Mn^{2+}-MMT in XNBR exhibit a homogenous distribution of the platy clay particles, which can be discerned in Fig. 115a/c. Lamella stacks with a size of about 100 nm are found for the Zn^{2+}-MMT composite, with high dispersibility. This should lead to strong polymer-filler interactions that could have a reinforcing effect on the mechanical strength and on the stability against chloroform and crude oil. The manganese cation exchanged montmorillonite is distributed in a similar manner, but the lamella packages appear to be slightly bigger with a thickness of approximately 25 nm.
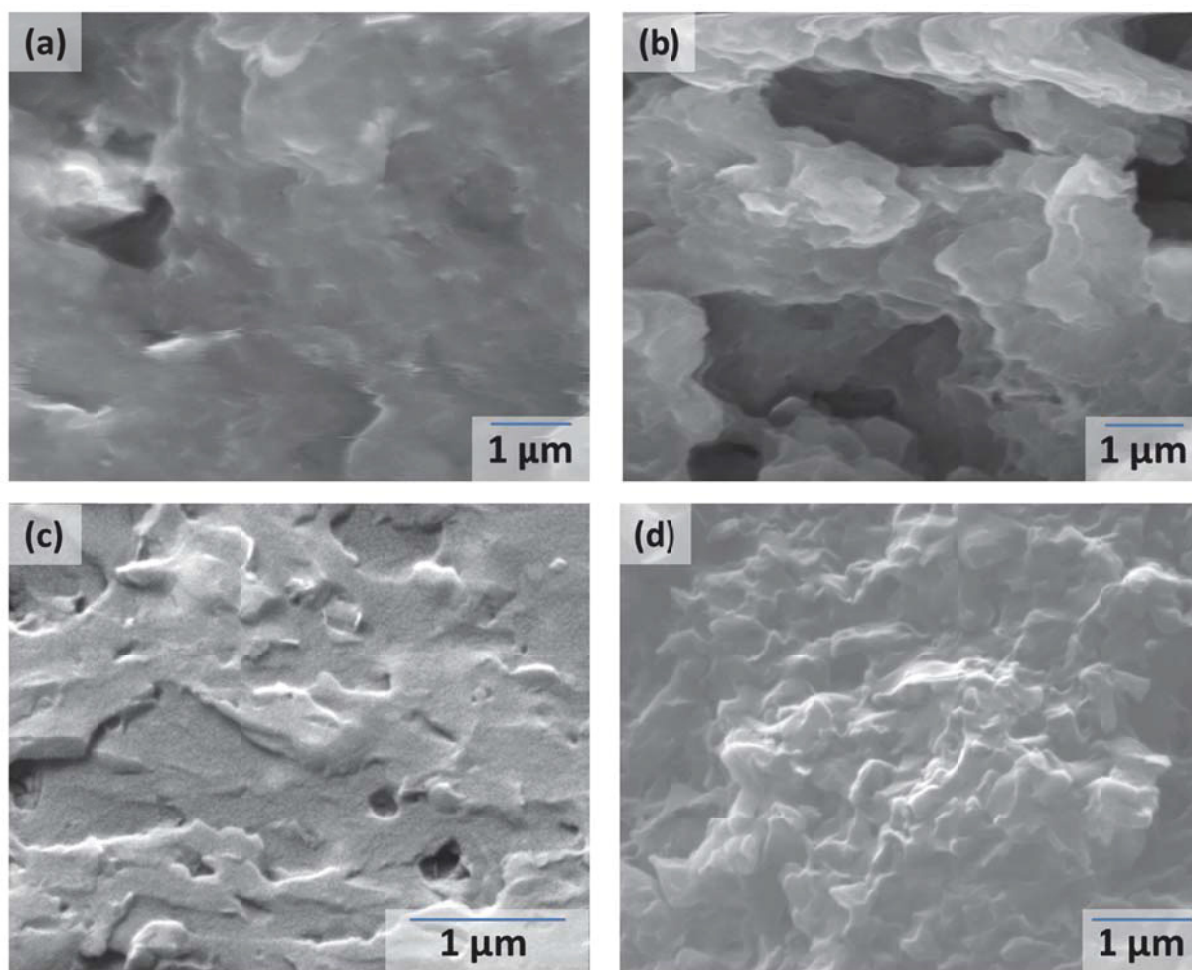
Fig. 115: SEM micrographs of the cross section of cryogenically broken XNBR-montmorillonite composite films. (a) 2wt.-% Zn^{2+}-MMT; (b) 7 wt.-% Zn^{2+}-MMT; (c) 2 wt.-% Mn^{2+}-MMT; (d) 5 wt.-% Mn^{2+}-MMT.

The crack surface of a thin XNBR composite loaded with 7 wt.-% of zinc cation exchanged clay resembles that of a typical brittle crack. The particles are evenly distributed and are located on the edges of the scaly structures, which can be discerned by the brightness differences due to more intense electron backscattering by the inorganic filler particles (see Fig. 115b). A composite film comprising 5 wt.-% Mn^{2+}-MMT exhibits a similar distribution of the clay particles, and brittle crack surface (see Fig. 115d).

Scanning electron microscopy reveals that the cation exchanged montmorillonite particles are evenly distributed in the XNBR matrix of the prepared composite films with a high dispersibility. The resulting strong polymer-filler interactions due to the high filler surface would have a reinforcing effect on the mechanical strength. On the other hand this would also lead to more brittle elastomer composites. These strong interactions should also improve the chemical resistance, which would be pivotal for the preparation of sealants.

4.5.2   *Determination of mechanical properties*

As the mechanical properties of elastomers are strongly influenced by polymer-filler interactions, tensile testing measurements have been conducted to investigate the effect of the method of incorporation of the filler material on the XNBR samples. The reference material is crosslinked by the conventional method using zinc oxide and exhibits high stress and strain at break (see Table 24 and Fig. 116a).

In a first attempt 5 wt.% Zn^{2+}-MMT were incorporated into zinc oxide crosslinked XNBR latex by dispersing the latex dispersion with the MMT dispersion (method II). This leads to an improved stiffness of the composite, whereas the strain at break and the stress at break are diminished. The incorporation of 10 wt.-% layered silicate leads to very brittle composite films that are not suitable for tensile testing sample preparation (see Table 24).

Crosslinking of XNBR using Zn^{2+}-MMT leads to deterioration of the stiffness and the stress at break, whereas the elongation at break is increased (see Fig. 116a). Higher content of layered silicate leads to embrittlement of the samples, thus reducing the elongation at break to 470 %.and the stress at break to 12.7 MPa as well, the stiffness however is increased.

Therefore it is concluded, that 2 wt.-% of Zn^{2+}-MMT are sufficient to achieve crosslinking of the XNBR latex. Higher contents of this particular cation exchanged MMT lead to a deterioration of the mechanical properties.

Table 24: Mechanical properties of XNBR composite films containing cation exchanged montmorillonite and ZnO

method	sample	E_t (MPa)	ε_B (%)	σ_B (MPa)
I	ZnO	1,78	690	43,75
II	ZnO / 5 wt.-% Zn^{2+}-MMT	2,82	428	15,33
	ZnO / 10 wt.-% Zn^{2+}-MMT	Films too brittle for die cutting of samples		
III	2 wt.-% Zn^{2+}-MMT	0,91	732	17,75
	7 wt.-% Zn^{2+}-MMT	1,89	470	12,67
	2 wt.-% Mn^{2+}-MMT	1,32	377	8,21
	2 wt.-% Mn^{2+}-MMT (25,3 Jcm^{-2})	n.d.	251	12,29
	5 wt.-% Mn^{2+}-MMT (25,3 Jcm^{-2})	3,17	412	15,16

The addition of 2 wt.% Mn^{2+}-MMT as crosslinking agent (method III), however, leads to crosslinked films, but the tensile properties are deteriorated, except the stiffness, which is correlated with the tensile modulus. Subsequent UV exposure results in improved stiffness, while strain and stress at break are increasing with increasing irradiation time, resulting in radiation doses of 25.3 Jcm^{-2} (see Fig. 116b). Composites comprising of 5 wt.-% Mn^{2+}-MMT show increased stiffness, almost twice the value of the reference material.
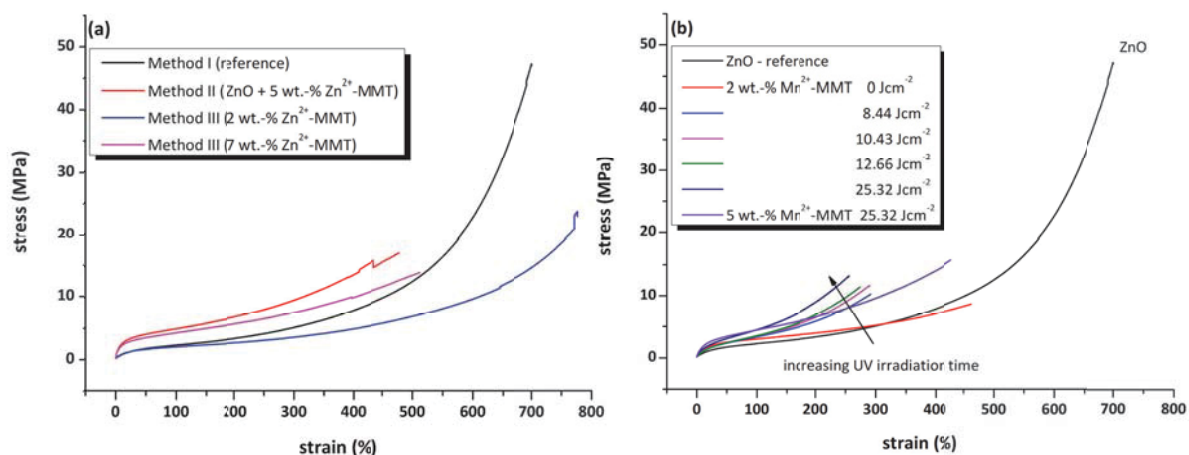
Fig. 116: Stress-strain curves of selected XNBR-MMT composite films. (a) different methods of sample preparation employing Zn^{2+}-MMT (b) influence of subsequent UV crosslinking on XNBR-Zn^{2+}-MMT composites which are prepared in accordance to method III.

Regarding the use of alternative methods for the crosslinking of XNBR latex it is found, that the tensile properties such as stress and strain at break are deteriorated, while the stiffness of the materials is improved. It has to be stated that the main aim of this recent work is the improvement of the solvent resistance of XNBR by the employment of bivalent cation exchanged montmorillonites.

4.5.3 *Investigation of solvent resistance*

The degree of swelling of thin crosslinked XNBR samples is determined in crude oil at room temperature and compared to a reference material. Due to the addition of Zn^{2+}-MMT to ZnO crosslinked XNBR the swelling is decreased by 15 %. Crosslinking in accordance to method III leads to further improvement of the swelling stability, but with increasing MMT content, the degree of swelling is increased. This may be caused by surface cracking and porosity, as a result of the determined embrittlement (see Fig. 117). In contrast to this an increase of the

content of manganese cation exchanged montmorillonite leads to a decrease of the swelling in crude oil to 105 %, without any UV treatment.
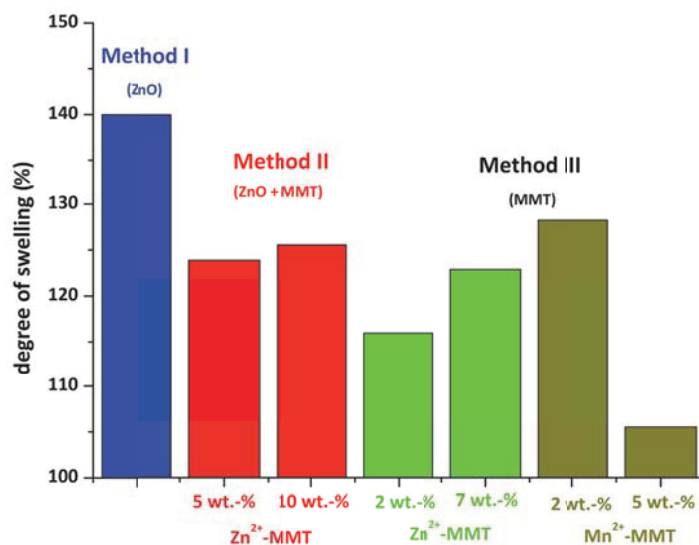
Fig. 117: Swelling of thin XNBR films using crude oil as testing fluid at RT for 48 hours compared to conventionally crosslinked XNBR.

Additional UV exposure using a Ga-doped mercury lamp to obtain a dual-crosslinked XNBR composite material (similar to the work Lenko and Schlögl) with improved resistance against crude oil and chloroform is performed.[89] The degree of swelling in crude oil of composite films containing of 2 wt.-% montmorillonite (Zn^{2+}/Mn^{2+}) is decreased by 10 % as a result of UV exposure, (dose of 12.7 Jcm^{-2}). As composites containing 7 wt.-% MMT exhibit a deteriorated swelling behaviour no UV irradiation experiments are conducted. Crosslinked XNBR composites with a montmorillonite content of 5 wt.-% also feature an increase of the degree of swelling of 17 %, which is followed by a slight decrease with increasing irradiation time (see Fig. 118a). This may be caused by the formation of surface cracking due to UV exposure, resulting in higher absorption of crude oil.
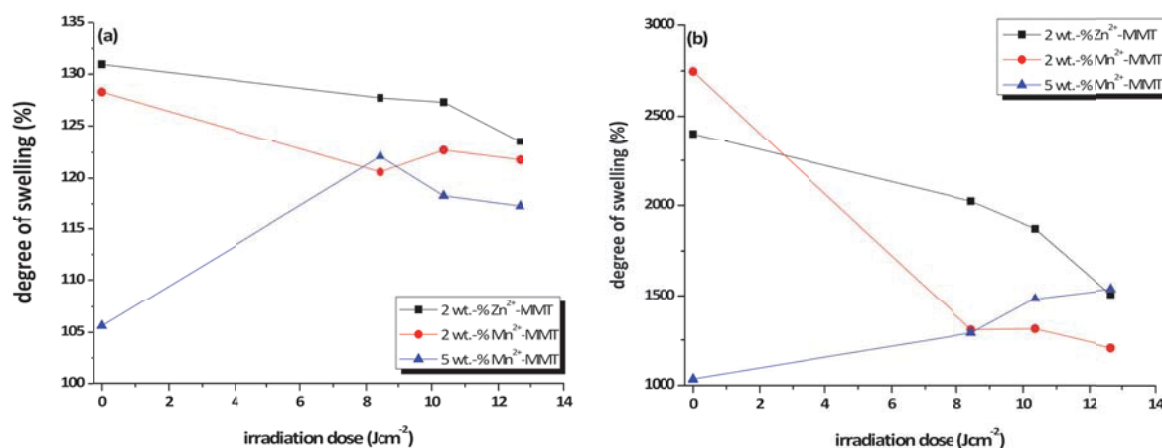
Fig. 118: Swelling of UV exposed XNBR composite samples versus irradiation dose. Immersion fluids: (a) crude oil; (b) chloroform. The lines are a guide to the eye.

To determine a distinctive tendency of the degree of swelling of UV irradiated XNBR, composite samples are immersed in chloroform, which is a more appropriate solvent for XNBR. It is evident that a radiation dose of 8.33 Jcm^{-2} leads to a decrease of 350 % of the degree of swelling for Zn^{2+}-MMT crosslinked samples, employing 2 wt.-% the functional additive. At an irradiation dose of 12.6 Jcm^{-2} a degree of swelling of 1500 % is obtained as a result of the formation of covalent crosslinks. For composites comprising 2 wt.-% Mn^{2+}-MMT the degree of swelling is almost halved upon the first irradiation step, further exposure results in a slight decrease to a total of 1200 %.

As mentioned before, an increase of the degree of swelling for composites films comprising 5 wt.-% of Mn^{2+}-MMT is found. That may be caused by chain scission due to UV-exposure or the increased surface areas that are created by the formation of microcracks. However the employment of manganese cation exchanged montmorillonite as crosslinking aid results in a better solvent stability compared to ZnO crosslinked films and Zn^{2+}-MMT as crosslinking agent.

4.5.4   *Conclusions*

It is demonstrated that the conventional crosslinking agent ZnO can be substituted with zinc or manganese cation exchanged montmorillonites, making the preparation of thin solvent resistant films feasible. Due to the high dispersibility of the filler particles, strong polymer-filler interactions occur, which lead to embrittlement of the film samples, thus reducing the

strain and stress at break. Subsequent UV crosslinking leads to a slight improvement of the failure stress; however, the strain at break is further deteriorated.

The main aim, to improve the solvent resistance, especially crude oil, has been achieved. This would be pivotal for the preparation of novel sealant or protective coating materials in contact with crude oil. Compared to conventional crosslinked XNBR, the montmorillonite crosslinked composites exhibit improved swelling behaviour in crude oil and chloroform. Subsequent UV exposure leads to further diminishing of the degree of swelling for composites comprising 2 wt.-% Zn^{2+} or Mn^{2+}-MMT, while a composite containing 5 wt.-% Mn^{2+}-MMT shows deterioration of the swelling properties due to formation of surface cracking. Therefore it is concluded that the optimum amount of Mn^{2+}-MMT is in between 2 and 5 wt.-%.

The use of functionalised montmorillonites as alternative crosslinking agents for XNBR may find application for solvent resistant protective coatings for metals or sealants in contact with seawater and crude oil. As crosslinking agents are immobilised in the interlayer galleries of the MMT, no leaching due to swelling can take place.

VI.   OVERALL CONCLUSIONS

1.   ALTERNATIVE METHODS OF PVA CROSSLINKING

Three different concepts of crosslinking of poly(vinyl alcohol) (PVA) have been investigated with emphasis on the determination of crosslinking mechanisms and the reduction of solubility/swelling behaviour in deionised water as testing fluid.

E-beam crosslinking of PVA. Doping of PVA with triallyl isocyanurate (TAIC), however, did not work out as intended, because the crosslinking aid tends to bleed out of the matrix. As the crosslinking aid TAIC is considered noxious and harmful to water organisms and the swelling properties of PVA composites are not significantly improved, the employed electron beam crosslinking concept has not been further pursued.

UV crosslinking of PVA. Upon doping of PVA with $FeCl_3$ a photoreactive polymeric material has been obtained, which exhibits (1) strong changes of the refractive index, (2) changes in optical absorption and (3) a significant improvement of the swelling behaviour of PVA in deionised water after UV irradiation. It is found that the mechanism of crosslinking is based on a photoreduction of Fe^{3+} to Fe^{2+}, which results in photobleaching as well as the formation of macroradicals that recombine, thus forming crosslinks in PVA. Photolithographic patterning results in topographical features (after development in deionised water) and outstanding contrast behaviour, which is achieved by UV induced modulation of the refractive index and the photobleaching effect.

Azosulphonate doped PVA. Doping of PVA with aryl azosulphonate dyes has been used to prepare a new photoreactive and water-based resist material, with the possibility to tune the polarity and the optical contrast behaviour of the material by UV light. Heat treatment is employed to immobilise the photoactive dyes, which leads to a strong improvement of the swelling behaviour for materials containing the dicarboxylic acid AZOII. The UV initiated decomposition of the dyes has no influence on the swelling behaviour in deionised water. Spectroscopic analysis revealed that an ionic decomposition mechanism of the azosulphonate dopant is prevalent. The obtained resist materials are applicable for photolithographic patterning. They exhibit excellent contrast behaviour as a result of UV induced cleavage of the chromophore, which can be visualised by phase contrast imaging. As

the azosulphonate moieties exhibit high thermal stability, so the applicability in high temperature environments is given. As nitrogen gas evolves upon UV exposure due to the cleavage of the azo groups, microcellular foaming applications with the possibility to prepare patterned foamed areas may be considered.

2. FUNCTIONALISED INORGANIC PARTICLES

A number of concepts have been pursued to prepare modified inorganic particles ranging from metal cation exchanged montmorillonites (MMT) to photoactive particles, bearing aryl azosulphonate moieties on their surface.

Metal cation exchanged montmorillonite. Transition metal cation exchanged montmorillonites have been prepared for the application as ion donor materials for crosslinking reactions, with emphasis on crosslinking XNBR latex to either substitute commercial crosslinking agents and to enhance the solvent stability of latex films. Additionally, a Fe^{3+} cation exchanged montmorillonite has been prepared in a similar manner, until no more iron ions are leached out. The major aim of the intercalation of Fe^{3+} ions was the immobilisation of the UV reactive species aiming at the photochemical crosslinking of polymers. This has been demonstrated for PVA, which can be crosslinked by UV light, when loaded with the modified montmorillonite.

Amino acid intercalated montmorillonite. Cation exchange reactions have been employed to immobilise amino compounds with functional groups, such as carboxylic, mercapto or sulphonic acid moieties, into the interlayer galleries of montmorillonite. Whilst the absorption of glycine and L-cysteine has been well studied and documented by a number of authors, the immobilisation of taurine to introduce sulphonic acid groups has not been reported yet.

The prevalent acid treatment of MMT leads to increased delamination of the clay mineral as well as to an increased organophilicity, which results in a higher intercalated organic content. MAXS patterns suggest that the d_{001} spacing is increased due to intercalation of the amino compounds, and mono- and bilayer formation can be determined for taurine intercalated MMT. The new two-step process of acid activation and amino acid intercalation

for the preparation of enhanced clay minerals leads to increased organic content as well as repulsion of interlayer water.

Surface functionalised particles. Photoreactive silica and montmorillonite particles with immobilised aryl azosulphonate moieties were obtained by surface silanisation followed by diazotisation reactions. Photolysis experiments of aqueous particle suspensions have been conducted, showing that the surface modified particles exhibit the photolytic behaviour of aryl azosulphonates. Moreover, a photoinduced destabilisation of the particle dispersions has been observed. Thermogravimetric measurements reveal high weight losses, which contribute to the successful immobilisation of organic substance.

3. ORGANIC-INORGANIC COMPOSITE MATERIALS

A variety of organic-inorganic composite materials, most of them comprising poly(vinyl alcohol) as matrix polymer, have been prepared and the resistance against dissolution in deionised water as well as the particular mechanism of crosslinking and the particle distribution has been investigated.

UV reactive PVA-Fe^{3+}-MMT nanocomposites. Fe^{3+} cation exchanged montmorillonite has been employed as iron ion donor for photochemical crosslinking of PVA. Besides very strong polymer-filler interactions, covalent crosslinks are formed, which result in significant improvement of the stability of the composites against water uptake. Due to the photobleaching caused by reduction of photoactive Fe^{3+} to Fe^{2+}, the crosslinking of comparatively thick substrates is feasible. The montmorillonite platelets are distributed evenly alongside the cross section of prepared samples with an almost parallel orientation. Also delamination of the platelets is observed, resulting in particle sizes ranging from 15 to 100 nm.

Composite materials comprising PVA and organo modified montmorillonite. The utilisation of amino acid intercalated montmorillonites as functional filler materials for PVA has led to some not anticipated results, such as the vanishing of the melting point during DSC measurements for activated MMT. Furthermore it has been found that the use of acid activated and organo modified MMT leads to an improved water resistance compared to sodium MMT.

Employment of UV reactive particles for crosslinking of PVA. The introduction of photoreactive inorganic particles (SiO_2 and montmorillonites), bearing azo sulphonate moieties on their surface, in poly(vinyl alcohol) makes a photoassisted tuning of material properties feasible. Dual crosslinking by heat treatment, followed by subsequent UV exposure leads to outstanding water resistance for composite materials comprising montmorillonite. This leads to highly crosslinked systems, which may be employed for protective coatings or barrier materials with phototuneable properties. As the decomposition of the immobilised dyes leads to the formation of nitrogen gas, micropores may be formed. The UV induced cleavage of the chromophore leads to the formation of hydroxyphenyl ($-C_6H_5OH$) or phenyl ($-C_6H_5$) groups, which remain on the particle surface.

Vinyl-modified particles for e-beam crosslinking of PVA. The electron beam exposure of PVA composites comprising silica particles with vinyl groups on their surface does not lead to highly crosslinked samples, hence the reactivity of the double bonds is not given and the matrix polymer undergoes chain scission caused by the ionising radiation.

Improvement of solvent resistance of XNBR. It has been demonstrated that transition metal cation exchanged montmorillonites (Zn^{2+}/Mn^{2+}) can be applied as crosslinking agents for XNBR latex, instead of conventional crosslinking using zinc oxide. To enhance the solvent stability further, additional crosslinking chemicals are used, thus attaining a dual crosslinking mechanism by physical interactions with the filler particles and covalent crosslinks, which are formed by the UV induced thiol-ene reaction. Experimental data clearly show that composites comprising manganese cation exchanged MMT exhibit better swelling stability in both crude oil and chloroform compared to the ZnO crosslinked samples. However, it has to be stated that the employment of MMT as functional filler leads to deterioration of the mechanical properties, mainly by embrittlement of the obtained samples.

4.   OUTLOOK

As an overview on possible fields of application of water-based and environmentally benign materials (UV reactive PVA, montmorillonites and their composites) is presented in the concluding section, the possible future progress in these fields of work is discussed in this section of the thesis.

The preparation of flexible polymer waveguides employing $PVA:FeCl_3$ as well as azosulphonate-doped PVA, by the means of photolithographic patterning should be highlighted. As these new photoreactive materials are water-based and can be developed with water after patterning, this would be an environmentally benign alternative to common resist materials. Furthermore, the barrier properties of the UV curable system $PVA:FeCl_3$ against non-polar organic solvents and fatty acids at different humidity levels would be of great interest for the application as biomedical products and coatings intended for food packaging.

In order to prevent leaching of azosulphonate compounds, the coupling reaction as well as the composition of the composite should be further optimised to allow for almost complete conversion of the carboxylic moieties, which should result in full immobilisation. Investigations concerning changes of the polarity of the composites due to decomposition of the photoactive species, as well as changes of permeability should be investigated in further work.

The activation and organic modification of layered platy alumosilicates such as montmorillonites provides a wide field of possible applications, ranging from solid state catalysts to fillers for polymers or as carrier materials of functional groups by immobilisation in the interlayer galleries or onto the surface.

Additional attempts to activate montmorillonite by the employment of mineral acids (e.g. HNO_3, H_3PO_4, H_2SO_4) may lead to changes of the morphology of the platy clay and increase the dispersibility of the particles as well. These activated MMTs may be employed for further modification steps or as catalytic materials.

As the organic modification of activated clays leads to an increase of the intercalated organic content, the intercalation of a number of amino compounds could be employed to immobilise functional moieties in the interlayer galleries of the montmorillonite. These clay minerals may be employed as stationary phases in the field of chromatography, for the removal of dyes out of water or as sequestrant for heavy metal ions.

As neat PVA exhibits outstanding barrier properties against non-polar organic compounds, the determination of barrier properties for organic-inorganic PVA composite materials under

different environmental conditions may be of interest. The investigation of the influence of aerial humidity on the diffusion of volatile compounds through crosslinked composite membranes is pivotal for the preparation of barrier layers. As some of the obtained composite samples can be employed for hydrogels for biomedical applications, the determination of cytotoxicity and further investigations concerning leaching out of crosslinking aids would be crucial.

VII.   REFERENCES

1.   Kuschel, V. Klimaschutzbericht 2012: Wien, Umweltbundesamt GmbH; ISBN: 978-3-99004-194-9, **2012**.

2.   Arbeitsgruppe "Papier, Karton und Pappe": Di-isobutylphthalat in Papieren und Kartons für den Kontakt mit Lebensmitteln, Sitzungsprotokoll; Bundesinstitut für Risikobewertung (BfR), Berlin, Germany, **2007**.

3.   Council of Europe, Committee of Ministers: Paper and board materials and articles intended to come into contact with foodstuffs: Resolution AP(2002)/1, **2002**.

4.   Public health committee, Committee of experts on materials coming into contact with food, Coatings intended to come into contact with foodstuffs, Council of Europe Policy Statement, **2008**.

5.   Escabasse, J.Y.; Ottenio, D. *Food Additives and Contaminants* **2002**, *19*, 79–92.

6.   VERORDNUNG (EG) Nr. 1935/2004 DES EUROPÄISCHEN PARLAMENTS UND DES RATES über Materialien und Gegenstände, die dazu bestimmt sind, mit Lebensmitteln in Berührung zu kommen und zur Aufhebung der Richtlinien 80/590/EWG und 89/109/EWG: EG Nr. 1935/2004, **2004**.

7.   Kielhorn, J.; Pohlenz-Michel, C.; Schmidt, S.; Mangelsdorf, I. Concise International Chemical Assessment Document 57: GLYOXAL: Geneva, **2004**.

8.   Schauberger, J.G. Polymere als Barrierematerialien für Karton. Master Thesis, **2009**.

9.   Schauberger, J.G.; Riess, G.; Kern, W. *Journal of Applied Polymer Science*.

10.   Trepanier, F.; Manivannan, G.; Changkakoti, R.; Lessard, R.A. *Can. J. Phys* **1993**, *71*, 423–428.

11.   Schauberger, J.G.; Riess, G.; Kern, W. *Journal of Applied Polymer Science* **2013**.

12.   Cox, M.; Rus-Romero, J.R.; Sheriff, T.S. *Chemical Engineering Journal* **2001**, *84*, 107–113.

13.   Knopp, D.; Tang, D.; Niessner, R. *Anal Chim Acta* **2009**, *647*, 14–30.

14.   Herrmann, W.O.; Haehnel, W. *Ber. dtsch. Chem. Ges. A/B* **1927**, *60*, 1658–1663.

15.   Amiya, S.; Tsuchiya, S.; Qian, R.; Nakajima, A. *Pure Appl. Chem.* **1990**, *62*, 2139–2146.

16.   Finch, C.A., Ed. Poly(vinylalcohol): Properties and applications; Wiley: London, New York, **1973**.

17.   Svensson, K.; Binderup, M.-L.; Brede, C.; Fabech, B.; Hallikainen, A.; Hellstrom, T.; Petersen, J.H.; Sveinsdottir, S., Eds. Adhesives in food contact materials and articles: proceedings from a Nordic seminar. June 2001.

18. Busch, J.R.; Francis, W. Gelled coating compositions and method of making same, US 3864294, **1972.**

19. So, J.-H.; Oh, M.-H.; Lee, J.-D.; Yang S.-M. *J Chem Eng Jpn* **2001**, *34*, 262–268.

20. SANCO D3/AS : 2005: European Commission, SYNOPTIC DOCUMENT of the European Commission, Provisional list of monomers and additives notified to European Commission as substances, which may be used in the manufacture of plastics and coatings intended to come into contact with foodstuffs, **2005**.

21. Mawad, D.; Martens, P.J.; Odell, R.A.; Poole-Warren, L.A. *Biomaterials* **2007**, *28*, 947–955.

22. Pal, K.; Banthia, A.; Majumdar, D. *Journal of Materials Science: Materials in Medicine* **2007**, *18*, 1889–1894.

23. Peppas, N.A.; Huang, Y.; Torres-Lugo, M.; Ward, J.H.; Zhang, J. *Annu Rev Biomed Eng* **2000**, *2*, 9–29.

24. Lagaron, J.M.; Nunez, E. *Journal of Plastic Film and Sheeting* **2012**, *28*, 79–89.

25. Zhang, Z.; Britt, I.J.; Tung, M.A. *J. Appl. Polym. Sci.* **2001**, *82*, 1866–1872.

26. Cava, D.; Cabedo, L.; Gimenez, E.; Gavara, R.; Lagaron, J.M. *Polymer Testing* **2006**, *25*, 254–261.

27. Braun, D.; Walter, E. *Colloid & Polymer Science* **1980**, *258*, 795–801.

28. More, S.M.; Kulkarni, R.V.; Sa, B.; Kayane, N.V. *J. Appl. Polym. Sci* **2010**, *116*, 1732–1738.

29. Phillipp, W.; Hsu, L.-C. *NASA Technical Paper 1407* **1979**.

30. Pal, K.; Banthia, A.K.; Majumdar, D.K. *AAPS PharmSciTech* **2007**, *8*, E142.

31. Bandyopadhyay, A.; Sarkar, M.; Bhowmick, A.K. *J Mater Sci* **2005**, *40*, 5233–5241.

32. Kotoky, T.; Dolui, S.K. *Journal of Sol-Gel Science and Technology* **2004**, *29*, 107–114.

33. Mansur, H.S.; Mansur, A.P. *Mater. Res. Soc. Symp. Proc. Vol. 873E* **2005**, *Vol. 873E*.

34. Navarra, M.; Fernicola, A.; Panero, S.; Martinelli, A.; Matic, A. *Journal of Applied Electrochemistry* **2008**, *38*, 931–938.

35. Tamaki, R.; Chujo, Y. *Appl. Organometal. Chem* **1998**, *12*, 755–762.

36. Gudeman, L.F.; Peppas, N.A. *J. Appl. Polym. Sci.* **1995**, *55*, 919–928.

37. Guiot, O.; Tighzert, L.; Coqueret, X. *European Polymer Journal* **1999**, *35*, 565–570.

38. Taleb, M.F.A.; El-Mohdy, H.L.A.; El-Rehim, H.A.A. *Journal of Hazardous Materials* **2009**, *168*, 68–75.

39. Zhao, L.; Mitomo, H.; Zhai, M.; Yoshii, F.; Nagasawa, N.; Kume, T. *Carbohydrate Polymers* **2003**, *53*, 439–446.

40. Park, K.R.; Park, S.; Kwon, I.; Young, C.N. *Applied Chemistry* **2003**, *7*, 459–462.

41. Barichard, A.; Israëli, Y.; Rivaton, A. *J. Polym. Sci. A Polym. Chem* **2008**, *46*, 636–642.

42. El-Khodary, A. *Physica B: Condensed Matter* **2009**, *404*, 1287–1294.

43. Kumar, G.; Chandramani, R. *Acta Physica Polonica A* **2010**, *117*, 917–920.

44. Manivannan, G.; Nikolov, O.; Kardinahl, T.; Keune, W.; Franke, H.; Changkakoti, R.; Lesssard, R.A. *SPIE Proc.* **1994**, *2042*, 98–109.

45. Bulinski, M.; Iova, I.; Belea, A.; Kuncser, V.; Filoti, G. *Journal of Materials Science Letters* **2000**, *19*, 27–28.

46. Kuncser, V.; Avramescu, A.; Filoti, G.; Rotaru, P.; Podgorsek, R.; Biebricher, M.; Franke, H. *Journal of Alloys and Compounds* **1997**, *256*, 269–275.

47. Kuncser, V.; Filoti, G.; Avramescu, A.; Podgorsek, R.; Biebricher, M.; Franke, H. *Journal of Alloys and Compounds* **1997**, *257*, 285–292.

48. Filoti, G.; Kuncser, V.; Franke, H.; Kardinahl, T.; Manivannan, G. *Journal of Radioanalytical and Nuclear Chemistry* **1995**, *190*, 315–320.

49. Changkakoti, R. *Opt. Eng* **1993**, *32*, 2240.

50. Kandori, K.; Ishikawa, T. *Colloid & Polymer Science* **2004**, *282*, 1118–1125.

51. Kowalonek, J.; Kaczmarek, H.; Bajer, D. *Macromol. Symp* **2010**, *295*, 114–118.

52. Tang, Z.; Wei, J.; Yung, L.; Ji, B.; Ma, H.; Qiu, C.; Yoon, K.; Wan, F.; Fang, D.; Hsiao, B.S.; Chu, B. *Journal of Membrane Science* **2009**, *328*, 1–5.

53. Blaya, S.; Carretero, L.; Madrigal, R.F.; Ulibarrena, M.; Fimia, A. *Applied Physics B: Lasers and Optics* **2002**, *74*, 603–605.

54. Liou, F.J.; Niu, G.C.C.; Wang, Y.J. *J. Appl. Polym. Sci.* **1992**, *46*, 1967–1972.

55. Gung, Y.W.; Kuo, S.M.; Wang, Y.J. *Biomaterials* **1997**, *18*, 367–371.

56. Overberger, C.G.; O'Shaughnessy, M.T.; Shalit, H. *J. Am. Chem. Soc.* **1949**, 2661.

57. Nuyken, O.; Voit, B. *Macromol. Chem. Phys.* **1997**, *198*, 2337–2372.

58. Nuyken, O., Ed. Encyclopedia of Polymer Science and Engineering p.143; Wiley & Sons: New York, **1985**.

59. Sheppard, C.S., Ed. Encyclopedia of Polymer Science and Engineering p158; Wiley & Sons: New York, **1985**.

60. Matusche, P.; Nuyken, O.; Voit, B.; van Damme, M. *Journal of Macromolecular Science, Part A* **1997**, *34*, 201–209.

61. Riess, G. Neue Arylazosulfonate und ihre Reaktionen. Diploma Thesis: Münchberg, **1990**.

62. Voit, B.; Braun, F.; Gernert, M.; Sieczkowska, B.; Millaruelo, M.; Messerschmidt, M.; Mertig, M.; Opitz, J. *Polym. Adv. Technol.* **2006**, *17*, 691–693.

63. Franzke, D.; Scherer, C.; Nuyken, O.; Wokaun, A. *Journal of Photochemistry and Photobiology A: Chemistry* **1997**, *111*, 47–50.

64. Nuyken, O.; Presenz, U. *Polymer Bulletin* **1988**, *20*, 335–341.

65. Trogisch, S.; Loppacher, C.; Braun, F.; Grafström, S.; Voit, B.; Eng, L.M. *Macromol. Symp.* **2002**, *184*, 261–274.

66. Staško, A.; Szaboova, K.; Cholvad, V.; Nuyken, O.; Dauth, J. *Journal of Photochemistry and Photobiology A: Chemistry* **1993**, *69*, 295–304.

67. Chassin, P. *Bull. Groupe franc. Argiles* **1969**, 71–88.

68. Effenberger, F.; Schweizer, M.; Mohamed, W.S. *Journal of Applied Polymer Science* **2009**, *112*, 1572-1578.

69. Wang, J.; Merino, J.; Aranda, P.; Galvan, J.-C.; Ruiz-Hitzky, E. *J. Mater. Chem* **1999**, *9*, 161–167.

70. Pavlidou, S.; Papaspyrides, C.D. *Progress in Polymer Science* **2008**, *33*, 1119–1198.

71. Kaufmann, A. Preparation of activated Montmorillonite, organic modification and characterisation of its nanocomposites with PVOH. Bacchelor thesis: Leoben, **2012**.

72. Puchleitner, R. Two-Step Organo-Modification of Layered Silicates. Master Thesis: Leoben, **2011**.

73. Vlasova, M.; Dominguez-Patiño, G.; Kakazey, N.; Dominguez-Patiño, M.; Juarez-Romero, D.; Enríquez Méndez, Y. *Sci Sintering* **2003**, *35*, 155–166.

74. Marina Vargas Rodríguez, Y.; Beltrán, H.I.; Vázquez-Labastida, E.; Linares-López, C.; Salmón, M. *J. Mater. Res* **2007**, *22*, 788–800.

75. Tyagi, B.; Chudasama, C.D.; Jasra, R.V. *Applied Clay Science* **2006**, *31*, 16–28.

76. Hart, M.P.; Brown, D.R. *Journal of Molecular Catalysis A: Chemical* **2004**, *212*, 315–321.

77. Kwon, O.-Y.; Park, K.-W.; Jeong, S.-Y. *Bull. Korean Chem. Soc.* **2001**, *22*, 678–684.

78. Bel'chinskaya, L.; Kozlov, K.; Chitechan, S.; Bondarenko, A.; Petukhova, G.; Gubkina, M. *Protection of Metals* **2008**, *44*, 275–279.

79. Demolon, M.A.; Wey, R. *Academie des Sciences - Séance du 18 Janvier* **1954**, 389–393.

80. Ravichandran, J.; Sivasankar, B. *Clays and Clay Minerals* **1997**, *45*, 854–858.

81. Wang, T.-H.; Liu, T.-Y.; Wu, D.-C.; Li, M.-H.; Chen, J.-R.; Teng, S.-P. *Journal of Hazardous Materials* **2010**, *173*, 335–342.

82. Malferrari, D.; Brigatti, M.F.; Laurora, A.; Pini, S.; Medici, L. *Journal of Hazardous Materials* **2007**, *143*, 73–81.

83. Liu, P.; Zhang, L. *Separation and Purification Technology* **2007**, *58*, 32–39.

84. Reddy, C.R.; Iyengar, P.; Nagendrappa, G.; Prakash, B.S.J. *Catal Lett* **2005**, *101*, 87-91.

85. Laszlo, P. *Pure Appl. Chem.* **1990**, *62*, 2027–2030.

86. Laszlo, P.; Mathy, A. *Helv. Chim. Acta* **1987**, *70*, 577–586.

87. Shi, Q.; Tan, S.; Yang, Q.; Jiao, Z.; Ouyang, Y.; Chen, Y. *J. Wuhan Univ. Technol.-Mat. Sci. Edit.* **2010**, *25*, 725-729.

88. Tan, S.-Z.; Zhang, K.-H.; Zhang, L.-L.; Xie, Y.-S.; Liu, Y.-L. *Chin. J. Chem.* **2008**, *26*, 865–869.

89. Lenko, D.; Schlögl, S.; Temel, A.; Schaller, R.; Holzner, A.; Kern, W. *J. Appl. Polym. Sci.* **2013**, n/a.

90. Abollino, O.; Giacomino, A.; Malandrino, M.; Mentasti, E. *Applied Clay Science* **2008**, *38*, 227–236.

91. Hothi, B.; Lechene, V.; Robinson, J.; Sheriff, T.S. *Polyhedron* **1997**, *16*, 1403–1406.

92. Gerstl, Z. *Clays and Clay Minerals* **1980**, *28*, 335–345.

93. McBride, M.B. *Clays and Clay Minerals* **1975**, *23*, 103–107.

94. Rozenson, I. *Clays and Clay Minerals* **1976**, *24*, 271–282.

95. Rozenson, I. *Clays and Clay Minerals* **1976**, *24*, 283–288.

96. Rozenson, I. *Clays and Clay Minerals* **1978**, *26*, 88–92.

97. David, P.G. *J. Chem. Soc., Chem. Commun.* **1972**, 1294.

98. Qian, X.; Liao, M.; Zhang, W. *Polymer International* **2007**, *56*, 399-408.

99. Alexandre, M.; Dubois, P. *Materials Science and Engineering: R: Reports* **2000**, *28*, 1–63.

100. Hang, P.T. *Clays and Clay Minerals* **1970**, *18*, 203–212.

101. Khan, A.; Nurnabi, M.; Bala, P. *Journal of Thermal Analysis and Calorimetry* **2009**, *96*, 929–935.

102. Benincasa, E.; Brigatti, M.F.; Lugli, C.; Medici, L.; Poppi, L. *Clay Minerals* **2000**, *35*, 635–641.

103. Jang, S.D.; Condrate, R.A. *Journal of Inorganic and Nuclear Chemistry* **1972**, *34*, 1503–1509.

104. Khan, A.H.; Bala, P.; Rahman, A.M.; Nurnabi, M. *Dhaka Univ. J. Sci.* **2012**, *60*.

105. Brigatti, M.F.; Lugli, C.; Montorsi, S.; Poppi, L. *Clays and Clay Minerals* **1999**, *47*, 664–671.

106. Santana, H.; Paesano, A.; Costa, A.C.S. de; Di Mauro, E.; Souza, I.G. de; Ivashita, F.F.; Souza, C.M. de; Zaia, C.T.B.V.; Zaia, D.A.M. *Amino Acids* **2010**, *38*, 1089–1099.

107. Yu, R.; Wang, S.; Wang, D.; Ke, J.; Xing, X.; Kumada, N.; Kinomura, N. *Catalysis Today* **2008**, *139*, 135–139.

108. Busca, G. *Chem. Rev.* **2007**, *107*, 5366–5410.

109. Harmer, M.A.; Sun, Q. *Hoelderich Special Issue* **2001**, *221*, 45–62.

110. Cheng, W.; McCown, M. *Journal of Chromatography A* **1985**, *318*, 173–185.

111. Kulkarni, S.A.; Ogale, S.B.; Vijayamohanan, K.P. *Journal of Colloid and Interface Science* **2008**, *318*, 372–379.

112. Kim, Y.; Choi, Y.; Kim, H.K.; Lee, J.S. *Journal of Power Sources* **2010**, *195*, 4653–4659.

113. Greesh, N.; Hartmann, P.C.; Cloete, V.; Sanderson, R.D. *Journal of Colloid and Interface Science* **2008**, *319*, 2–11.

114. Kim, Y.; Lee, J.S.; Rhee, C.H.; Kim, H.K.; Chang, H. *Journal of Power Sources* **2006**, *162*, 180–185.

115. Zhao, Y.; Xu, Z.; Wang, X.; Lin, T. *Langmuir* **2012**, *28*, 6328–6335.

116. Zhang, K.; Chen, H.; Chen, X.; Chen, Z.; Cui, Z.; Yang, B. *Macromol. Mater. Eng.* **2003**, *288*, 380–385.

117. Griesser, T.; Track, A.; Koller, G.; Ramsey, M.; Kern, W.; Trimmel, G. In Interface Controlled Organic Thin Films; Al-Shamery, K., Horowitz, G., Sitter, H., Rubahn, H.-G., Eds.; Springer Berlin Heidelberg, **2009**, pp 113-117.

118. Reddy, S.; Arzt, E.; del Campo, A. *Adv. Mater.* **2007**, *19*, 3833–3837.

119. Mattausch, H.; Laske, S.; Ðuretek, I.; Kreith, J.; Maier, G.; Holzer, C. *Polym Eng Sci* **2013**, *53*, 1001–1010.

120. Balek, V.; Málek, Z.; Cásenský, B.; Niznanský, D.; Šubrt, J.; Vecerníková, E.; Römich, H.; Pilz, M. *Journal of Sol-Gel Science and Technology* **1997**, *8*, 591–594.

121. Brinker, C.; Scherer, G. Sol-Gel Science: The Physics and Chemistry of Sol-Gel Processing; Academic Press Inc., **1990**.

122. Nishiura, K.; Takaki, T.; Nakaura, M. *MRS Proc.* **2006**, *951*.

123. Guo, R.; Ma, X.; Hu, C.; Jiang, Z. *Polymer* **2007**, *48*, 2939–2945.

124. Dean, K.M.; Do, M.D.; Petinakis, E.; Yu, L. *Composites Science and Technology* **2008**, *68*, 1453–1462.

125. Duquesne, S.; Lama, C.; Bras, M.; Delobel, R.; Recourt, P.; Gloaguen, J.M. *Composites Science and Technology* **2003**, *63*, 1141–1148.

126. Grunlan, J.C.; Grigorian, A.; Hamilton, C.B.; Mehrabi, A.R. *J. Appl. Polym. Sci* **2004**, *93*, 1102–1109.

127. Paranhos, C.M.; Soares, B.G.; Oliveira, R.N.; Pessan, L.A. *Macromol. Mater. Eng.* **2007**, *292*, 620–626.

128. Kokabi, M.; Sirousazar, M.; Hassan, Z.M. *European Polymer Journal* **2007**, *43*, 773–781.

129. Nho, Y.C.; Park, K.R. *J. Appl. Polym. Sci.* **2002**, *85*, 1787–1794.

130. Sirousazar, M.; Kokabi, M.; Hassan, Z.M.; Bahramian, A.R. *Journal of Macromolecular Science, Part B* **2012**, *51*, 1335–1350.

131. Follain, N.; Joly, C.; Dole, P.; Bliard, C. *Carbohydrate Polymers* **2005**, *60*, 185–192.

132. Nam, S.Y.; Nho, Y.C.; Hong, S.H.; Chae, G.T.; Jang, H.S.; Suh, T.S.; Ahn, W.S.; Ryu, K.E.; Chun, H.J. *Macromol. Res.* **2004**, *12*, 219–224.

133. Schauberger, J.G.; Riess, G.; Schmuck, M.; Kriechbaum, M.; Kern, W. *Applied Clay Science* **2013**.

134. Elliott, J.E.; Macdonald, M.; Nie, J.; Bowman, C.N. *Polymer* **2004**, *45*, 1503–1510.

135. Chrońska, K.; Przepiórkowska, A. *J. Appl. Polym. Sci.* **2009**, *114*, 1984–1991.

136. Obreja, P.; Cristea, D.; Budianu, E.; Rebigan, R.; Kuncser, V.; Bulinski, M.; Filoti, G. *Progress in Solid State Chemistry* **2006**, *34*, 103–109.

137. Hesse, M.; Meier, H.; Zeeh, B. Spektroskopische Methoden in der organischen Chemie: 102 Tabellen; Thieme: Stuttgart [u.a.], **2005**.

138. Strähle, J.; Rossi, R.; Schweda, E. Jander-Blasius: Lehrbuch der analytischen und präparativen anorganischen Chemie; S. Hirzel Verlag: Stuttgart, **2006**.

139. EN 455-2:2009+A1:2011. Medical Gloves for Single Use - Part 2: Requirements and Testing for Physical Properties, **2009**.

140. Rogošić, M.; Mencer, H.J.; Gomzi, Z. *European Polymer Journal* **1996**, *32*, 1337–1344.

141. Kenney, J.F.; Willcockson, G.W. *J. Polym. Sci. A-1 Polym. Chem.* **1966**, *4*, 679–698.

142. Harris, H.E.; Kenney, J.F.; Willcockson, G.W.; Chiang, R.; Friedlander, H.N. *J. Polym. Sci. A-1 Polym. Chem.* **1966**, *4*, 665–677.

143. Krimm, S.; Liang, C.Y.; Sutherland, G.B.B.M. *J. Polym. Sci* **1956**, *22*, 227–247.

144. Socrates, G. Infrared and raman characteristic group frequencies: Tables and charts; John Wiley & Sons: West Sussex, **2007**.

145. Ming Yang, J.; Chih Chiu, H. *Journal of Membrane Science* **2012**, *419–420*, 65–71.

146. Kumar, G.V.; Chandramani, R. *Applied Surface Science* **2009**, *255*, 7047–7050.

147. Mahendia, S.; Tomar, A.K.; Kumar, S. *Materials Science and Engineering: B* **2011**, *176*, 530–534.

148. Shehap, A.M. *Egypt. J. Solids* **2008**, *31*, 75–91.

149. Mohsin, M.; Hossin, A.; Haik, Y. *J. Appl. Polym. Sci.* **2011**, *122*, 3102–3109.

150. David, F.; David, P.G. *J. Phys. Chem* **1976**, *80*, 579–583.

151. McKnight, D.M.; Kimball, B.A.; Runkel, R.L. *Hydrol. Process.* **2001**, *15*, 1979–1992.

152. Rabie, S.M.; Abdel-Hakeem, N.; Moharram, M.A. *J. Appl. Polym. Sci* **1990**, *40*, 1163–1176.

153. Sharma, R.; Sud, L.V. *Acta Polym* **1982**, *33*, 356–357.

154. Kocaokutgen, H.; Gümrükçüoğlu, I.E. *Journal of Thermal Analysis and Calorimetry* **2003**, *71*, 675–679.

155. Holt, B.D.; Engelkemeir, A.G. *Anal. Chem.* **1970**, *42*, 1451–1453.

156. Falk, M. *Spectrochimica Acta Part A: Molecular Spectroscopy* **1984**, *40*, 43–48.

157. Mustroph, H.; Epperlein, J. *J. Prakt. Chem.* **1981**, *323*, 755–775.

158. Xu, W.; Johnston, C.; Parker, P.; Agnew, S. *Clays and Clay Minerals* **2000**, *48*, 120–131.

159. Lerot, L.; Low, P. *Clays and Clay Minerals* **1976**, *24*, 191–199.

160. Lerot, L.; Poncelet, G.; Fripiat, J.J. *Materials Research Bulletin* **1974**, *9*, 979–987.

161. Cloos, P.; Laura, R.D. *Clays and Clay Minerals* **1972**, 259–270.

162. Greene-Kelly, R. *Mineral Mag.* **1955**, 604–615.

163. Xie, W.; Gao, Z.; Liu, K.; Pan, W.-P.; Vaia, R.; Hunter, D.; Singh, A. *Thermochimica Acta* **2001**, *367-368*, 339–350.

164. van Koster Groos, A.F.; Guggenheim, S. *American Mineralogist* **1984**, *69*, 872–879.

165. van Koster Groos, A.F.; Guggenheim, S. *Clays & Clay Minerals* **1986**, *34*, 281–286.

166. Shuali, U. *Clay Minerals* **1991**, *26*, 497–506.

167. Heinz, H.; Vaia, R.A.; Krishnamoorti, R.; Farmer, B.L. *Chem. Mater.* **2006**, *19*, 59–68.

168. Lagaly, G. *Clay Minerals* **1981**, *16*, 1–21.

169. Malferrari, D.; Brigatti, M.F.; Marcelli, A.; CHU, W.; Wu, Z. *Applied Clay Science* **2010**, *50*, 12–18.

170. Rissing, C.; Son, D.Y. *Organometallics* **2008**, *27*, 5394–5397.

171. Bolto, B.; Tran, T.; Hoang, M.; Xie, Z. *Progress in Polymer Science* **2009**, *34*, 969–981.

172. Burshe, M.C.; Sawant, S.B.; Joshi, J.B.; Pangarkar, V.G. *Separation and Purification Technology* **1997**, *12*, 145–156.

173. Chuang, W.-Y.; Young, T.-H.; Chiu, W.-Y.; Lin, C.-Y. *Polymer* **2000**, *41*, 5633–5641.

174. Carrado, K.A. *Clays and Clay Minerals* **1996**, *44*, 506–514.

175. Suzuki, K.; Mori, T.; Kawase, K.; Sakami, H.; Iida, S. *Clays and Clay Minerals* **1988**, *36*, 147–152.

176. Yoshioka, Y.; Nagano, M. *Kobunshi Kagaku* **1952**, 36.

177. Nagai, N.; Mima, S.; Kuribayashi, S.; Sagane, N. *Kobunshi Kagaku* **1955**, 199w.

178. Sakurada, I.; Hosono, M. *Kobunshi Kagaku* **1945**, 151.

179. Aurela, B.; Ohra-aho, T.; Söderhjelm, L. *Packag. Technol. Sci* **2001**, *14*, 71–77.

180. N., N. Konformität von Lebensmittelverpackungen: Migration und Abklatschen; 2006. Available online: http://www.hubergroup.info/lang/deu/tipdf/19103D.PDF.

VIII.   APPENDIX

1. TABLE HEADINGS

2.   FIGURE CAPTIONS

3.   FIGURES

3.1   AZOSULPHONATE DOPED PVA
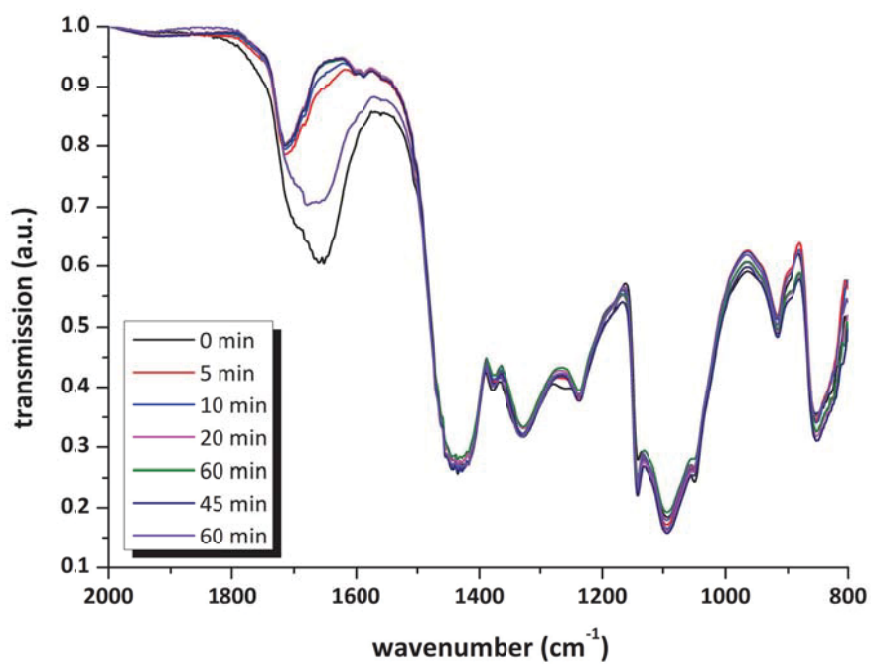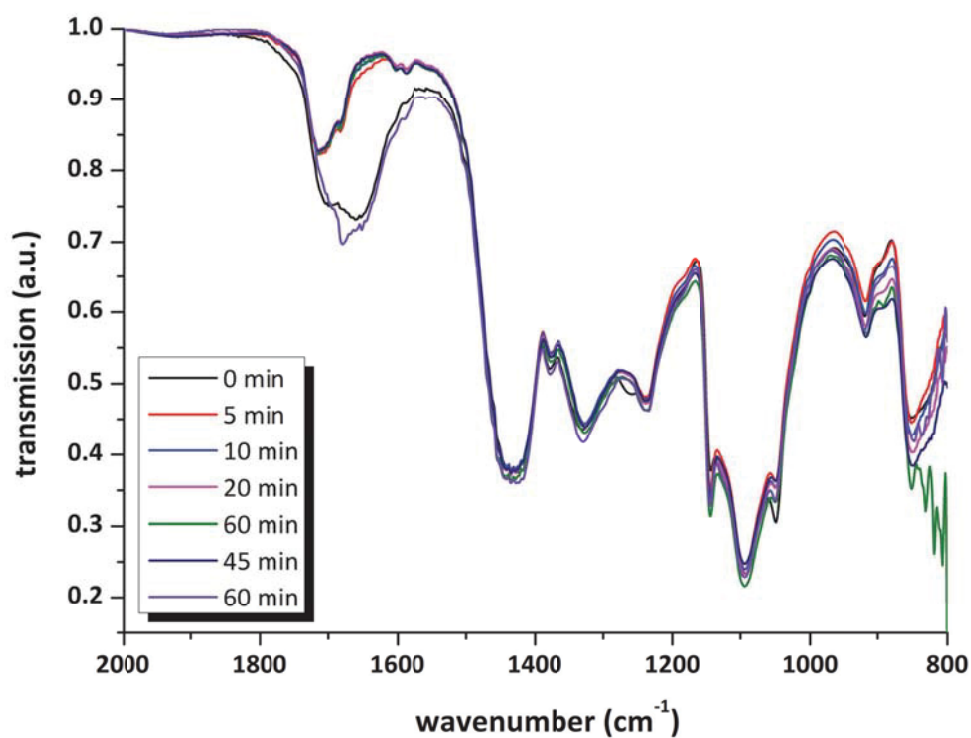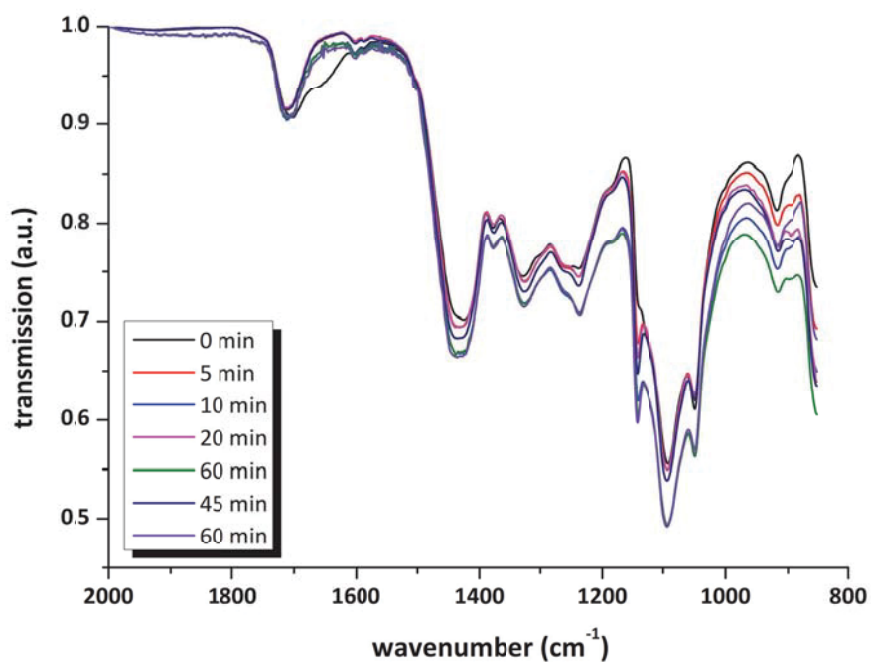
3.1.1   *Annealing*

P 1:   Changes of FTIR spectra of PAII.1 (coated CaF_2 platelet) upon annealing at 100 °C in a circulating air oven.
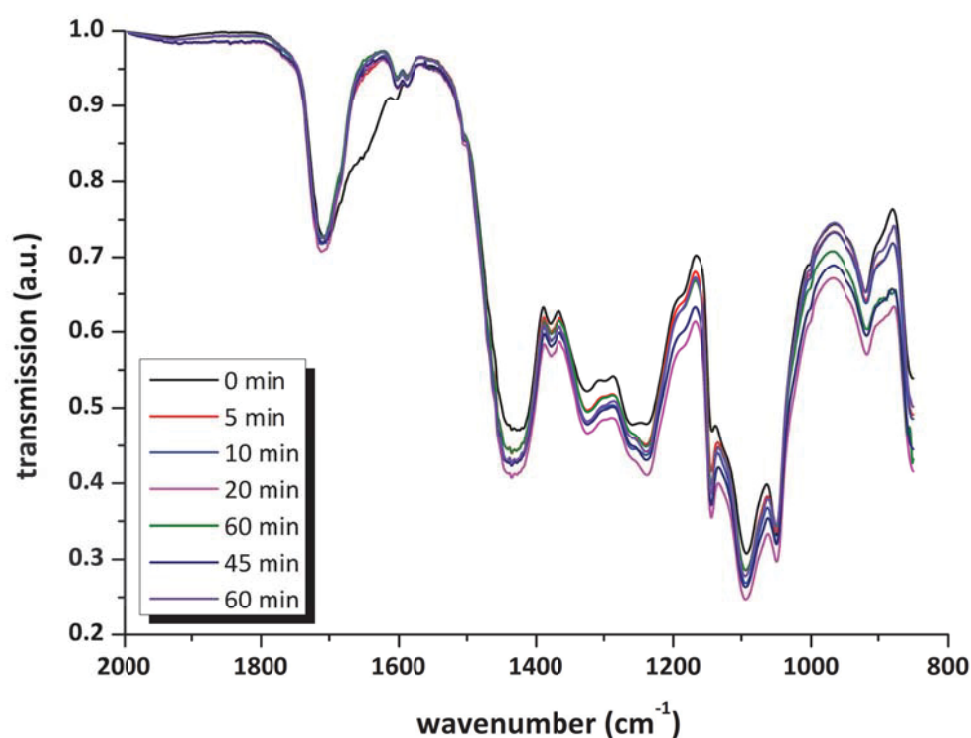
P 2: Changes of FTIR spectra of PAII.2 (coated CaF_2 platelet) upon annealing at 100 °C in a circulating air oven.

P 3: Changes of FTIR spectra of PAII.3 (coated CaF_2 platelet) upon annealing at 100 °C in a circulating air oven.
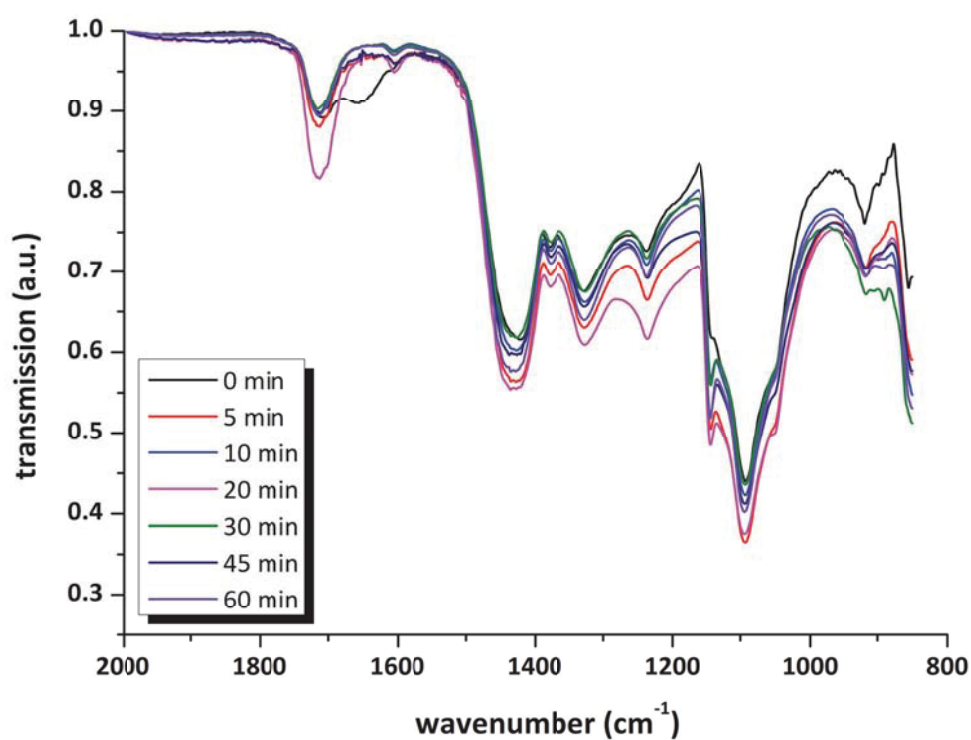
P 4: Changes of FTIR spectra of PAII.4 (coated CaF$_2$ platelet) upon annealing at 100 °C in a circulating air oven.
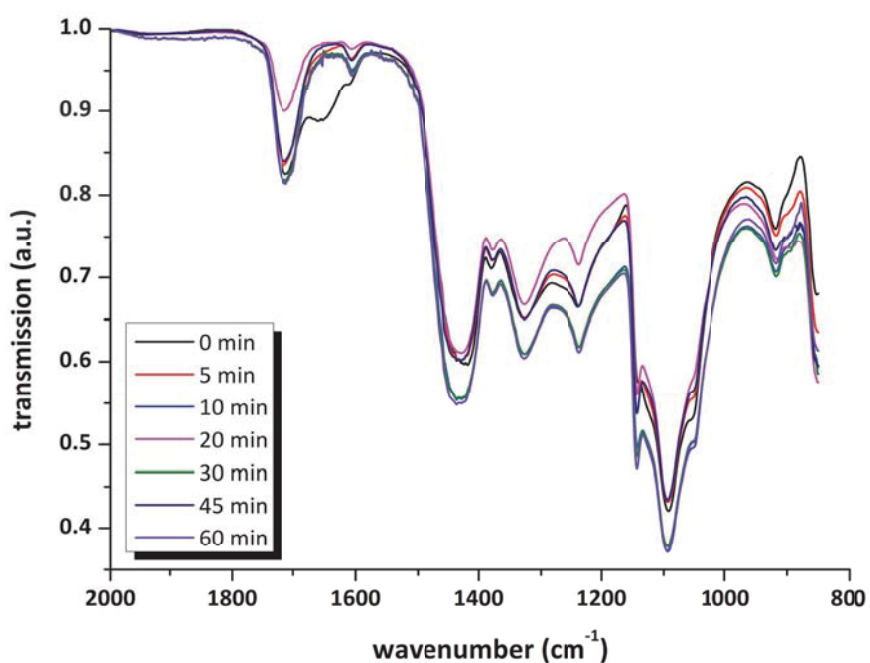

P 5: Changes of FTIR spectra of PAII.5 (coated CaF$_2$ platelet) upon annealing at 100 °C in a circulating air oven.
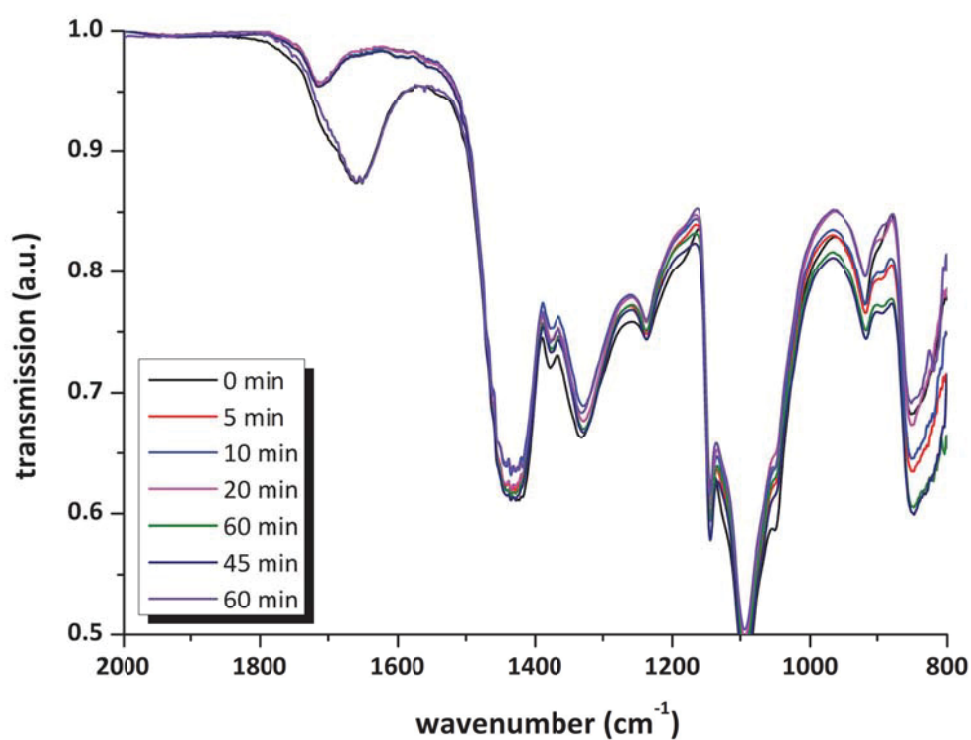
P 6: Changes of FTIR spectra of PAIII.1 (coated CaF_2 platelet) upon annealing at 100 °C in a circulating air oven.

P 7: Changes of FTIR spectra of PAIII.2 (coated CaF_2 platelet) upon annealing at 100 °C in a circulating air oven.

P 8: Changes of FTIR spectra of PAIII.3 (coated CaF$_2$ platelet) upon annealing at 100 °C in a circulating air oven.

P 9: Changes of FTIR spectra of PAIII.4 (coated CaF$_2$ platelet) upon annealing at 100 °C in a circulating air oven.

P 10:   Changes of FTIR spectra of PAIII.5 (coated CaF$_2$ platelet) upon annealing at 100 °C in a circulating air oven.
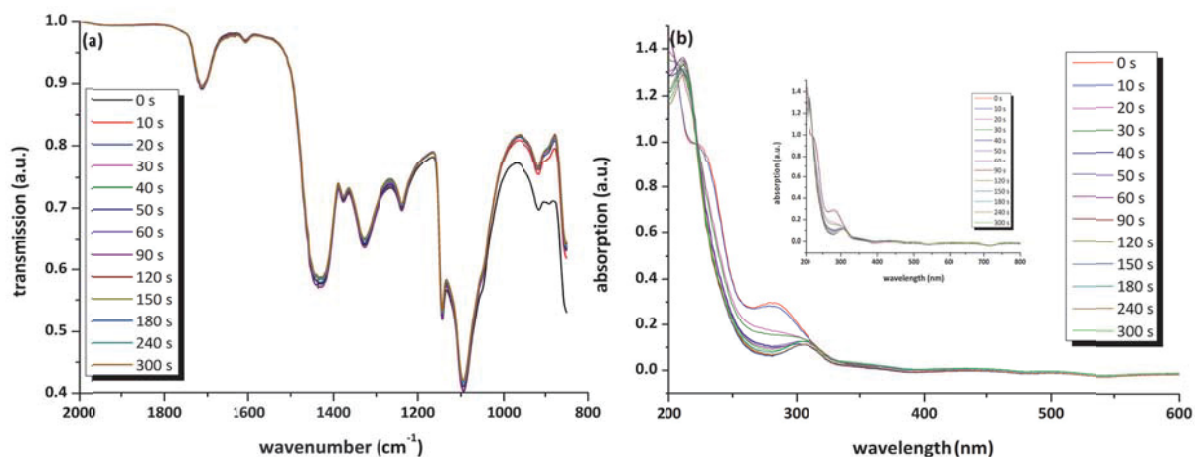
3.1.2   *Photolysis*
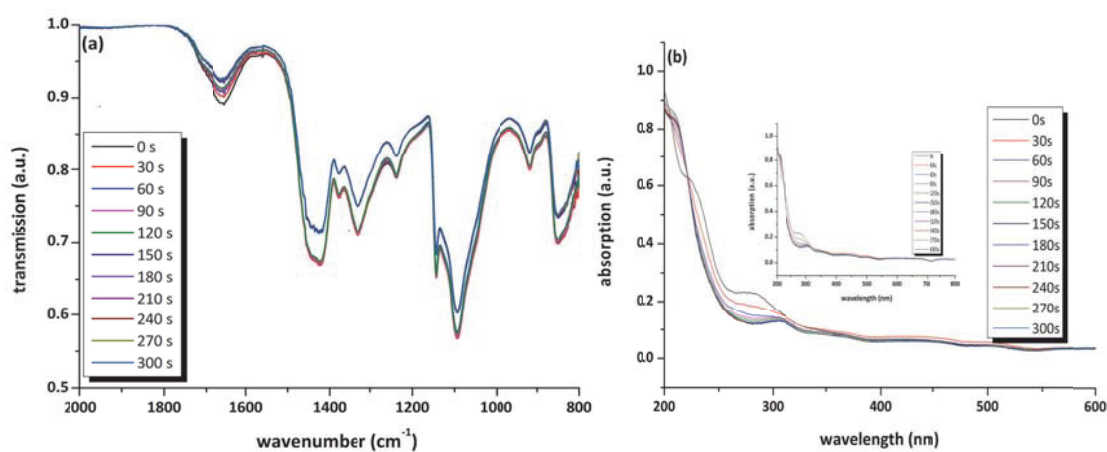
P 11:   UV irradiation kinetics of FTIR transmission (a) and UV-Vis absorption spectra (b) of annealed thin PAII.1 films coated onto a CaF$_2$ substrate. UV light is emitted by a high pressure Hg lamp with an intensity of 9.25 mWcm^{-2}.
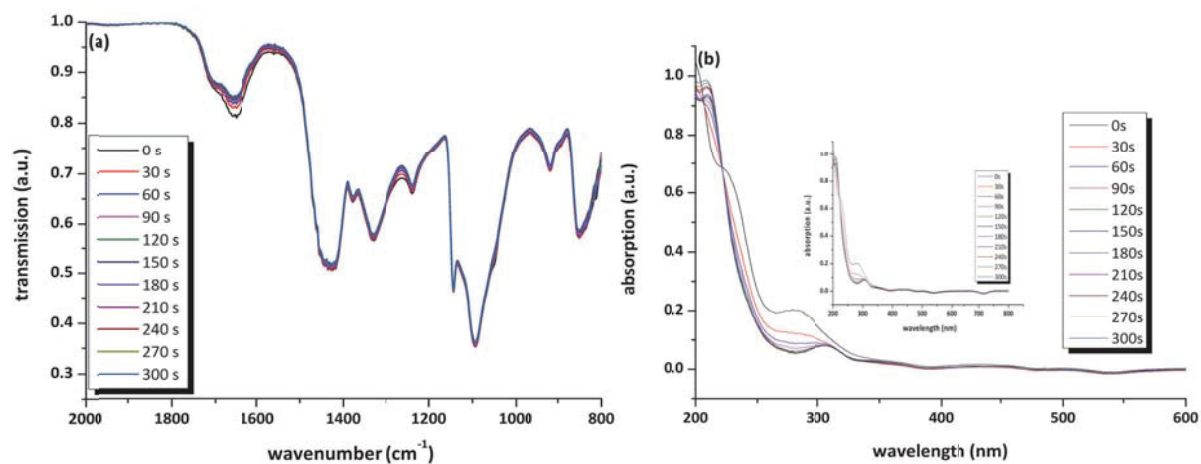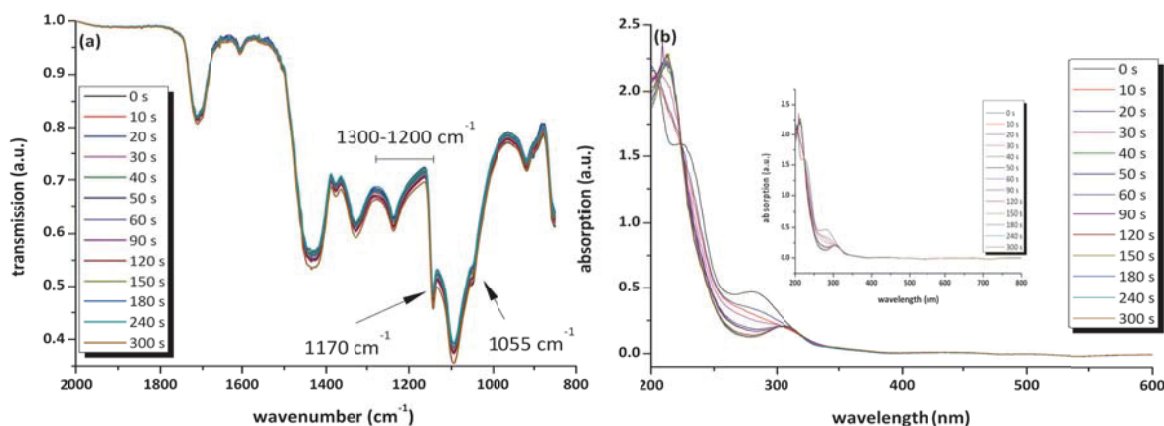
P 12:   UV irradiation kinetics of FTIR transmission (a) and UV-Vis absorption spectra (b) of annealed thin PAII.2 films coated onto a CaF_2 substrate. UV light is emitted by a high pressure Hg lamp with an intensity of 9.25 mWcm^{-2}.
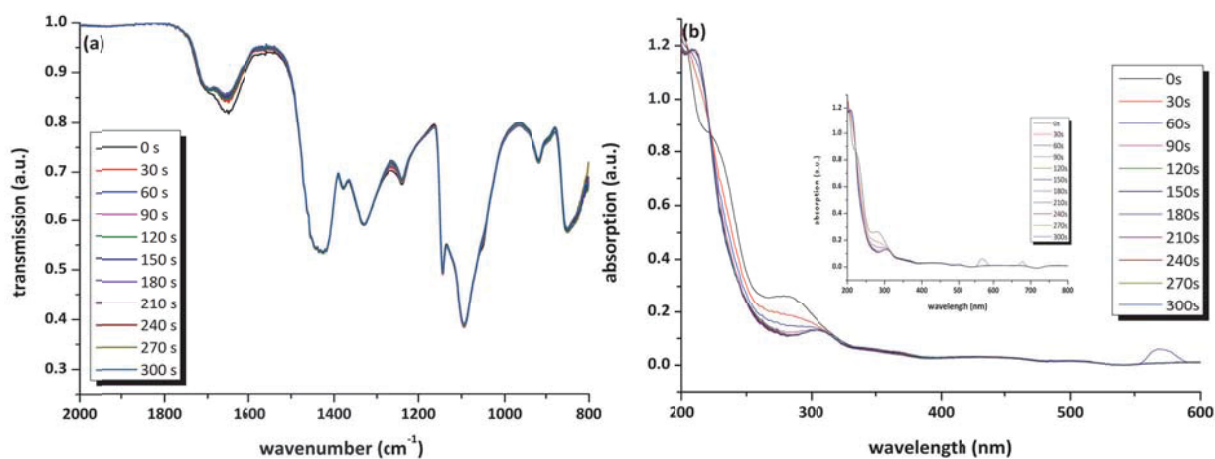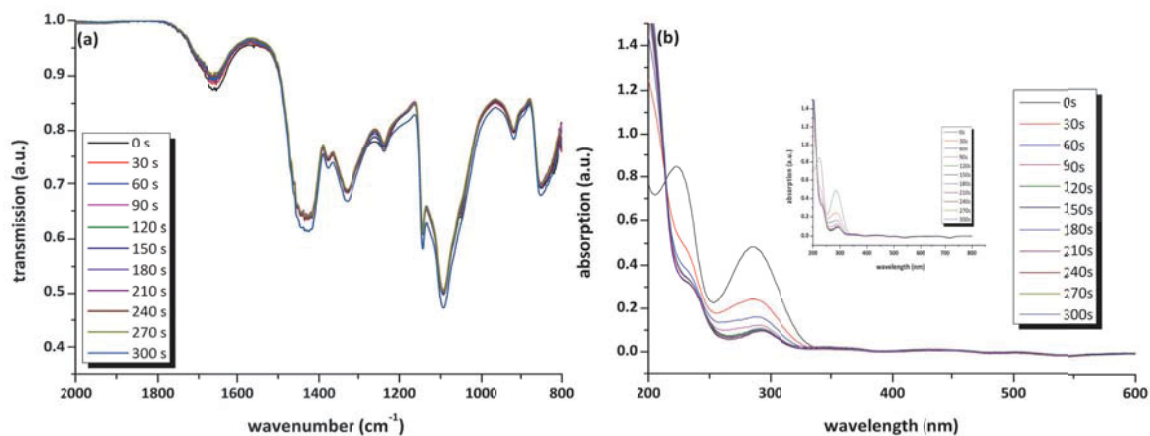

P 13:   UV irradiation kinetics of FTIR transmission (a) and UV-Vis absorption spectra (b) of annealed thin PAII.3 films coated onto a CaF_2 substrate. UV light is emitted by a high pressure Hg lamp with an intensity of 9.25 mWcm^{-2}.
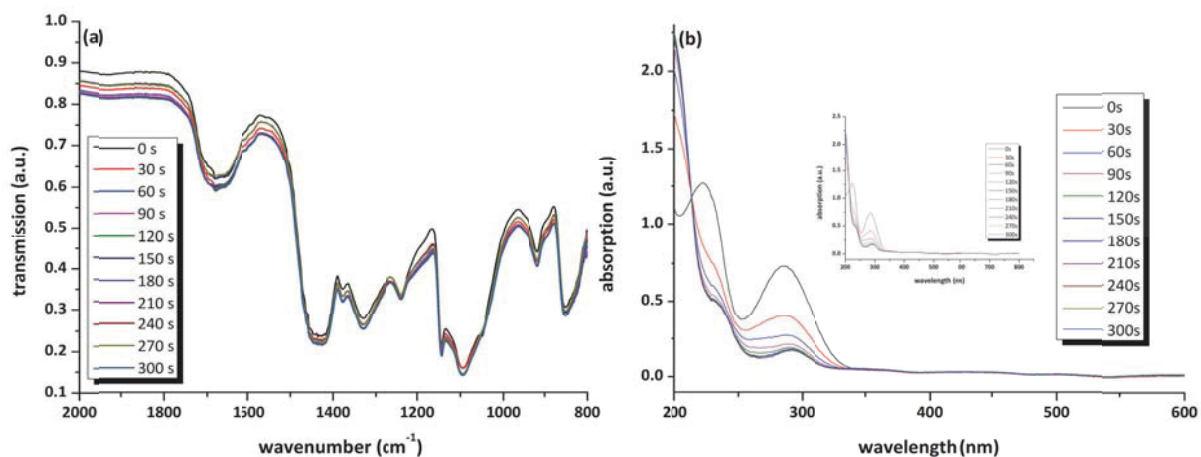
P 14: UV irradiation kinetics of FTIR transmission (a) and UV-Vis absorption spectra (b) of annealed thin PAII.4 films coated onto a CaF$_2$ substrate. UV light is emitted by a high pressure Hg lamp with an intensity of 9.25 mWcm^{-2}.
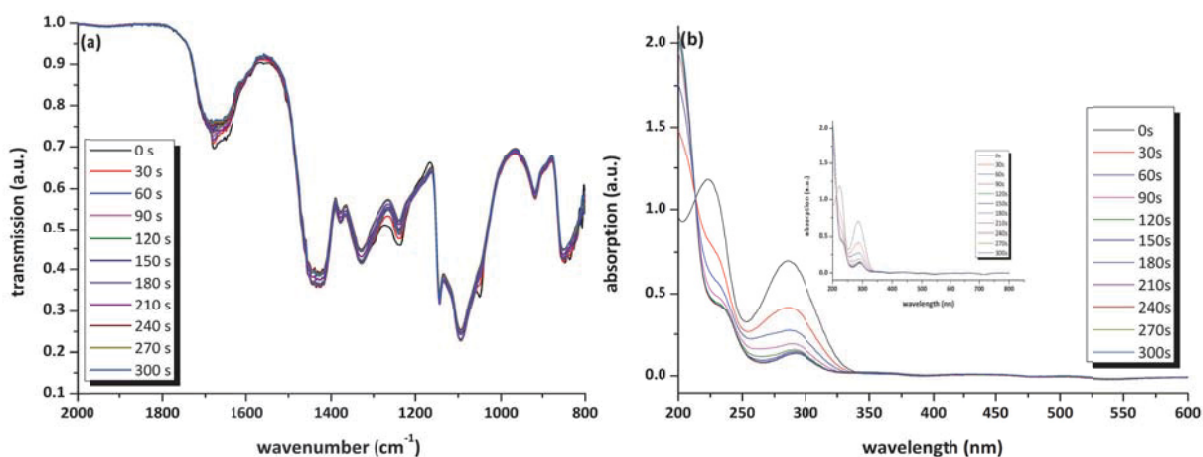

P 15: UV irradiation kinetics of FTIR transmission (a) and UV-Vis absorption spectra (b) of annealed thin PAII.5 films coated onto a CaF$_2$ substrate. UV light is emitted by a high pressure Hg lamp with an intensity of 9.25 mWcm^{-2}.
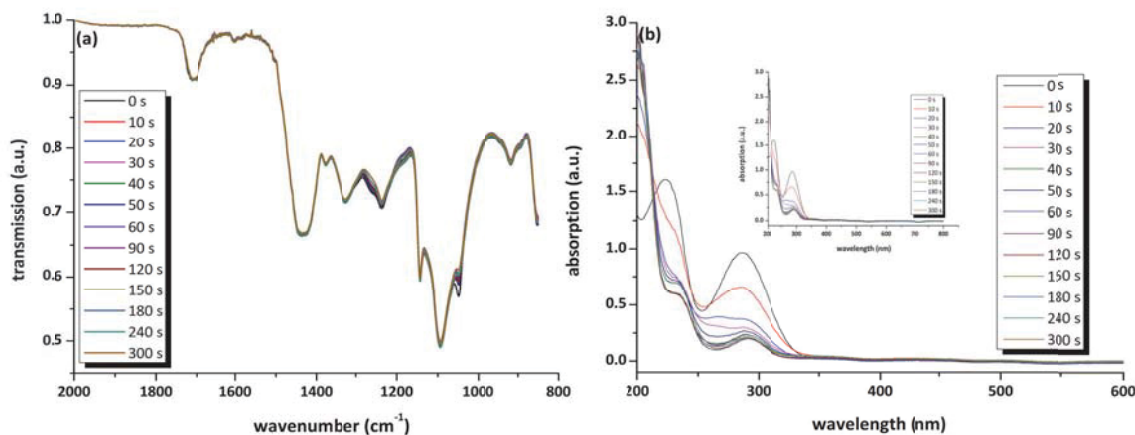

P 16: UV irradiation kinetics of FTIR transmission (a) and UV-Vis absorption spectra (b) of annealed thin PAIII.1 films coated onto a CaF$_2$ substrate. UV light is emitted by a high pressure Hg lamp with an intensity of 9.25 mWcm^{-2}.

P 17:   UV irradiation kinetics of FTIR transmission (a) and UV-Vis absorption spectra (b) of annealed thin PAIII.2 films coated onto a CaF$_2$ substrate. UV light is emitted by a high pressure Hg lamp with an intensity of 9.25 mWcm^{-2}.
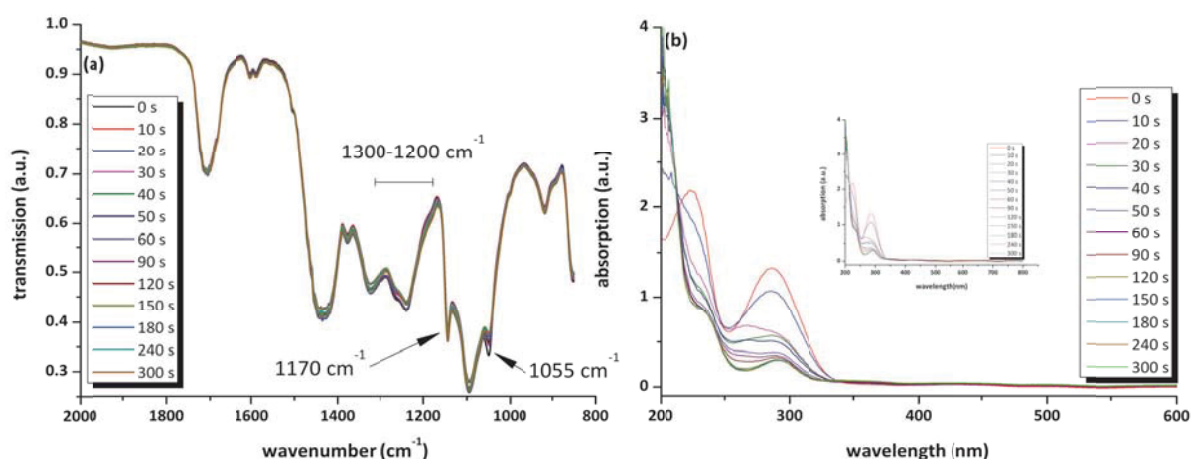

P 18:   UV irradiation kinetics of FTIR transmission (a) and UV-Vis absorption spectra (b) of annealed thin PAIII.3 films coated onto a CaF$_2$ substrate. UV light is emitted by a high pressure Hg lamp with an intensity of 9.25 mWcm^{-2}.

P 19:   UV irradiation kinetics of FTIR transmission (a) and UV-Vis absorption spectra (b) of annealed thin PAIII.1 films coated onto a CaF$_2$ substrate. UV light is emitted by a high pressure Hg lamp with an intensity of 9.25 mWcm^{-2}.

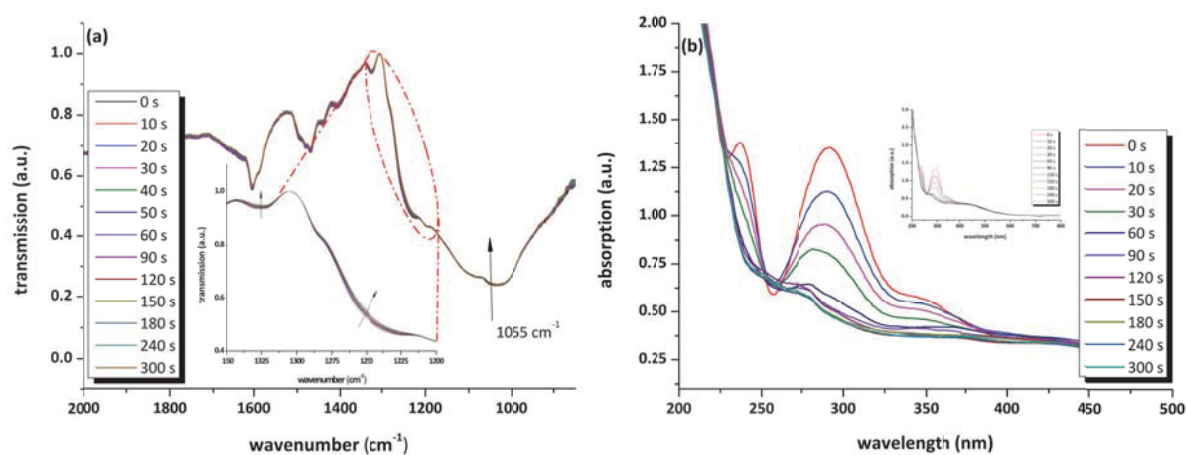P 20:   UV irradiation kinetics of FTIR transmission (a) and UV-Vis absorption spectra (b) of annealed thin PAIII.5 films coated onto a CaF_2 substrate. UV light is emitted by a high pressure Hg lamp with an intensity of 9.25 $mWcm^{-2}$.

## 3.2   SURFACE FUNCTIONALISED PARTICLES

3.2.1   *Photolysis*

P 21:   (a) FTIR spectra of thin layers surface modified fumed silica particles **P2** deposited on CaF_2 platelets. (b) UV-Vis absorption spectra of an aqueous **P2** particle dispersion upon irradiation with a spot curing emitter with an intensity of 9.25 $mWcm^{-2}$.
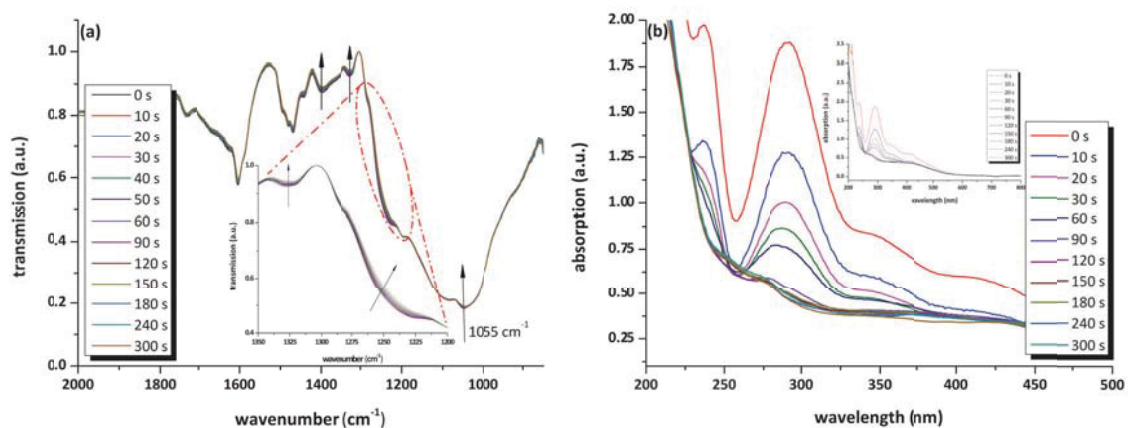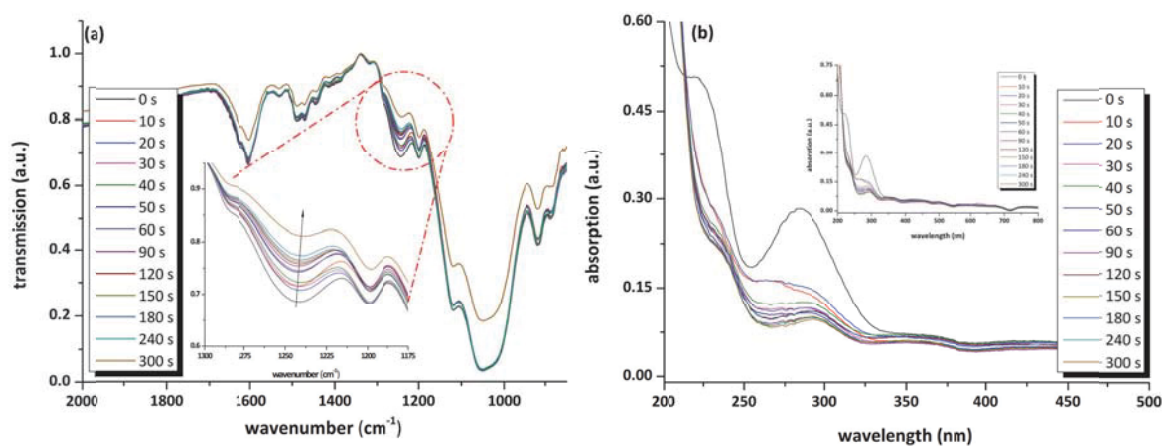
P 22:   (a) FTIR spectra of thin layers surface modified fumed silica particles **P3** deposited on CaF$_2$ platelets. (b) UV-Vis absorption spectra of an aqueous **P3** particle dispersion upon irradiation with a spot curing emitter with an intensity of 9.25 mWcm^{-2}.
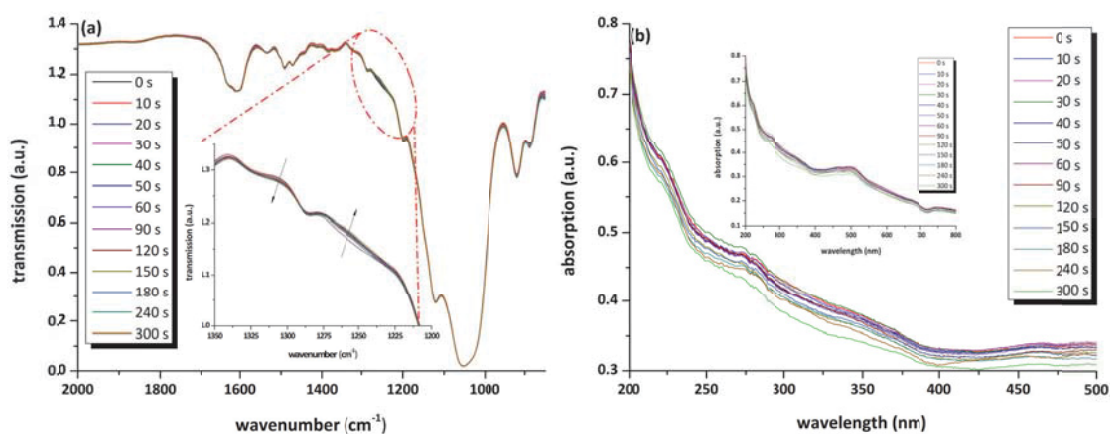
P 23:   (a) FTIR spectra of thin layer of surface modified montmorillonite (**MMTb**) deposited on CaF$_2$ platelets. (b) UV-Vis absorption spectra of an aqueous MMT dispersion upon irradiation with a spot curing emitter with an intensity of 9.25 mWcm^{-2}.
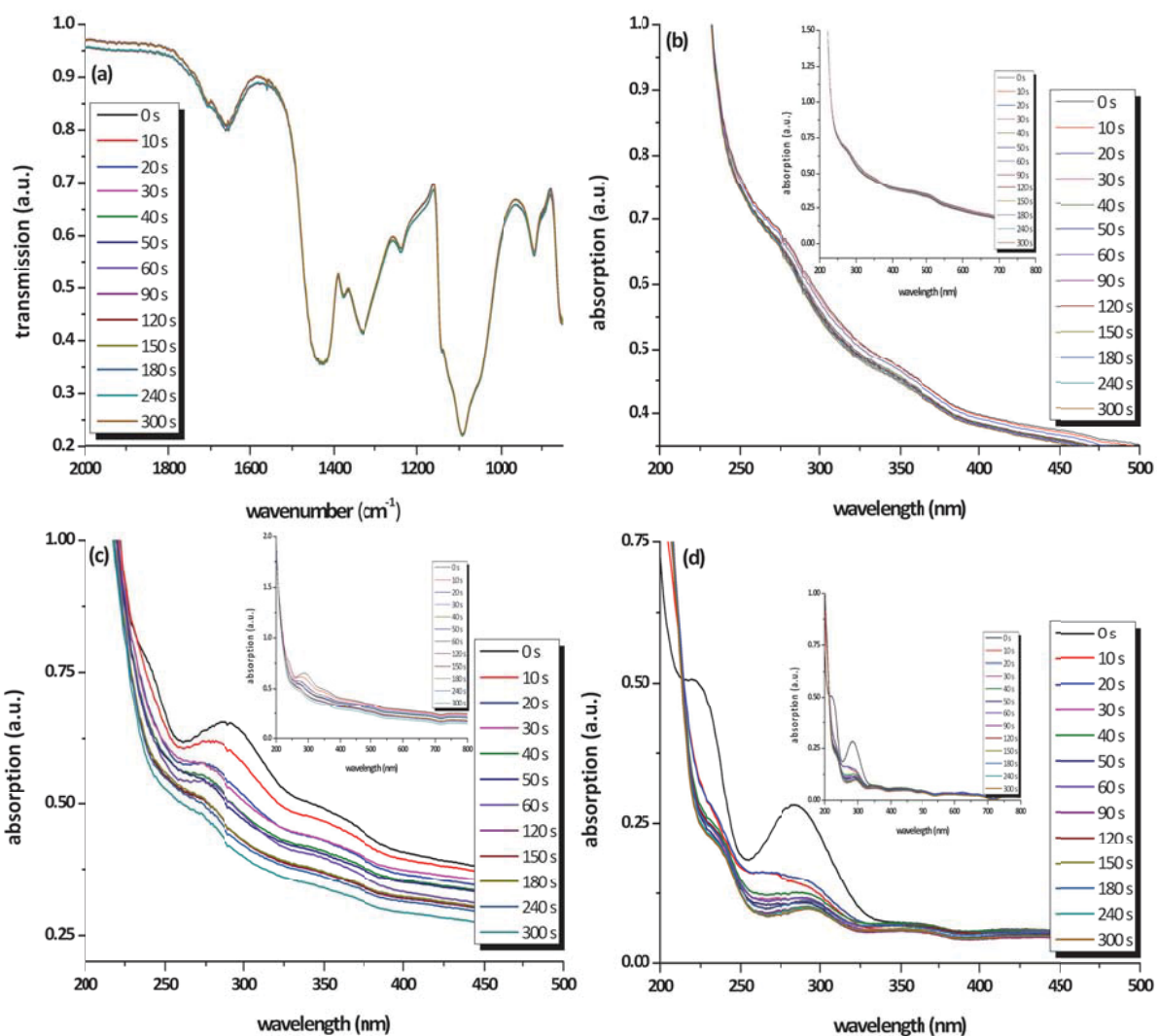
P 24:   (a) FTIR spectra of thin layer of surface modified montmorillonite (**MMTd**) deposited on CaF$_2$ platelets. (**b**) UV-Vis absorption spectra of an aqueous MMT dispersion upon irradiation with a spot curing emitter with an intensity of 9.25 mWcm^{-2}.
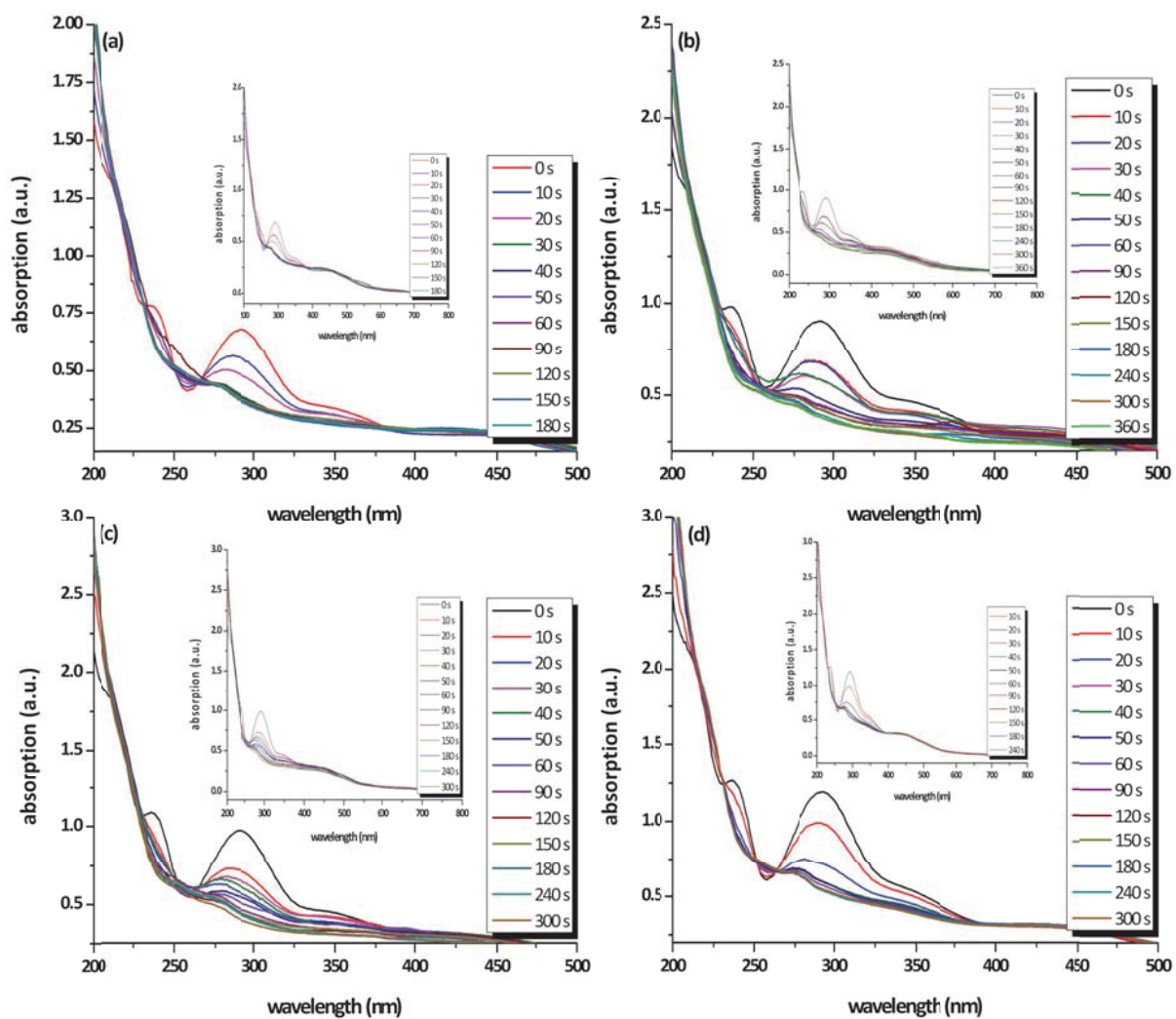
3.3   USE OF UV REACTIVE PARTICLES FOR THE CROSSLINKING OF PVA

P 25:   UV exposure kinetics of azosulphonate doped PVA comprising 2.5 wt.-% of surface modified montmorillonites (a/b) FTIR and UV-Vis spectra of PMMTa_1; (c) PMMTc_1; (d) PMMTd_1. Exposure is performed using a high pressure mercury vapour emitter with an output intensity of 9.25 Wcm^{-2}.

P 26:   UV exposure kinetics of PVA composites comprising 5 wt.-% of surface modified silica particles: (a) PP1_2; (b) PP2_2; (c) PP3_2 and (d) nanoparticles PNP2. Exposure is performed using a high pressure mercury vapour emitter with an output intensity of 9.25 Wcm^{-2}.
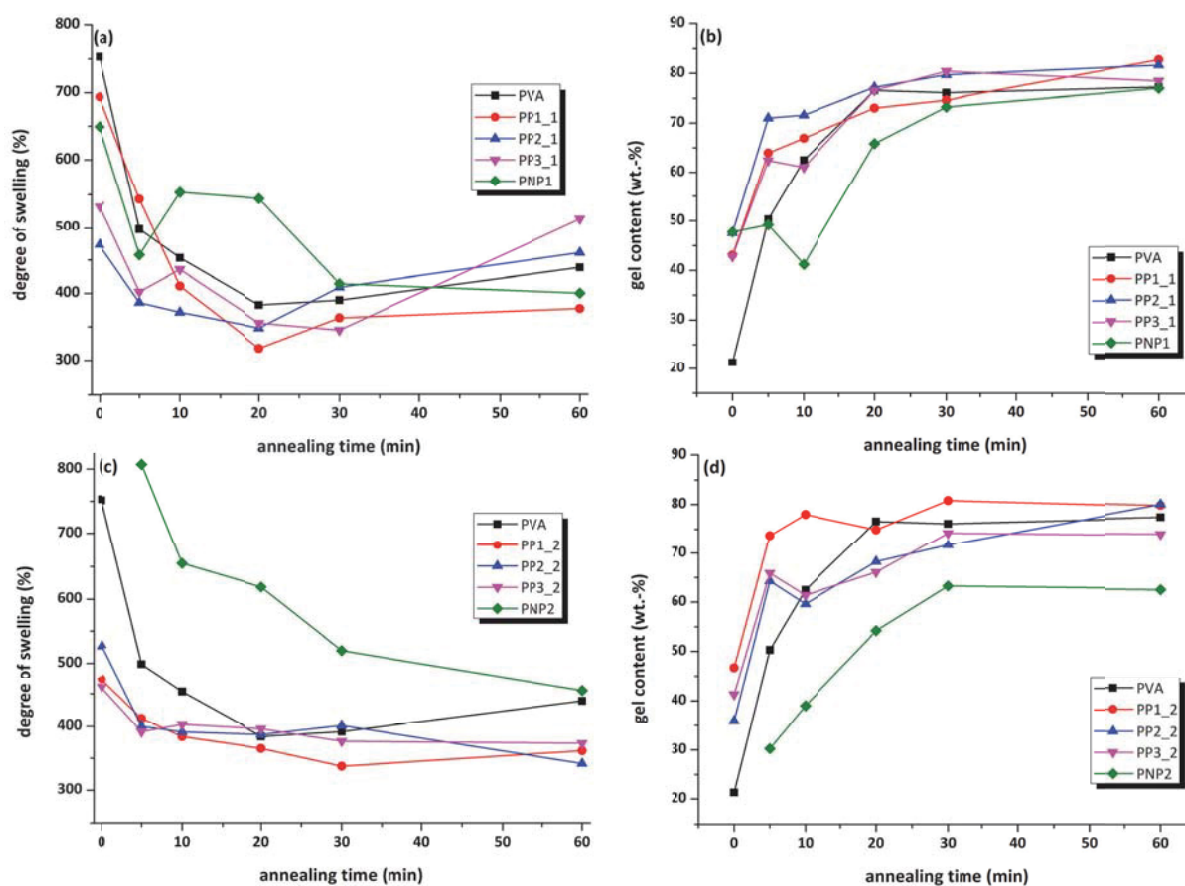
P 27: Changes of swelling behaviour of PVA-silicon particle composite films due to thermal treatment. (a/b) composites containing 2.5 wt.-% of particles; (c/d) 5 wt.-% particles.
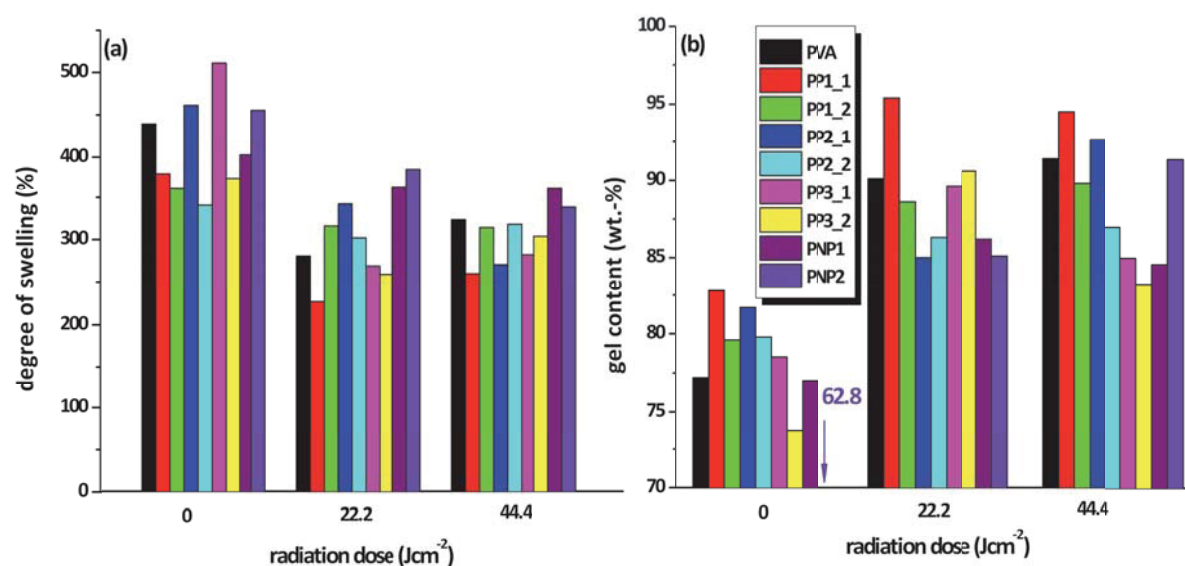
P 28: Sol-gel analysis of heat treated PVA-MMT composite films which undergo subsequent UV exposure with a medium pressure mercury vapour lamp with an output intensity of 740 mWcm^{-2}. (a) degree of swelling; (b) gel content.

4.   CURRICULUM VITAE

Personal information

Schauberger / Jörg Guido; MSc

Address	Münzenbergstrasse 18/2, 8700 Leoben (Austria)
Mobile	+43 650/4615946
E-Mail	jgschauberger@gmail.com
Nationality	Austria
Date of birth	28/07/1982
Gender	Male

Education and work experience

08/2009 –10/2013 University of Leoben

Doctoral program

Chemistry of plastics and analytical chemistry
PhD Thesis: "Alternative methods for the crosslinking of poly(vinyl alcohol) by the use of functionalised inorganic particles - A water-based approach towards environmentally benign coating materials "

10/2008 – 06/2009 University of Leoben

Master program "Polymer engineering and science" (MSc)

Material development and characterisation
Master Thesis: "Polymers as barrier coatings for cardboard "

10/2001 – 10/2008 University of Leoben

Bachelor program "Polymer engineering and science" (BSc)

Bachelor Thesis: "Modification and characterisation of Polyhydroxybutyrate produced by bacteria "

09/1992 – 06/2000 BRG Michaelerplatz, Steyr

Matriculation exam

Focus on natural sciences and Latin

Work experience

08/2009 – 10/2013

Researcher / PhD Student

Contribution to student training (supervision of bachelor theses)
- Rainer Puchleitner: "Characterisation of reaction kinetics of UV curable acrylate resins"
- Andreas Kaufmann: "Preparation of activated Montmorillonite, organic modification and characterisation of its nanocomposites with PVOH"
- Martin Spörk: "Investigations of the catalytic activity of montmorillonites in the field of condensation reactions "

Crosslinking of water soluble polymers
Modification of inorganic surfaces
Characterisation of polymer-filler interactions
Synthesis and characterisation of UV reactive polymers and particles

Chair of Chemistry of Polymeric Materials, Otto-Glöckel-Strasse 2/4, 8700 Leoben

10/2008 – 06/2009

Master Thesis

Development of migration barriers for food packaging based on cardboard

Chair of Chemistry of Polymeric Material, Otto-Glöckel-Strasse 2/4, 8700 Leoben

03/2008, 04/2008 – 07/2008 (1 month full time, 3.5 months part time 25 h)

Internship

Development of vacuum infusion resins

Cytec Surface Specialties Austria GmbH, Leechgasse 21, 8010 Graz

08/2007 – 09/2007; 08/2006 – 09/2006 (4 months)

Internship

Compounding of Polypropylene and injection moulding of test specimen

Borealis Polyolefine GmbH, St.-Peter-Straße 25, 4021 Linz

12/2006 – 06/2007, 03/2005 – 06/2005 (11 months)

Scientific project staff

Characterisation of biopolymers
Processing of biopolymer-wood-composites

Institute of Chemistry and Technology of Materials, Graz University of Technology, Stremayrgasse 9, 8010 Graz

08/2005 – 09/2005, 04/2004 (3 months)

Internship

Quality assurance
Extrusion of PVC window frame profiles
Maintenance of extrusion machinery

IFN-Internorm Bauelemente GmbH & Co KG, Am Teichfeld 6, 4152 Sarleinsbach

Other work experience

Organic Farm Hörezedt
- Maintenance of farm machinery
- Caretaking of pasture land and fish ponds

BMW Motoren Steyr GmbH
- Spare parts logistics
- Maintenance of machinery
- Assembly of diesel engines and quality assurance

	Voestalpine AG
	  • Cleaning personal
	APM HandelsgesmbH
	  • Eventmanagement
	AGRU Oberflächentechnik GmbH
	  • Incoming goods department and logistics

Publications	
Papers in referred journals	Schauberger, J. G.; Rieß, G.; Kern, W. (2013): "UV crosslinking of Fe^{+3} doped poly(vinyl alcohol) - characterization of optical properties and swelling behaviour". - in: Journal of applied polymer science, Volume 129, Issue 6, 15 September 2013, Pages: 3623–3628, DOI: 10.1002/app.39109. Schauberger, J. G.; Rieß, G.; Kern, W. (2013): **Cover Image** in: Journal of Applied Polymer Science, Volume 129, Issue 6, 15 September 2013, Page: i, Article first published online : 19 JUN 2013, DOI: 10.1002/app.39080 Schauberger, J. G.; Rieß, G.; Kern, W. (2013): "Preparation of UV reactive montmorillonite and characterisation of its nanocomposites with poly(vinyl alcohol)". - in: Journal of applied polymer science, Volume 130, Issue 1, 5 October 2013, Pages: 665–672, DOI: 10.1002/app.39198
Lecture or presentation	Schauberger, J. G.; Riess, G.; Kern, W.: "Preparation of UV-reactive montmorillonite and characterisation of its nanocomposites with poly (vinyl alcohol)" - at: ASPM 2013. Bled: 03. – 05. 04. 2013 Schauberger, J.; Kaufmann, A.; Puchleitner, R.; Schlögl, S.; Rieß, G.; Kern, W.: "Improvement of the chemical resistance of elastomers using organo-modified filler materials based on layered silicates." - at: NGF RubberCon 2012. Oslo: 14.05.2012 Schauberger, J.; Rieß, G.; Kaufmann, A.; Kern, W.: "UV-sensitizing of poly(vinyl alcohol) using cation-exchanged montmorillonite." - at: XXIVth IUPAC Symposium on Photochemistry. Coimbra: 15.07.2012
Poster presented within an academic meeting	Rieß, G.; Schauberger, J.; Muhr, N.; Kern, W.: "Silica nanoparticles bearing a photoreactive shell." - at: European Symposium of Photopolymer Science. Turin am: 04.09.2012 Rieß, G.; Schauberger, J.; Koschell, K.; Kern, W.: "Novel silica nanoparticles with photoactive diazosulfonate groups. - at: XXIV IUPAC Symposium of Photochemistry. Coimbra (Portugal): 16.07.2012 Manhart, J.; Schlögl, S.; Schauberger, J.; Kern, W.: "Photochemical cross-linking of poly(vinyl alcohol): New strategies towards water-developable photoresists." - at: XXIVth IUPAC Symposium on Photochemistry. Coimbra: 15.07.2012 Schauberger, J.; Puchleitner, R.; Yue, L.; Rieß, G.; Kern, W.: "Optimization of double-bond conversion of acrylic UV-curable resin formulations". - at: The 27th Annual Meeting of the Polymer Processing Society. Marrakesh: 10.05.2011